From the Institute of Pathobiochemistry

at the University Medical Center of the Johannes Gutenberg University

Broader Functional Role of Meprin β in the Murine Brain and in the APP/V717I Mouse Model

Dissertation to attain the degree of

Doctor rerum naturalium (Dr. rer. nat.)

From the faculties of Biology and Medicine

at Johannes Gutenberg University Mainz

Submitted by Maximilian Keller

Born 06.04.1993 in Omsk

Mainz, October 2025

This work was completed between March 2022 and September 2025 at the Institute of Pathobiochemistry at the University Medical Center of the Johannes Gutenberg University Mainz.

Dean of the faculty of Biology: Univ.-Prof. Dr. Eckhard Thines

1. Supervisor: Univ.-Prof. Dr.

2. Supervisor: Univ.-Prof. Dr.

1. Reviewer: Univ.-Prof. Dr.

2. Reviewer: Univ.-Prof. Dr.

Chair of Disputation: Univ.-Prof. Dr.

Date of Disputation: 04.12.2025

Zusammenfassung

Die Alzheimer-Krankheit (AD) ist eine sich weltweit rasch ausbreitende Gesundheitskrise, deren Fallzahlen sich aufgrund der steigenden Lebenserwartung bis 2050 voraussichtlich mehr als verdoppeln werden. Früher fälschlicherweise als einfache senile Demenz diagnostiziert, wird AD heute durch eine Kombination aus klinischen Untersuchungen, Bildgebung des Gehirns (MRT, PET) und spezifischen Biomarkern wie Amyloid-beta (Aβ) und Tau diagnostiziert. Die Pathologie umfasst Neurodegeneration, die durch die Ansammlung fehlgefalteter Proteine und chronischer Entzündungen verursacht wird.

AD manifestiert sich hauptsächlich in zwei Formen: der seltenen, früh auftretenden familiären AD (FAD) und der weitaus häufigeren, spät auftretenden sporadischen AD. Die vorherrschende Erklärung, die Amyloid-Hypothese, geht davon aus, dass die Anhäufung von Aβ die primäre auslösende Ursache ist. Dieser toxische Prozess erfolgt über den amyloidogenen Stoffwechselweg der Verarbeitung des Amyloid-Vorläuferproteins (APP), dem der schützende nicht-amyloidogene Stoffwechelweg gegenübersteht. Dieser schützende Weg wird durch positive Lebensstilfaktoren wie gesunde Ernährung und regelmäßige Bewegung unterstützt.

Aktuelle Forschungsbemühungen gehen über Aβ und Tau hinaus und untersuchen die Rolle spezifischer Proteasen im Gehirn, wie z. B. Meprin β, welches als Risikofaktor für AD identifiziert wurde. Während aktuelle Therapien weitgehend nur eine Linderung der Symptome bieten, konzentrieren sich zukünftige Strategien auf Interventionen, die frühzeitig im Krankheitsverlauf auf die Kernpathologie abzielen können.

Hier berichten wir, dass die Überexpression von Meprin β das Lernverhalten von Mäusen auf verhaltensbezogener und elektrophysiologischer Ebene beeinflusst. Wir zeigen, dass die NMDA- und AMPA-Rezeptorlevel unverändert bleiben, wobei die N-Terminomik-Analyse Brevican als potenziellen Kandidaten für die beobachteten Effekte identifiziert. Gleichzeitig zeigt die Überexpression von Meprin β in einem AD-Mausmodell (APP/Ld) keine beobachtbaren Unterschiede im Lernverhalten. Die Analyse von löslichem Aβ im Kortex und Hippocampus ergab, dass Mäuse mit Meprin-β-Überexpression in einem APP/Ld-Hintergrund mehr Aβ produzieren als APP/Ld-Tiere. Die höheren Aβ-Spiegel führen nicht zur Bildung von Plaques, während wir eine intrazelluläre Akkumulation beobachten.

Summary

Alzheimer's Disease (AD) is a rapidly growing global health crisis, with case numbers projected to more than double by 2050 due to increasing life expectancy. Historically misdiagnosed as simple senile dementia, AD is now diagnosed through a combination of clinical assessments, brain imaging (MRI, PET), and specific biomarkers like amyloid-beta (Aβ) and tau. Pathology involves neurodegeneration caused by the accumulation of misfolded proteins and chronic inflammation.

AD primarily manifests in two forms: the rare, early-onset familial AD (FAD), driven by gene mutations that lead to the overproduction of Aβ, and the far more common, late-onset sporadic AD, which results from the impaired clearance of Aβ from the brain. The dominant explanation, the amyloid hypothesis, posits that the accumulation of is the primary initiating pathological event. This toxic process occurs via the amyloidogenic pathway of amyloid precursor protein (APP) processing, which is contrasted by the protective non-amyloidogenic pathway. This protective pathway is supported by beneficial lifestyle factors, including healthy diets and regular exercise.

Current research efforts extend beyond Aβ and tau to explore the role of specific proteases in the brain, such as meprin β, which has been identified as a risk factor for AD. While current treatments largely offer only symptomatic relief, future strategies are focused on interventions that can target the core pathology early in the disease course to modify or prevent its progression.

Here, we report that the overexpression of meprin β affects learning in mice on the behavioral and electrophysiological level. We show that NMDA- and AMPA receptor levels are not altered, while N-terminomics analysis reveals brevican as a potential candidate to explain the observed effects. Simultaneously, overexpression of meprin β in an AD mouse model background (APP/Ld) shows no observable differences in learning and behavior. Analysis of soluble Aβ in the cortex and hippocampus revealed that meprin β-overexpressing mice in an APP/Ld background produce more Aβ than APP/Ld animals. The higher Aβ levels do not translate into the formation of plaques, whereas we observe intracellular accumulation.

List of Abbreviations

AD – Alzheimer's Disease

ADAM – A Disintegrin and Metalloproteinase

ALS – Amyotrophic Lateral Sclerosis

AMPA – α-amino-3-hydroxy-5-methyl-4-isoxazolepropionic acid receptor

ApoE – Apolipoprotein E

APP – Amyloid Precursor Protein

Aβ – Amyloid Beta

BACE1 – Beta-Site APP-Cleaving Enzyme 1

CNS – Central Nervous System

CPSG – Chondroitin Sulfate Proteoglycan

CS – Chondroitin Sulfate

CSF – Cerebrospinal Fluid

CT – Computed Tomography

DASH – Dietary Approaches to Stop Hypertension

ECM – Extracellular Matrix

FAD – Familial Alzheimer's Disease

FDA – U.S. Food and Drug Administration

fEPSP – Field Excitatory Postsynaptic Potential

FUS – Focused Ultrasound

GWAS – Genome-Wide Association Study

HD – Huntington's Disease

HFS – High-Frequency Stimulation

HSV-1 – Herpes Simplex Virus Type 1

HUNTER – High-efficiency Undecanal-based N-Termini EnRichment

I/O – Input/Output

KO – Knockout

Ld – London mutation (APP V717I)

LRP1 – Low-Density Lipoprotein Receptor-Related Protein 1

LTD – Long-Term Depression

LTP – Long-Term Potentiation

MEA – Microelectrode Array

MIND – Mediterranean-DASH Intervention for Neurodegenerative Delay

MMP – Matrix Metalloproteinase

MRI – Magnetic Resonance Imaging

MS – Multiple Sclerosis

MVB – Multivesicular Body

MWM – Morris Water Maze

NASH – Non-Alcoholic Steatohepatitis

NMDA – N-Methyl-D-Aspartate receptor

NSAID – Nonsteroidal Anti-Inflammatory Drug

PAGE – Polyacrylamide Gel Electrophoresis

PBM – Photobiomodulation

PD – Parkinson's Disease

PNN – Perineuronal Net

PrP – Prion Protein

PSEN – Presenilin

PT – Probe Trial

PTPσ – Protein Tyrosine Phosphatase Sigma

PV+ – Parvalbumin-positive

sAPP – Soluble Amyloid Precursor Protein

SDS – Sodium Dodecyl Sulfate

Swe – Swedish mutation (APP K670N/M671L)

TMT – Tandem Mass Tag

TPS – Transcranial Pulse Stimulation

UPS – Ubiquitin–Proteasome System

Table of Contents

1. Introduction

1.1 Alzheimer's Disease: History, Diagnosis, and the Growing Dementia Crisis

Alzheimer's disease (AD) is becoming more common worldwide. Typically, the risk of developing AD increases sharply with age, especially after 65. As life expectancy rises and more people reach older ages, the number of Alzheimer's cases grows accordingly (Li et al., 2022; Hebert et al., 2001; Monfared et al., 2022). Projections show that the number of people with AD will more than double by 2050, mainly because of the increasing age of the population, not because the disease is becoming more common at younger ages (Javaid et al., 2021; Stevenson-Hoare et al., 2023). Nonetheless, some studies suggest that the risk of developing AD at a given age may be declining in some high-income countries, likely due to better education and improved management of cardiovascular risk factors (Langa, 2015).

Before AD was formally identified in the early 20th century, symptoms were described in more general terms as part of "senile dementia" or age-related mental decline. There was no clear distinction between different types of dementia, and the condition was often seen as a natural, inevitable part of aging. Dementia-like symptoms were noted in ancient texts, often described as a general decline in memory and reasoning in old age. For example, the Old Testament references being kind to elders whose minds fail them (Bonid et al., 2017). Medieval physicians, such as Avicenna (980–1037 CE), already tried to distinguish between different forms of cognitive decline. Still, the concept of "senile dementia" persisted, and there was little attempt to separate what we now call AD from other causes of cognitive impairment (Taheri-Targhi et al., 2019; Vatanabe et al., 2020). Additionally, without brain imaging or pathology, descriptions relied on observable symptoms like memory loss, confusion, and behavioral changes. Only from the 20th century onward AD was recognized as a distinct disease thanks to advances in medical science and pathology.

AD is diagnosed by combining an assessment of symptoms with tests that help rule out other causes and detect changes in the brain**.** It is based on evaluating memory and thinking problems, supported by brain scans and sometimes lab tests. Clinicians usually look for gradual and progressive memory loss and other cognitive problems by applying interviews and simple mental tests to check thinking, memory, and daily functioning (McKhann et al., 1984). Simultaneously, blood tests and other lab work are performed to rule out other conditions that

might cause similar symptoms, such as vitamin deficiencies or thyroid problems (Weller & Budson, 2018). Lastly, scans like MRI or CT are used to look for brain changes typical of AD and to exclude other brain diseases. These advanced imaging techniques (like PET scans) and biomarker tests (from spinal fluid or blood) can provide more specific evidence of Alzheimer's but are not always used in routine practice (Kim et al., 2022). AD biomarkers include CSF markers (like amyloid-beta and tau), blood and fluid biomarkers (such as specific proteins and microRNAs) and ocular biomarkers like retinal thickness changes detected by imaging (Zabel et al., 2025). Brevican, for example, is a brain-specific protein that is part of the extracellular matrix (ECM) and perineuronal nets (PNN). Recent research suggests that fragments of brevican in blood or cerebrospinal fluid may serve as potential biomarkers for distinguishing between different types of dementia, including AD (Jonesco et al., 2020). There, tests were developed to detect two brevican fragments - N-brevican (N-Brev) and brevican-A (Brev-A). The ratio of these fragments can help distinguish AD from other dementias, but unfortunately does not clearly separate AD from healthy controls (Jonesco et al., 2020). Some brevican peptides are lower in vascular dementia compared to AD and controls, suggesting brevican may help differentiate between these two specific dementia types (Minta et al., 2020; Morawski et al., 2012).

Research funding for age-related diseases, including AD and other chronic conditions, has significantly increased in recent years (Jin et al., 2015; Li, 2019). This shift reflects growing recognition of the health and economic impact of an aging population, leading to more resources and attention for research in this area (Katiyar et al., 2020). The National Institute on Aging in the US, for example, has seen its budget triple from 2015 to 2020, with much of this new funding directed toward AD and related dementias (Bernard et al., 2020). As funding for AD research has increased overall, support for other age-related diseases has likewise expanded, since growth in AD research tends to draw resources into the broader field of age-related illnesses South and East Asia are seeing the quickest increases in the number of people with AD, while high-income countries in Western Europe and Japan have the highest prevalence rates due to their older populations (Ji et al., 2024; Javaid et al., 2021). Nevertheless, a large study from Stephan et al. (2018) shows that among these high-prevalence countries, age-standardized dementia incidence rates have actually decreased by over 50% in both men and women over the last decade, even as overall prevalence remains high. China is experiencing a dramatic increase in AD cases, driven by its large and rapidly aging

population. The total number of people affected is rising faster here than anywhere else, and similar trends are seen in India and neighboring countries (Ji et al., 2024; Javaid et al., 2021). By 2040, 71% of people with dementia will live in low- and middle-income countries, especially in Asia (Kalaria et al., 2024).

AD is typically dependent on several different lifestyle factors such as diet, physical activity and gut health. A healthy diet, regular movement, and a balanced gut microbiome can help protect the brain and may delay or reduce the risk of AD**.** Diets rich in vegetables, fruits, whole grains, legumes, fish, and healthy fats (like the Mediterranean, DASH, or MIND diets) are associated with a lower risk of AD (Baranowski et al., 2020; Kepka et al., 2022; Zhang et al., 2020). These diets provide antioxidants, polyunsaturated fatty acids, and polyphenols, which reduce inflammation and oxidative stress - key contributors to AD. At the same time, unhealthy diets high in saturated fats and simple sugars increase AD risk (Stefaniak et al., 2022). Regular exercise reduces AD risk and slows cognitive decline by improving blood flow, reducing inflammation, and increasing brain-derived neurotrophic factor (BDNF), which supports brain health (Khemka et al., 2023; De La Rosa et al., 2020). A healthy gut microbiome, shaped by diet and exercise, supports brain health via the gut-brain axis. Gut dysbiosis is linked to increased inflammation and AD pathology, while a diverse microbiome may protect against neurodegeneration (Zhou et al., 2023; Kesika et al., 2020).

To fully understand how these health benefits work and to evade the risk of getting sick, we need to understand the pathology of this disease in detail. Neurodegeneration refers to the progressive loss of structure and function of neurons, ultimately leading to their death. This process underlies many disorders, including AD, Parkinson's disease (PD), Huntington's disease (HD) and amyotrophic lateral sclerosis (ALS). These diseases share several core features, despite differences in symptoms and the brain regions affected: the accumulation of misfolded proteins, impairment of critical cellular processes, chronic activation of inflammatory pathways and ultimately neuronal death (Hou et al., 2019; Sanghai & Tranmer, 2023; Noori et al., 2020; Gao et al., 2018). In all cases, toxic protein buildup, such as amyloid-β and tau in AD, α-synuclein in PD, and TDP-43 in ALS, drives protein aggregation and cellular dysfunction (Spires-Jones et al., 2017). A major contributing mechanism is the failure of protein clearance systems, which disrupt proteostasis and allow harmful aggregates to persist (Sanghai & Tranmer, 2023; Noori et al., 2020; Tan et al., 2019). This is compounded by reduced

energy production, increased oxidative stress and chronic activation of brain immune cells, which altogether fuel persistent neuroinflammation (Singh et al., 2023). The incidence of these disorders rises sharply with age, reflecting the gradual decline of cellular repair mechanisms over the lifespan (Sanghai & Tranmer, 2023; Hou et al., 2019). Ultimately, these converging processes trigger inflammasome activation, progressive loss of neuronal function, and defective protein folding or clearance.

However, the most common treatment procedures focus on symptom relief, slowing disease progression and improving quality of life. Standard pharmacological treatments include cholinesterase inhibitors like Donepezil and are widely used to improve or stabilize memory and cognitive symptoms in mild to moderate AD. Then NMDA receptor antagonists like Memantine are prescribed for moderate to severe AD to help with memory, attention, and daily functioning (Buccellato et al., 2023; Breijyeh & Karaman, 2020). Recently, monoclonal antibodies (Aducunumab and Lecanemab) were conditionally approved by the FDA, which target amyloid β (Aβ) plaques in the brain. These drugs aim to slow disease progression, though their clinical benefits are modest and they require careful patient selection and monitoring (Rahman et al., 2023; Beshir et al., 2022).

Unfortunately, these treatment options are very limited and only improve symptoms for a short period, leading to growing interest in alternative and complementary therapies. Several non-drug and non-invasive options, herbal remedies, lifestyle interventions, and repurposed medications show promise for managing AD symptoms and potentially slowing disease progression. Focused Ultrasound (FUS) and Transcranial Pulse Stimulation (TPS) are non-invasive brain stimulation techniques that have shown benefits in animal and early human studies, potentially improving cognitive function and altering disease progression by affecting the blood-brain barrier and brain activity (Sovrea et al., 2025). Infrared light therapy or photobiomodulation (PBM), especially during sleep, may enhance brain waste clearance and reduce amyloid buildup, with preclinical and early clinical evidence supporting its safety and potential effectiveness (Semyachkina-Glushkovskaya et al., 2023; Wang et al., 2024). Ayurvedic and traditional Chinese medicine herbs such as turmeric, Brahmi, Ashwagandha, and Ginkgo biloba contain compounds with antioxidant, anti-inflammatory, and neuroprotective effects. These may improve memory, reduce neurodegeneration, and enhance quality of life, though more rigorous clinical trials are needed (Kumar, 2019; Peng et al., 2024).

As described, multiple factors contribute to the onset of AD. Although the variants share core pathological features and clinical manifestations, it is essential to distinguish between the two major forms.

1.2 Pathophysiology of AD

Familial Alzheimer's disease (FAD) is a rare, inherited form of Alzheimer's disease caused by specific genetic mutations, as it accounts for only 1–5% of all Alzheimer's cases. FAD is characterized by an early age of onset (often before age 65, sometimes as early as the 30s or 40s) and is passed down in families in an autosomal dominant pattern, meaning each child of an affected parent has a 50% chance of inheriting the disease (Breitner et al., 1984)**.** FAD is caused by mutations in one of three genes: APP (amyloid precursor protein), PSEN1 (presenilin 1), or PSEN2 (presenilin 2). These mutations lead to abnormal processing of APP, resulting in amyloid β (Aβ), a protein that accumulates in the brains of people with AD (Andrade-Guerrero et al., 2023; Bird, 1994). The clinical symptoms of FAD are similar to those of sporadic Alzheimer's, including progressive memory loss, cognitive decline, and behavioral changes. However, FAD often progresses more rapidly and may include additional neurological symptoms such as seizures or myoclonus (involuntary muscle jerks) in some families (Tang et al., 2016).

Sporadic AD is the most common form of AD, accounting for about 95% of all cases. Unlike familial AD, sporadic AD does not result from inherited gene mutations and typically develops later in life. Its exact cause is unknown, but it is believed to arise from a complex interplay of aging, genetic risk factors, and environmental influences (Piaceri et al., 2013; Theron et al., 2023). Most cases occur in people over 65 years old, often referred to as late-onset AD (Masters et al., 2015). While certain genetic alleles (like APOE ε4) increase the risk, there is no deterministic single mutation as seen in FAD. Furthermore, genome-wide association studies (GWAS) have identified many risk genes, including TREM2, SORL1, ABCA7 or PICALM, that have substantial effects but not as severe as the APOE ε4 variant (Theron et al., 2023; Rajabli et al., 2023; Bellenguez et al., 2022; Karch et al., 2015).

However, some factors have a protective effect against AD. There is strong evidence that certain genetic mutations and variants can protect against both familial and sporadic AD. The most well-established protective mutations are the APOE allele ε2 and the APP A673T (Icelandic) mutation. The APOE ε2 variant is associated with a significantly lower risk of

developing AD compared to the common ε3 and high-risk ε4 alleles, due to more efficient clearance of Aβ from the brain. Its protective effect is seen in both sporadic and familial cases, and it may also slow disease progression (Corder et al., 1994). The rare mutation A673T in APP reduces the formation of Aβ, the peptide that accumulates in AD brains. It protects against both sporadic and familial forms, even when other pathogenic mutations are present (Shimohama et al., 2024). Carriers of the mutation additionally show reduced levels of soluble APPβ (sAPPβ) in cerebrospinal fluid and plasma, while levels of sAPPα (a product of the non-amyloidogenic pathway) are increased (Wittrahm et al., 2023). Also, the mutation is associated with better cognitive performance in old age and protection against age-related cognitive decline, even in the absence of AD (Maloney et al., 2014; Jónsson et al., 2012). Another very interesting factor is the APOE ε3 Christchurch (R136S) mutation. It was identified in a person with a high-risk familial AD mutation (PSEN1 E280A) who did not develop dementia. This rare variant appears to confer resilience against tau pathology via inhibition of the cGAS-STING-IFN pathway (Naguib et al., 2025).

The amyloid hypothesis has been the dominant model for explaining AD for decades. It proposes that the accumulation of Aβ peptides in the brain is the primary cause of AD, triggering downstream events like tau pathology, neurodegeneration, and cognitive decline. Aβ plaques appear early in AD, and low cerebrospinal fluid Aβ1-42 and amyloid-PET positivity precede symptoms by years (Selkoe & Hardy, 2016; Karran & De Strooper, 2022). Recent anti-amyloid antibody therapies (e.g., aducanumab) can remove amyloid plaques and have shown modest slowing of cognitive decline in some patients, though the clinical benefit is debated and may require early intervention (Selkoe & Hardy, 2016; Karran & De Strooper, 2022). This suggests Aβ accumulation is an *initiating* event in the disease cascade (Kametani & Hasegawa, 2018), which may explain why many anti-amyloid therapy trials have failed when treatment is given after significant neuronal damage (Hamm et al., 2017; Samaey et al., 2019). The most effective window for Aβ-targeted therapies may be during the preclinical phase, before extensive neurodegeneration, so before neuroinflammation starts and the disease course cannot be prevented anymore (Hamm et al., 2017; Samaey et al., 2019). Because said processes are so closely linked and flow into one another, it's hard to pinpoint exactly where one ends and the next begins, making them difficult to explain clearly.

In FAD, Aβ accumulation is mainly the result of higher APP processing, whereas in late-onset AD, studies indicate that Aβ clearance rates are markedly impaired (Jack et al., 2010; Korte et al., 2020). Therefore, addressing excessive Aβ production is particularly relevant for FAD, while improving clearance is the key challenge in sporadic AD. Although abnormal processing or clearance of APP is recognized as the earliest sign, there remains no reliable theory explaining why this occurs. However, new hypotheses are emerging: there is growing evidence that viral DNA is frequently found in the brains of people with AD and may contribute to disease risk and pathology. The relationship remains under active investigation. Herpes simplex virus (HSV)-1 DNA has been detected within amyloid plaques in AD brains, with studies showing up to 90% of plaques containing HSV-1 DNA in AD patients. This association is much stronger in AD brains than in normal-aged brains (Wozniak et al., 2009). Consequently, HSV-1 infection can trigger Aβ accumulation and tau hyperphosphorylation - both hallmarks of AD - in cell and animal models (Wozniak et al., 2009; Harris & Harris, 2018). The risk appears to be higher in individuals carrying the APOE-ε4 gene variant, which may make the brain more susceptible to viral effects.

Interestingly, there is a well-documented inverse relationship between cancer and AD: cancer patients have about a 35–40% lower risk of AD, and vice versa (Zhang et al., 2015). This phenomenon has been observed in multiple large epidemiological studies and meta-analyses. The inverse association holds across different types of cancer and persists after adjusting for confounding factors such as age, education, and genetic risk (e.g., APOE status) (Ospina-Romero et al., 2020; Musicco et al., 2013). A possible reason could be that cancer and AD involve opposite cellular processes. Cancer is characterized by uncontrolled cell growth and reduced cell death (apoptosis), while AD features increased cell death and impaired cell survival (Bhardwaj et al., 2023; Shafi, 2016). Proteins like p53 and PIN1 are implicated in both diseases but act in opposite directions, respectively. For example, high PIN1 activity promotes cancer but protects against AD, while low PIN1 increases AD risk but reduces cancer risk (Lanni et al., 2020). Further, some genes are upregulated in AD but downregulated in cancer, and vice versa, suggesting a genetic basis for the phenomenon (Anyomi et al., 2025). Hence, the inverse relationship between cancer and AD is robust and supported by strong epidemiological evidence. This insight is driving new research into shared mechanisms and potential therapeutic targets that are used in both diseases.

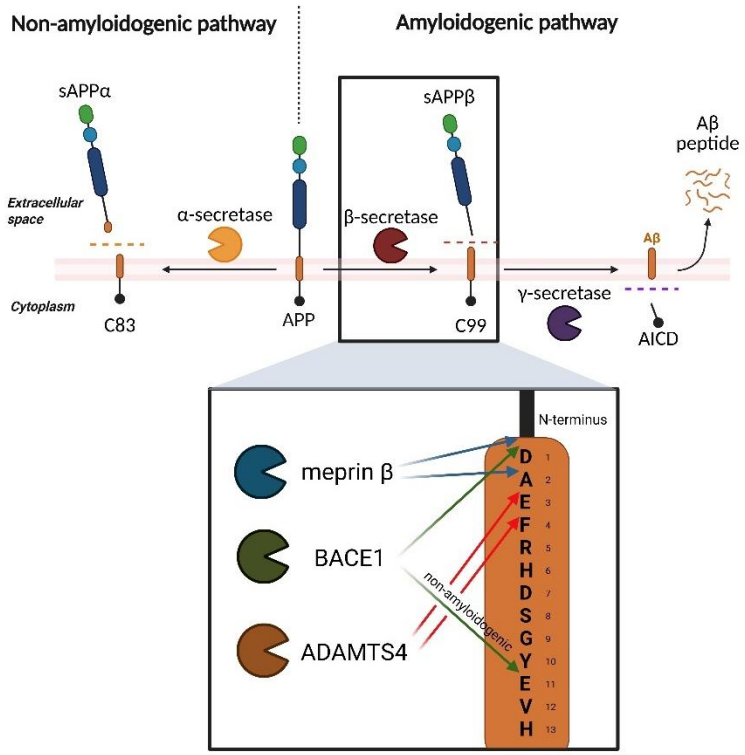

Figure 1 – Sequential cleavage of APP generates different metabolites through two main routes. In the non-amyloidogenic pathway, APP is first cleaved by α-secretase, releasing soluble APPα (sAPPα) and producing the membrane-bound fragment C83. Subsequent cleavage by γ-secretase precludes amyloid-β (Aβ) formation and is regarded as protective against AD. In contrast, the amyloidogenic pathway begins with β-secretase cleavage, yielding soluble APPβ (sAPPβ) and a longer C-terminal fragment that is further processed by γ-secretase to release Aβ peptides, which are prone to aggregation. BACE1 and other alternative β-secretases cleave at different positions of the Aβ domain, generating the full-length and N-terminally truncated Aβ species.

1.3 Aspects of Alzheimer's Disease

As noted earlier, certain factors can be protective against AD. To determine what makes these mutations “protective,” it is essential to understand their underlying molecular mechanisms.

The dominant view in current research is that Aβ accumulation is the earliest detectable pathological event in AD, with changes detectable in the brain years before symptoms appear (Jack et al., 2010). There is growing evidence that other changes, such as reduced cerebral blood flow, may occur in parallel, potentially triggered by not-accumulated Aβ oligomers (Korte et al., 2020). Other early changes, such as white matter disruption and hippocampal network activity alterations, are closely linked to Aβ but do not precede it (Collij et al., 2021; Goutagny & Krantic, 2013). Early changes in theta and gamma rhythms in the hippocampus may serve as a potential early biomarker for Alzheimer's disease, aiding in early diagnosis and treatment (Goutagny & Krantic, 2013).

Non-amyloidogenic processing of APP is a key pathway that prevents the formation of Aβ peptides, which are central to AD pathology. This pathway not only avoids toxic Aβ production

but also generates neuroprotective fragments. In the non-amyloidogenic pathway, APP is first cleaved by α-secretase, producing a soluble fragment called sAPPα. This prevents the formation of Aβ because the α cleavage site is within the Aβ region of APP, making further processing impossible (Jacobsen & Iverfeldt, 2011; Al-Kuraishy et al., 2023). The remaining membrane-bound fragment is then cleaved by γ-secretase, resulting in non-toxic peptides (Coronel et al., 2018) (Figure 1). Compounds like NSAIDs, statins, flavonoids, and caloric restriction can promote non-amyloidogenic processing, often by inhibiting pathways that favor amyloidogenic cleavage or by activating SIRT1 and related gene expression (Tang, 2005). Induction of autophagy (e.g., by Terminalia chebula extract) can shift APP processing toward the non-amyloidogenic pathway, again potentially reducing Aβ generation. sAPPα, the main product of non-amyloidogenic processing, supports neuronal survival, growth, and synaptic function, and may protect against neurodegeneration unrelated to AD (Coronel et al., 2018; Zhao et al., 2022). In addition, non-amyloidogenic APP fragments can positively influence metabolism in both the brain and peripheral tissues (Al-Kuraishy et al., 2023). By enhancing this pathway, it may be possible to simultaneously reduce Aβ burden and promote neuronal health, a strategy supported by several molecular targets and interventions currently under investigation (Jacobsen & Iverfeldt, 2011; Tang, 2005; Zhao et al., 2022).

As already mentioned, on the other side, we have the amyloidogenic pathway. Amyloidogenic processing of APP is the pathway that leads to the production of Aβ peptides, which are central to AD pathology. This process involves sequential cleavage of APP by β-secretase and γ-secretase, resulting in several distinct molecular species, including the neurotoxic Aβ peptides. APP exists in several isoforms due to alternative splicing of its mRNA. The main human APP isoforms are APP695 (which is also the most common form and exists predominantly in neurons) and APP751 & APP770 (which are more abundant in non-neuronal tissue) (Multhaup, 1994; Zhang et al., 2011).

APP and Aβ, while central to AD, have key physiological roles in the healthy brain and body. APP supports brain development, synaptic function, and neuroprotection by promoting neurite outgrowth, neuronal migration, synaptogenesis, and acting as a cell adhesion molecule for network formation (Al-Kuraishy et al., 2023; Müller & Zheng, 2012, Sosa et al., 2017). Its non-amyloidogenic fragments (P3, C83, sAPPα) protect neurons from apoptosis and oxidative stress (Al-Kuraishy et al., 2023). At normal levels, Aβ aids homeostatic synaptic plasticity,

supports neuronal survival, protects against excitotoxicity, and may function as an antimicrobial peptide (Galanis et al., 2020). APP expression is largely neuron-specific, especially at synapses (Guo et al., 2011), but can change with mutations (e.g., presenilin 1) or after nerve injury, affecting distribution and highlighting its role in damage response (Woodruff et al., 2014; Rodkin et al., 2021).

During amyloidogenic processing, APP is first cleaved by the β-site of APP cleaving enzyme (BACE1), producing a soluble fragment (sAPPβ) and a membrane-bound C-terminal fragment (C99) (Cho et al., 2022), while the acidic environment of endosomes is particularly important for β-secretase activity (Sinha et al., 1999). The C99 fragment is subsequently cleaved by γ-secretase, producing Aβ peptides - most notably Aβ1/11-40 and Aβ1/11-42 (Vetrivel & Thinakaran, 2006), as well as the APP Intracellular Domain (AICD), a small fragment with potential signaling functions (Kienlen-Campard et al., 2008). The Aβ1-42/Aβ1-40 ratio is a key factor in pathology, with FAD mutations often elevating this ratio and thereby promoting disease (Kienlen-Campard et al., 2008; Kim & Bezprozvanny, 2021; Zhao et al., 2020). Importantly, plaques contain a diverse range of truncated and post-translationally modified Aβ peptides, including N-terminal variants (e.g., Aβ2-40/42, Aβ3-40/42, Aβ4-40/42), C-terminal variants (e.g., Aβ1-37, Aβ1-38, Aβ1-39, Aβ1-43), and chemically altered forms such as pyroglutamylated, isomerized, and oxidized species (Drummond et al., 2022; Güntert et al., 2006). For the N-truncated peptides, alternative proteases have been described, such as ADAMTS4 or meprin β (Bien et al., 2012; Schönherr et al., 2016; Marengo et al., 2022). Meprin β, for example, fulfills numerous proteolytic functions in the body and was recently identified as a risk factor for AD (Patel et al., 2017). Interestingly, meprin β is not only able to produce N-truncated x-40/42 species *but also* the 'full-length' 1-x peptides (Schönherr et al., 2016).

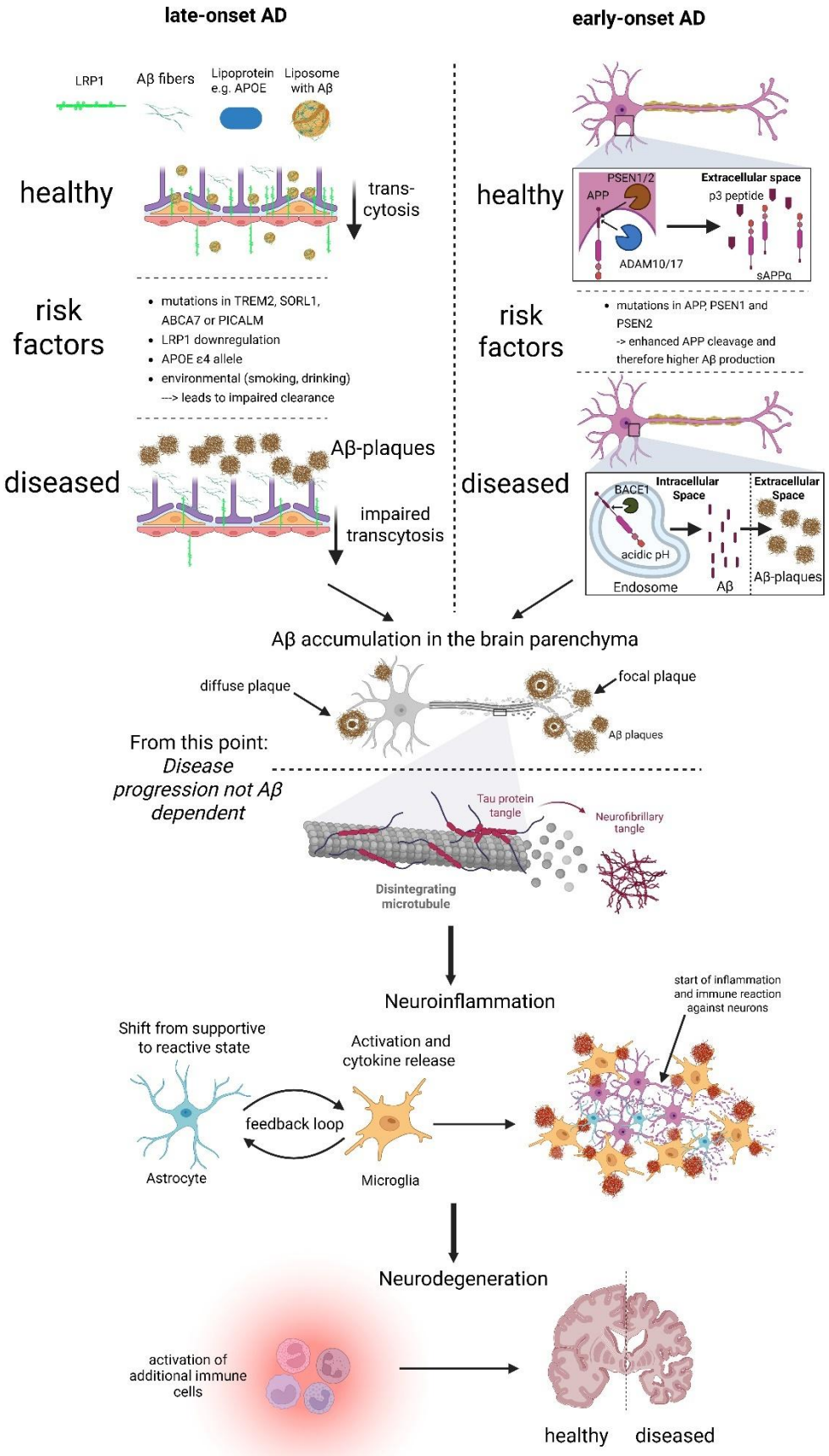

(Figure caption on next page)

Figure 2 – Two different pathways lead to AD. Early-onset AD is mainly driven by genetic mutations that alter the production of Aβ. In contrast, late-onset AD involves mutations that act as risk factors, primarily affecting clearance mechanisms and Aβ transport rather than its production. Both pathways result in the extracellular buildup of Aβ, ultimately forming plaques. Once plaque accumulation triggers tau pathology, inflammation, and degeneration of brain tissue, targeting Aβ becomes merely symptom-relieving without the potential to cure the disease. As neurons degenerate, inflammation increases, creating a vicious cycle. Immune cells become activated, further degrading tissue, which eventually leads to the severe and phenotypic symptoms of AD.

Generation of Aβ1–40 and Aβ1–42 peptides requires several cleavage steps that are separated from each other. To produce Aβ1–40 peptides, the γ-secretase sequentially cleaves at positions Aβ49, Aβ46, Aβ43 and finally at Aβ40. Similar to this sequence, Aβ1–42 is obtained by sequential γ cleavage at Aβ48, Aβ45 and Aβ42 (Steiner et al., 2008). In the brains of AD patients, the Aβ1–42 to Aβ1–40 ratio is usually skewed toward Aβ1–42, with this peptide serving as the aggregation-prone core of plaques due to its increased hydrophobicity (Jenkins et al., 1996; Xu et al., 2022; Wall et al., 2016; Nguyen et al., 2016). Interestingly, this ratio is altered in people with the Icelandic mutation (A673T). *In vitro* genome editing to introduce A673T in human cells with familial AD mutations also lowers Aβ secretion (Tremblay et al., 2021). Some studies suggest that the mutant Aβ forms fewer oligomers and has a much lower binding affinity to synaptic receptors, resulting in reduced neurotoxicity and aggregation (Limegrover et al., 2020)**.** Interestingly, meprin β, one of the alternative β-secretases, is not able to cleave APP with the Icelandic mutation because the mutation disrupts the sequence specificity required for meprin β's enzymatic activity at this site (Schönherr et al., 2016). The inability of meprin β to cleave and form Aβ peptides could be the reason for less Aβ production and, therefore, be responsible for the protective effect.

A central paradox in AD research is that Aβ peptides are generated inside neurons, yet the hallmark amyloid plaques are found outside cells. As described, Aβ is produced intracellularly through sequential cleavage of APP primarily in endosomes and the trans-Golgi network (Sinha & Lieberburg, 1999; Vassar et al., 1999; Mañucat-Tan et al., 2018). After its generation, Aβ is actively transported and secreted into the extracellular space through several mechanisms. Mostly, it is directly secreted via the classical secretory pathway involving vesicular trafficking and exocytosis. Additionally, Aβ is packaged into intraluminal vesicles within multivesicular bodies (MVBs), which fuse with the plasma membrane to release exosomes containing Aβ into the extracellular space. Endocytic recycling also plays a role, where APP and its fragments, including Aβ, are internalized and recycled back to the cell surface for release. Moreover, autophagy-dependent pathways facilitate Aβ secretion, with

impaired autophagy leading to reduced extracellular Aβ and increased intracellular accumulation (Rajendran et al., 2006; Selkoe et al., 1996; Arbo et al., 2019; Deng et al., 2021). Active transporters, such as ABC transporters and LRP1, further assist in exporting Aβ across the plasma membrane and the blood-brain barrier (BBB), aiding in its clearance from the brain (Sinha & Lieberburg, 1999; Vassar et al., 1999; Nilsson et al., 2013; Storck et al., 2018). Disruption of these transporters can result in Aβ buildup and plaque formation. Once in the extracellular space, Aβ can aggregate into oligomers and protofibrils, eventually forming insoluble amyloid plaques, a hallmark of AD pathology (Takahashi et al., 2002). The presence of exosomal proteins within plaques supports the significant role of exosome-mediated export in plaque formation (Deng et al., 2021; Nilsson et al., 2013).

Additionally, Aβ is found in several tissues of the body outside the brain. Aβ is present in the blood, liver, kidneys, skin, skeletal muscle, aorta, platelets, and other peripheral tissues. These peripheral sites play important roles in Aβ metabolism, clearance and may even contribute to its production in the brain, since peripheral tissues not only clear brain-derived Aβ but can also produce it, as demonstrated in skin fibroblasts (Shigemori et al., 2022). The liver plays a particularly important role in Aβ clearance, with liver disease linked to increased blood Aβ levels (Tsoy et al., 2024). In the periphery, Aβ interacts with various proteins that can influence its aggregation and toxicity (Yi et al., 2024). These peripheral Aβ levels can impact the brain's Aβ burden, as Aβ from the periphery is able to enter the brain and exacerbate pathology. Notably, peritoneal dialysis has been shown to effectively reduce Aβ levels in both humans and mice, highlighting a promising peripheral strategy for AD therapy (Bu et al., 2018; Jin et al., 2017).

Aβ metabolism in the liver is a critical component of systemic Aβ clearance, with the liver acting as the primary peripheral organ responsible for removing circulating Aβ from the blood. This process involves rapid hepatic uptake, endocytosis by hepatocytes, enzymatic degradation, and excretion into bile, thereby maintaining low plasma Aβ levels and influencing brain Aβ burden in the brain (Ghiso et al., 2004). The liver rapidly removes Aβ from the bloodstream, accounting for over 60% of plasma Aβ clearance in animal models. Hepatocytes capture Aβ primarily via endocytosis, with the low-density lipoprotein receptor-related protein 1 (LRP1) playing a central role in mediating Aβ uptake from the circulation (Ghiso et al., 2004). After degradation, Aβ and its fragments are excreted into the bile and eliminated via the

gut. Biliary excretion becomes especially relevant at higher Aβ concentrations, and enterohepatic recirculation may influence systemic Aβ levels. Hepatobiliary and enterohepatic cycles are modulated by transporters such as ABCA1, ABCG2, and MDR1, which can be targeted pharmacologically to enhance Aβ clearance (Ghiso et al., 2004; Bhattacharjee & Roy, 2022). Recent research also highlights the interplay between hepatic cholesterol metabolism and Aβ processing, as well as the impact of liver steatosis and inflammation on Aβ degradation (Hone et al., 2003). Liver steatosis, non-alcoholic steatohepatitis (NASH), and other hepatic pathologies impair Aβ clearance by downregulating LRP1 and altering the expression of Aβ-degrading enzymes. Restoration of normal hepatic cholesterol metabolism and targeting hepatic Aβ clearance pathways are emerging as potential therapeutic strategies (Huang et al., 2022). Studies in animal models and primates show that circulating Aβ crosses the BBB and accumulates in the brain, co-localizing with amyloid plaques, making the BBB is not a complete barrier to Aβ. Specialized transport systems, such as the receptor for advanced glycation end products (RAGE), allow Aβ from the blood to enter the brain, while other systems (like LRP1) help remove Aβ from the brain to the blood (Petrushanko et al., 2023; Zlokovic et al., 1993; Mackic et al., 2002).

AD has long been recognized as a neurodegenerative disorder characterized by the accumulation of misfolded proteins, primarily Aβ plaques and tau neurofibrillary tangles. In recent years, a substantial body of research has demonstrated that these proteins exhibit “prion-like” properties: they can misfold, self-propagate, and spread from cell to cell within the brain, templating the misfolding of native proteins and driving disease progression (Walker et al., 2016; Watts & Prusiner, 2018). This mechanism is strikingly similar to that of classical prion diseases, such as Creutzfeldt-Jakob disease, where the prion protein (PrP) misfolds and induces further misfolding in a self-perpetuating cycle (Fornari et al., 2019). However, unlike classical prion diseases, there is no strong evidence that AD is infectious among individuals under natural conditions. Nevertheless, the prion-like hypothesis has unified the understanding of neurodegenerative diseases, highlighting shared mechanisms of protein misfolding, aggregation, and propagation. Experimental models show that injection of Aβ or tau aggregates into the brains of transgenic mice induces the formation and spread of plaques and tangles, recapitulating key features of AD pathology (Goedert et al., 2015; Duyckaerts et al., 2019). That’s why it is of particular interest to stop or interfere with the disease in its initial stages, because later intervention only lightens the symptoms.

1.4 The APP/swe-BACE1 Research Bias

Early therapeutic strategies indicate that eliminating Aβ plaques or preventing their formation can yield beneficial outcomes, such as improved cognitive function (Fani et al., 2021; Van Dyck et al., 2023). However, currently approved FDA treatments do not cure the disease; they only slow its progression during the early stages (Fani et al., 2021; Van Dyck et al., 2023).

Many of these studies focus on the protease BACE1, as it plays a central role in the development of Aβ and amyloid plaques and is the major β-secretase (Sims et al., 2023; Cole et al., 2008). As described, Aβ peptides are formed by the proteolytic processing of APP through the sequential action of β- and γ-secretases (Ridler, 2018). In addition to the classical 'full-length' Aβ species (Aβ1-40, Aβ1-42), numerous variants with different N-terminal modifications have been described (Sergeant et al., 2003; Dunys et al., 2018; Bayer, 2021). The exact physiological role of these N-terminally truncated Aβ species (Aβx-40/x-42) is still controversially discussed. At the same time, they have been identified as major components of extracellular amyloid deposits in the human brain (Bayer et al., 2014). In fact, N-terminally truncated species account for up to 70 % of the Aβ forms detected in brain samples from patients with advanced Alzheimer's disease (Wildburger et al., 2017; Wiltfang et al., 2001; Wirths & Zampar, 2019). As BACE1 is not able to generate N-terminally truncated Aβ peptides, but only peptides with 1- and 11-x start positions, mouse models facilitating BACE1 cleavage might not be an optimal solution to address AD pathology, due to the absence of a large portion of plaque species.

The leading mouse model utilized in current AD research is the APP/swe (K670N/M671L) mouse model, which may overlook important pathological factors, because of favored BACE1 cleavage (Armbrust et al., 2022). Therefore, focusing on APP/swe mouse models alone is not sufficient and might be partially misleading for the study of AD.

Interestingly, meprin β cannot proteolytically process APP with the Swedish mutation (Thal et al., 2022). The Swedish mutation alters the amino acid sequence around the β cleavage site, leading to the loss of a large proportion of potential N-truncated Aβ species. Instead, these models focus heavily on enhanced processing by BACE1, resulting in a biased representation of Aβ diversity compared to the full spectrum of Aβ in patient brains. To reduce the influence of BACE1-derived Aβ, we employed an AD mouse model with a γ-secretase-site mutation: APP/V717I (APP/Ld). Of note, the plaque-causing mutation in APP/Ld animals is not due to a

mutation in Presenilin, but rather due to a mutation in the sequence and the expression of the APP protein (Dewachter et al., 2000).

1.5 Proteases in the Brain

Proteases are vital enzymes in the central nervous system that regulate protein breakdown, playing key roles in both normal brain functions and disease processes. Important protease families include matrix metalloproteinases (MMPs), calpains, the ubiquitin-proteasome system (UPS), serine proteases, caspases, and lysosomal proteases. Physiologically, they support synaptic remodeling, axon guidance, protein turnover and are essential for learning, memory, and neural circuit formation (Vafadari et al., 2016; Baudry et al., 2016; Bingol et al., 2011; Yoshida et al., 1999; Bai & Pfaff, 2011). Accordingly, dysregulated protease activity contributes to protein aggregation, synaptic loss, neuronal death and neuroinflammation, which are key features of neurodegenerative diseases like Alzheimer's and Parkinson's. The UPS and lysosomal proteases maintain synaptic plasticity by degrading proteins (Bingol et al., 2011; Baudry et al., 2024), while certain MMPs are critical for dendritic spine remodeling and long-term potentiation (Vafadari et al., 2016; Ferrer-Ferrer & Dityatev, 2018; Hedge & Upadhya, 2007). This dual role of proteases in both supporting neural health and driving degeneration makes them important therapeutic targets and biomarkers in CNS disorders (Davidson & Pickering, 2023; Lech et al., 2019; Church et al., 2025; Wang et al., 2020).

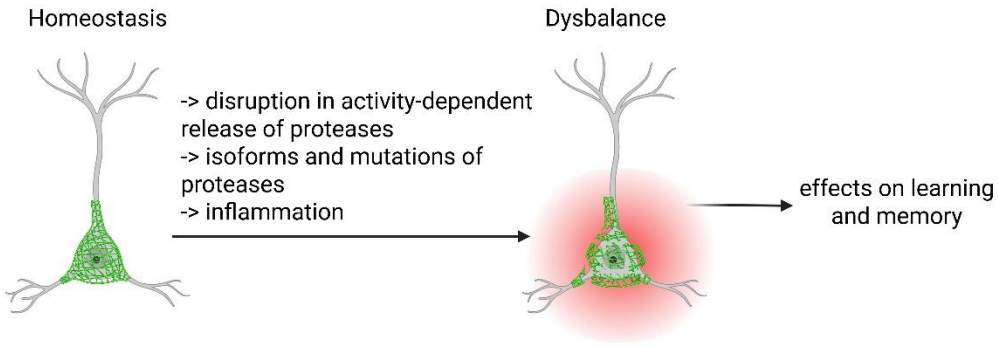

Figure 3 – The perineuronal net is important in stabilizing neuronal outgrowth and synapse stability. Proteases and mutations can lead to disruption of PNN components, resulting in inflammation and learning impairments.

As already mentioned, α- and β-secretases are key enzymes in the brain that control how APP is processed. While BACE1 is widely recognized as the principal β-secretase responsible for initiating Aβ production in AD, research has identified several alternative β-secretases that can also process APP. Notably, BACE2, a close homolog of BACE1, and other proteases such as cathepsin B, have been shown to cleave APP at or near the β-secretase site, sometimes

generating distinct Aβ species or influencing amyloidogenic and non-amyloidogenic pathways (Hussain et al., 2000). Also, meprin β is an alternative β-secretase that is responsible for N-terminally truncated Aβ species (Schönherr et al., 2016). These alternative enzymes contribute to the diversity of Aβ peptides found in the brain, impacting disease progression and representing additional therapeutic targets. Understanding the roles, substrate specificities, and physiological relevance of these alternative β-secretases is crucial for developing more effective AD interventions.

Meprin β is an extracellular metalloprotease with unique roles in the brain, particularly in neurodegeneration and is directly implicated in AD pathology. Truncated Aβ species (Aβ2-x) that were cleaved by meprin β are highly prone to aggregation and may accelerate amyloid plaque formation (Gindorf et al., 2020; Schönherr et al., 2016). However, recent studies reveal an increasingly broad role for meprin β in the brain, extending beyond its known functions to include synaptic and behavioral effects. For example, overexpression of meprin β in mouse brains leads to mild cognitive impairment, hyperactivity, and altered exploratory behavior, effects partly linked to its role in APP processing but also involving cleavage of other neuronal proteins such as latrophilin-3 (Armbrust et al., 2025). Additionally, meprin β influences blood-brain barrier (BBB) regulation by modulating tight junction proteins in brain endothelial cells: overexpression decreases these proteins and increases BBB permeability, whereas knockout mice exhibit tighter barriers and reduced brain water content. Meprin β also activates other proteases, including ADAM10 - the primary α-secretase - highlighting complex interactions within protease networks that are relevant to neurodegeneration (Broder & Becker-Pauly, 2013; Becker-Pauly & Pietrzik, 2017; Armbrust et al., 2025).

Overexpression of proteases such as BACE1, ADAM10, and ADAM17 has been shown to profoundly impact processes like cell signaling, inflammation, tissue remodeling, and neurodegeneration. These enzymes regulate the shedding of membrane proteins and cytokine activity, with clear links to diseases such as AD, cancer, and fibrosis (Luo et al., 2011; Buchanan et al., 2017; Gnosa et al., 2022; Li et al., 2018; Katakowski et a., 2009). Despite the growing understanding of how overexpressed proteases contribute to disease, no study has yet examined the effects of meprin β overexpression in neurons in an AD animal model. Given that a previous study showed that meprin β knockout alters Alzheimer's pathology (Marengo et al., 2022), the novel aim is to investigate what happens when meprin β is overexpressed, in order

to better understand its role in the context of neurodegeneration and protease network dynamics.

1.6 Meprins

Over the last few years, other enzymes, such as ADAMTS4 and meprin β, have been described to act as alternative β-secretases and generate Aβ peptides. For instance, knockout of ADAMTS4 in mice abolished the production of Aβ peptides starting at position 4 (Walter et al., 2019). Likewise, APP cleavage by meprin β was shown to generate soluble N-terminally truncated Aβ peptides starting mainly at position 2, giving this secretase a role in the amyloidogenic pathway (Bien et al., 2012).

Meprins are oligomeric proteases that can be either anchored in the plasma membrane or secreted into the extracellular space. They are composed of one or two evolutionarily related subunits, α and β (Jiang et al., 2000). The genes encoding these subunits are located on separate chromosomes: in humans, the meprin α gene resides on chromosome 6, whereas its murine ortholog is on chromosome 17. In contrast, the meprin β gene is found on chromosome 18 in both humans and mice (Gorbea et al., 1993).

Meprin α occurs in two forms: a membrane-bound heterooligomer containing both α and β subunits, and a secreted homooligomer composed exclusively of α subunits (Bertenshaw, Norcum, & Bond, 2003). Oligomers containing the β subunit are generally membrane-associated but can also be cleaved, producing an active soluble form.

Meprin β is a metalloprotease, but its cleavage specificity differs from that of other matrix metalloproteinases (MMPs): meprin β preferentially targets acidic amino acids, MMPs cleave primarily between neutral and hydrophobic residues (Schönherr et al., 2016; Bickenbach et al., 2025). Their active sites also differ in zinc coordination and overall structure, influencing substrate recognition. Both enzyme families can degrade extracellular matrix proteins such as collagen IV, nidogen-1, and fibronectin; however, unlike MMPs, meprin β does not act on intact collagen I (Kruse et al., 2004, Bien et al., 2012, Jefferson et al., 2012). The distinctive substrate preference for glutamate (E) and aspartate (D) makes meprin β essential in the brain, as no known other protease has this specific motif sequence.

Certain proteases are involved in AD and their flawed control may contribute to the onset and progression. The expression of cerebral proteases, involved in APP processing and extracellular

matrix remodeling, shows that ADAM10, ADAMTS1, Cathepsin D, and meprin β have significantly higher mRNA expression in sporadic AD subjects versus controls, while ADAMTS1, Cathepsin D, and meprin β also show an increase at the protein level. This indicates that transcriptional events affecting brain proteases are activated in AD patients (Medoro et al., 2019).

Additionally, hinting at meprin β as a risk factor for AD, we came across a study checking for polygenic risk scores in AD (Patel et al., 2018). This study used whole-exome sequencing to investigate genetic risk factors for sporadic AD. Specifically, the protein-coding regions of DNA were analyzed, which are most likely to carry disease-causing mutations. The study involved 132 individuals with AD and 53 cognitively normal controls, using postmortem brain samples from the Brains for Dementia Research (BDR) program in the UK. One gene highlighted was meprin β (*MEP1B*). A specific genetic variant in *MEP1B*, known as rs173032, was found to occur significantly more often in individuals with AD than in controls. This gene was found in a nonsingleton variant analysis, meaning that this is a specific trait in a wide part of the population rather than being a specific mutation in an individual. The association of *MEP1B*-rs173032 with AD was identified through a method called 'burden analysis', which tests whether multiple variants of many genes collectively occur more often in cases than controls. It's particularly useful for detecting the cumulative effect of rare or subtle variants that might not show up as significant on their own. Intriguingly, the *MEP1B*-rs173032 variant codes for a synonymous mutation, meaning that both versions translate into the same amino acid at position 537 (S537). However, even though the protein sequence is identical, synonymous mutations can still have functional effects. For example, they can affect how efficiently or accurately the protein is made, alter mRNA stability or folding, or influence splicing. Conclusively, the difference between rs173032 and wt *MEP1B* isn't in the protein's structure, but potentially in how much, how fast, or when the meprin β protein is produced. These subtle regulatory effects can still contribute to disease pathology, especially in a complex disorder like AD.

Meprin β's cellular localization, regulation, and isoforms are well characterized in several tissues, especially the kidney and skin. Meprin β is primarily expressed on the plasma membrane of epithelial cells, especially in the brush border of kidney proximal tubules and intestinal epithelial cells. It is also found in certain leukocytes, cancer cells, and in the stratum

granulosum of the human epidermis, just beneath the stratum corneum (Bond et al., 2005; Becker-Pauly et al., 2007). For the brain, no reliable data about the localization of meprin β has been published yet. The expression of meprin β is tightly controlled at both gene and protein levels and regulatory elements and transcription factor binding sites have been identified in the gene's promoter regions. Additionally, alternative splicing generates different mRNA isoforms, which produce at least two mRNA isoforms: the standard β (2.5 kb) and the β' (2.7 kb) isoform, with β' mostly found in carcinoma cells. These isoforms arise from the alternative use of 5' exons in the *MEP1B* gene (Jiang et al., 2000). Additional protein variants (e.g., G45R, G89R, E110G and R238Q) have been identified in association with cancer, affecting activity, stability, invasion and cellular localization (Gellrich et al., 2021; Bickenbach et al., 2025). Although overexpression is uncommon, it can occur following disease or injury. Expression levels and localization may shift in response to tissue damage, inflammation, or cancer, often correlating with disease severity (Bond et al., 2005; Becker-Pauly et al., 2007), and have also been observed in patients at risk for AD (Patel et al., 2018).

Additionally, it was shown that meprin β is also responsible for TREM2 cleavage, a risk protein in AD patients (Berner et al., 2020). Building on the findings of Marengo et al. (2022) on meprin β knockout models, along with studies such as the one identifying the *MEP1B*-rs173032 variant, the literature provides strong evidence that meprin β has a broader role in the brain.

1.7 The Delicate Balance of Proteolytic Regulation

Proteases in the brain have dual roles because they are involved in both normal physiological processes and pathological conditions. Their activity can support healthy brain function or contribute to disease, depending on context, concentration, and regulation. While proteases are crucial in neuronal development (e.g., Reelin) (Fatemi et al., 2005), synaptic plasticity, memory formation (Yoshida et al., 1999; Almonte et al., 2011) and protein quality control (Türker et al., 2021), their disruption triggers harmful pathological effects such as cell death (apoptosis, necrosis, neurodegeneration) and inflammation (Mathews & Levy, 2016). One illustrative example is thrombin, a protease whose effects are context-dependent. At low concentrations, thrombin may promote cell survival, whereas elevated levels or prolonged exposure can induce cell death or trigger inflammatory responses (Bae et al., 2009). By analogy, this thesis proposes that meprin β may similarly exhibit dual roles.

Moreover, the interconnected roles between proteases can be illustrated through the molecular mechanisms underlying learning. Proteases are critical for learning and memory, as they regulate synaptic plasticity. Through controlling protein synthesis and degradation at synapses, they support long-term potentiation (LTP) and long-term depression (LTD), the fundamental cellular processes underlying cognitive functions. The UPS contributes both to the formation of new memories and to the destabilization of old ones during retrieval, enabling memory updating (Patrick et al., 2023; Hedge et al., 2017). Subsequently, serine proteases and MMPs reshape the extracellular environment, facilitating the structural synaptic changes required for learning (Tsilibary et al., 2014; Salazar et al., 2015). The dual roles of proteases, supporting both neural plasticity and degeneration, highlight their importance as both therapeutic targets and biomarkers in CNS disorders. We think that, based on its established functions in other tissues, there is a promising chance that meprin β contributes to extracellular matrix (ECM) remodeling also in the brain (Kronenberg et al., 2010).

1.8 Perineuronal Nets

As previously noted, numerous proteases have the capacity to remodel the ECM, of which the PNN is a key component. PNNs are specialized, lattice-like structures made of extracellular matrix molecules that wrap around certain neurons in the central nervous system (Sorg et al., 2016). They play a crucial role in regulating brain plasticity, stabilizing neural circuits, and protecting neurons (Steulet et al., 2017). In more detail, PNNs are composed primarily of chondroitin sulfate proteoglycans (CSPGs), hyaluronan, tenascins, and link proteins. These components assemble into a stable, reticular sheath surrounding the soma and proximal dendrites of select neurons, particularly parvalbumin-expressing (PV+) inhibitory interneurons, while leaving openings for synaptic contacts (Figure 3) (Fawcett et al., 2019; Testa et al., 2019). This unique molecular composition enables them to act as both a physical barrier and a signaling interface, influencing memory formation and neuroprotection (Li et al., 2023). The molecular architecture is highly conserved but shows regional and cell-type specificity, with variations in sulfation patterns and protein composition influencing PNN function (Fawcett et al., 2019; Testa et al., 2019).

PNN formation occurs late in postnatal development, coinciding with the closure of critical periods of heightened plasticity, by stabilizing mature neural circuits (Mirzadeh et al., 2018). Experimental removal or enzymatic digestion of PNNs in adults reopens these critical periods,

reinstating juvenile-like plasticity, learning, and memory, but may also increase vulnerability to excitotoxicity and maladaptive plasticity (Testa et al., 2019). Additionally, PNNs are essential for the maintenance of long-term memories and the regulation of synaptic homeostasis. They protect neurons from oxidative stress and neurotoxicity, partly by acting as ion exchangers and scavenging redox-active molecules (Morawski et al., 2015).

Alterations in PNN structure or expression are implicated in a range of neurological and psychiatric disorders, including schizophrenia and bipolar disorder (Steulet et al., 2017). Moreover, PNN loss is an early and progressive event in AD, driven largely by microglial activation and neuroinflammation (Crasper et al., 2020). Consequently, activated microglia in AD brains engulf and degrade PNNs, especially near amyloid plaques. This loss is proportional to plaque burden and precedes the loss of PV+ interneurons, further exacerbating neurodegeneration and inflammation. Also, disrupted PNNs make neurons more susceptible to toxic insults and impair their ability to maintain normal brain rhythms and memory (Reichelt et al., 2020).

Due to the immense influence of PNNs, they are increasingly recognized as promising therapeutic targets. Modifying PNNs to enhance plasticity may help restore memory and learning in AD and age-related cognitive decline (Li et al., 2024). Additionally, disrupting or remodeling PNNs can reactivate plasticity in the adult brain, facilitating recovery after spinal cord injury or stroke (Li et al., 2024).

1.9 Learning and Memory

PNNs are specialized ECM structures that surround certain neurons and play a crucial role in regulating brain plasticity. Their influence on learning and memory is significant, as they help balance the brain's need for both stability and adaptability. PNNs mature during development and are closely linked to the closure of critical periods - windows when the brain is highly plastic and able to form new connections. Once PNNs form, they stabilize existing synapses and restrict further plasticity, which helps consolidate learned information but limits new learning in adulthood (Sanchez et al., 2023). By enwrapping neurons, PNNs promote the stabilization of synaptic contacts, supporting the retention of long-term memories (Carulli et al., 2019). PNNs are essential for the recall of remote (long-lasting) memories. Disrupting PNNs, by enzymatic removal or genetic modifications, can impair the retrieval of established

memories but may enhance relearning or the formation of new memories through PNN receptor PTPσ-signalling (Carulli et al., 2019; Lesnikova et al., 2021; Thompson et al., 2017). For example, the KO of Brevican, a main building block of the PNN, shows a strong impairment in LTP formation, seen in electrophysiological experiments (Brakebusch et al., 2002).

Learning at the molecular level involves activity-dependent changes in synaptic strength, a process called synaptic plasticity. Central to this are NMDA and AMPA receptors, which mediate glutamatergic transmission. During learning, repeated activation of a synapse leads to the removal of the magnesium block in NMDA receptors, allowing calcium influx, which then triggers intracellular signaling cascades that strengthen the synapse - often by inserting more AMPA receptors into the postsynaptic membrane (Brown et al., 2022). PV+ interneurons, a class of fast-spiking inhibitory GABAergic neurons, regulate the timing and synchronization of excitatory neuron firing, shaping the temporal window for NMDA receptor activation (Wingert et al., 2021; Klimczak et al., 2021). By controlling network oscillations and excitatory-inhibitory balance, PV+ interneurons, which are primarily surrounded by the PNN, help gate plasticity, ensuring that only specific patterns of activity result in lasting changes (Sigal et al., 2019). Thus, learning emerges from a finely tuned interplay between excitatory signaling, NMDA/AMPA receptor dynamics, and inhibitory control by PV+ interneurons.

An aspect particularly interesting and relevant to our study is that the brain employs activity-dependent release of proteases to remodel synapses, thereby facilitating learning and memory. Established key proteases like MMPs, tPA, neurotrypsin, neuropsin, calpains, and the UPS are activated by neuronal activity and regulate synaptic plasticity, dendritic spine growth, and synaptogenesis (Meighan et al., 2006; Madani et al., 1999; Nagy et al., Frischknecht et al., 2008; Bingol & Schumann, 2006). These enzymes act on the ECM and synaptic proteins to promote structural and functional changes essential for long-term potentiation (LTP) and new neural connections. Proper regulation is critical: both insufficient and excessive protease activity can impair cognitive function.

1.10 Therapeutic Potential

In AD, changes in PNN composition and dysregulation of protease activity contribute to impaired plasticity, memory loss, and neuronal damage. Targeted therapeutic strategies involving PNNs and proteases have shown promise in restoring cognitive function and reducing

pathology in preclinical models, but the therapeutic window is narrow due to the need to balance enhanced plasticity with preservation of neuroprotection (Reichelt et al., 2019).

With age and in AD, PNNs undergo modifications that increase their inhibitory effect on plasticity. These changes involve altered glycan sulfation patterns - specifically, an increase in chondroitin-4-sulfate (C4S) and a decrease in chondroitin-6-sulfate (C6S) - which are associated with diminished synaptic adaptability and memory impairments. Both human and animal studies demonstrate that disruption or loss of PNNs correlates with cognitive decline and synaptic dysfunction in AD (Yang et al., 2021; Yang et al., 2017).

MMPs, ADAMTS, cathepsins, and components of the UPS are also dysregulated in AD. Some of these enzymes exacerbate disease by promoting amyloid and tau accumulation, whereas others, like protease nexin-1 (PN-1), are neuroprotective and support synaptic health. Reduced activity of these protective proteases is associated with increased neuronal degeneration and hindered neurite outgrowth (Li et al., 2020).

Therapeutically, modulating PNNs through enzymatic digestion, antibody targeting of inhibitory glycan motifs, or restoring permissive sulfation patterns has been shown to recover synaptic plasticity and memory in experimental AD models (Reichelt et al., 2019). Similarly, correcting protease imbalances has reduced amyloid and tau pathology while improving cognitive outcomes. However, such interventions require caution, as excessive degradation of PNNs or uncontrolled protease activity may lead to further neurodegeneration (Chocron et al., 2022; Crasper et al., 2020).

While these findings offer encouraging possibilities for therapy, their translation into clinical practice remains complex. Human applications must account for the regional and cell-type-specific functions of PNNs and proteases, as well as the delicate trade-off between promoting plasticity and maintaining neuronal protection. Ongoing advancements in biomarker development and high-resolution proteomic and glycomic profiling are helping to define patient subgroups and optimal therapeutic windows, bringing these novel strategies closer to clinical relevance.

1.11 Aim of Study

AD is a complex neurodegenerative disorder driven by Aβ accumulation, tau pathology, synaptic dysfunction, and neuroinflammation. Research has historically focused on BACE1 as the primary β-secretase, largely due to the widespread use of APP/swe mouse models, which favor BACE1 cleavage and fail to capture the diversity of N-terminally truncated Aβ species present in human AD brains. Meprin β, an alternative β-secretase, generates these N-terminally truncated peptides and is implicated in ECM remodeling, PNN integrity, and synaptic regulation. Evidence from genetic studies and KO mice indicates that meprin β contributes to AD pathology, but its broader physiological and pathological roles in neurons remain poorly understood.

Proteases in the brain play dual roles, supporting both normal neuronal function and neurodegeneration. Additionally, the BACE1-focused research bias limits our understanding of the full proteolytic network, including the interactions between meprin β and other enzymes that modulate neurodegeneration. Exploring these pathways is crucial for capturing the complexity of AD pathology and for identifying protease-mediated mechanisms that may influence both disease progression and neuronal resilience.

We previously demonstrated that meprin β is able to cleave APP (Schönherr et al., 2016), and subsequent research in APP/Ld x $mep^{Cre;KO/KO}$ animals confirmed that Aβ levels are lower compared to APP/Ld mice (Marengo et al., 2022). Meprin β also performs important functions in other tissues, such as the kidney and intestine, particularly in ECM remodeling. Although the ECM composition in the brain differs from these peripheral tissues, likely, some brain ECM proteins are also substrates for meprin β, given its endogenous expression in the central nervous system.

Keeping this in mind, the aims of this study were:

- To move beyond BACE1-centered mouse models and investigate a model with a more balanced expression of alternative proteases capable of cleaving APP.
- To confirm that meprin β can cleave APP *in vivo*, contributing to increased Aβ levels, building on previous findings from meprin β knockout studies.
- To explore additional potential functions of meprin β in the brain, particularly its role in extracellular matrix remodeling.

2. Materials

2.1 Chemicals

- 4’,6-diamidino-2-phenylindole (DAPI) - Thermo Fisher Scientific
- 40% Acrylamide 19:1 Bis-Acrylamide - BioRad, Munich, Germany
- 40% Acrylamide 29:1 Bis-Acrylamide - BioRad, Munich, Germany
- Acetic acid - Merck, Darmstadt
- Amersham™Protran® Nitrocellulose Blotting Membrane 0.45µm - Roth, Karlsruhe
- Ammoniumpersulfate (APS) - Sigma-Aldrich
- Bicine - Carl Roth
- BioRad Precision Plus Protein™ All Blue Prestained Protein Standards, 10 to 250kDa - BioRad Laboratories
- Biozym Agarose
- Bis-Tris - Carl Roth
- Bovine Serum Albumin (BSA) - Sigma-Aldrich
- Bromphenol blue - Roth, Karlsruhe
- Chondroitinase Buffer (ChABC) - Sigma-Aldrich
- cOmplete™, EDTA-free Protease inhibitor - Roche
- Cryoprotective solution - AG Lutz, Mainz
- CutSmart® Buffer - New England BioLabs
- Deoxycholate - Sigma-Aldrich
- Desoxynucleotide-tri-phosphate (dNTP) - NEB
- Diethanolamine (DEA)
- Dimethyl sulfoxide (DMSO) - Sigma-Aldrich
- Doxycycline hyclate - Sigma-Aldrich
- Dulbecco’s Modified Eagle Medium (DMEM) - Gibco
- Ethanol - Roth
- Ethylenediaminetetraacetic acid (EDTA) - Carl Roth
- EZ link™ sulfo-NHS-LC-LC-Biotin - ThermoFisher
- Fetal Calf Serum (FCS) - Invitrogen
- FluoromountTM Aqueous Mounting Medium - Sigma Aldrich
- Formic acid 98-100% - Merck

- Glutamax (100x) - Gibco
- Glycerol - Carl Roth
- Glycine - Merck
- HEPES - Invitrogen
- Hydrochloric acid (HCl) - Carl Roth
- Iodoacetamid - Sigma-Aldrich
- Isofluran-Piramal - Piramal Critical Care Deutschland GmbH
- Isopropanol - Carl Roth
- Ketamine (HCl)/Xylazin in 0.9% NaCl
- L-Glutamine - Invitrogen
- Lipofectamine®2000 - Invitrogen
- Magnesium chloride (MgCl2) - Carl Roth
- Methanol - Carl Roth
- Midori Green - NIPPON Genetics EUROPE GmbH
- Na-Pyruvate - Sigma-Aldrich
- NaCl - Roth
- NeutrAvidin 29201 - ThermoFisher
- Nonidet-P40 - Roche
- Opti-MEM - Invitrogen
- OrangeG 6x - New England BioLabs
- PageRuler™ prestained Protein Ladder, 10 to 180kDa - ThermoFisher Scientific
- Paraformaldehyde (PFA) - Sigma-Aldrich
- PhosSTOP™ - Roche
- Phosphate buffered saline (PBS) - Life Technologies
- Polyethyleneimine (PEI) MAX - Polysciences, INC
- Ponceau S - Sigma-Aldrich
- Potassium chloride (KCl) - Sigma-Aldrich
- Powdered milk - Roth
- Roti Load® (4x protein loading buffer) - Carl Roth
- Roti® Histofix 4% - Roth
- Skim Milk Powder - Carl Roth

- Sodium azide (NaN_3) - Carl Roth
- Sodium chloride (NaCl) - Carl Roth
- Sodium di-hydrogen phosphate (NaH_2PO_4) - Merck
- Sodium dodecyl sulfate (SDS) - BioRad
- Sodium hydroxide (NaOH) - Merck
- Sodium pyruvate - Invitrogen
- Sucrose - Roth
- Synthetic Aβ peptides - VCPBIO
- TEMED (N,N,N+,N+-Tetramethylendiamine) - BioRad
- Trichloroacetid acid (TCA) - Sigma-Aldrich
- Tris-hydrochloride (Tris-HCl) - Carl Roth
- Tris(hydroxymethyl)aminomethan (TRIS) base - Roth
- Triton-X 100 - Sigma-Aldrich
- TRIS-HCl - Roth
- Trypan blue - Gibco
- Trypsin/EDTA - Invitrogen
- Tween20 in TBS - Roth

2.2 Antibodies (against):

- ABCB1/MDR1 (rabbit, 1:1000 (WB), sc-8313, Santa Cruz)
- ADAM10 (rabbit, 1:1000 (WB), Ab19026, Millipore)
- AKT (rabbit, 1:1000 (WB), 9272, Cell Signaling)
- AMPA (rabbit, 1:500 (WB), 2460, Cell Signalling)
- ApoE (rabbit, 1:500 (WB), Ab83)
- Aβ (mouse, 1:500 (WB) 1:100 (IP), IC16, Jäger et al., 2009)
- Aβ (mouse, 1:100 (WB), mabn639, Millipore)
- Aβ2-x (rabbit, 1:500 (IHC), pAb77, Savastano et al., 2015)
- α-tubulin (mouse, 1:1000 (WB), 62204, Invitrogen)
- β-Actin (rabbit, 1:5000 (WB), A5060, Sigma-Aldrich)
- Dynabeads® M-280 Mouse IgG (sheep, 11202D, Invitrogen)
- FOXO1 (rabbit C29H4, 1:1000 (WB), 2880, Cell Signaling)
- GAPDH (mouse GA1R, 1:1000 (WB), Invitrogen)

- GSK3β (mouse, 1:1000 (WB), 610202, BD Biosciences)
- HA-tag (mouse, 26183, Thermo)
- LDL-R (rabbit, 1:1000 (WB), C500291, LSBio)
- LRP1 (rabbit, 1:1000 (WB), β-chain, Pietrzik et al., 2002)
- meprin β (goat, 1:3000 (WB), AF2895, R&D Systems)
- Neurexin-3 (rabbit, 1:1000 (WB), 48004, Cell Signaling)
- Neurocan (rabbit, 1:500, PA5-79718, Thermo)
- NMDAR1a (mouse, 1:1000 (WB), clone 54.1, 32-0500, Thermo)
- NMDAR2a (mouse, 1:1000 (WB), MA5-27692, Invitrogen)
- NMDAR2b (mouse, 1:1000 (WB), MA1-2014, Invitrogen)
- PCSK9 (rabbit, 1:1000 (WB), 31762, abcam)
- PSD95 (mouse, 1:2000 (WB), 610495, BD)

2.3 Secondary Antibodies (against):

- mouse IgG (goat-AlexaFluor488, 1:1000 (IF), 150077, abcam)
- mouse IgG (donkey-HRP, 1:5000 (WB), Jackson Immunoresearch)
- rabbit IgG (goat-HRP, 1:10000 (WB), Sigma-Aldrich)
- rabbit and mouse IgG (goat-IRDye 680CW, 1:5000 (WB), Licor Biotech LLC)
- rabbit and mouse IgG (goat-IRDye 800CW, 1:5000 (WB), Licor Biotech LLC)
- goat IgG (donkey-IRDye 800CW, 1:5000 (WB), Licor Biotech LLC)
- goat IgG (rabbit-HRP, 1:3000 (WB), Sigma-Aldrich)

2.4 Kits

- ELISA Aβ1-40 - IBL, Hamburg, Germany
- ELISA Aβ1-42 - IBL, Hamburg, Germany
- NucleoBond® Xtra Midi EF - MACHEREY-NAGEL GmbH & co. KG, Düren
- Pierce™BCA Protein Assay Kit - Thermo Scientific, Rockford
- Syn-PER™ Synaptic protein extraction reagent - Thermo Fisher, Darmstadt, Germany

2.5 Antibiotics

- Ampicillin
- Penicillin/Streptomycin (Pen/Strep) - Invitrogen

2.6 Laboratory Equipment

- Agarose gel documentation imager - INTAS, Göttingen, Germany
- Agarose gel electrophoresis chamber - Biometra, Göttingen, Germany
- Amersham™ Nitrocellulose membrane 0.2µm - Sigma-Aldrich, Taufkirchen, Germany
- Anthos microplate reader 2010 - Anthos Labtec, Salzburg, Austria
- Aspirator - StarLab
- BioRad Mini Trans-Blot® Cell - BioRad Laboratories
- BioRad Mini-PROTEAN® Tetra Cell Casting Module - BioRad Laboratories
- BioRad power Pac 300 - BioRad, Munich
- Biometra compact - AnalytikJena
- Blotting paper - A.Hartenstein
- Bunsen burner Campingaz Labogaz 470
- Cell culture dishes (10 cm) - Sarstedt, Nümbrecht
- Centrifuge 54150 - Eppendorf
- Centrifuge Biofuge stratos (rotor #3335 and #8172) - Hereaus, Hanau
- Centrifuge Heraeus Fresco - Kendro, Langenselbold, Germany
- Centrifuge Mikro200R - Hettich
- Centrifuge universal 32 - Hettich, Tuttlingen
- ChemiDoc MP - BioRad Laboratories
- CM2050S Cryostat - Leica
- CO_2 Incubator HERACell 240 - New Brunswick, USA
- Countess 3 FL - Thermo Fisher Scientific
- CryoTube™ Vials - Thermo Scientific
- Dewar vessel - KGW isotherm
- DYNAL magnetic bead seperator - Invitrogen
- Falcons - GreinerBio One GmbH, Frickenhausen
- Freezer -20°C - Liebherr, Germany
- Freezer -80°C - Heraeus, Hanau, Germany
- Fridge +4 °C – Liebherr, Germany
- Fridge +4 °C - Privileg, Germany
- Glass pipettes - Hirschmann®Techcolor, Germany

- Glassware - Schott, Mainz, Germany
- Gloves - StarLab International GmbH
- Heating Block - Grant, Berlin, Germany
- HeraSafe 2030i sterile bench - Thermo Fisher
- Hotplate VMS-A - VWR
- Immobilon-P Membrane, PVDF 0.45µm - Millipore, Schwalbach, Germany
- ImmersolTM 518 F - Zeiss
- Incubator (bacteria) - Binder, Tuttlingen, Germany
- Integra VacuSafe sterile bench - Nunc, Wiesbaden
- KL1500LCD Lichtquelle - Schott
- Leica DM5500B - Leica microsystems, Wetzlar, Germany
- LSM710 Confocal Microscope - (Zeiss, Jena, Germany)
- Magnetic stirrer - Heidolph, Kehlheim, Germany
- Micropipette puller model P-97 - Sutter instruments
- Microscope CKX41 - Olympus
- Microwave - Micromaxx, Real
- Mini Centrifuge - Starlab International GmbH
- Mini Protein III, Western Blotting System - BioRad, Munich, Germany
- Mini-Peristaltic Pump 2 - Harvard Apparatus
- MiniTrans-Blot® Cell - Biorad, Munich, Germany
- Mr. Frosty™ freezing container - Thermo Fisher, Darmstadt, Germany
- NanoDrop™ - Thermo Fisher Scientific
- Olympus BX-51 microscope - Olympus, Hamburg, Germany
- Optima™ MAX-XP Ultracentrifuge - (Beckman Coulter, CA, USA)
- Pasteur pipettes - Roth, Karlsruhe
- pH meter - inoLab, Weilheim
- pH-meter - Mettler Toledo, Gießen, Germany
- Pipette controllers accu jet ® S - VWR
- Pipettes 1 µl-1 ml - Eppendorf, Hamburg
- Plastic pipettes - Sarstedt, Nümbrecht
- Precellys24 - PeqLab

- Reaction tubes - Shaker Infors, Boltmingen Schweiz
- Rocky® 3D - Labortechnik Frödel
- Scale - Sartorius Kissling
- Scale PCB - Kern
- T3 Thermocycler - Biometra, Göttingen, Germany
- Table Centrifuge Minifuge plus - StarLab
- Test-tube rotator 34528 - Snijders
- Thermomixer 5436 - Eppendorf
- Timer TR118 - Roth
- TipOne - Starlab International GmbH
- TLA120.2 rotor - Beckman Coulter, CA, USA
- Trans-Blot® SD Semi-dry transfer - Biorad, Munich, Germany
- Ultrasonic Cleaner - VWR
- Vacusafe - Integra Biosciences
- Ventana Benchmark XT - Roche, Basel, Switzerland
- Vortex - StarLab International GmbH
- Vortex-Genie 2TM - Bender & Hobein AG
- Vortexer IKA Labortechnik VF2 - Janke & Kunkel
- Water Bath - Grant Instruments
- Water Bath GFL1086 - GFL, Burgwedel, Germany
- WIS shaking incubator - Witeg, Germany

2.7 Programs (Software)

- ADAP software - Anthos
- GraphPad Prism 8.0.2 - GraphPad Software, La Jolla
- ImageJ 1.54g
- Leica LAS X
- MEROPS peptidase database 12.5 - Rawlings et al., 2018
- Microsoft Office 2016
- SnapGene V5
- SnapGeneViewer 5.0.5 - GSL Biotech LLC
- Zeiss ZEN microscopy software 14.0.24.201 – Zeiss

3. Methods

3.1 Molecular Methods

3.1.1 Genomic DNA Preparation for Genotyping

To prepare genomic DNA for genotyping, we began by collecting a small piece of tissue (e.g., ear punches) and placing it into an Eppendorf tube. We added 0.5 ml of Tail Lysis Buffer (100 mM Tris-HCl, 5 mM EDTA, 0.2% SDS, 200 mM NaCl, pH 8) to the tube containing the tissue piece. Next, we added 5 µL of a 20 mg/ml Proteinase K solution to each sample, mixed thoroughly and incubated the samples overnight at 50–55°C with shaking. Efficient digestion is essential for successful DNA extraction; incomplete digestion can result in poor DNA yield. To enhance digestion, we ensured vigorous shaking throughout the incubation. After digestion, we centrifuged the tubes at maximum speed for 10 minutes to pellet undigested material such as hair. Lastly, we transferred the supernatant to a new Eppendorf tube.

To precipitate the DNA, we added 0.5 ml of isopropanol to each tube. The tubes were gently reversed a few times to mix. Next, the samples were centrifuged at top speed for 10 minutes at 4°C to pellet the DNA. The supernatant was discarded and the DNA pellet was washed by adding 70% ethanol. Subsequently, the samples were centrifuged again at top speed for 10 minutes. After centrifugation, we carefully removed the ethanol (by decantation). The DNA pellet was dried at room temperature for 1 h. Once dry, the DNA was resuspended in 50 µL of nuclease-free water (dH_2O) by pipetting up and down with a P200 pipette. For genotyping by PCR, we used 2 µL of the resuspended DNA as the template in a 20 µL PCR reaction.

3.1.2 PCR/Genotyping

To accurately determine the genotype of each mouse and to support the establishment of new strains or the maintenance of existing colonies, we used a polymerase chain reaction (PCR) assay to amplify specific regions of the extracted genomic DNA. PCR is a widely adopted molecular biology technique that enables the selective amplification of DNA sequences through the enzymatic action of DNA polymerase.

Each PCR reaction contained a pair of sequence-specific single-stranded primers, deoxynucleoside triphosphates (dNTPs) as the building blocks for DNA synthesis, a reaction

buffer to maintain optimal conditions and the DNA template extracted from mouse tissue. Typically, a 2 µL aliquot of the DNA extract was used for each reaction.

PCR amplification generally involves 30 to 40 thermal cycles, each comprising specific temperature steps that allow for DNA denaturation, primer annealing, and strand elongation. The reaction is initialized by heating the double-stranded DNA to 95 degrees Celsius for approximately 40 seconds to separate the strands into single-stranded templates.

Next, the annealing step is carried out by lowering the temperature to between 55 and 65 degrees Celsius for about 30 seconds, allowing primers to hybridize to their complementary sequences on the single-stranded DNA. The precise annealing temperature and duration depend on the specific sequence and base composition of the primers used.

The elongation step follows, during which DNA polymerase extends the primers by incorporating dNTPs, synthesizing a new DNA strand complementary to the template. The temperature for this step varies depending on the enzyme used, but typically falls between 72 and 80 degrees Celsius. A final elongation step is sometimes included to ensure that any remaining single-stranded DNA is fully extended. This step is usually conducted at a temperature of 70 to 75 degrees Celsius for 5 to 15 minutes.

For each genotyping assay, primers were designed using SnapGene software. The corresponding sequences and PCR reaction schemes are described in detail below.

To detect transgenic animals harboring a heterozygous NEX-Cre mutation, we used the following primers:

Primers	**Sequence**	**Gene**
Forward (fwd) transgenic (TG)	5’ TCTTTTTCATGTGCTCTTGG 3’	NEX
Reverse (rev) TG	5’ CGCGCCTGAAGATATAGAAGA 3’	NEX
Fwd CB1 (wt)	5’ CAAGAAATGAGAACCGTGTC 3’	CB1
Rev CB1 (wt)	5’ GTTCTCCTTGAACGATGAGA 3’	CB1

Table 1 – Sequence of primers used to detect the NEX-Cre mutation in mice. CB1 primers were used to detect the wild-type sequence of the gene, while the NEX Primers hybridized to the mutation.

Primers for CB1 were used as an internal PCR control (IPC). Bands for IPC were at the height of 543bp. Detected bands at the height of 390 bp indicated the presence of the transgene for NEX. The reaction scheme was as follows:

Component	**µl per reaction**
Nuclease-free water	10.25
10x VWR key buffer (with 15 mM $MgCl_2$)	2.5
$MgCl_2$ (25 mM)	3.5
dNTPs (10 mM)	0.5
Primer NEX fwd	1
Primer Nex rev	1
Primer CB1 fwd	1.25
Primer CB1 rev	1.5
Taq DNA Polymerase (5 U/µL)	0.5
DNA template	2
Total amount per reaction	24

Table 2 – Ingredients needed for PCR reaction. A master mix containing all components except the DNA was prepared first and distributed into all tubes. The DNA of each sample was then added to each tube and mixed thoroughly.

PCR-cycler program for DNA synthesis:

Cycles	**Time**	**Temperature**
1x	3 min	95°C
27x	45 s	95°C
27x	45 s	55°C
27x	45 s	72°C
1x	3 min	72°C

Table 3 – To compare wild-type and transgenic animals, the samples were incubated according to the protocol outlined in this table. The steps highlighted in gray were repeated 27 times, followed by a final elongation step. Subsequently, the samples were either stored at 4 °C or immediately loaded onto an agarose gel.

To detect animals harboring a *Mep1b*-KI Rosa26 knock-in, we used the following primers:

Primers	**Sequence**	**Gene**
Fwd TG and wt	5' AAAGTCGCTCTGAGTTGTTATC 3'	Rosa26
Rev TG	5' TGTCGCAAATTAACTGTGAATC 3'	Rosa26
Rev wt	5' GATATGAAGTACTGGGCTCTT 3'	Rosa26

Table 4 - Sequence of primers used to detect the ROSA26 mutation in mice, which was the promoter for the knock-in of the meprin β gene. The first reverse primer was hybridizing to the wt sequence, while one hybridized to the transgenic region. Genotyping of heterozygous animals therefore resulted in two bands (fwd TG/wt + rev TG and fwd TG/wt + rev wt) and one band for wt animals (fwd TG/wt + rev wt).

The forward primer was used as an initiation point of synthesis, both for the resulting TG and wt band. Detected bands at the height of 380 bp indicated the presence of the Rosa26 transgene, while bands at the height of 570 bp originated from wt DNA. The reaction scheme was as follows:

Component	**µl per reaction**
Nuclease-free water	16.6
10x VWR extra buffer	2.5
dNTPs (10 mM)	0.4
Primer Rosa26 fwd (TG and wt)	1
Primer Rosa26 rev (TG)	1
Primer Rosa26 (wt)	1
Taq DNA Polymerase (5 U/µL)	0.5
DNA template	2
Total amount per reaction	25

Table 5 - Ingredients needed for PCR reaction. A master mix containing all components except the DNA was prepared first and distributed into all tubes. The DNA of each sample was then added to each tube and mixed thoroughly.

PCR-cycler program for DNA synthesis:

Cycles	Time	Temperature
1x	3 min	95°C
35x	30 s	95°C
35x	30 s	56°C
35x	50 s	72°C
1x	3 min	72°C

Table 6 - To compare wild-type and transgenic animals, the samples were incubated according to the protocol outlined in this table. The steps highlighted in gray were repeated 35 times, followed by a final elongation step. Subsequently, the samples were either stored at 4 °C or immediately loaded onto an agarose gel.

To detect transgenic animals heterozygously expressing human APP/Ld, we used the following primers:

Primers	Sequence	Gene
Fwd TG	5’ CCGATGGGTAGTGAAGCAATGGTT 3’	APP/Ld
Rev TG	5’ TGTGCCAGCCAACAGAGAAAA 3’	APP/Ld

Table 7 - Sequence of primers used to detect the London mutation for APP in mice.

The reaction scheme was as follows:

Component	µl per reaction
Nuclease-free water	13.3
10x VWR extra buffer	2
dNTPs (10 mM)	0.4
PrimerAPP/Ld rev	0.8
Primer APP/Ld fwd	0.8
Taq DNA Polymerase (5 U/µL)	0.2
DNA template	2
Total amount per reaction	19.5

Table 8 - Ingredients needed for PCR reaction. A master mix containing all components except the DNA was prepared first and distributed into all tubes. The DNA of each sample was then added to each tube and mixed thoroughly.

PCR-cycler program for DNA synthesis:

Cycles	Time	Temperature
1x	10 min	95°C
35x	20 s	95°C
35x	30 s	64°C
35x	30 s	72°C
1x	7 min	72°C

Table 9 - To compare wild-type and transgenic animals, the samples were incubated according to the protocol outlined in this table. The steps highlighted in gray were repeated 30 times, followed by a final elongation step. Subsequently, the samples were either stored at 4 °C or immediately loaded onto an agarose gel.

3.1.3 Gel Electrophoresis

Separation of DNA fragments for genotyping was performed by agarose gel electrophoresis. Depending on the size of the DNA fragments, different percentages of agarose were used in the gel. Appropriate amounts of agarose powder were dissolved in TAE (40 mM Tris-acetate, 1 mM EDTA, pH 8.0) by boiling. For the visualization of the DNA, the intercalating agent Midori Green Advance (Nippon Genetics, MG04) was added to a final concentration of 0.5 µl/100 ml and the agarose solution was cast into a cast frame. The DNA samples were supplemented with a loading dye solution (5x Orange G) and separated at 80 V for an appropriate amount of time.

3.1.4 Transformation of Competent Bacteria

For co-transfection experiments with meprin β and NDMA1a receptor, we needed to amplify the *Mep1b* plasmid. For this, we utilized competent E. coli DH5α bacteria that were transformed with a vector (pLBCX-Meprin-β-HA) containing the *Mep1b* gene. Transformation refers to the introduction of exogenous DNA into competent bacterial cells, a naturally occurring process that can be exploited for plasmid amplification. In this experiment, 5 µL of KLD reaction mix containing the purified DNA product was added to 50 µL of chemically competent DH5α cells. The mixture was incubated on ice for 20 minutes, followed by a heat shock at 42°C for 45 seconds to facilitate DNA uptake. Subsequently, 500 µL of LB medium was added to the cells, and the suspension was incubated at 37°C for 1 hour in a thermocycler (Biometra, Göttingen, Germany) to allow recovery and expression of antibiotic resistance.

Finally, 100 µL of the transformed cell suspension was plated onto LB agar plates and incubated overnight at 37°C to enable colony formation.

3.1.5 Midi Prep

Following transformation, single colonies were selected from LB agar plates and inoculated into 5 ml of LB medium supplemented with 100 µg/ml ampicillin. The cultures were incubated at 37°C for 6 hours with vigorous shaking. For large-scale plasmid preparation, the starter cultures were diluted 1:1000 into 300 ml of fresh LB medium containing 100 µg/ml ampicillin and incubated overnight at 37°C under constant agitation. The following day, plasmid DNA was purified using the NucleoBond Xtra® Plasmid DNA Purification Kit (Macherey-Nagel), following the manufacturer's instructions for the endotoxin-free Midi Plus protocol.

3.1.6 Determination of DNA Concentration

DNA concentration was measured using the NanoDropOne™ spectrophotometer (ThermoFisher Scientific) by applying 1 µL of purified DNA directly onto the measurement pedestal. Absorbance was recorded at 260 nm to determine nucleic acid concentration, while sample purity was assessed using the A260/A280 ratio.

3.1.7 Proteomics

Samples (n = 3 per genotype) were processed according to TMT HUNTER workflow (Weng et al., 2019). Precipitated proteins were re-constituted in 1 ml (1% SDS, 1× complete EDTA-free Protease Inhibitor Cocktail (Roche), 50 mM HEPES pH 8). Protein concentration was determined using Pierce BCA Protein Assay Kit (Thermo). One hundred micrograms of proteins of each sample were reduced and alkylated by mixing with 24 mM TCEP, 80 mM Chloroacetamide for 1 h at 25°C in the dark. First clean-up was performed with SP3 beads (1:20 w/w protein to beads ratio) and ethanol (EtOH) added to 50% (v/v) with mixing for 15 min at 25°C to induce protein binding. Then, the supernatant was removed and the beads were washed three times with 80% EtOH. To commence with TMT labeling, beads were resuspended in 22.5 µL6 M Guanidine hydrochloride, 30 µL 0.5 M HEPES (pH 8), and 4.5 µL 125 mM TCEP at 25°C for 30 min. Isobaric tandem mass tags (0.8 mg TMT6plex reagents (Thermo)) were dissolved in 57µL EtOH by occasional vortexing for 5 min. Samples were separated with TMT6plex reagents and labeling was performed by adding a label to each bead-bound protein sample (one tag per sample) and mixing for 1.5 h at 25°C in the dark. Labeling

was stopped by adding 8 µL 8% hydroxylamine for 30 min at 25°C. A second clean-up was done by combining each group of samples and adding EtOH to 80% for 15 min at 25°C. Then, the supernatant was removed, and the beads were washed three times with 80%EtOH. Beads were spun down to remove any remaining liquid, then reconstituted in 200 mM HEPES (pH 8). Digestion was performed with trypsin (1:50 enzyme to protein ratio) overnight at37°. Ten microliters of the supernatant (corresponding to 15 µg of protein) was taken as a pre-HUNTER and the rest (HUNTER) was labeled with undecanal by adding EtOH to 40%, 12 µL undecanal 97% and sodium cyanoborohydride to 30 mM final concentration for 1 h at 37°C. Labeled peptide solution was then acidified with Trifluoroacetic acid (TFA) to pH 3 and undecanal clean-up was performed using Sep-Pak tC18 Cartridges 1 cc(Waters). Conditioning and equilibration were performed with methanol and 40% EtOH, 0.1% TFA, respectively. Samples were added and 0.1% TFA and the flow-through was collected. Collected fractions were dried in a Speedvac for 3h, then freeze-dried overnight. Desalting of the Pre-HUNTER and HUNTER samples was done with 10 µL Pierce C18 Spin Tips (Thermo) and Sep-Pak C18 Cartridges 1 cc (Waters), respectively. Eluted peptides were vacuum dried and stored at −20°C until analysis. Samples were resuspended in 3% ACN with 0.1% TFA and injected for LC–MS analysis. Chromatographic separation was performed on a Dionex U3000 nano HPLC system equipped with an Acclaim PepMap100 C18 column (2 µm particle size,75 µm × 500 mm) coupled online to a mass spectrometer. The eluents used were eluent A: 0.05% FA, eluent B: 80% ACN + 0.04%FA. For pre-HUNTER samples, the separation was performed over a programmed 90-minute run. Initial chromatographic conditions were 4% B for 2 min followed by linear gradients from 4%to 50% B over 60 min, then 50%–90% B over 5 min, and 10 min at90% B. Following this, an inter-run equilibration of the column was achieved by 13 min at 4% B. For HUNTER samples, the separation was performed over a programmed 220-minute run. Initial chromatographic conditions were 4% B for 2 min followed by linear gradients from 4% to 50% B over 180 min, then 50%–90%B over 10 min, and 13 min at 90% B. Following this, an inter-run equilibration of the column was achieved by 15 min at 4%B. A constant flow rate of 300 nL/min was employed. Wash runs were performed between each sample injection. Data acquisition following separation was performed on a QExactive Plus (Thermo). Full scan MS spectra were acquired (350–1400 m/z, resolution 70 000) and subsequent data-dependent MS/MS scans were collected for the 10 or 15 most intense ions (Top10 or Top15) for pre-HUNTER and HUNTER, respectively, via HCD activation at NCE 33 (resolution 17 500). Dynamic

exclusion (40s duration) and a lock mass (445.120025) were enabled. Raw data were analyzed against a database containing a re-viewed Uniprot mouse proteome (Mus musculus) (17530 sequences) and common contaminants (cRAP). The search was performed on Proteome Discoverer 2.2 using a SequestHT search engine with 10 ppm and 0.02 Da precursor and fragment ion tolerances, respectively. Digestion with Trypsin_R (semi)with a max of two missed cleavages was applied. Oxidation of methionine (15.995 Da), acetyl (42.011 Da), and TMT6plex(229.163 Da) at the peptide N-terminus was set as a dynamic modification. Carbamidomethylation (57.02146 Da) on cysteine and TMT6plex on lysine was set as a static modification. For labeling efficiency calculations, TMT6plex on lysine was set as a dynamic modification. Strict parsimony criteria have been applied, filtering peptides and proteins at 1% FDR

3.2 Cell Biological Methods

3.2.1 Primary Hippocampal Neuronal Culture

Six-well plates were prepared by coating with polyornithine (Sigma, P4538) 1:100 in Hank's balanced salt solution (HBSS) (Gibco HBSS without calcium, without magnesium, without phenol red, 14175129) and placed in an incubator for at least 1 hour at 37°C. Each well was then washed 3 times with Millipore water and aspirated, before 1ml of plating medium which consists of MEM (Gibco, 31095-031), 10% horse serum (Gibco, 26050070), 0.6% glucose (Fluka, 16646153) and 500µL glutamine (Gibco, 11539876) was added to each well and the plate placed back in the incubator. All preparation instruments were autoclaved before use. Mice were decapitated at P0 and the brain was removed using curved forceps and eye scissors via the foramen magnum and along the sagittal suture. The parietal bones were folded back using forceps and the brain was transferred into a 3.5cm petri dish, which was filled with HBSS for neurons and placed on ice. Under the dissection microscope, the cerebellum and brain stem were removed and the hemispheres were separated. The hippocampi were isolated and transferred to tubes with 5ml HBSS on ice. The tissue was washed 3 times with ice-cold HBSS under sterile conditions. Activated trypsin (Gibco, Trypsin-EDTA (0,5 %), without phenol red, 15400-054) was added and the sample was incubated for 20 minutes in a water bath at 37°C. DNase (Sigma, DN25100MG) was then added and incubation continued for an additional 5 minutes. After the tube was removed and the trypsin was aspirated away. The tissue was then

washed twice with HBSS and once more with plating medium. The tissue was then homogenized with 2ml of plating medium using flamed glass pipettes (Marienfeld) with increasingly narrow tips. The cell suspension was added to a 50ml Falcon tube through a cell sieve (Greiner, EASYstrainer 40µM, 542040). Live cells were quantified using Trypan blue (Sigma-Aldrich, T8154) in the Neubauer chamber. 1 million cells per well of the 6-well plate were seeded in plating medium. After 30 minutes, the plating medium was aspirated and neuron medium, which consisted of Neurobasal Medium A (Gibco, 10888-022), glutamine (Gibco, 11539876) and B27 supplement (Gibco, 17504044), was pipetted in from the edge of the well. At approximately 2 days *in vitro* (DIV), 2.5µL cytosine arabinoside (AraC) per 500µL of medium is added to each well. At 7 DIV, a medium change with maturation medium consisting of neuronal medium (BrainPhys, 05790) and SM1 Neuronal Supplement (NeuroCult, 05711) took place. This medium change occurred weekly. At ~21 DIV, the culture was ready for the biotinylation assay.

3.2.2 Standard Cell Culture

Cells were maintained at 37 °C in a humidified incubator with 5% CO_2 in 10 cm culture dishes. Subculturing was performed under sterile conditions using the manufacturer-recommended medium for each specific cell line. Adherent cells were detached by trypsinization, resuspended in fresh culture medium, and seeded at appropriate dilutions depending on the growth characteristics of the respective cell line.

3.2.3 Cryopreservation and Thawing of Cells

To minimize morphological and genetic alterations, cells were cryopreserved following standard protocols. Adherent cells were washed with phosphate-buffered saline (PBS) after removal of the culture medium. Subsequently, cells were incubated with sufficient trypsin solution at 37 °C for approximately 2-5 minutes to achieve detachment. Cells were then resuspended in culture medium and centrifuged at 1200 rpm for 4 minutes. The resulting cell pellet was resuspended in fresh culture medium supplemented with 10% dimethyl sulfoxide (DMSO) and transferred to cryovials.

Cryovials were placed in a Mr. Frosty™ freezing container to ensure a controlled cooling rate of approximately 1 °C per minute, which is optimal for preserving cell viability during freezing. For thawing, cryopreserved cells were rapidly warmed in 37 °C culture medium, followed by centrifugation at 160g for 4 minutes to remove residual DMSO and minimize cytotoxic effects.

The pelleted cells were then resuspended in fresh culture medium and seeded onto 6 cm^2 culture plates for continued growth.

3.2.4 Transient Transfection with PEI

HEK293T cells were seeded into 6-well plates at a density of 0.3×10^6 cells per well. After 24 hours of incubation under standard culture conditions, cells were transiently transfected with plasmid DNA encoding *Mep1b.*

To optimize transfection efficiency, the culture medium was first replaced with serum-free Opti-MEM™ 30 minutes before transfection, allowing cells to adapt to serum-free conditions. Plasmid DNA and polyethylenimine (PEI) were prepared in a 1:4 ratio (w/w) and diluted in 60 µL of serum-free medium per well. The DNA-PEI complexes were then added to the cells and incubated for 4 hours. Following this incubation period, the transfection medium was replaced with standard growth medium consisting of DMEM supplemented with 10% fetal calf serum (FCS) and 1% penicillin/streptomycin.

3.2.5 Cell Lysis and Protein Extraction

Twenty-four hours after transfection or compound treatment, cells were harvested for protein extraction. Lysis was performed using NP-40 lysis buffer composed of 50 mM Tris-HCl (pH 7.4), 150 mM NaCl, 5 mM EDTA, 1% Nonidet P-40 (v/v), and 0.02% sodium azide (v/v). The buffer was freshly supplemented with a protease inhibitor cocktail (Complete, Roche) to prevent protein degradation during the extraction process.

1 ml of ice-cold PBS was added to the wells of the 6-well plate. Cells were scraped and collected in an Eppendorf tube, kept on ice. Cell suspension was washed and resuspended in 40 µl lysis buffer. The lysate was left on ice for 20 min. Following lysis, cell debris and insoluble material were removed by centrifugation at 20,000g for 20 minutes at 4 °C using a refrigerated microcentrifuge. The resulting clear supernatants, containing the soluble protein fraction, were carefully transferred to fresh microcentrifuge tubes and stored on ice or at −80 °C until further analysis.

3.2.6 TCA Precipitation of Secreted Proteins

Cell culture supernatants were collected at 24 or 48 h post-transfection, before the addition of protease inhibitors. To remove cellular debris and larger particles, supernatants were first

centrifuged at 500g for 5 minutes at 4 °C, followed by a second centrifugation step at 5,000g for 5 minutes at 4 °C.

To facilitate protein aggregation, 2% (v/v) sodium deoxycholate (DOC) was added to each sample, followed by brief vortexing. Samples were then incubated on ice for 30 minutes. Subsequently, 200 µL of 100% trichloroacetic acid (TCA) was added to 1 ml of the sample, vortexed thoroughly, and incubated on ice for an additional 30 minutes to allow protein precipitation. After incubation, samples were centrifuged at 15,000g for 15 minutes at 4 °C. The supernatants were carefully aspirated and discarded. The resulting protein pellets were washed three times with 500 µl of ice-cold acetone to remove residual TCA. Each wash was followed by centrifugation at 15,000g for 5 minutes at 4 °C, and the supernatants were discarded after each step. The final pellet was air-dried at room temperature. For SDS-PAGE analysis, pellets were resuspended in 95 µL of 1x PAP buffer. To improve solubilization, 2 µL of 2 N NaOH was added, followed by vortexing and incubation at room temperature for 15 minutes. Proteins were then denatured by heating at 95 °C for 5 minutes and subsequently loaded onto an SDS-PAGE gel for analysis.

3.2.7 Uptake Experiments (Huntingtin)

On Day 1, 7.5×10^5 cells were seeded per well in a 12-well plate and incubated overnight under standard culture conditions. On Day 2, a 0.1 nM solution of ^{125}I-labeled Aβ (^{125}I-Aβ) was prepared in OptiMEM by adding 156 µl of the radioactive stock to 4 ml of OptiMEM medium.

To initiate the experiment, the cells were starved by replacing their growth medium with OptiMEM and incubating for 1 hour at 37 °C. If possible, the growth medium was replaced with OptiMEM the evening before to enhance starvation. After the starvation period, the medium was carefully removed from each well, and 1 ml of the 0.1 nM ^{125}I-Aβ solution was added to each well. The cells were then incubated for 1 hour at 37 °C to allow ligand binding and internalization.

During the incubation, two aliquots of the radioactive medium were collected to serve as input samples by transferring 1 ml of medium into labeled tubes and keeping them on ice. Meanwhile, 2 ml Eppendorf tubes for precipitation were prepared by adding 1 µl of trichloroacetic acid (TCA) and 50 µl of bovine serum albumin (BSA, 2 mg/ml) to each tube, and the tubes were labeled according to the corresponding samples.

After the 1-hour incubation, the culture plate was placed on ice to halt further internalization. The cells were washed five times with 1 ml of ice-cold phosphate-buffered saline (PBS), carefully aspirating the wash solution each time to remove unbound ligand. Following the washes, 0.8 ml of PBS adjusted to pH 2.0 was added to each well and incubated for 5 minutes at 4 °C to elute surface-bound but non-internalized ligand. The supernatant was collected into the corresponding pre-labeled tubes and kept on ice. The PBS pH 2.0 wash was repeated by adding another 0.8 ml to each well, incubating for an additional 5 minutes at 4 °C, then collecting the supernatant and pooling it with the first wash. This pooled fraction represented ligand bound to the cell surface but not internalized.

To collect internalized ligand, 1 mL of 0.2 N sodium hydroxide (NaOH) was added to each well to lyse the cells. The lysate from each well was transferred into the corresponding labeled 2 ml Eppendorf tube. Then, 0.8 ml of PBS was added to each lysate and mixed thoroughly by pipetting. This combined lysate represented the internalized fraction.

To separate free iodine from protein-bound ^{125}I-Aβ, proteins were precipitated by adding TCA. For the PBS fractions (surface-bound ligand), 900 µl of 15% TCA was added to each tube containing the pooled PBS pH 2.0 washes. For the lysate samples, 80 µl of 100% TCA was added to each tube. All samples were incubated at 4 °C for 30 minutes to allow complete protein precipitation. Following incubation, the samples were centrifuged at 10,000g for 20 minutes at 4 °C. The supernatants, which contained free radioactive iodine, were carefully transferred into fresh pre-labeled Eppendorf tubes, leaving behind the pellets containing protein-bound ^{125}I-Aβ.

All fractions were retained in their respective tubes for subsequent analysis. The second measurement consisted of the combined supernatants from the PBS pH 2.0 washes and corresponded to ^{125}I-Aβ bound to the cell surface but not internalized. The third measurement involved the lysate samples and reflected internalized ^{125}I-Aβ. The fourth measurement corresponded to the input medium containing the original 0.1 nM ^{125}I-Aβ used for incubation. All samples were quantified using γ-counter protocol #6, with each sample measured three times for 180 seconds to ensure accuracy and reproducibility.

3.3 Biochemical Methods

3.3.1 BCA Assay

To quantify the total protein concentration in cell or tissue lysates, we performed a bicinchoninic acid assay (BCA) using the Pierce™ BCA Protein Assay Kit (Thermo Fisher). Briefly, peptide bonds in the proteins reduce Cu^{2+} ions from copper (II) sulfate to Cu^{+} ions. Subsequently, two molecules of bicinchoninic acid chelate each Cu^{+} ion, resulting in the formation of a purple-colored complex. The intensity of this color change correlates directly with the protein concentration and can be quantified by measuring the absorbance of the purple complex at 562 nm using a plate reader. For the assay, 1 ml of a 50:1 mixture of solutions A and B was added to 50 µL of a 1:10 dilution of each sample, as well as to a standard curve prepared with known concentrations of bovine serum albumin (BSA). The reaction mixtures were incubated for 30 minutes at 60°C. Absorbance values of samples and standards were recorded at 562 nm using a plate reader and analyzed using ADAP version 1.6 software (Anthos Labtec Instruments).

3.3.2 Synthetic Aβ Solubilization

Synthetic Aβ1-40 and Aβ1-42 peptides (PSL, Heidelberg) were used as controls for Aβ quantification. Peptides were solubilized using the 1,1,1,3,3,3-hexafluoroisopropanol (HFIP) method. Briefly, lyophilized peptide vials were equilibrated to room temperature prior to solubilization. HFIP (100%, Sigma-Aldrich) was added at a ratio of 1 ml per 1 mg of peptide to achieve a final concentration of 1 mg/ml. The suspension was incubated at room temperature for 1 hour with intermittent vortexing to ensure complete dissolution. Samples were subsequently sonicated in a water bath sonicator for 10 minutes, with tubes maintained in an upright position throughout the process.

Following solubilization, the peptide solution was aliquoted into 10 µL portions and dried using a SpeedVac concentrator at room temperature for approximately 6 hours. The aliquots were again reconstituted in 1x PAP buffer (0.36M Bis-Tris, 0.16M Bicine, 15% w/v Sucrose, 1% SDS, 0.0075% Bromphenolblue), resulting in a concentration of 1 µg/µL, and stored at −80 °C until further use.

For immunoblot analysis, individual 10 µL peptide aliquots in 1xPAP buffer were loaded onto an 8M urea SDS-PAGE gel without prior heating. Proteins were separated electrophoretically

and transferred onto a PVDF membrane. The membrane was then immersed in MilliQ water and boiled for 3 minutes to enhance epitope exposure. Subsequent immunodetection was carried out according to the standard protocol described under “Urea SDS-PAGE and Western Blotting”.

3.3.3 Immunoprecipitation of Aβ

Soluble fractions from mouse protein extracts were used for immunoprecipitation (IP). Magnetic Dynabeads (M-280 Sheep Anti-Mouse IgG, 11201D, Invitrogen), coated with sheep anti-mouse IgG, were activated with the monoclonal antibody (mAb) IC16 following the manufacturer’s protocol (direct IP method) and subsequently added to the lysates. IC16, which recognizes residues 1–16 of the human Aβ sequence, was used at a final concentration of 1:100[28].

For immunoprecipitation, total Aβ was extracted from soluble brain lysates by mixing each sample with concentrated detergent buffer containing 50 mM HEPES (pH 7.4), 150 mM NaCl, 0.5% (v/v) Nonidet P-40, 0.05% (w/v) SDS, and a protease inhibitor cocktail (Roche Applied Science), resulting in a 1X dilution. After overnight incubation at 4 °C, the samples were washed three times with 1× PBS containing 0.1% (w/v) BSA, followed by a final wash in 10 mM Tris–HCl (pH 7.5).

The samples were then heated to 95 °C in 25 µL of sample 1x PAP buffer (0.36 M Bis–Tris, 0.16 M bicine, 1% [w/v] SDS, 15% [w/v] sucrose, and 0.0075% [w/v] bromophenol blue), and the resulting supernatants were loaded for analysis which is further described in the "Urea SDS PAGE" section.

3.3.4 Urea Sodium Dodecyl Sulfate (SDS) Polyacrylamide Gel Electrophoresis (PAGE) and Western Blotting

Immunoprecipitated Aβ peptides from soluble fractions were separated using 1 mM 10% polyacrylamide 8 M urea SDS gels, as previously described in Marengo et al. (2022). To distinguish Aβ40 from Aβ42, resolving gels were prepared with a final concentration of 0.3 M H_2SO_4. Peptides were then transferred onto an Immobilon-P PVDF membrane via semi-dry western blotting (Bio-Rad) at 47 mA per membrane for 30 minutes.

Membranes were boiled in MilliQ water for 3 minutes, then blocked in 5% powdered milk in TBST (20 mM Tris, 137 mM NaCl, 0.1% [v/v] Tween-20) for at least 30 minutes. Immunostaining was performed overnight using the IC16 antibody (1:1000). Following washes in TBS-T, membranes were incubated with a fluorescent secondary goat anti-mouse antibody (1:5000, IRDye680, Li-COR). Immunoreactive bands were detected using a fluorescence imager (BioRad, ChemiDoc™, Imaging System, USA).

3.3.5 Standard SDS PAGE and Western Blotting

Samples for analysis were prepared in SDS loading buffer (4X Roti-Load, Carl Roth, Germany) and boiled at 95 °C. Protein extracts were separated by standard SDS PAGE, transferred onto nitrocellulose membranes (Amersham Hybond ECL), and then blocked in 5% (*w*/*v*) milk powder in TBS-T. The percentage of the gel was determined based on the size of the protein of interest. Soluble fractions were used to detect total soluble N-APP (sAPP), using an anti-N-terminal APP antibody (22C11, MAB348, Millipore). Moreover, the following antibodies were used for detection: HA-tag for meprin β (Sigma-Aldrich, H6908), sAPPβ (gift from Becker-Pauly lab), sAPPα (Biolegend, 805701), IC16 (own production), GAPDH (Invitrogen, PA1-987), α-tubulin (Invitrogen, 62204), and meprin β antibody (R&D, AF2895).

For Western blotting of synaptosome proteins, 20-30 µg of lysate was loaded. Soluble (S2) fraction samples were incubated in Chondroitinase ABC buffer (50 mM Tris-HCl, 50 mM Sodium Acetate, 50 mM NaCl, 2 mM $MgCl_2$, 0.1% BSA, pH 8) from *Proteus vulgaris* (Sigma Aldrich, C3667) for 30 min at 37°C. Chondroitinase ABC digests the perineural nets and aids the visualization of the protein bands in Western blotting experiments. Then, synaptosome or S2 fraction samples (pooled Hippocampi and single Cortices) were prepared in 1x SDS loading buffer (4X Roti-Load, Carl Roth, Germany) and boiled at 95 °C. Protein extracts were separated by SDS PAGE, transferred onto nitrocellulose membranes (Amersham Hybond ECL), and then blocked in 5% (w/v) milk powder in TBST. The samples were analyzed for the expression of several different synaptic proteins using the following antibodies: NMDAR1a (Invitrogen, 32-0500), NMDAR2a (Santa Cruz, sc-515148), NMDAR2b (Invitrogen, MA1-2014), AMPAR 2/3/4 (Cell Signaling, 2460), brevican (Invitrogen, PA5-31444), Neurocan (Thermo, PA5-47563), α-tubulin (Invitrogen, 62204), GAPDH (Invitrogen, PA1-987) and anti-HA-tag (Roche, 11867427001). To visualize multiple proteins at once, we utilized fluorescent secondary

antibodies. Depending on the specific antibody's species, we paired the secondary antibodies accordingly with a combination of the following dyes: IRDye800CW and IRDye680CW (both for goat@mouse, Li-COR). This approach allowed us to see multiple proteins of interest efficiently on a single membrane.

3.3.6 Sandwich Enzyme-Linked Immunosorbent Assay (ELISA)

Human Aβ1–42 concentrations were determined using the commercially available ELISA kit (27718, IBL International) following the manufacturer's instructions. In brief, the soluble fraction was diluted at a ratio of 1:50 before being added to wells coated with anti-human Aβx–42 (44A3) antibody and incubated overnight at 4 °C. After washing, the wells were incubated for 1 hour with HRP-conjugated anti-human Aβ1–x (82E1). Following additional washing steps, TMB solution was added as a substrate, and the reaction was stopped using 1N H_2SO_4. Optical density (OD) values were measured at 450 nm using a microplate reader (Anthos, 2010).

3.3.7 Biotinylation

To assess changes in protein expression on the cell surface of primary neurons, surface biotinylation was performed. To start, cells were placed on ice to inhibit endocytosis, and medium was aspirated. Cells were washed three times with ice-cold PBS, then incubated for 40 minutes at 4°C in a solution containing 0.3 mg/ml sulfo-NHS-LC-LC-biotin (ThermoFisher, 21335) in PBS to biotinylate surface proteins. Following biotinylation, cells were washed four times with 50 mM NH_4Cl solution to neutralize and remove any unbound biotin.

After a final wash with PBS, cells were lysed with RIPA buffer (150 mM NaCl, 10 mM TRIS-HCl, 1 mM EDTA, 1% Triton X-100, 0,1% SDS, 0,1% Sodium deoxycholate), and total protein concentration was measured to ensure equal protein loading. Equal protein amounts were incubated overnight at 4°C with 30 µl NeutrAvidin agarose beads (ThermoFisher, 29201) for specific binding and precipitation of biotinylated proteins. The beads were subsequently washed twice with RIPA buffer, and bound proteins were eluted by boiling at 95°C in SDS loading buffer. Finally, proteins were analyzed by SDS-PAGE followed by Western blotting to quantify changes in surface protein expression.

3.4 Microscopy & Imaging

3.4.1 Immunofluorescence – Free-Floating Slices (Aβ Plaques and Meprin β Expression)

Mouse brains were first perfused with PBS and then 4% paraformaldehyde (PFA) and subsequently embedded in Tissue Freezing Medium (Leica). Sagittal sections of 30 µm thickness were prepared using a CM3050S cryostat (Leica) and transferred into 48-well plates containing cryoprotective solution (25% glycerol, 25% polyethylene glycol, 50% PBS). Sections were stored at 4 °C until further processing. For IF, cryosections of mouse brains were post-fixed in 4% paraformaldehyde overnight and processed as free-floating slices. All washing steps were carried out using 0.01 M phosphate-buffered saline (PBS). To block non-specific binding and permeabilize the tissue, sections were incubated for 2 hours at room temperature in PBS containing 0.8% Triton X-100 and 7% normal donkey serum (Dianova, 017-000-121).

Primary antibody incubation was performed for three days at 4 °C in PBS supplemented with 2% bovine serum albumin (IgG-free, protease-free; Jackson ImmunoResearch, 001-000-161, via Dianova), 0.05% sodium azide, and 0.3% Triton X-100. The following primary antibodies were applied: goat anti-meprin β (1:40, Thermo Fisher Scientific, PA5-47474), rabbit anti-VGLUT1/2 (1:500, Synaptic Systems, 135503), and an alpaca-derived FluoTag®-X2 anti-PSD95-AZDye 568 nanobody (1:200, NanoTag/Synaptic Systems, N3702-AF568-L).

Following primary incubation, sections were washed with PBS and incubated for 2 hours at room temperature with the respective secondary antibodies and DAPI (0.5 µg/ml, AppliChem, A4099,0005) in PBS containing 2% bovine serum albumin and 0.05% sodium azide. Secondary antibodies used were IRDye 680RD donkey anti-goat IgG (1:200, Li-COR) and Alexa Fluor 488-conjugated donkey anti-rabbit IgG (H+L) (1:200, Jackson ImmunoResearch).

After final washes in PBS, sections were mounted using Fluoromount-G (Thermo Fisher Scientific) and stored protected from light until further processing for microscopy. The subcellular localization of meprin β in hippocampal neurons of wild-type and meprin β-overexpressing mice in sagittal brain slices from the CA3 region of the murine hippocampus was imaged using a Zeiss LSM 710 confocal laser scanning microscope. Quantification of colocalization of observed proteins was performed in ImageJ by splitting RGB channels,

thresholding (triangle method), and using the “Image Calculator” to determine overlap area fractions (in %).

To assess Aβ plaque deposition in meprin β-overexpressing mice in an APP/Ld background, brain sections were processed according to the standard protocol described before, with the following modification for antigen retrieval: prior to permeabilization, sections were treated with 88% formic acid for 10 minutes at room temperature to enhance epitope accessibility by disrupting protein cross-links.

Following antigen retrieval, permeabilization and blocking, sections were incubated with the primary antibody IC16 (mouse monoclonal, 1:500) to detect Aβ. Nuclear counterstaining was performed using DAPI (1 µg/ml). For visualization of IC16 labeling, a goat anti-mouse AF 488-conjugated secondary antibody (1:1000) was applied. Fluorescence signals were acquired and analyzed accordingly. Meprin β-overexpressing APP/Ld mice were compared to control animals expressing only the APP/Ld transgene.

3.4.2 Immunohistochemistry and DAB Staining of Sagittal Brain Sections

Sagittal brain slices were fixed in 4% paraformaldehyde, cryoprotected in sucrose, and cut at 30 µm thickness using a cryostat. Free-floating sections were rinsed in phosphate-buffered saline (PBS), permeabilized with 0.3% Triton X-100, and incubated in a blocking solution containing 5% normal serum. Slices were then incubated overnight at 4 °C with the primary antibody (pAB77) diluted in blocking buffer. Antibody pAb77 was raised against residues 2-14 of the Aβ peptide, detecting N-truncated Aβ2-x peptides (Savastano *et al.*, 2015). After washing in PBS, sections were incubated with a biotinylated secondary antibody followed by the avidin–biotin complex (ABC) reagent. Diaminobenzidine (DAB) was used as the chromogenic substrate, and the reaction was monitored under a microscope to achieve optimal signal intensity. Sections were rinsed thoroughly, mounted on glass slides, dehydrated through graded alcohols, cleared in xylene, and coverslipped with mounting medium for microscopic analysis.

3.5 *In Vivo* Methods (Animal Work)

3.5.1 Animals Breeding

hAPP[V717I][31] mice (APP/Ld) were crossed with NEX$^{Cre;TG/wt}$ × ROSA26$^{Mep1b\text{-}HA}$ animals (mepβ$^{Cre;TG/wt}$), resulting in animals overexpressing meprin β in an APP/Ld background (mepβ$^{Cre;TG/wt}$ x APP/Ld). Overexpression was specific to the cortex and hippocampus. APP/Ld, mepβ$^{Cre;TG/wt}$ × APP/Ld and mepβ$^{Cre;wt/wt}$ (wt) animals were maintained on a 12h light/dark cycle with food and water *ad libitum*. During our experiments, we did not detect any gender-specific differences; therefore, we used mixed genders for all experiments. All animal studies were conducted in compliance with European and German guidelines for the care and use of laboratory animals and were approved by the Central Animals Facility of the University of Mainz and the ethical committee on animal care and use of Rhineland-Palatinate, Germany.

Meprin β-overexpressing (mepβ$^{Cre;TG/wt}$) and wild-type (mepβ$^{Cre;wt/wt}$) mouse strains were maintained on a 12 h light/dark cycle with food and water *ad libitum. NEX$^{Cre;TG/wt}$ × Rosa26$^{Mep1b\text{-}HA}$* (mepβ$^{Cre;TG/wt}$ or mepβ$^{Cre;wt/wt}$) mice were generated by crossing *Rosa26$^{Mep1b\text{-}HA}$* mice (Armbrust et al., 2025) with *NEX$^{Cre;TG/wt}$* mice (Peters et al., 2021). The animals were a gift from Christoph Becker-Pauly (Institute of Biochemistry - Kiel), have a C57BL/6 background and breeding was genetically refreshed every 4-6 generations with wild-type C57BL/6 animals. All animal studies were conducted in compliance with European and German guidelines for the care and use of laboratory animals and were approved by the Central Animal Facility of the University of Mainz and the ethical committee on animal care and use of Rhineland–Palatinate, Germany.

3.5.2 Behavioral Experiments – Morris' Water Maze

To minimize potential experimenter-induced stress, animals were habituated to the presence of the experimenter. This was achieved by daily visits to the animal facility for four consecutive days prior to the start of behavioral testing. During these sessions, the experimenter interacted gently with the animals to allow them to become familiar with handling and presence, thereby reducing anxiety-related responses. Following this habituation period, behavioral experiments were initiated.

For behavioral analysis, 8-month-old mice were tested (n=5/7 animals per group). Spatial learning and memory were assessed by the Morris' Water Maze hidden platform task performed as previously described with minor modifications[28]. Briefly, the water maze (diameter 120 cm) was filled with clear water (21-22 °C) one centimeter above the platform. Prominent symbols around the maze provided abundant extra-maze cues. The platform stayed in the same quadrant from day 1 to 4, and the animals were released from four different positions at the pool perimeter. Mice performed four trials per day on 4 consecutive days with a maximum length of 90 seconds. Each day, the animals were released into the water from different locations outside the platform (d1 – north, south, east, west; d2 – W-E-S-N; d3 – S-W-N-E; d4 – E-N-W-S). If mice did not find the platform within the given time, they were gently guided to the platform. Mice were allowed to stay on the platform for 10 s to memorize the surrounding cues. On the fifth experimental day, a probe trial (60 s) without the platform was performed. Basal motor activity was evaluated by swimming speed. Learning was assessed by measuring the escape latency to find the platform. Memory capabilities were characterized by the number each mouse crossed the former platform location at the probe trial and the latency to reach the former location. To further assess the ability to memorize the location of the platform, the time spent in the right quarter of the platform was measured. For vision abilities, a visible platform task was done after the learning assessment on day 6. It consisted of three trials in a row, starting opposite the platform that was indicated by a table tennis ball 15 cm above the platform. No mouse failed this task, showing that all tested mice were capable of seeing the cues.

A computerized video recording system registered the moving path and duration in water maze tests automatically. The hardware consisted of an IBM-type AT computer combined with a video digitizer and a CCD video camera. The software used for data acquisition and analysis was EthoVision XT® release 8.0 (Noldus Information Technology, Utrecht, the Netherlands).

3.5.3 Organ Dissection and Lysis

Animals were anesthetized by intraperitoneal injection of ketamine solution at a dose of 10 µL per gram of body weight. Depth of anesthesia was assessed by testing the pedal withdrawal reflex. Animals that showed no response to toe pinch and additionally no reaction to spraying 70% ethanol onto their face were considered deeply anesthetized.

Blood was collected via cardiac puncture into the left ventricle while the heart was still beating. Approximately 0.5 ml of blood was drawn and allowed to coagulate at room temperature. During this period, cerebrospinal fluid (CSF) was obtained by puncturing the cisterna magna using a glass capillary.

Following blood and CSF collection, organs of interest, including the brain, liver, and kidney, were harvested. After 5 minutes, the coagulated blood was centrifuged at maximum speed to separate the serum, which was then transferred to a fresh tube. All tissues and CSF samples were immediately flash-frozen in liquid nitrogen and stored at −80 °C until further processing.

For protein extraction, tissues were homogenized in RIPA buffer supplemented with protease inhibitors at a 1:10 (w/v) ratio, using a glass dounce homogenizer. The homogenates were incubated on ice for 30 minutes and subsequently centrifuged at maximum speed for 10 minutes at 4 °C. The resulting supernatants were collected, and protein concentrations were determined using the BCA assay.

3.5.4 Dissection of Organs and Animals: Tissue Lysis for Aβ Analysis

Animals were euthanized by cervical dislocation, and their brains were extracted. For meprin β characterization, the brains were dissected to isolate the cortex and hippocampus. Brain regions from three to five mice per group were pooled and homogenized in a buffer containing 320 mM sucrose, 10 mM HEPES, and 1 mM EDTA at a 1:6 (weight-to-volume) ratio. The homogenates were centrifuged at 18,000g for 30 min, after which the soluble extract was removed, and the pellet was resuspended in 1% NP-40 lysis buffer (150 mM NaCl, 50 mM Tris–OH, pH 8.0). Lysates were then centrifuged again at 18,000g for 30 minutes, and the supernatants were collected for further analysis.

For Aβ analysis, hemispheres of the cortex and the pooled hippocampi were mechanically homogenized in 0.04% DEA buffer (0,4% DEA, 0.1 M NaCl) using the same ratio described above and subsequently ultracentrifuged at 120,000g for 60 minutes (TLA120.2 rotor, Beckman Coulter). The DEA buffer-extracted supernatant (soluble fraction) was collected, while the pellet was resuspended in 800 µL of 0.01 M PBS containing 2% SDS for further use. PBS and SDS protein extracts were either analyzed directly or stored at –80 °C until further use. All buffers were supplemented with protease (cOmplete, Roche) and phosphatase inhibitor cocktails (PhosSTOP, Roche) before use.

3.5.5 Perfusion of animals

Perfusion was not performed in experiments involving blood and CSF collection, as sufficient vascular and intracranial pressure is required for their extraction, which is only maintained while the animal is physiologically alive. In contrast, perfusion was conducted for immunofluorescence applications to reduce background signal from blood-derived autofluorescence.

Mice were anesthetized with ketamine as described previously. The left ventricle was cannulated and connected to a peristaltic pump set to deliver ice-cold phosphate-buffered saline (PBS) at a flow rate of 2 ml/min. Simultaneously, the right atrium was incised to allow efflux of blood and perfusate. The perfusion was carried out for 5–7 minutes, depending on the size of the animal, resulting in effective replacement of blood with PBS. This step was critical to minimize background fluorescence that could interfere with subsequent immunofluorescent labeling.

3.5.6 Synaptosome isolation

Animals (n=9) were sacrificed by cervical dislocation and their brains were removed. For further characterization, brains were dissected into the cortex and hippocampus. To obtain enough protein, three hippocampi from each group were pooled. Functional synaptosomes were isolated as recommended by the manufacturer (ThermoFisher, 87793). Briefly, brain regions were weighed and mechanically homogenized in an appropriate amount of Syn-PER reagent. First, the homogenate was centrifuged at 1200g for 10 minutes. The supernatant was transferred to a fresh tube. After centrifugation at 15,000g for 20 minutes, the pellet was resuspended in Syn-PER reagent to a final concentration of 4-5 µg/µl, resulting in the synaptosome fraction. The synaptosome fraction was aliquoted and snap frozen for further analysis. The homogenate after the first centrifugation step and an aliquot of the supernatant after the last centrifugation step were snap frozen as well, resulting in the homogenate and S2 (cytosolic) fraction, respectively. The Syn-PER reagent was supplemented with protease inhibitor cocktails prior to use (cOmplete, Roche).

3.5.7 Electrophysiology

Mice were deeply anesthetized with 4 vol% isoflurane until loss of involuntary reflexes. Then they were quickly decapitated, the brain immediately removed and put into the ice-cold (4°C)

choline-based artificial cerebrospinal fluid (cACSF) perfused with carbogen (95% oxygen [O_2] and 5% carbon dioxide [CO_2]). This cutting solution contained (in mM): NaCl (87), KCl (2.5), $NaH_2PO_4 + H_2O$ (1.25), choline chloride (37.5), $NaHCO_3$ (25), and D-glucose (25), $CaCl*2H_2O$ (0.5), $MgCl_2$ (7) and at a pH of 7.4. Next, the brain was placed on the stage of a vibratome (VT1200 S, Leica) in an orientation to cut horizontal brain slices with a thickness of 400 µm. Slices containing the distinctive hippocampal structures were selected and put into a storage chamber filled with normal, carbonated ACSF containing (in mM): NaCl (125), NaH_2PO_4 (1.25), KCl (2.5), $NaHCO_3$ (25), D-glucose (25), $CaCl_2*2H_2O$ (2), $MgCl_2$ (1) and kept at room temperature. Slices rested in ACSF for at least 40 min before individual slices were transferred onto a multi-electrode array (MEA) chip of a two-chamber MEA system (MEA2100 System, Multi-Channel Systems MCS GmbH), which was constantly perfused with normal ACSF at 32°C. Each glass MEA chip consisted of 60 electrodes, each with a diameter of 30 µm and spaced with a 200 µm interelectrode distance (60MEA200/30iR; Multi-Channel Systems MCS GmbH). Each brain slice was placed optimally to have well-positioned stimulating electrodes in the CA3 region and recording electrodes in the CA1 region of the hippocampus. A platinum grid was placed on top of the slices to stabilize their position. Slices were allowed to settle on the MEA chip for a minimum of 30 min before any recordings began. The electrophysiological recording protocols were generated and applied by Multi Channel Experimenter 2.2 software (Multi Channel Systems MCS GmbH) using a 50 kHz sampling rate and a Butterworth highpass 2.0 Order Filter with a 200 Hz cutoff.

Input/output (I/O) curves of extracellularly recorded field postsynaptic potentials (fEPSPs) were generated by electrical stimulation of one MEA electrode, starting with a voltage pulse of 500 mV at a stimulus duration of 100 µs, then gradually increasing the pulse intensity by +500 mV until a maximum stimulation intensity of 5000 mV was reached. The duration between each voltage pulse stimulation was 40 s.

The paired-pulse protocol used a stimulation intensity that resulted in a fEPSP equal to approximately 30% of the maximum evoked fEPSP amplitude from the input/output curve protocol. Paired pulses had a 50 ms interstimulus interval.

To test the strength of synaptic long-term potentiation (LTP), fEPSPs were recorded with the same stimulus intensity selected for the paired-pulse protocol, on a slice-wise basis. Baseline

stimulations for LTP were applied for 10 min, consisting of one stimulation per minute. Then, LTP was induced by applying a high-frequency stimulation (HFS) at 100 Hz for 1 s, followed by 60 min of baseline stimulation every 60 s. The level of HFS-induced LTP was analyzed by normalizing the mean amplitudes from the last 10 min of baseline recordings after HFS (50–60 min) to the mean of the amplitude of the initial 10 min baseline recordings before HFS. These data were compared to recordings against the independent control pathway that was generated by a second stimulation electrode located in the direction of the subiculum, as it cannot generate long-term plasticity changes in CA1. The Multi-Channel Analyzer 2.2 (Multi-Channel Systems MCS GmbH) software was used to record the peak value of each fEPSP amplitude.

All electrophysiological data were analyzed using the Multi-Channel Analyzer 2.2 software, Microsoft Office Excel (Microsoft), and GraphPad Prism (GraphPad Software).

3.5.8 Statistical analysis and illustrations

All graphs and statistical analyses were prepared using GraphPad Prism 8 software (La Jolla, CA). Western blots were quantified by densitometry analysis using ImageJ v.1.52 (NIH, USA). The individual statistical tests were described in the respective figure descriptions (ns: $p > 0.05$; *: $p \leq 0.05$; **: $p \leq 0.01$; ***: $p \leq 0.001$). The figures were created with Microsoft PowerPoint, BioRender.com and/or GraphPad.

4. Results

4.1 Part I:

Meprin β Modulates Brevican Proteolysis Impairing Neural Plasticity and Memory Formation

4.1.1 Generation of a Targeted Meprin β-Overexpressing Mouse Model

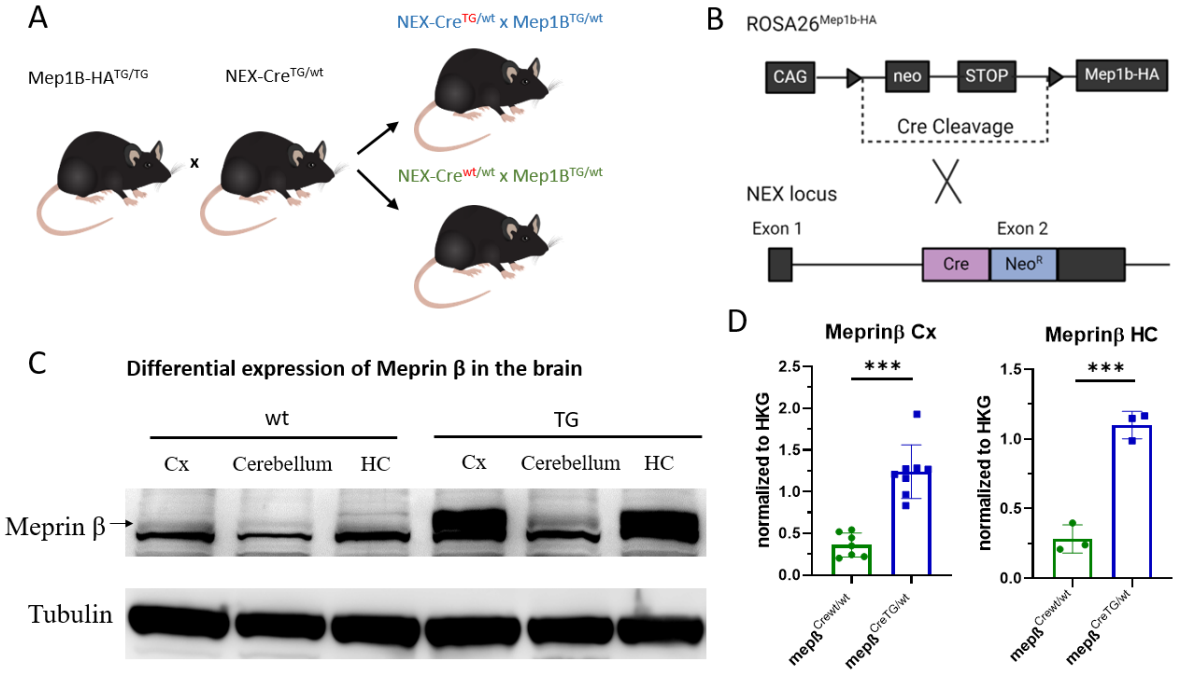

Figure 4 - Generation of a targeted meprin β overexpression in cortical and hippocampal neurons. (A) Homozygous transgenic *Rosa26*$^{Mep1b\text{-}HA}$ mice were crossed with heterozygous *NEX*^{Cre} mice, yielding *NEX*$^{Cre;wt/wt}$ × *Rosa26*$^{Mep1b\text{-}HA}$ (mepβ$^{Cre;wt/wt}$) and *NEX*$^{Cre;TG/wt}$ × *Rosa26*$^{Mep1b\text{-}HA}$ (mepβ$^{Cre;TG/wt}$) offspring. **(B)** For cortex- and hippocampus-specific overexpression of meprin β, we employed the NEX-Cre mouse model, where Cre recombinase expression is directed by NEX regulatory sequences. This was achieved by substituting the NEX coding region with a Cre cassette via homologous recombination. **(C)** Western blot analysis across different brain regions of *NEX*$^{Cre;wt/wt}$ × *Rosa26*$^{Mep1b\text{-}HA}$ (wild-type) and *NEX*$^{Cre;TG/wt}$ × *Rosa26*$^{Mep1b\text{-}HA}$ of 8-month-old mice showed elevated meprin β expression specifically inside the cortex and hippocampus of *NEX*$^{Cre;TG/wt}$ × *Rosa26*$^{Mep1b\text{-}HA}$ transgenic animals. **(D)** Densitometric quantification of meprin β in cortex and hippocampus of *NEX*$^{Cre;wt/wt}$ × *Rosa26*$^{Mep1b\text{-}HA}$ and *NEX*$^{Cre;TG/wt}$ × *Rosa26*$^{Mep1b\text{-}HA}$ mice from several experiments, normalized to tubulin.

We previously described a learning and memory-related effect of meprin β in the brain beyond its role in APP processing (Marengo et al., 2022). Behavioral analysis revealed that meprin β KO animals outperformed their wild-type littermates, suggesting an enhanced ability for memory consolidation. To further investigate this, we established a mouse model that overexpresses meprin β in neurons of the hippocampus and cortex, the brain regions primarily responsible for learning and memory formation (Figure 4A).

To generate a targeted meprin β-overexpression in the cortex and hippocampus, we utilized the previously described NEX-Cre mouse model, where the Cre recombinase is expressed under control of the regulatory sequences of NEX, a gene that encodes a neuronal basic helix-loop-helix protein. The coding region of NEX (exon 2) was replaced by a Cre cassette using homologous recombination (Figure 4B) (Goebbels et al., 2006). Animals harboring this mutation were crossed with meprin β knock-in animals as described in (Peters et al., 2021). The knock-in was generated by cloning murine meprin β cDNA into STOP-EGFP-ROSA-CAG targeting vector and inserting it into the Rosa26 locus of embryonic stem cells by homologous recombination.

This breeding resulted in heterozygous meprin β-overexpressing offspring (mepβ$^{Cre;TG/wt}$) with consistent expression of meprin β specifically in the hippocampus and cortex. Figure 4C shows the expression of meprin β in wild-type mice and the novel mepβ$^{Cre;TG/wt}$ mouse model: apart from low endogenous meprin β expression in mepβ$^{Cre;wt/wt}$ (wild-type) animals and the cerebellum of mepβ$^{Cre;TG/wt}$ mice, we can see a significant increase in meprin β expression in the cortex and hippocampus of mepβ$^{Cre;TG/wt}$ animals.

Densitometric analysis of Western blots revealed that meprin β was overexpressed approximately threefold in the cortex and fivefold in the hippocampus of transgenic mice compared to endogenous meprin β levels in wild-type controls (Figure 4D).

4.1.2 Meprin β Overexpression in Cortex and Hippocampus Leads to Severe Impairment in Learning and Memory

After generating the mouse model, we aimed to compare learning and memory performance in a behavioral experiment between mepβ$^{Cre;wt/wt}$ and mepβ$^{Cre;TG/wt}$ animals. To investigate this, we utilized the Morris Water Maze (MWM) paradigm test (Figure 5A).

Clear differences between mepβ$^{Cre;TG/wt}$ and mepβ$^{Cre;wt/wt}$ animals emerged as early as the third day of training. Mepβ$^{Cre;wt/wt}$ animals could locate the platform significantly faster by the fourth training day, whereas meprin β-overexpressing mice showed no evidence of learning (Figure 5B). The time required to locate the platform remained constant from the first to the last training day for mepβ$^{Cre;TG/wt}$ mice, indicating a pronounced learning impairment (Figure 5B). Furthermore, during the probe trial (PT), these animals took significantly longer to find the former platform location compared to mepβ$^{Cre;wt/wt}$ counterparts (Figure 5C). Although the

time to locate the platform decreased for mepβ$^{Cre;TG/wt}$ animals during the probe trial, suggesting minimal learning, this effect was likely coincidental: analysis of the time spent in the correct quadrant of the water tank revealed that meprin β-overexpressing mice failed to exhibit directed swimming towards the platform's original location (Figure 5D).

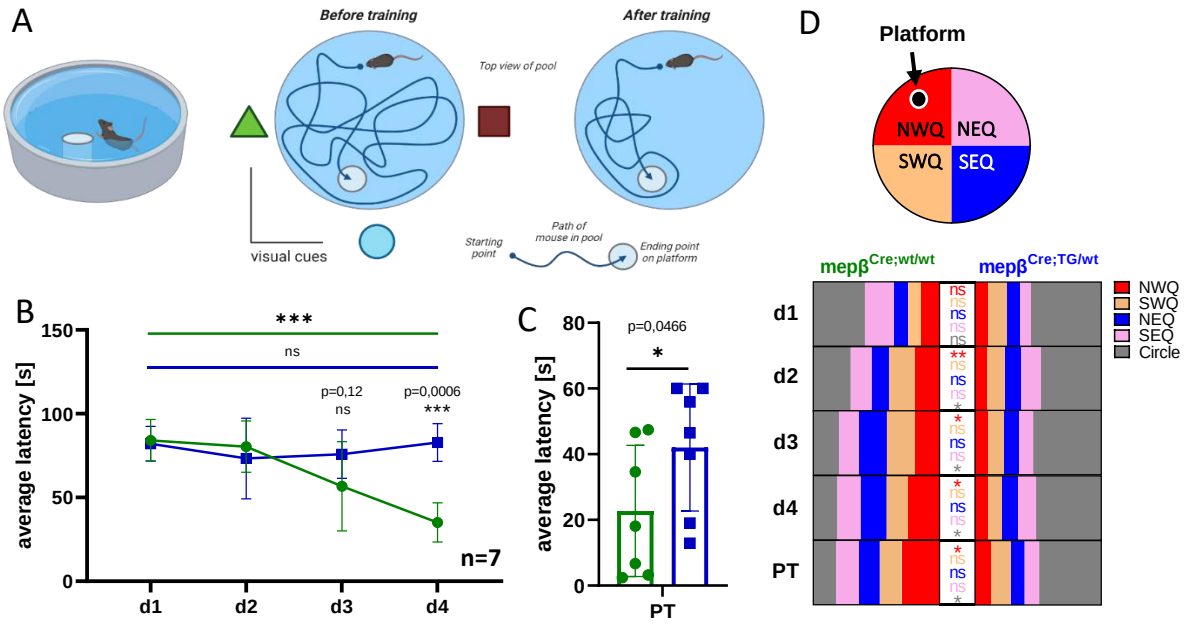

Figure 5 - Meprin β overexpression leads to severe cognitive impairment. Spatial learning and memory tests utilizing the Morris water maze (MWM) paradigm were carried out on 8-month-old meprin β-overexpressing mice and their wild-type counterparts (n=7). **(A)** Schematic overview of the MWM paradigm test: the platform is submerged under water, but the animals have visual cues on the wall of the water tank for navigation. Training lasts for four days, with four trials per day. **(B)** The average escape latency in each trial was measured for the four training days. On day four, the meprin β-overexpressing animals showed a significant learning deficit compared to mepβ$^{Cre;wt/wt}$ mice (p=0.006). The data shown is the mean ±SEM of four different trials performed on each day. Statistical analysis was performed using an unpaired parametric t-test. **(C)** On probe trial (PT) day, the platform was removed and the latency to reach the former platform location was measured. Similar to the final training day, significant cognitive deficits can be observed for meprin β-overexpressing mice compared to mepβ$^{Cre;wt/wt}$ animals (p=0.0466). Statistical analysis was conducted using an unpaired Mann-Whitney U test due to the data's non-normal distribution, as determined by the Shapiro-Wilk test. **(D)** The water tank was divided into four equal quarters, with the platform located in the NWQ quarter. The time spent by the animals in each of the four quarters or circling the water tank (grey area) was measured. It is observable that after the second day, the mepβ$^{Cre;wt/wt}$ animals spent significantly more time in the correct quarter, although this difference is not directly reflected in latency for finding the platform. Additionally, after the second day, mepβ$^{Cre;wt/wt}$ animals spent significantly less time circling the platform. Statistical analysis was performed using an unpaired parametric t-test.

In contrast, mepβ$^{Cre;wt/wt}$ animals displayed a clear preference for the correct quadrant, indicating effective learning and spatial memory already on day two. Additionally, mepβ$^{Cre;wt/wt}$ animals spent significantly less time circling the water tank compared to meprin β-overexpressing animals (Figure 5D).

Additionally, we did not observe any differences in swimming velocity between the animals, indicating that the mutation did not cause locomotor deficiencies and that the observed

effects were not due to impaired swimming abilities (Figure 6). The higher swimming speed on probe trial day is likely due to the shortened swimming time (60 instead of 90 seconds), since the animals are swimming faster in the first seconds of the experiment compared to the last seconds.

In summary, transgenic mice exhibit substantial learning impairments in the MWM paradigm test. Together with prior findings showing beneficial effects of meprin β KO on learning (Marengo et al., 2022), these results suggest that meprin β may play a significant role in learning and behavioral processes.

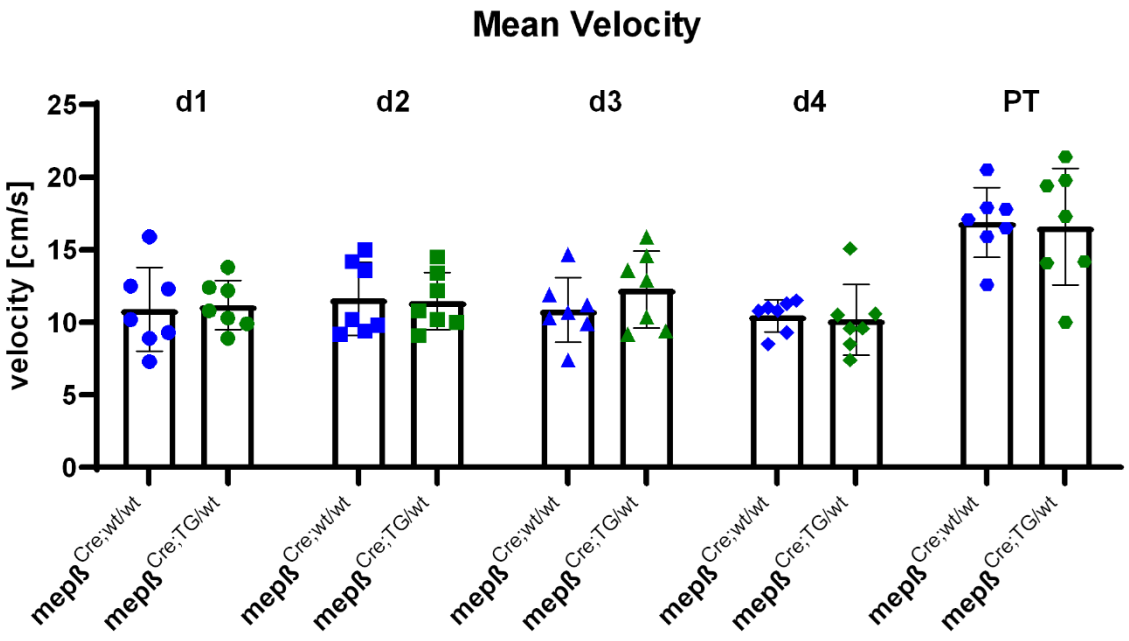

Figure 6 - Mean velocity does not change between the tested groups in the MWM test. During the training phase, mice swam for 90 seconds per session, while during the PT, they swam for 60 seconds. Analysis of swimming speed revealed no significant differences between the wt and transgenic groups across all testing days in the MWM paradigm test. These findings indicate that the animals exhibit no locomotor impairments, suggesting that observed differences in performance are unrelated to motor function.

4.1.3 Meprin β Localizes to Axons and Synapses and Co-localizes with PSD-95 in Overexpressing Neurons

Identifying the subcellular localization of meprin β in neurons has been technically challenging, largely due to low endogenous expression levels and limited sensitivity of available antibodies. Using a transgenic mouse model that overexpresses meprin β in cortical and hippocampal neurons, we employed confocal microscopy to examine its distribution in sagittal brain slices, focusing on the CA3 region of the hippocampus (Figure 7C). This area was selected based on findings showing that meprin β-overexpressing mice exhibit impairments in spatial learning in

the MWM and because higher endogenous protein levels of meprin β were detected in the hippocampus compared to other brain areas (Marengo et al., 2022). To determine the precise localization of meprin β overexpression in neurons, we took advantage of the fact that meprin β was tagged with an HA epitope. We could observe that meprin β is mostly overexpressed at the cell soma, with low axonal and synaptic expression as well, when compared to controls that had no expression of HA-tagged meprin β (Figure 7A). Control stainings, only incubated with the secondary antibody, showed an acceptable background signal (Figure 7B).

Next, to compare overexpression to endogenous expression, we stained with an antibody directed against meprin β (Figure 8A). In wild-type animals, the meprin β signal was primarily perinuclear, likely reflecting retention in the endoplasmic reticulum. In contrast, overexpressing mice showed stronger staining intensity throughout the soma, with additional localization in axons and synaptic regions, as already shown in the anti-HA-tagged staining. To assess synaptic distribution more specifically, we performed co-staining with the presynaptic marker VGLUT and the postsynaptic marker PSD-95 (Figure 8B). The overlap between meprin β and VGLUT appeared as yellow, while the overlap between meprin β and PSD-95 was visualized as magenta, and between VGLUT and PSD-95 as cyan. While the yellow and cyan signals did not differ substantially between wild-type and overexpressing animals, the magenta signal was notably more prominent in the overexpression condition, indicating an increased postsynaptic presence of meprin β (Figure 8C). These findings align with previous behavioral data suggesting a synaptic mechanism underlying the cognitive impairments observed in these animals. For control stainings (Figure 9), brain slices were incubated only with secondary antibodies used in Figure 8 to exclude background staining. No significant background signal was detected. PSD95 was labeled using a primary antibody directly conjugated to a fluorophore.

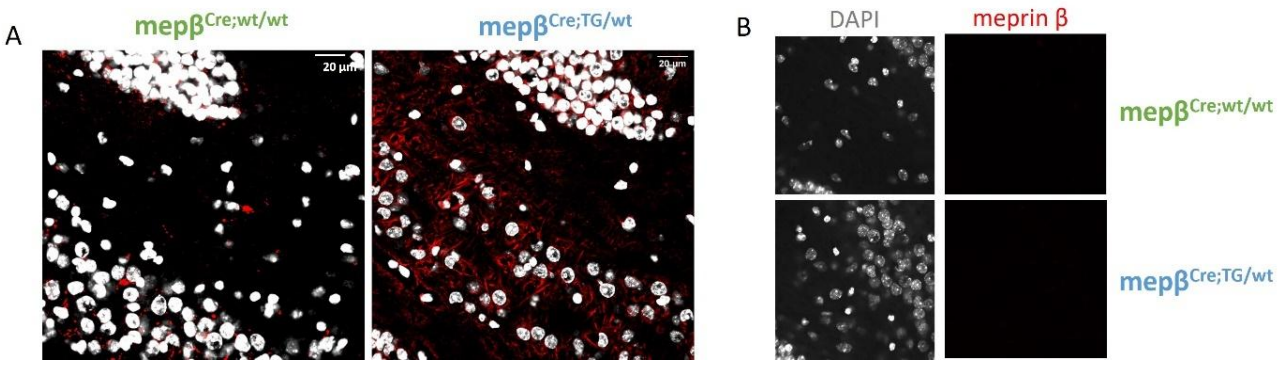

Figure 7 – Meprin β overexpression in neuronal cell bodies, synapses, and axons of transgenic animals compared to animals not expressing HA-tagged meprin β. (A) Immunofluorescent staining of HA-tagged transgenic meprin β in mepβ$^{Cre;wt/wt}$ and mepβ$^{Cre;TG/wt}$ animals with an anti-HA tag antibody to visualize the overexpression of meprin β. Pseudo-colors: Grey (DAPI, 1:200), red (mouse anti-HA, 2-2.2.14 Invitrogen, 1:100; donkey anti-mouse IgG-IRDye680RD, Li-Cor Biosciences, 1:200). **(B)** Control stainings that were incubated only with the secondary antibody IRDye680RD (925-68074, Li-Cor Biosciences, 1:200, rabbit).

Figure 8 - Subcellular localization of meprin β in hippocampal neurons of wild-type and meprin β-overexpressing mice. Sagittal brain slices (thickness: 30 µm) from the CA3 region of the murine hippocampus were imaged using a Zeiss LSM 710 confocal laser scanning microscope. The following acquisition settings were used: DAPI (grey) was excited at 405 nm (pinhole 41.9 µm, gain 850), VGLUT (green, Alexa Fluor 488) at 488 nm (pinhole 51.4 µm, gain 750), PSD-95 (blue, Alexa Fluor 568) at 543 nm (pinhole 59.4 µm, gain 900), and meprin β (red, IRDye 680 detected via the Atto680 channel) at 633 nm (pinhole 67.8 µm, gain 1200). Pixel dwell time was 54.93 µs, frame size 1912 × 1912 pixels, and line averaging was set to 16. Images were processed in ImageJ by subtracting background (rolling ball radius = 50 pixels), applying Gaussian blur (1 px), and slightly enhancing contrast. Scale bar: 20 µm. **(A)** Representative confocal images show meprin β (red) and DAPI (grey) staining in wild-type (mepβ$^{Cre;wt/wt}$) and meprin β-overexpressing (mepβ$^{Cre;TG/wt}$) animals, revealing increased signal and extended axonal and synaptic distribution in the latter, indicated by arrows. **(B)** Single-channel and merged images of DAPI (grey), VGLUT (green), PSD-95 (blue), and meprin β (red) in wild-type and overexpressing animals. Merged signals appear as yellow (meprin β + VGLUT), magenta (meprin β + PSD-95), and cyan (VGLUT + PSD-95). Zoomed-in views highlight overlapping patterns, indicated by arrows. **(C)** Schematic diagram of the CA3 region indicating the anatomical site of image acquisition. **(D)** Quantification of co-localization was performed in ImageJ by splitting RGB channels, thresholding (triangle method), and using the 'Image Calculator' to determine overlap area fractions (in %). Increased meprin β + PSD-95 co-localization was observed in overexpressing animals, with no observable changes in the other combinations.

(Figure caption on previous page)

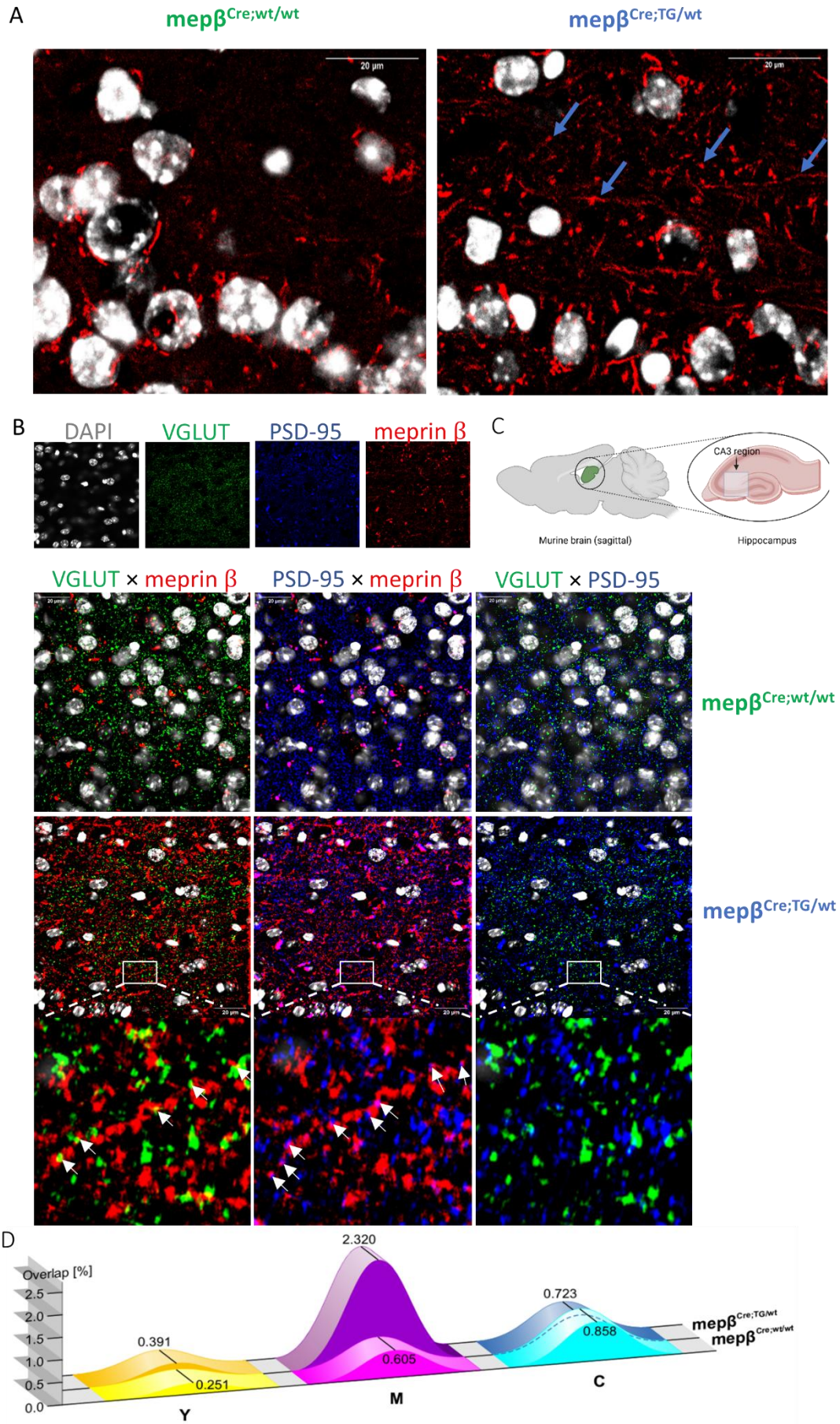

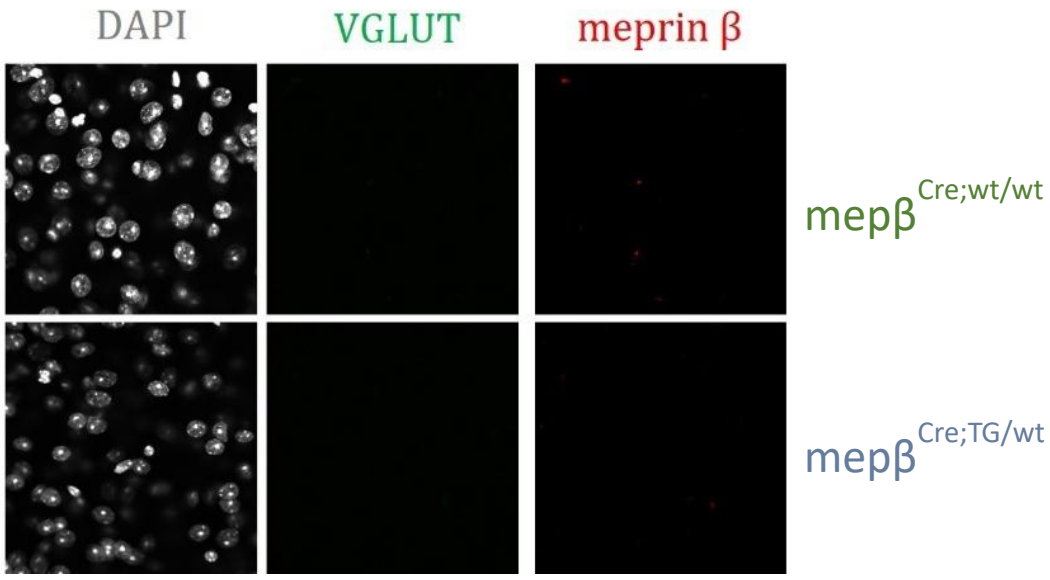

Figure 9 - **Control stainings that were incubated only with the secondary antibody.** PSD95 is absent, because it was stained only with a fluorophore-attached primary antibody. Pseudo-colors: Grey (DAPI), green (rabbit anti-VGLUT, 1:40, donkey anti-rabbit-AF488, 711-545-152 Jackson Lab. Biozol, 1:200), red (goat anti-meprin β, PA5-47474; ThermoFisher Scientific, 1:40; donkey anti-goat IgG-IRDye680RD, 925-68074, Li-Cor Biosciences, 1:200).

4.1.4 Meprin β-Overexpressing Animals Show Significantly Impaired Hippocampal LTP

As we have detected severe learning and memory differences in meprin β-overexpressing mice and additionally a higher presence at the post-synapse, we tested the impact of meprin β overexpression on long-term synaptic plasticity, a cellular model of learning and memory. Therefore, we carried out electrophysiological long-term potentiation (LTP) recordings of acute mepβ$^{Cre;wt/wt}$ and mepβ$^{Cre;TG/wt}$ mouse hippocampal tissue slices by use of the microelectrode array (MEA). A representative slice on the MEA chip can be seen in Figure 10A. First, we recorded baseline extracellular field excitatory postsynaptic potentials (fEPSPs) in the CA1 region at a stimulation intensity that evoked approximately 30% of the maximum evoked response from the input/output (I/O) curve, on an individual slice basis.

Following 10 minutes of stable baseline recordings, we applied electrical high-frequency stimulation (HFS) of 100Hz for 1 second at the Schaffer collaterals in area CA3. As an additional, independent control input, HFS of equal intensity was also exerted from another, second pathway onto CA1. As expected, this independent, second input failed to reveal any potentiation of synaptic fEPSPs in area CA1 (Figure 10B, grey dots). Representative evoked fEPSP traces from before and after the HFS for mepβ$^{Cre;wt/wt}$ (green) and mepβ$^{Cre;TG/wt}$ (blue) slices, and the control stimulation pathway (grey), can be seen in Figure 10C. Statistical analysis

of the fEPSPs was carried out based on the mean potentiation values of the last 10 minutes of the 60-minute recording period following HFS for each slice, relative to each of their baseline fEPSP amplitudes (Figure 10D). As expected, and shown in Figure 10D, LTP was successfully induced at CA1 synapses from mepβ$^{Cre;wt/wt}$ mice. The LTP induction after HFS in mepβ$^{Cre;TG/wt}$ mice, however, was significantly impaired. Meprin β overexpression resulted in a significantly lower hippocampal potentiation compared to the mepβ$^{Cre;wt/wt}$ mice, as well as having no statistical difference from the independent control pathway (Figure 10D).

In summary, mepβ$^{Cre;TG/wt}$ mice have a significantly impaired LTP in the CA3-CA1 pathway, which indicates functional impairment of the synaptic properties normally inducing NMDAR-dependent type of LTP. This further suggests potential behavioral deficits in hippocampal-dependent learning and memory tasks in these animals, and it might link those changes to functional alterations of postsynaptic AMPA and/or NMDARs.

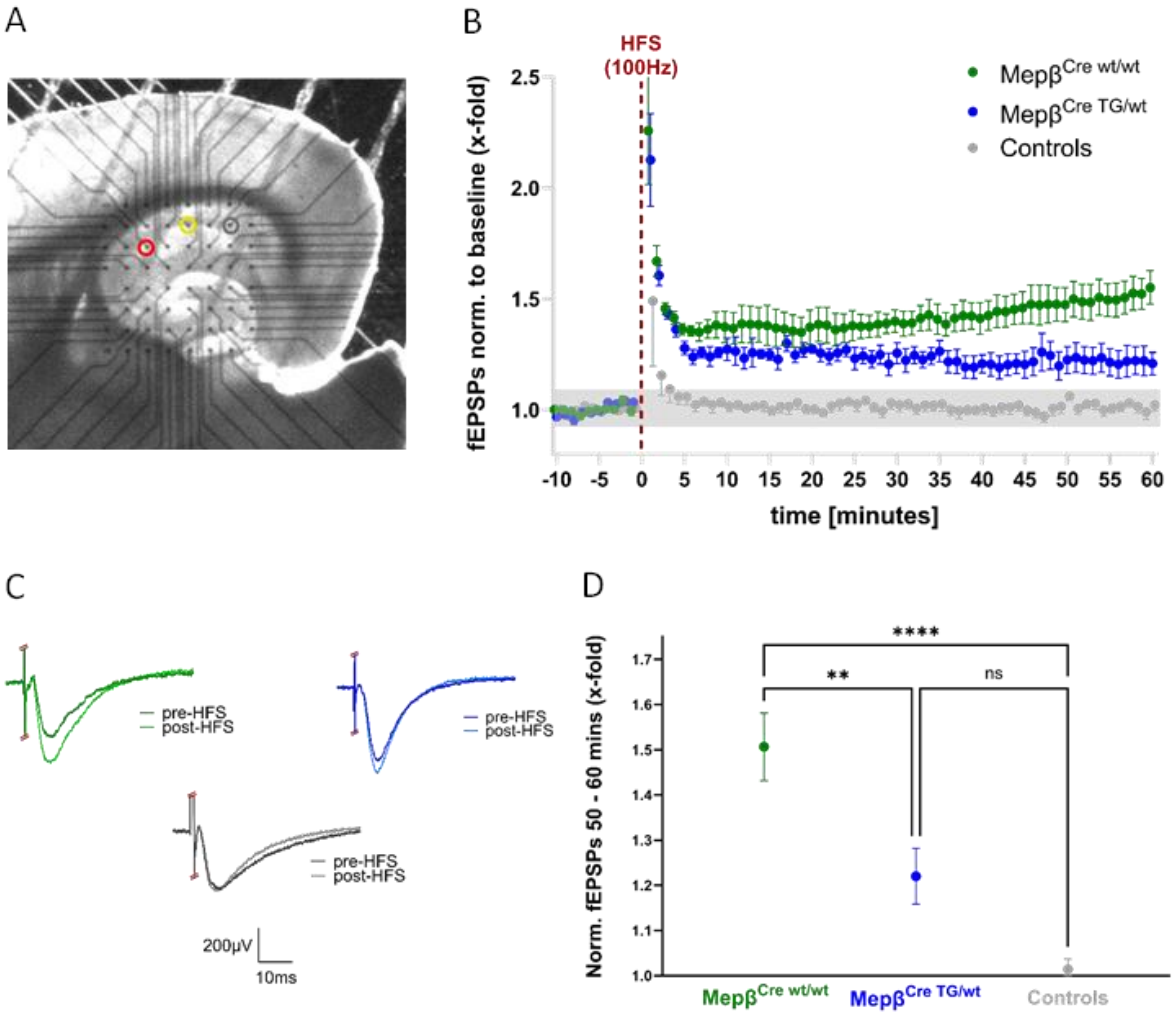

(Figure caption on next page)

Figure 10 - Meprin β-overexpressing mice show an impaired hippocampal LTP. Mepβ$^{Cre;wt/wt}$ mice (green) achieve a level of LTP that is significantly larger than both the control recordings (grey) and the mepβ$^{Cre;TG/wt}$ (blue) recordings. **(A)** Example of the location of stimulating electrode (red), recording electrode (yellow) and stimulating electrode of the independent control pathway (grey) along the Schaffer Collaterals. **(B)** Long-term potentiation (LTP) was induced at the Schaffer collaterals using a 100 Hz high-frequency stimulation (HFS) protocol and recorded in area CA1 using a microelectrode array (MEA) in mepβ$^{Cre;wt/wt}$ and mepβ$^{Cre;TG/wt}$ mice. Green dots represent the mepβ$^{Cre;wt/wt}$ recordings, blue dots represent mepβ$^{Cre;TG/wt}$ recordings and the grey dots represent the recordings taken from the independent control pathway. The graph shows mean +/- S.E.M. of the relative strength of potentiation of fEPSPs. Mepβ$^{Cre;wt/wt}$ n=7 slices from 6 mice. Mepβ$^{Cre;TG/wt}$ n = 7 slices from 4 mice. Control pathway n=6 slices from 5 mice. **(C)** Representative fEPSP traces from both mepβ$^{Cre;wt/wt}$ (green) and mepβ$^{Cre;TG/wt}$ (blue) genotypes, along with the traces from the independent control pathway (grey). The darker of each color shows fEPSPs before the 100Hz stimulation, the lighter of each color shows fEPSPs 60 minutes after the tetanic stimulation. **(D)** The relative strength of potentiation of the fEPSPs recorded at 50 to 60 minutes after the 100Hz stimulation shows that the mepβ$^{Cre;TG/wt}$ genotype has a significantly lower LTP than mepβ$^{Cre;wt/wt}$, as well as revealing no significant difference compared to the independent control pathway (p = 0.05). Statistical analysis using one-way ANOVA with post-hoc Tukey's multiple comparisons test. Graph shows mean +/- S.E.M.

4.1.5 Glutamatergic Receptor Expression at the Synapse is not Altered in Meprin β Overexpressing Animals

Glutamatergic signaling is central to excitatory neurotransmission and LTP, the cellular correlate of learning and memory. Meprin β commonly exhibits peak activity on the outer cellular membrane of the cell and in its soluble form, within the ECM (Arolas et al., 2012; Huguenin et al., 2008). Accordingly, we focused on membrane-bound key mediators in synaptic transmission to explain the observed effects. The two main regulators of synaptic excitatory transmission are the glutamatergic receptors, NMDA and AMPA. While NMDA receptors are required for LTP establishment, AMPA receptors are responsible for baseline synaptic transmission. Both receptors were examined by SDS PAGE and Western blotting to explore the potential variability in receptor expression between wild-type and meprin β-overexpressing mice, which might contribute to the establishment of cognitive impairment.

For a more accurate assessment of these receptors, we isolated and enriched synaptic proteins. We focused on the synaptosome fraction due to enriched membrane-bound synaptic proteins (Figure 12). To prove that synaptic proteins were enriched, the brain lysates before and after enrichment were analyzed using Western blotting. Figure 12 shows clearly that the synaptosome fraction had a significantly higher expression for NMDAR2a and NMDAR2b compared to non-synaptosome-enriched brain lysates, which was also underlined by densitometric analysis. The synaptosome isolation process involved dissecting the hippocampus and cortex and performing gradient centrifugation, resulting in the isolation of the cytosolic (S2) and synaptosome fractions (Figure 11A).

Next, we assessed levels of several different NMDA receptor subunits and the AMPA receptor. Western blot analysis revealed no significant differences in the expression levels of NMDA receptor subunits 1A, 2A, or 2B within this fraction (Figures 11B & 11C – data were collected in collaboration with Dayan Taghighah).

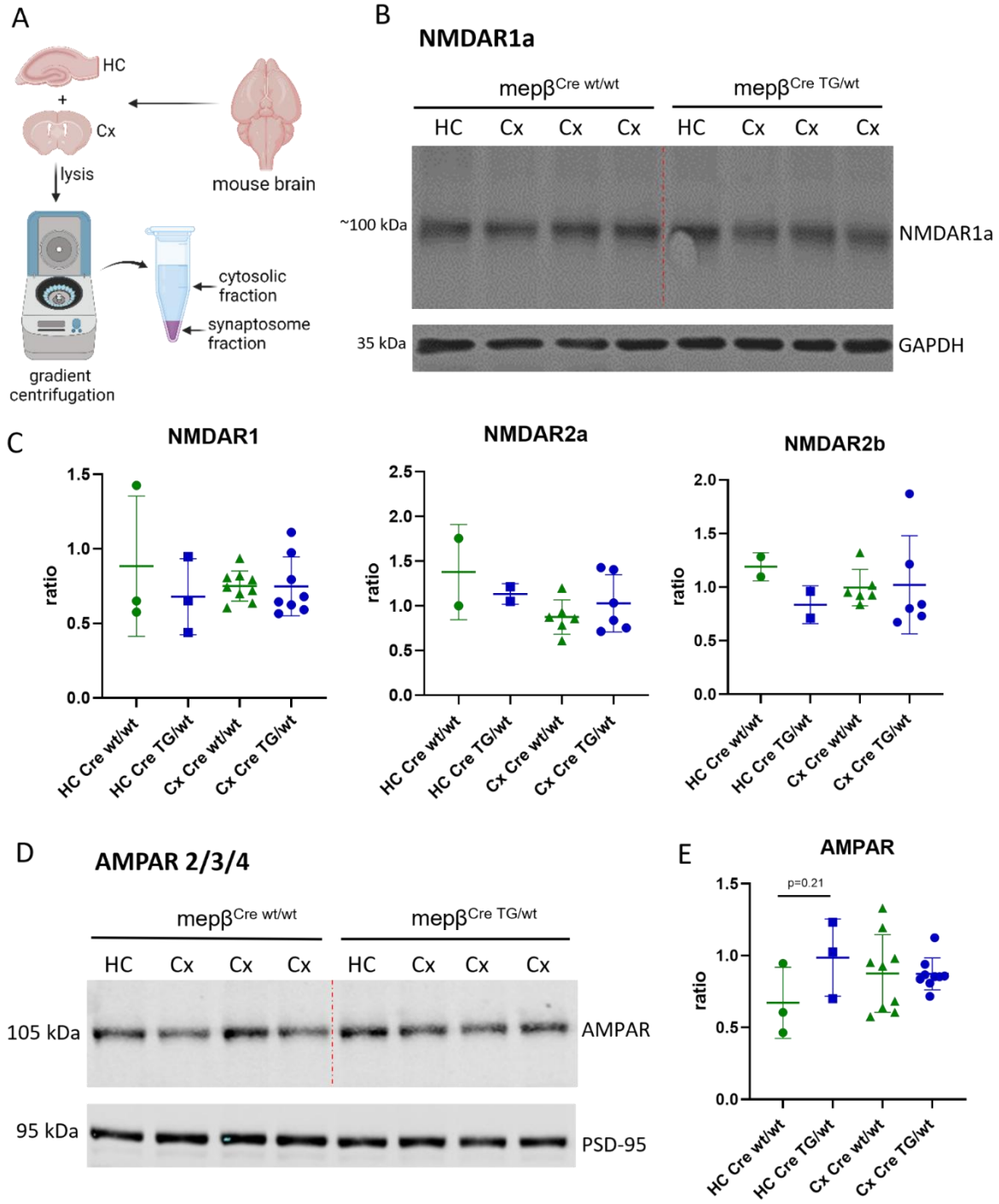

Figure 11 - Meprin β overexpression has no effect on NMDA- or AMPA-receptor expression at cortical or hippocampal synapses. Due to low yield in isolating the hippocampal synaptosome fraction, samples from two to three animals of the same genotype were pooled. Thus, each data point for the hippocampus represents multiple animals. For statistical analysis unpaired Student's t-test was used. **(A)** Schematic overview of the synaptosome isolation of the murine cortex and hippocampus. We used nine mice in three independent

experiments that were normalized to GAPDH. All animals used for Western analysis were 8 months of age. **(B)** Western blot targeting NMDAR subunit 1 and GAPDH for normalization. The dotted red line separates the mepβ$^{Cre;wt/wt}$ from the transgenic mepβ$^{Cre;TG/wt}$ samples. **(C)** Densitometric quantification of three different experiments using different animals. The respective subunit was normalized to GAPDH. **(D)** Representative Western blot of AMPA receptor subunits 2/3/4 and PSD-95 for normalization. The dotted red line separates mepβ$^{Cre;wt/wt}$ from mepβ$^{Cre;TG/wt}$ animals. **(E)** Densitometric quantification of three different experiments using different animals, normalized to PSD-95.

After examining the NMDA receptor subunits, we shifted our focus to the AMPA receptor, as it also plays an important role in learning and memory. Similar to the NMDA receptor, there was no difference in expression of the AMPA receptor between mepβ$^{Cre;wt/wt}$ mice and meprin β-overexpressing animals. A quantification across three independent experiments, each with distinct animal samples, did not reveal any statistically significant changes (Figure 11D&E – data were collected in collaboration with Dayan Taghighah). We observe a tendency towards a higher expression of the AMPA receptor in meprin β-overexpressing animals. However, this data indicates that the behavioral and electrophysiological effects of meprin β are not likely mediated by changes in NMDA or AMPA receptor expression. Instead, perhaps a more subtle synaptic alteration is responsible for the observed phenotype.

After establishing that the overall levels of glutamatergic receptors at the synapse remained unchanged, we next aimed to determine their more detailed subcellular localization. To this end, we employed a surface biotinylation assay. Synaptic surface proteins were biotinylated at 4 °C to prevent endocytosis, then cells were washed and surface-biotinylated proteins were compared with total protein levels (Figure 13).

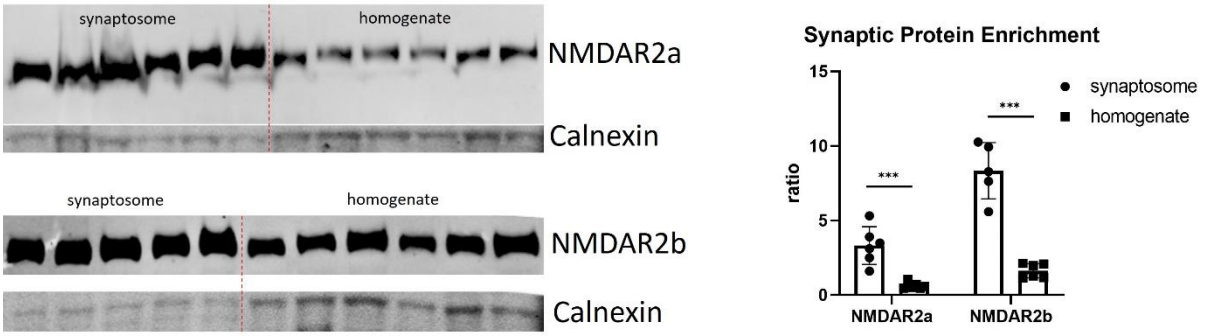

Figure 12 - Enrichment of synaptic proteins. The brains of mice were dissected into the cortex and hippocampus and homogenized. To address synaptic proteins more clearly, synaptic proteins were enriched using the Syn-PER extractions reagent as recommended by the manufacturer. Western blotting confirmed an enrichment of synaptic proteins (represented are NMDAR2a and NMDAR2b receptor subunits). Also, densitometric analysis revealed a clear enrichment after isolation with the Syn-PER reagent.

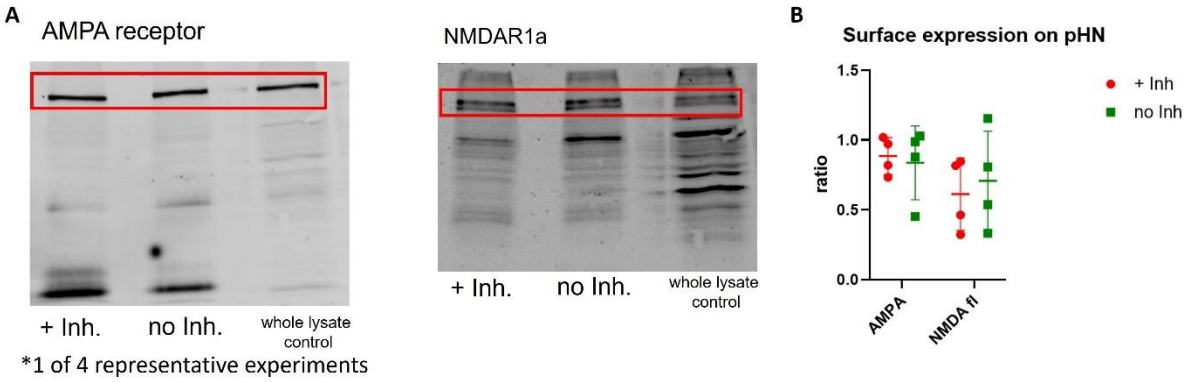

Figure 13 - Biotinalytion assay of glutamatergic receptors. Primary hippocampal neurons were extracted from P1 mice. For 72 hours, we inhibited the cells with meprin β inhibitor actinonin (final concentration 15 µg/ml) prior to the biotinylation. Western blotting reveals no differences in neither the AMPA- nor the NMDA-receptor expression (red boxes) on the surface of primary hippocampal neurons **(A)**, which is also observed over all four experiments **(B)**.

Due to breeding constraints, we were unable to generate primary neuronal cultures from meprin β-overexpressing animals and therefore used wt hippocampal neurons in both experimental conditions. One set of wt neurons was treated with the meprin β inhibitor actinonin for three consecutive days (with fresh addition every 8 hours, final concentration 15 µg/ml). Our working hypothesis was that meprin β influences the trafficking of glutamatergic receptors to the neuronal surface. In this scenario, meprin β inhibition should increase receptor surface expression, whereas in *in vivo* conditions, the normal expression of meprin β would decrease glutamatergic receptor levels and therefore impair LTP.

As shown in Figure 13, no significant differences in surface expression of AMPA- nor NMDAR1a receptors were observed between untreated wt neurons and actinonin-treated neurons. These results suggest that meprin β does not affect the membrane trafficking of these receptor subtypes.

We further analyzed the internalization dynamics of these receptors. Surface proteins were biotinylated at 4 °C and subsequently allowed to internalize during re-incubation at 37 °C. Samples were collected at defined time points, after which residual surface proteins were stripped to ensure that only internalized receptors retained biotin labeling. Western blot analysis demonstrated that AMPARs presumably undergo more rapid internalization than NMDAR1a receptors (Figure 14). For AMPARs, internalization reached near-maximal levels within 15 min, with no substantial increase detected up to 60 min (Figure 14A). In contrast,

NMDAR1a internalization continued to progress between 15 and 60 min, indicating a slower internalization rate compared to AMPARs (Figure 14B).

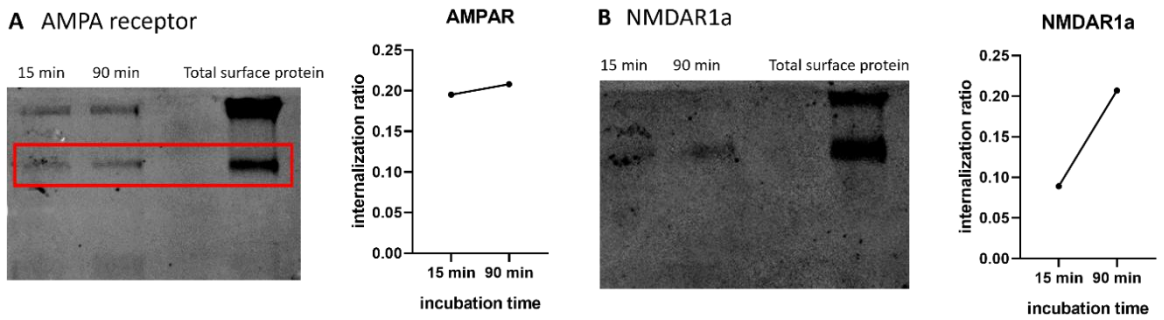

Figure 14 – Internalization dynamics of glutamatergic receptors. Primary hippocampal neurons were surface-biotinylated and re-incubated at 37 °C to allow receptor internalization. AMPARs **(A)** exhibited faster internalization than NMDAR1a **(B)**, reaching near-60 min levels within 15 min. For quantification, band intensities at 15 min and 60 min were normalized to the total surface protein expression of hippocampal neurons.

4.1.6 Assessment of IL6R, EAAT-2, and α-neurexin-3 Expression in Meprin β–Overexpressing Mice

Given that the experimental model involves overexpression of meprin β, a protease known to shed the interleukin-6 receptor (IL6R) (Arnold et al., 2017), we next focused on IL6R together with other proteins implicated in synaptic plasticity. In particular, EAAT-2, the main astrocytic glutamate transporter, is critical for maintaining extracellular glutamate homeostasis and preventing excitotoxicity (Kim et al., 2011), while α-neurexin-3 contributes to synapse organization and the regulation of excitatory transmission (Zhang et al., 2022). Together, these proteins provide a more complete perspective on how protease activity might influence neuroinflammatory signaling and plasticity-related processes. In our initial Western blot analyses, we did not detect consistent expression differences for α-neurexin-3 or IL6R (Figure 15). EAAT-2, however, exhibited considerable variability across animals, particularly in the cortex when comparing wild-type and meprin β-overexpressing groups. Moreover, preliminary data suggest lower EAAT-2 levels in the hippocampus of wild-type animals compared to meprin β overexpressors (Figure 15), though this observation is based on a single pooled sample and requires further validation.

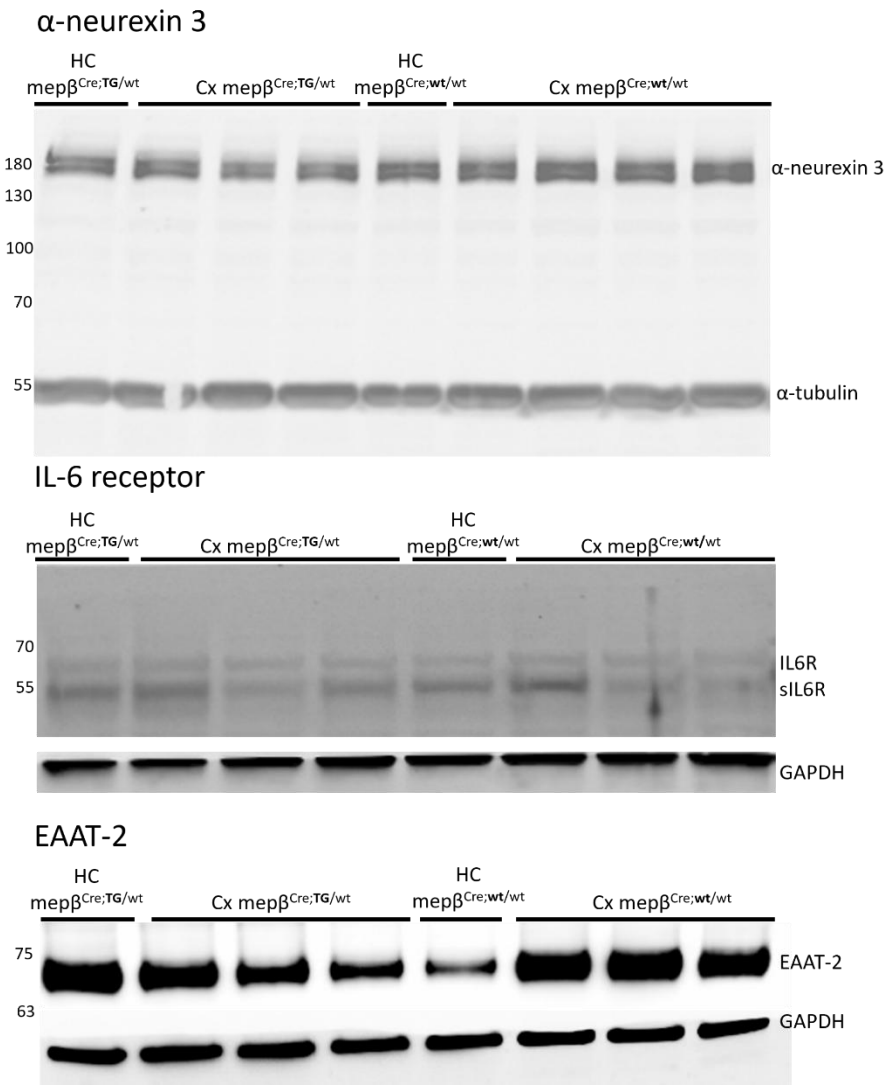

Figure 15 – Expression of further potential meprin β substrates. Western blots showing Neurexin-3 (~170 kDa), IL-6 receptor (soluble form ~55 kDa, membrane-bound form ~70 kDa), and EAAT-2 (~70 kDa). Molecular weight markers are indicated on the left for size reference. GAPDH (~37 kDa) and α-tubulin (~50 kDa) were used as loading controls and are shown below the respective blots.

4.1.7 Utilization of N-Terminomics for the Identification of Novel Substrates of Meprin β in the Murine Brain

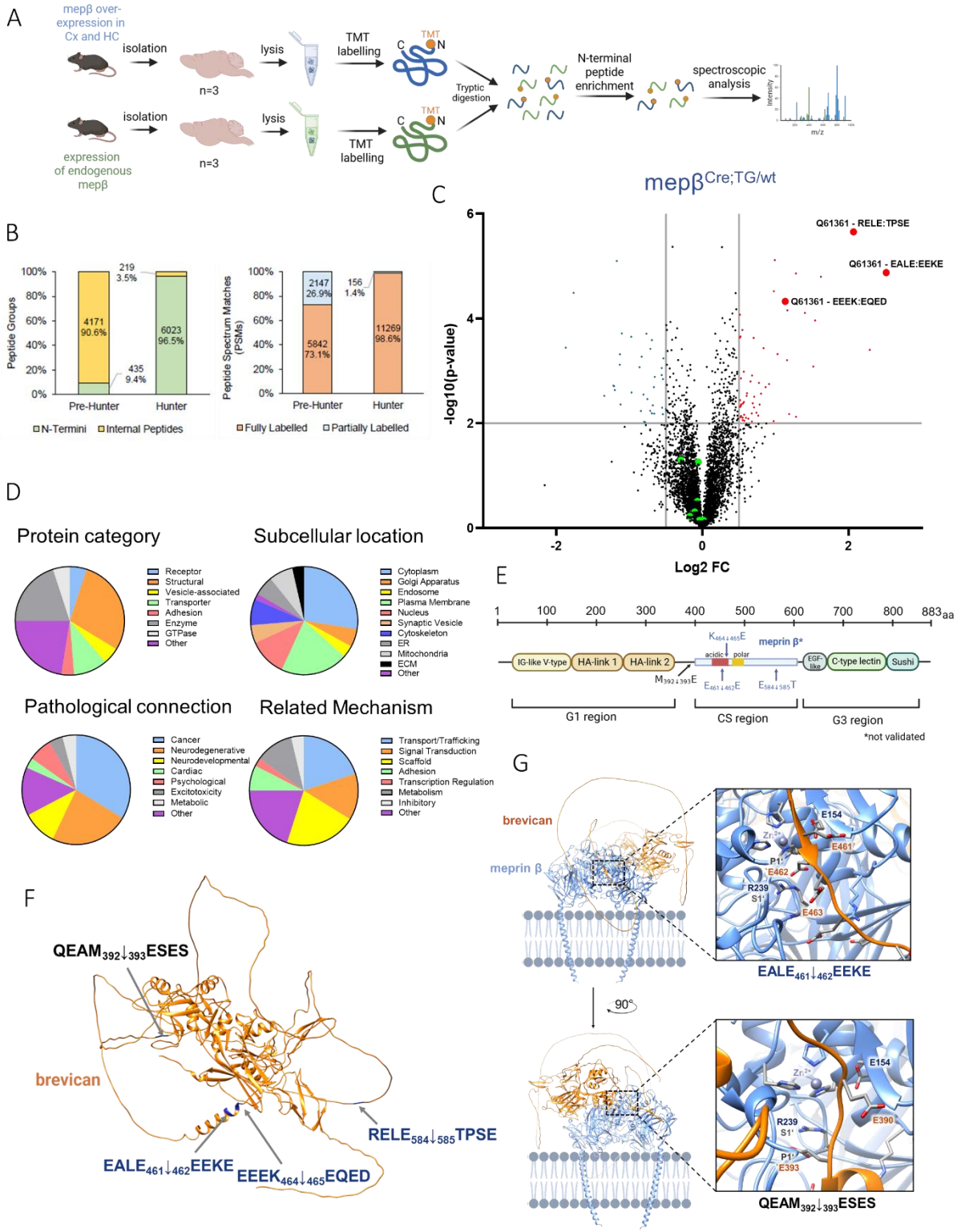

Figure 16 - Utilization of N-terminomics for the identification of novel substrates of meprin β within the brain. **(A)** Schematic overview of the N-terminomics process: N-terminal peptides were enriched using the TMT HUNTER protocol before spectroscopic analysis (n=3). **(B)** Quantification of enriched peptides pre- and post-HUNTER. **(C)** Volcano plot visualization of potential substrates: red dots show the overrepresented peptides in meprin β-overexpressing brains, and the blue dots show the underrepresented peptides. The threshold was set at $\log_2$

(difference) = ±0.5 and $-\log_{10}$ (p-value) = 2. Additionally, depicted are the P4-P4' amino acid residues surrounding the N-terminal cleavage site of the respective brevican peptide. The green dots in the center represent the detected peptides of NMDA and AMPA receptor subunits, confirming the absence of overrepresentation, consistent with the results from Western blotting experiments. **(D)** Categorization of obtained overrepresented peptides in different functional areas for visual overview. **(E)** Schematic overview of murine brevican and potential cleavage sites indicated by blue arrows as predicted by N-terminomics analysis. With a black arrow, an additional potential cleavage site by meprin β based on alpha fold modeling (G) is shown. **(F)** Predicted protein structure of brevican generated with AlphaFold 3 (Abramson et al., 2024) using the UniProt Consortium 2021 sequence (ID: Q61361) and illustrated with UCSF Chimera. Cleavage sites identified for meprin β by N-terminomics are labeled in blue, additional potential cleavage site is labeled in black. **(G)** Predicted structure of brevican (uniprot ID: Q61361) together with meprin β homodimer (uniprot ID: Q61361) generated with AlphaFold 3 using the UniProt Consortium 2021 sequence and illustrated with UCSF Chimera. The cleavage site E461↓E462 within brevican, identified by N-terminomics for meprin β, nicely fits into the first active site of the meprin β homodimer. The second active site aligns with the sequence QEAM392↓393ESES, suggesting a potential additional cleavage by meprin β at this site.

Our investigations into meprin β overexpression in cortical and hippocampal neurons led us to hypothesize that additional substrates for meprin β may exist in the brain, influencing learning and memory. To address mechanisms affected by meprin β processing and identify additional substrates, we employed N-terminomics using HUNTER analysis on brain lysates from meprin β-overexpressing and respective Cre-negative control animals (Figure 16A). A key benefit of this method is that it enables the enrichment of N-terminally truncated peptides from minimal sample quantities, allowing for a robust, sensitive, and scalable analysis. The HUNTER approach identified substantially more peptides than pre-HUNTER analysis, demonstrating the effectiveness of N-terminal peptide enrichment prior to MS analysis (Figure 16B). Using this approach, we discovered a set of N-terminal peptides that are significantly increased in meprin β-overexpressing animals (Figure 16C – red dots). Criteria for significant overrepresentation were defined as $-\log_{10} = 3$ (p-value) and $\log_2 = \pm 0.5$ (expression difference) (Figure 16C).

We observed particularly high enrichment values for brevican (Q61361), aligning with observations in astrocytes reported by Armbrust et al. (2025). Brevican is long known to affect synaptic plasticity (Brakebusch et al., 2002). Additionally, the cleavage site of the discovered overrepresented brevican peptides aligns well with the established meprin β cleavage motif (Schäffler et al., 2019) as meprin β prefers negatively charged residues, such as aspartate (D) and glutamate (E), at the P1 and P1’ positions. Given brevican's established involvement in LTP, this protein emerges as a potential proteolytic substrate for meprin β, supporting the observed behavioral and electrophysiological results.

Following the categorization of overrepresented peptides in meprin β-overexpressing animals, we observed a marked increase in potential substrates associated with the scaffolding of the cell (Figure 16D, 'protein category' - orange), the plasma membrane (Figure 16D, 'subcellular location' - green), influence in neurological pathologies (Figure 16D, 'pathological connection' - orange/yellow/red) and the scaffolding mechanism (Figure 16D, 'mechanism' – yellow). Additionally, NMDA- and AMPA-receptor subunits showed no significant overrepresentation nor underrepresentation in meprin β-overexpressing mice, further suggesting that both receptors play no substantial role in meprin β processing as indicated by Western blot analysis (Figure 16C – green dots).

N-terminomics analysis revealed multiple brevican peptides overrepresented in meprin β-overexpressing animals. Brevican is a dumbbell-shaped molecule comprising N-terminal (G1) and C-terminal (G3) domains, separated by a polar, negatively charged central spacer (Figure 16E). This spacer contains chondroitin sulfate (CS) attachment sites and meprin β cleavage sites identified by N-terminomics (indicated by blue arrows) (Figure 16E, F). Utilizing AlphaFold 3 (Abramson et al., 2024) and the UniProt Consortium 2021 sequence, we modeled brevican (ID: Q61361) with a meprin β homodimer (ID: Q61361) (Figure 16G). The cleavage site E461$_{\downarrow}$E462 within brevican, identified by N-terminomics for meprin β, aligns with the first active site of the meprin β homodimer, supporting our experimental N-terminomics data. The additional cleavage site at K464$_{\downarrow}$E465, in proximity, suggests that meprin β may shift the cleavage site by three amino acids or that cleavage at K464$_{\downarrow}$E465 occurs following initial cleavage at E461$_{\downarrow}$E462. The second active site aligns with the sequence QEAM392$_{\downarrow}$393ESES, indicating a potential additional cleavage by meprin β at this site. The absence of this cleavage site in the N-terminomics data could be due to methodological limitations or further downstream processing of brevican cleavage products by other proteases like ADAMTS4. Additionally, N-terminomics identified cleavage at E584$_{\downarrow}$T585. Although our AlphaFold modeling lacks validation for this site, it is considered probable, as it aligns with the cleavage preference of meprin β (Schäffler et al., 2019) and is likely accessible based on the predicted structure. However, our AlphaFold modeling does not account for glycosylation, which may impact accessibility and proteolytic processing by meprin β.

4.1.8 Meprin β Influence on PNN Proteins Brevican and Neurocan

The identification of brevican in the N-terminomics analysis of potential meprin β substrates provides a plausible explanation for the phenotype observed in transgenic meprin β-overexpressing mice. To assess the possibility of brevican proteolysis in meprin β-overexpressing animals, as well as potential accumulation in the absence of meprin β, we analyzed hippocampal and cortical samples from wild-type ($mep\beta^{Cre;wt/wt}$), meprin β knockout ($mep\beta^{KO/KO}$), and meprin β-overexpressing ($mep\beta^{Cre;TG/wt}$) mice using Western blotting (Figure 17). Given that brevican is an extracellular matrix protein, we examined the soluble "s2" fraction from the synaptosome isolation procedure to determine brevican levels. Our results revealed reduced brevican levels in $mep\beta^{Cre;TG/wt}$ mice, whereas no significant differences were detected between $mep\beta^{Cre;wt/wt}$ and $mep\beta^{KO/KO}$ mice, indicating that brevican does not accumulate in the absence of meprin β. Consistently, the same reduction in protein levels was observed in both cortex and hippocampus (Figure 17A&B).

The observation that we have no accumulation of brevican in meprin β KO brains can be attributed to the presence of alternative proteolytic enzymes capable of processing brevican. Notably, members of the ADAMTS (A Disintegrin and Metalloproteinase with Thrombospondin Motifs) family, such as ADAMTS4 and ADAMTS5, have been identified as key brevican-degrading enzymes (Nakamura et al., 2000). Studies have shown that these proteases can cleave brevican at specific sites, contributing to its turnover in the ECM. Furthermore, research indicates that in the context of spinal cord injury, the proteolysis of brevican is not significantly altered in ADAMTS4 or ADAMTS5 KO mice, suggesting compensatory mechanisms by other proteases (Stanton et al., 2011). These findings support the notion that brevican degradation is mediated by a network of proteolytic enzymes, ensuring its regulation even in the absence of meprin β.

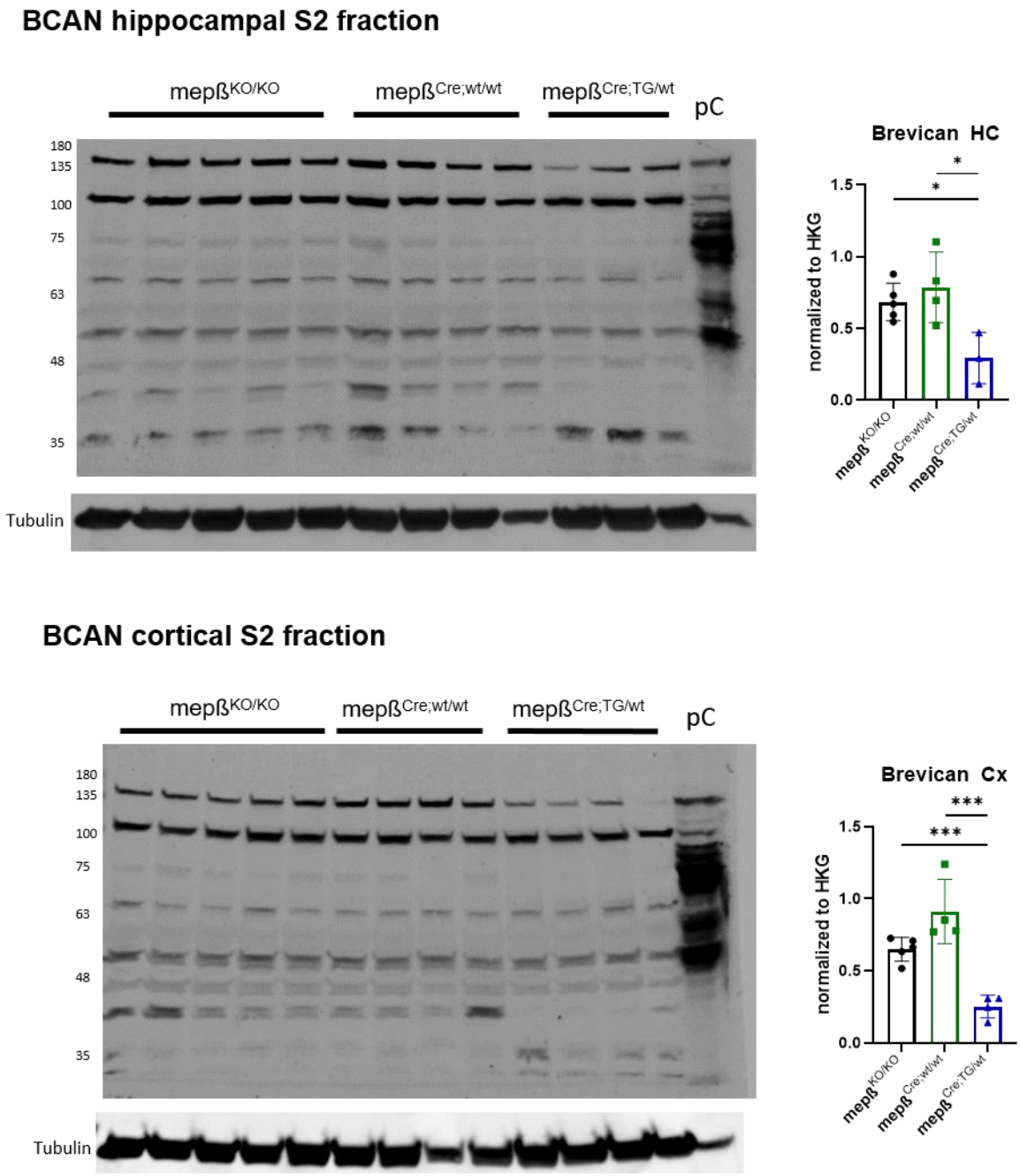

Figure 17 - Western blotting of brevican in the cytosolic fraction (S2) of cortical and hippocampal brain lysates, normalized to tubulin. pC; positive control (A) Western blot of hippocampal brain lysates. Different genotypes are indicated by horizontal bars: meprin KO (mepβ$^{KO/KO}$), wild-type (mepβ$^{Cre;wt/wt}$) and meprin β-overexpressing (mepβ$^{Cre;TG/wt}$) animals. On the right side, the densitometric quantification of detected brevican bands was conducted. We can see significant differences in brevican levels between wild-type & KO animals compared to meprin β-overexpressing brain lysates. **(B)** Western blot of cortical brain lysates. Different genotypes are indicated by horizontal bars: meprin KO (mepβ$^{KO/KO}$), wild-type (mepβ$^{Cre;wt/wt}$) and meprin β-overexpressing (mepβ$^{Cre;TG/wt}$) animals. On the right side, the densitometric quantification of detected brevican bands was conducted. We can see significant differences in brevican levels between wild-type & KO animals compared to meprin β-overexpressing brain lysates.

In addition to brevican, our N-terminomics analysis identified further extracellular matrix proteins associated with PNNs, including neurocan. While brevican remained the central focus of this study, we also performed initial investigations into neurocan, a related chondroitin sulfate proteoglycan and established PNN component. Our Western blot analyses revealed increased neurocan levels in meprin β-overexpressing (mepβ$^{Cre;TG/wt}$) animals, whereas wild-type (mepβ$^{Cre;wt/wt}$) and knockout (mepβ$^{KO/KO}$) mice displayed comparable expression. Interestingly, this expression pattern contrasted with that of brevican, which was reduced in meprin β-overexpressing brain lysates (Figure 18).

The observed increase in neurocan in meprin β-overexpressing animals may reflect broader alterations in extracellular matrix composition or stability induced by heightened meprin β activity. Given neurocan's reported roles in synaptic plasticity and memory regulation (Müller-Bühl et al., 2025), its upregulation could contribute to remodeling of PNNs in these mice, potentially compensating for or counterbalancing the reduction of brevican. Nevertheless, these findings should be considered preliminary and require further validation.

It is important to note that no positive control was available for neurocan detection, as we lacked access to a plasmid encoding neurocan and were therefore unable to generate an overexpression control in cell culture. Moreover, due to neurocan's large isoforms (~120–130 kDa and >200 kDa) and extensive posttranslational modifications, including glycosylation and proteolytic processing, multiple bands were detected within the relevant molecular weight range. To maintain consistency and avoid potential misinterpretation, we quantified only the upper band, which we interpret as representing the undigested, full-length protein. Lower bands likely reflect processed forms of neurocan, consistent with prior reports (Rauch et al., 1992).

Together, these experiments highlight distinct regulatory effects of meprin β on two major PNN components, brevican and neurocan, suggesting that meprin β overexpression may influence PNN organization through multiple molecular pathways.

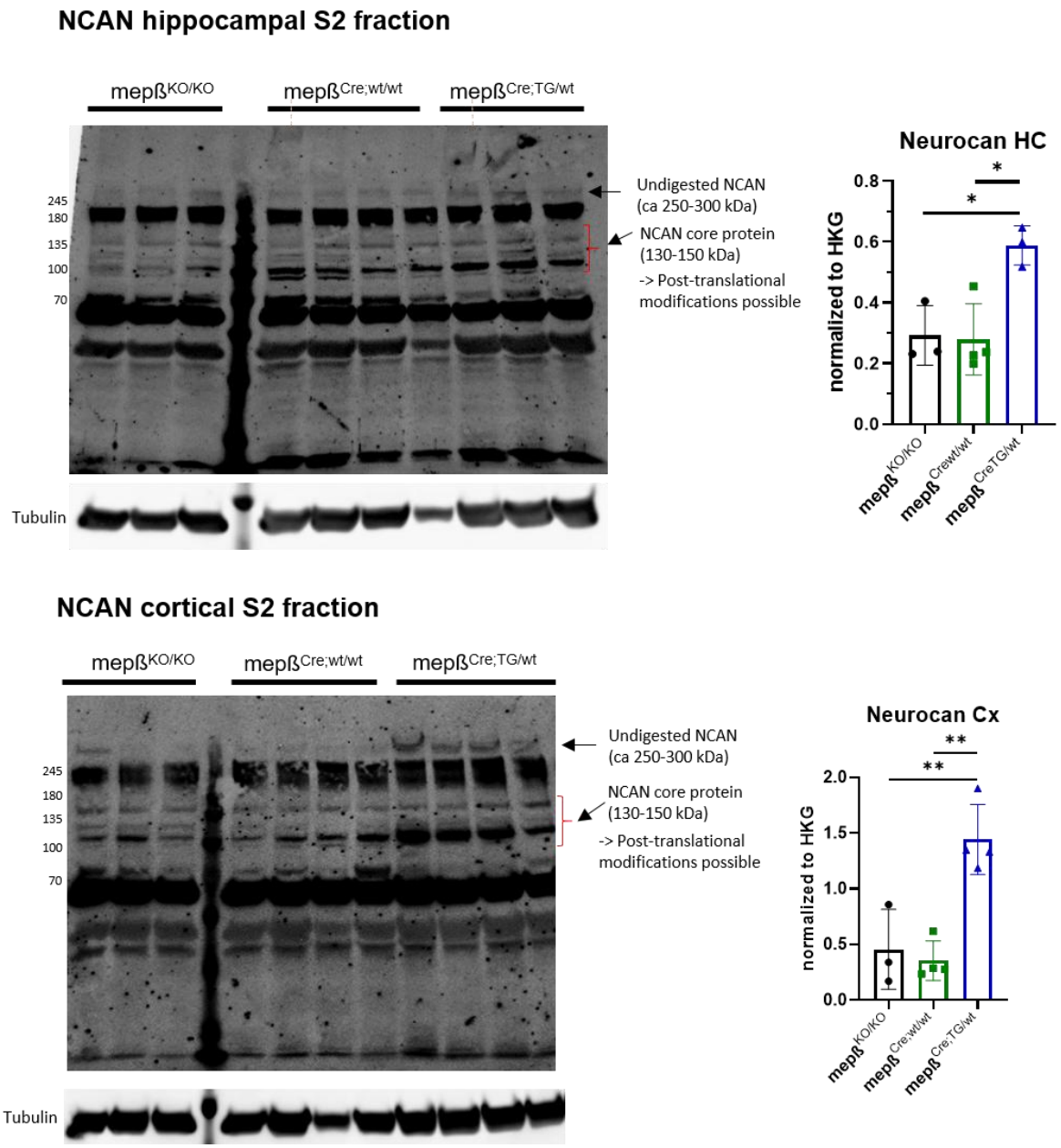

Figure 18 - Western blot analysis of neurocan in the cytosolic fraction (S2) of cortical and hippocampal brain lysates, normalized to tubulin. Please note that no positive control was available for these experiments. **(A)** Western blot of hippocampal brain lysates from animals of different genotypes: meprin β knockout (mepβ$^{KO/KO}$), wild-type (mepβ$^{Cre;wt/wt}$) and meprin β-overexpressing (mepβ$^{Cre;TG/wt}$). Densitometric quantification of neurocan bands is shown on the right. Increased neurocan levels are observed in meprin β overexpressing animals compared to both wild-type and meprin β KO mice. **(B)** Western blot of cortical brain lysates from the same genotypes. Quantification on the right similarly shows elevated neurocan levels in the meprin β-overexpressing group, suggesting altered regulation of neurocan expression.

4.1.9 Meprin β-Overexpressing Mice Display a Higher Hippocampal Network Excitability than Mepβ$^{Cre;wt/wt}$ Mice

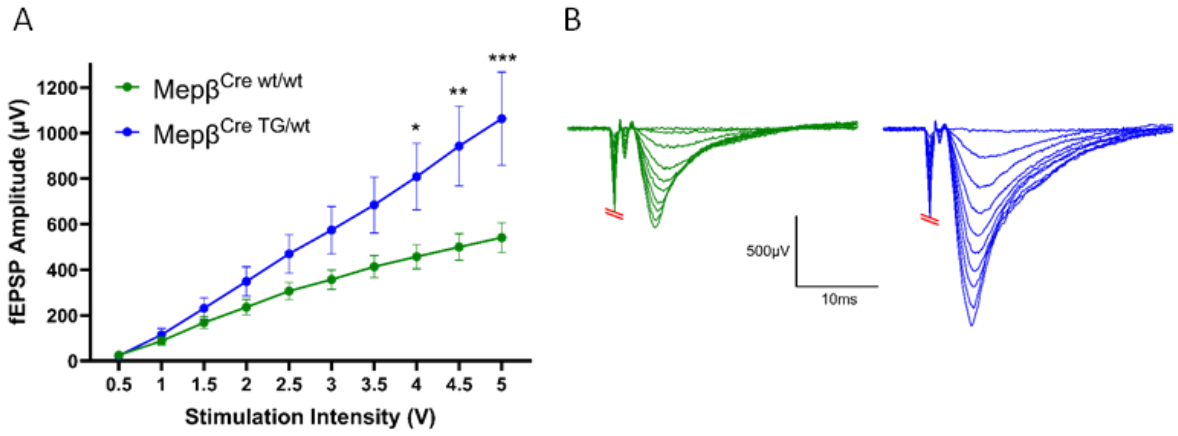

Figure 19 - Meprin β-overexpressing mice display a significantly higher evoked network activity than mepβ$^{Cre;wt/wt}$ mice. (A) Multi-Electrode Array (MEA) recordings displaying input/output (I/O) curves with the stimulation input ranging from 0.5V to 5V in 0.5V steps. The output was recorded as field excitatory postsynaptic potentials (fEPSPs). Statistical analysis using two-way ANOVA with post-hoc Šídák's multiple comparisons test. Graph shows mean +/- S.E.M. Mepβ$^{Cre;wt/wt}$ n = 10 slices from 4 mice. mepβ$^{Cre;TG/wt}$ n = 9 slices from 4 mice. p = 0.05. (**B)** Representative fEPSP traces were recorded from the gradually increasing stimulus intensity from the I/O curve for mepβ$^{Cre;wt/wt}$ (green) and mepβ$^{Cre;TG/wt}$ (blue) mice.

As changes in the brain ECM have been documented to influence AMPAR-dependent excitability, we next investigated whether an overexpression of meprin β in the mouse hippocampus affects the AMPAR-dependent excitability of the hippocampal neuronal network. We performed electrophysiological recordings of acute hippocampal slices by use of the MEA in the mepβ$^{Cre;TG/wt}$ and mepβ$^{Cre;wt/wt}$ mice. A series of electrical stimulations ranging from 0.5V to 5V, with step increases of 0.5V, was applied to one electrode of the MEA located below the Schaffer collaterals in the CA3 region of the brain slice. The resulting extracellular fEPSPs were recorded with the MEA electrode below the target region in CA1. The amplitude of these fEPSP signals allowed us to determine the excitability in the CA3 to CA1 signaling pathway.

Interestingly, the amplitude of the fEPSPs obtained from the mepβ$^{Cre;TG/wt}$ mice was significantly larger than those from mepβ$^{Cre;wt/wt}$ mice at stimulation intensities from 4V through to 5V (Figure 19A). Representative fEPSP traces with overlaid outputs from the input/output curve can be seen in Figure 19B.

4.1.10 Hippocampal Paired-Pulse Ratio is Unaffected by Meprin β Overexpression

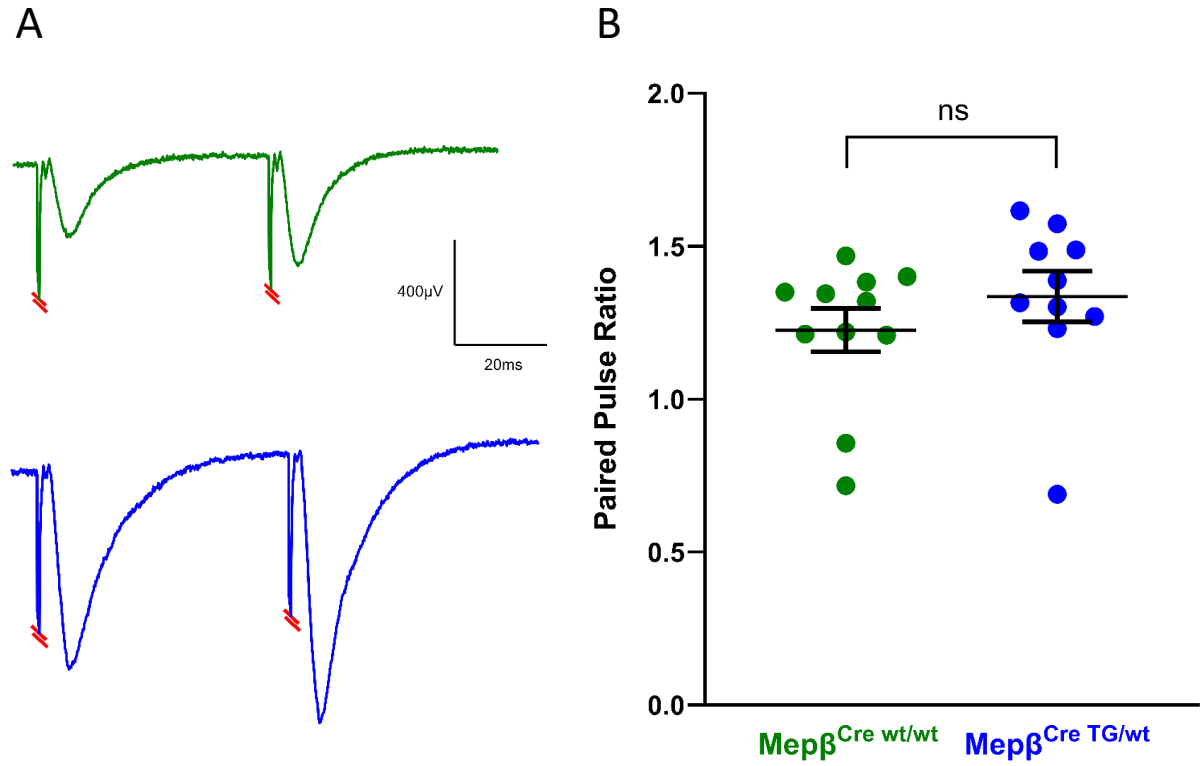

Figure 20 - Hippocampal Paired-Pulse Ratio is unaffected by meprin β overexpression. (A) Representative evoked fEPSPs from a paired-pulse stimulus in wild-type mepβ$^{Cre;wt/wt}$ (green) and mepβ$^{Cre;TG/wt}$ (blue) with a 50 ms interstimulus interval (ISI). **(B)** Analysis (unpaired t-test) of the ratio of the second evoked fEPSP to the first evoked fEPSP showing no difference between genotypes.

To further investigate whether the synaptic alterations observed in our model arise from pre- or postsynaptic mechanisms, we performed paired-pulse ratio (PPR) recordings in both wild-type and transgenic animals. The PPR is a classic electrophysiological approach to probe presynaptic release probability. In this paradigm, two stimuli are applied to the same afferent pathway in quick succession (interstimulus interval - ISI), and the amplitudes of the two corresponding postsynaptic responses are compared (Figure 20A). If the probability of neurotransmitter release at the presynaptic terminal is high, the readily releasable vesicle pool is more likely to be depleted by the first stimulus, resulting in a reduced second response (paired-pulse depression). Conversely, if release probability is low, the second response is often facilitated relative to the first, as residual calcium in the terminal enhances transmitter release (paired-pulse facilitation). The ratio between the first and second response amplitudes, therefore, serves as an indirect but reliable indicator of presynaptic release dynamics. By applying this measure, we sought to clarify whether the differences we observe at the synapse

originate primarily from presynaptic changes in release probability or whether they are instead mediated postsynaptically.

Our results showed no significant difference in PPR between wild-type and transgenic animals (Figure 20B). We concluded that overexpression of meprin β in the mouse hippocampus significantly increased neuronal network excitability between CA3 and CA1, and these changes are likely due to changes in brevican expression and alterations at the postsynapse. This interpretation integrates well with our broader dataset and working hypothesis, even though NMDA and AMPA levels did not change.

4.2 Part II:

Meprin β Elevates Hippocampal Soluble Aβ in an APP/V717I Mouse Model

4.2.1 Generation of the Mepβ$^{Cre;TG/wt}$ × APP/Ld Mouse Model

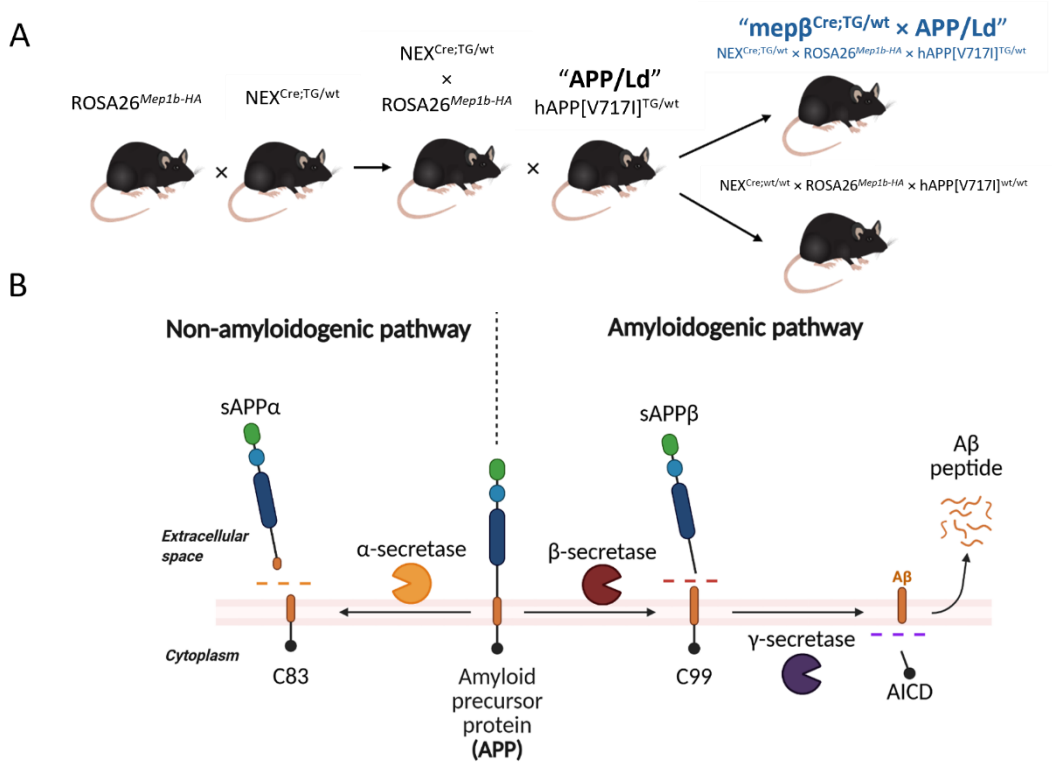

Figure 21 - Generation of a novel AD-mouse model overexpressing meprin β in cortical and hippocampal neurons. (A) Homozygous transgenic ROSA26$^{Mep1b-HA}$ mice were crossed with heterozygous NEX^{Cre} mice, yielding NEX$^{Cre;TG/wt}$ × ROSA26$^{Mep1b-HA}$ (mepβ$^{Cre;TG/wt}$) offspring. Double-transgenic mepβ$^{Cre;TG/wt}$ animals were crossed with hAPP[V717I]$^{TG/wt}$ (APP/Ld) animals, resulting in the triple-transgenic novel animal model NEX$^{Cre;TG/wt}$ × ROSA26$^{Mep1b-HA}$ × hAPP[V717I]$^{TG/wt}$ (mepβ$^{Cre;TG/wt}$ × APP/Ld). **(B)** Schematic depiction of the non-amyloidogenic and the amyloidogenic pathway. sAPPα is a product of the non-amyloidogenic pathway, whereas sAPPβ is a product of the amyloidogenic pathway.

To generate a novel AD mouse model, we crossed mice overexpressing meprin β with mice expressing human transgenic amyloid precursor protein (APP). Since we wanted to specifically investigate the function of meprin β, without influencing β-secretase cleavage, we deliberately refrained from mutating our animal model at the β cleavage site. Instead, we opted for the APP/Ld model, in which the mutation is located at the γ-cleavage site (V717I) (Tanghe et al., 2010). Furthermore, to demonstrate the specificity of meprin β on the β-secretase cleavage side, we additionally could not use any mouse model carrying the Swedish mutation, as the Swedish mutation in APP results in a higher affinity towards BACE1, simultaneously suppressing the cleavage activity of meprin β (Schönherr et al., 2016).

For targeted neuronal overexpression, we utilized the NEX-Cre mouse model, which was previously described. These NEX-Cre mice were crossed with previously characterized meprin β knock-in mice. The knock-in was created by integrating murine meprin β cDNA into the STOP-EGFP-ROSA-CAG targeting vector at the Rosa26 locus in embryonic stem cells via homologous recombination. The resulting mice selectively overexpressed meprin β in neurons of regions critical for learning and memory, notably the hippocampus and cortex—areas first affected in AD pathology. To further confirm the functional role, we bred the meprin β-overexpressing mice into the APP/Ld (V717I) AD mouse model. This cross yielded triple-transgenic animals ($NEX^{Cre;wt/wt}$ × $ROSA26^{Mep1b\text{-}HA}$ × $hAPP[V717I]^{TG/wt}$, abbreviated as $mep\beta^{Cre;TG/wt}$ × APP/Ld), allowing for detailed investigation of amyloidogenic pathway dynamics (Figure 21A).

An increased level of Aβ peptides typically correlates with elevated sAPPβ, a cleavage product generated via the amyloidogenic pathway. Previously, we reported that in mice overexpressing meprin β, significantly elevated levels of sAPPβ are observed, indicating a functional role of meprin β (Dissertation of Liana Marengo). For this analysis, we used a specific antibody that detects specifically only meprin β-cleaved sAPPβ. As meprin β truncates Aβ N-terminally at P2, it leaves an additional amino acid at the C-terminus of sAPPβ, which is recognized by this antibody. In contrast, APP/Ld animals exhibited significantly higher levels of sAPPα, reflecting a preferential non-amyloidogenic APP-processing. The shift toward increased sAPPβ production in $mep\beta^{Cre;TG/wt}$ × APP/Ld animals demonstrates enhanced proteolytic activity of meprin β toward APP, leading to greater amyloidogenic pathway activation and higher Aβ production, as illustrated in the Dissertation of Liana Marengo.

4.2.2 Elevated Aβ 1-40/42 Levels in the Hippocampus of Mepβ$^{Cre;TG/wt}$ × APP/Ld Animals

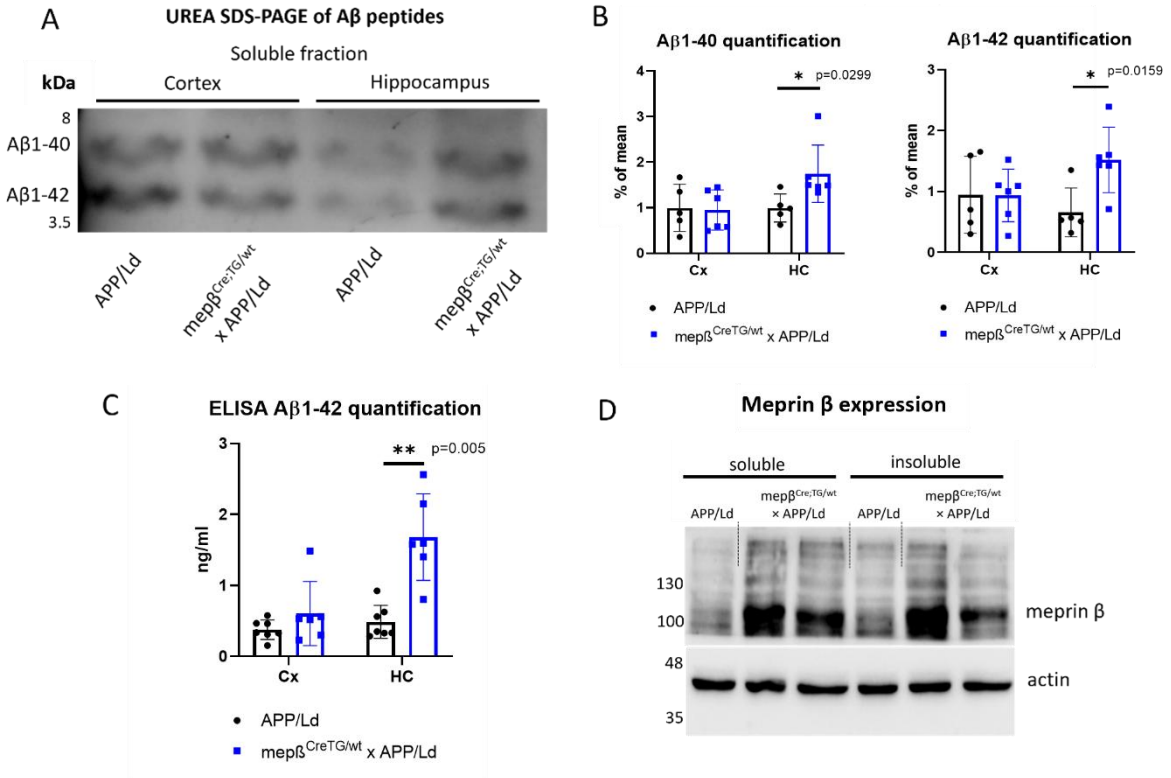

Figure 22 - Meprin β-overexpressing animals show elevated levels of soluble Aβ in the hippocampus. (A) UREA SDS-PAGE and subsequent Western blotting of cortical and hippocampal brain lysates show elevated levels of Aβ1-40 and Aβ1-42 in mepβ$^{Cre;TG/wt}$ × APP/Ld in the hippocampus compared to APP/Ld mice. **(B)** Densitometric quantification of five different experiments showed a significant increase in soluble Aβ1-40 and Aβ1-42 in hippocampal but not cortical neurons between mepβ$^{Cre;TG/wt}$ × APP/Ld and APP/Ld mice (unpaired t-test, n=5/6). **(C)** ELISA analysis showed increased levels of Aβ1–42 (***$p < 0.005$, *t*-test, $n = 6/7$) in soluble fractions of mepβ$^{Cre;TG/wt}$ × APP/Ld mice compared to APP/Ld mice. **(D)** Western blot of meprin β in APP/Ld and triple transgenic mepβ$^{Cre;TG/wt}$ × APP/Ld animals in the soluble and insoluble fractions of the brain. A stronger band intensity can be observed for meprin β-overexpressing animals in the soluble and membrane-bound fraction.

To evaluate the impact of meprin β overexpression in the APP/Ld mouse model, we quantified Aβ levels in the hippocampus and cortex and compared our novel mepβ$^{Cre;TG/wt}$ × APP/Ld with the APP/Ld model. Brains were isolated from 14-month-old animals, and the hippocampus and cortex were dissected separately. Using high-speed ultracentrifugation, we separated soluble fractions from insoluble components. Since we were interested in early disease pathology, our focus was on the soluble fraction. Insoluble components were only processed to check for membrane-bound meprin β.

Aβ levels in the soluble fraction were immunoprecipitated and analyzed using Urea SDS-PAGE, a technique suitable for detecting subtle differences in molecular weight of peptides such as Aβ1-40 and Aβ1-42. Figure 22A provides a representative blot illustrating soluble brain lysates

from APP/Ld and mepβ$^{Cre;TG/wt}$ × APP/Ld animals. In the hippocampus, we observed elevated levels of Aβ1-40/42, whereas no significant differences were detected in the cortex.

Quantitative densitometric analysis across 5 and 6 replicates (APP/Ld and mepβ$^{Cre;TG/wt}$ × APP/Ld groups, respectively) confirmed a significant increase in Aβ1-40/42 levels (Figure 22B) specifically in the hippocampus. Subsequently, Aβ1-42-specific ELISA confirmed the increased soluble Aβ1-42 levels in the hippocampus, aligning with the Western blot results (Figure 22C). Together with the shift to elevated meprin β-specific sAPPβ levels (Dissertation of Liana Marengo), this effect is observed likely due to meprin β's non-canonical APP cleavage. Additionally, to validate meprin β overexpression in our mouse model, we analyzed meprin β expression levels and observed higher expression in mepβ$^{Cre;TG/wt}$ × APP/Ld compared to APP/Ld animals in the soluble and the membrane-bound fraction (Figure 22D).

In summary, our findings demonstrate a clear effect of meprin β overexpression on Aβ levels specifically in the hippocampus. Interestingly, the cortex did not exhibit increased Aβ levels, suggesting region-specific factors influencing protease activity, potentially reflecting differences in environmental or regulatory conditions between the hippocampus and cortex in a later stage of pathology.

4.2.3 Intraneuronal Aβ Accumulation Without Plaque Formation in Neurons of Mepβ$^{Cre;TG/wt}$ × APP/Ld Mice

After detecting elevated hippocampal Aβ levels in mepβ$^{Cre;TG/wt}$ × APP/Ld animals, we next investigated whether this increase also translates into plaque deposition within the brain. To address this, we performed immunohistochemistry (IHC) on brain slices of 4-month-old APP/Ld and mepβ$^{Cre;TG/wt}$ × APP/Ld mice using an antibody specifically recognizing N-terminally truncated Aβ species (Aβ2-x), kindly provided by Prof. Oliver Wirths (University of Göttingen). No extracellular plaque deposits could be observed in the brains analyzed, neither in APP/Ld nor in mepβ$^{Cre;TG/wt}$ × APP/Ld brains (Figure 23A&B). Instead, we detected intracellular accumulation of Aβ, predominantly localized around the neuronal soma in the pyramidal layer of the CA1 region of the hippocampus in mepβ$^{Cre;TG/wt}$ × APP/Ld animals (Figure 23B(ii)). Such intracellular or perinuclear deposits are of particular relevance, as several studies have suggested that intraneuronal Aβ is highly toxic and may contribute to early synaptic and neuronal dysfunction (Welikovitch et al., 2020). This signal also translated into cortical neurons

but was less intense or common (Figure 23B(i)). It is important to note the age of the animals used. At this age, the APP/Ld model typically does not yet display extracellular plaque pathology, which usually begins to manifest around 10-12 months of age (Kukreja et al., 2014). Nonetheless, we had anticipated an accelerated Aβ pathology in the mepβ$^{Cre;TG/wt}$ × APP/Ld mice, similar to 5xFAD animals, due to the overexpression of meprin β, which was not the case.

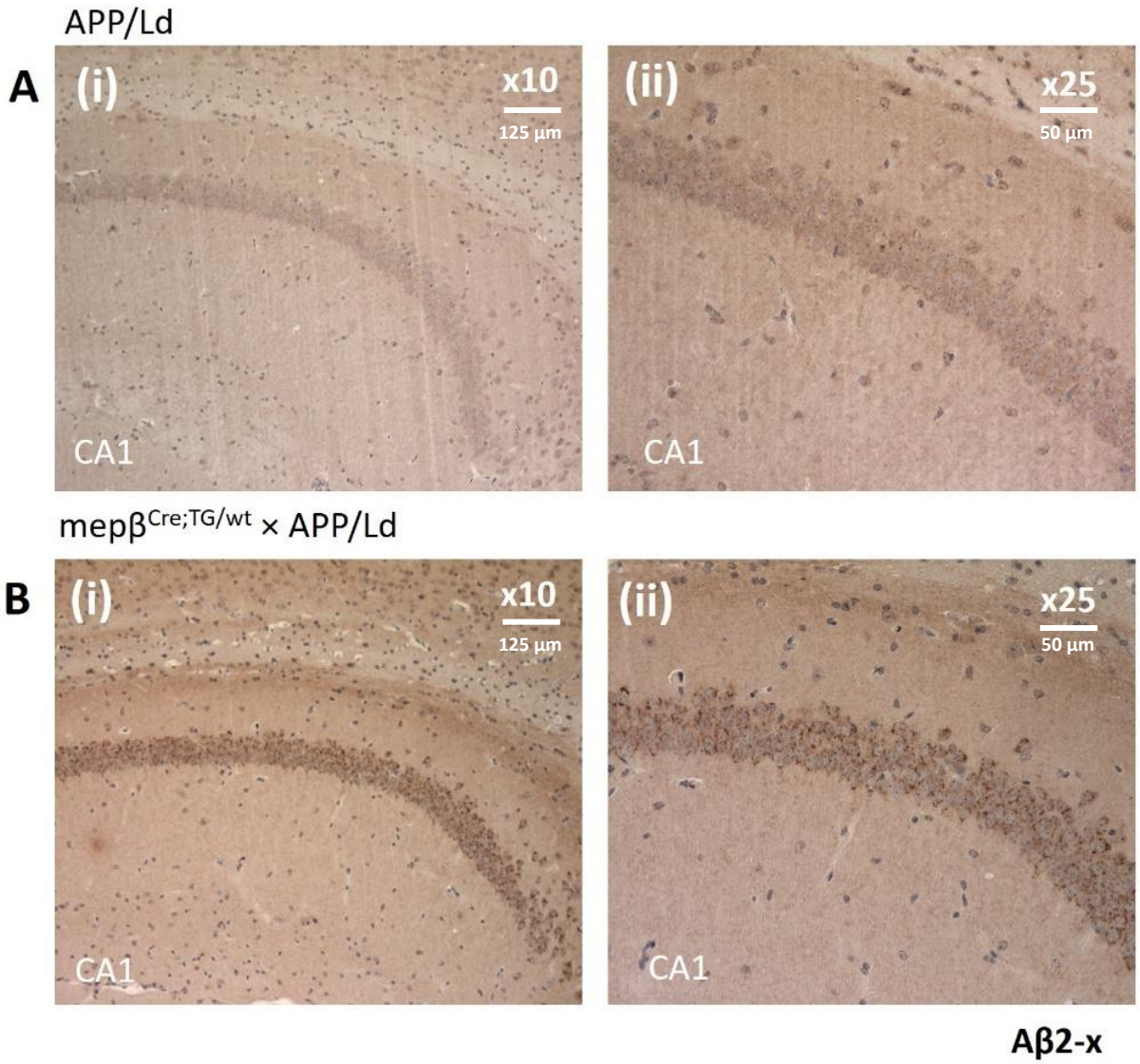

Figure 23 – DAB staining of hippocampal brain slices of 4-month-old animals with Aβ2-x-specific antibody pAb77 (brown) and counterstaining of nuclei with hematoxylin (blue). (A) No meprin β-derived Aβ plaque deposits are visible in APP/Ld animals. The earliest expected plaques in this mouse model are manifested around 10 months of age. **(B)** In mepβ$^{Cre;TG/wt}$ × APP/Ld animals, no plaque deposition was visible. Nevertheless, intracellular or perinuclear accumulation could be detected in this novel mouse model, especially in the pyramidal cell layer of the CA1 region. Sporadically, also intracellular accumulation of Aβ can be seen in the cortical neurons.

To determine whether Aβ distribution changes in older animals, we extended our analysis to 12- and 18-month-old mice (Figures 24 & 25). For these experiments, we applied immunofluorescence staining with IC16, an antibody detecting Aβ, instead of the Aβ2-x-

specific antibody. As expected, APP/Ld mice exhibited robust extracellular plaque deposition at both 12 and 18 months of age in the hippocampus and cortex. In the 12-month-old group, we see many Aβ deposits, especially in the border region between the CA1 and the subiculum (Figure 24A(i) – white arrows) and in the cortex (Figure 24A(i) – red arrows). The plaque load does not change between the 12-month-old and 18-month-old animals (Figure 24A(i) & Figure 25A(i)). Surprisingly, similar to the 4-month-old mepβ$^{Cre;TG/wt}$ × APP/Ld group, we can diffusely detect perinuclear accumulation (white arrow) in addition to plaque deposits (red arrows) of Aβ in the cortex of 12-month-old APP/Ld animals (Figure 24 A(ii)&(iii)). Intracellular accumulation of Aβ in APP/Ld animals appears transient, as it is no longer detectable in 18-month-old animals.

Intriguingly, no plaque pathology was detectable in mepβ$^{Cre;TG/wt}$ × APP/Ld animals, although elevated meprin β expression increases amyloidogenic APP processing and thereby should promote plaque formation. In turn, we can see pronounced perinuclear Aβ peptide accumulation in the pyramidal cell layer of the hippocampus (Figure 24B (ii)&(iii)) and diffusely in the cortex (Figure 24B(i)) similar to 4-month-old animals of the same genotype, which is exacerbated in 18-month-old mepβ$^{Cre;TG/wt}$ × APP/Ld brains (Figure 25A(ii)). Further examination showed elevated intracellular Aβ in the subiculum, the pyramidal cell layer of the hippocampus and the cortex (Figure 25B (i)-(iii)). Interestingly, we saw no accumulation in other parts of the hippocampus, such as the granule cell layer of the dentate gyrus (Figure 25 B(iiii)). Upon closer examination, Aβ expression appears to be localized within vesicles or compartmentalized inside the cell (Figure 25C & D – white arrows).

Thus, the immunofluorescence analysis in older animals confirmed our initial findings: overexpression of meprin β drives Aβ accumulation within neurons but does not lead to extracellular plaque formation. The most striking observation is therefore the divergence of mepβ$^{Cre;TG/wt}$ × APP/Ld animals from APP/Ld mice, where plaques failed to develop altogether despite pronounced intraneuronal Aβ. This unexpected result suggests a fundamentally different mechanism of Aβ handling and deposition in the presence of meprin β overexpression.

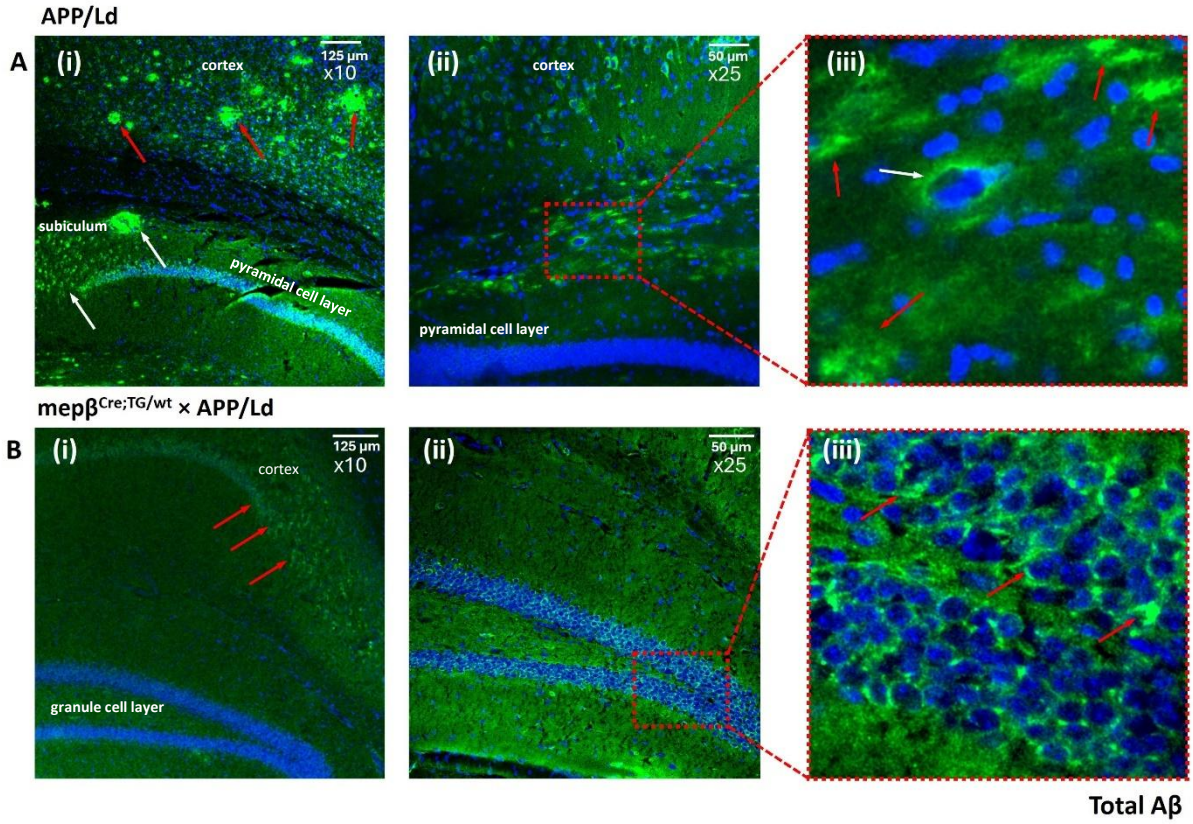

Figure 24 - Immunofluorescence staining of hippocampal brain slices of 12-month-old animals with the Aβ-specific antibody IC16 detecting Aβ (green) and counterstaining of nuclei with DAPI (blue). Brain slices were stained primarily with mouse anti-Aβ (IC16; 1:50) and DAPI (Invitrogen - D1306; 1:10000) and secondarily with goat anti-mouse-AF488 (Invitrogen - A11001, 1:500). **(A)** In APP/Ld animals, abundant plaque deposition was observed, particularly at the border of the subiculum and the CA1 region of the hippocampus (Ai - white arrows) and in the cortex (Ai - red arrows). In addition, sporadic intracellular accumulation of Aβ could be detected in cortical neurons (Aii, Aiii). **(B)** In mepβ$^{Cre;TG/wt}$ × APP/Ld animals, no extracellular plaques were visible. Nevertheless, intracellular or perinuclear accumulation of Aβ was detected, especially in the pyramidal cell layer of the CA1 region of the hippocampus (Bii, Biii) and in cortical neurons (red arrows, Bi). Compared to 4-month-old animals, the intracellular signal appeared more pronounced in this cohort.

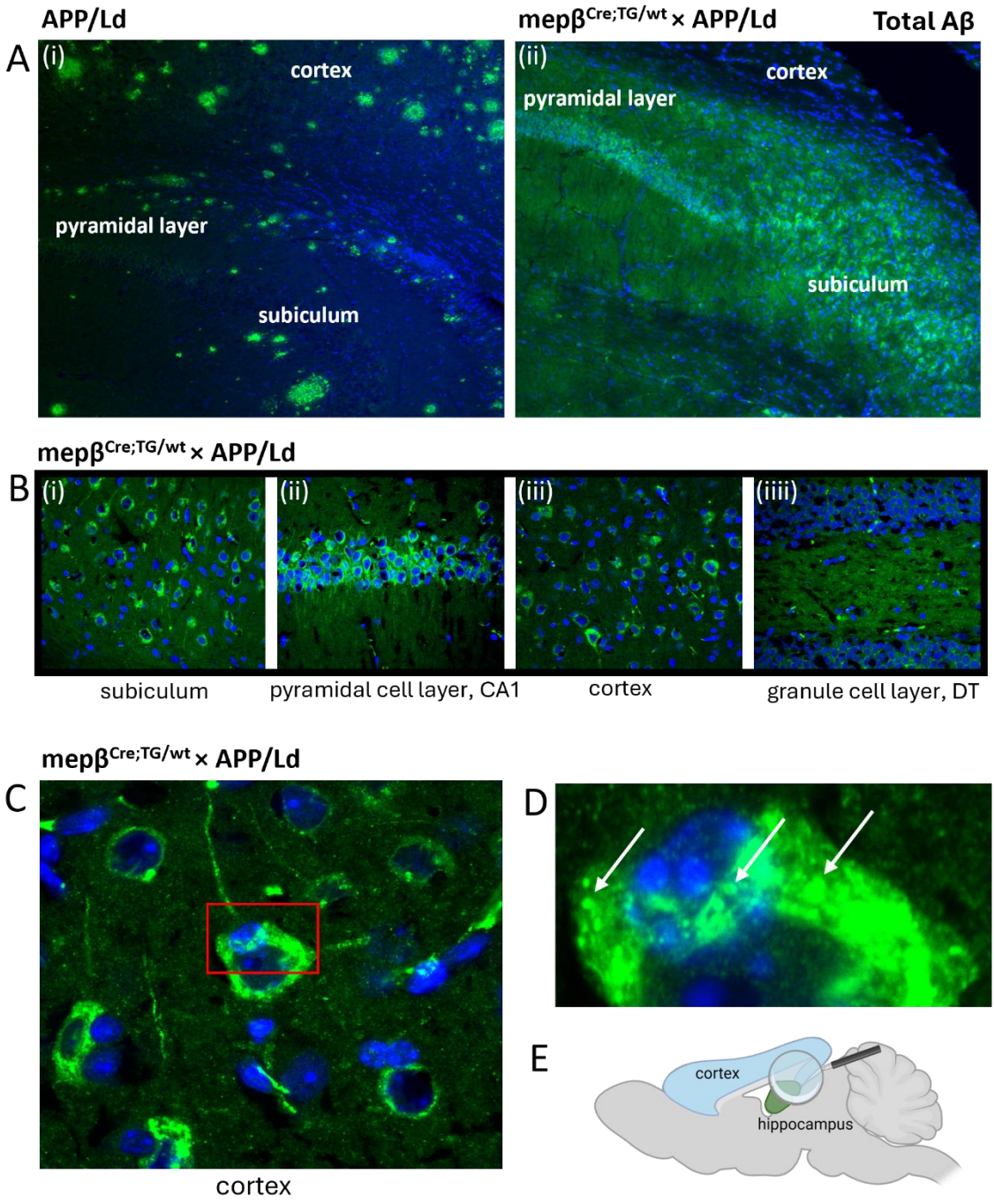

Figure 25 – Immunofluorescence staining of hippocampal brain slices of 18-month-old animals with the Aβ-specific antibody IC16, detecting Aβ (green) and counterstaining of nuclei with DAPI (blue). Brain slices were stained primarily with mouse anti-Aβ (IC16; 1:50) and DAPI (Invitrogen - D1306; 1:10000) and secondarily with goat anti-mouse-AF488 (Invitrogen - A11001, 1:500). **(A)** In APP/Ld animals, abundant extracellular plaque deposition was detected in the cortex and hippocampus **(i)**, whereas mepβ$^{Cre;TG/wt}$ × APP/Ld animals showed no extracellular plaques **(ii)**. Instead, intracellular Aβ accumulation was observed in the subiculum and pyramidal cell layer of the hippocampus **(ii)**. **(B)** Intracellular Aβ was detected in the subiculum, the pyramidal cell layer of the hippocampus, and the cortex of mepβ$^{Cre;TG/wt}$ × APP/Ld animals **(i–iii)**, but not in the dentate gyrus (DT) **(iiii)**. **(C)** Closer examination indicates that Aβ accumulation is confined within vesicular structures inside the cell (red box). **(D)** Enlarged view of the region highlighted in (C). **(E)** Overview of the area of interest analyzed by immunofluorescence staining.

4.2.4 APP/Ld × mepβ$^{Cre;TG/wt}$ Animals Show Increased Hippocampal Excitability, But No Change in the Strength of LTP Induction

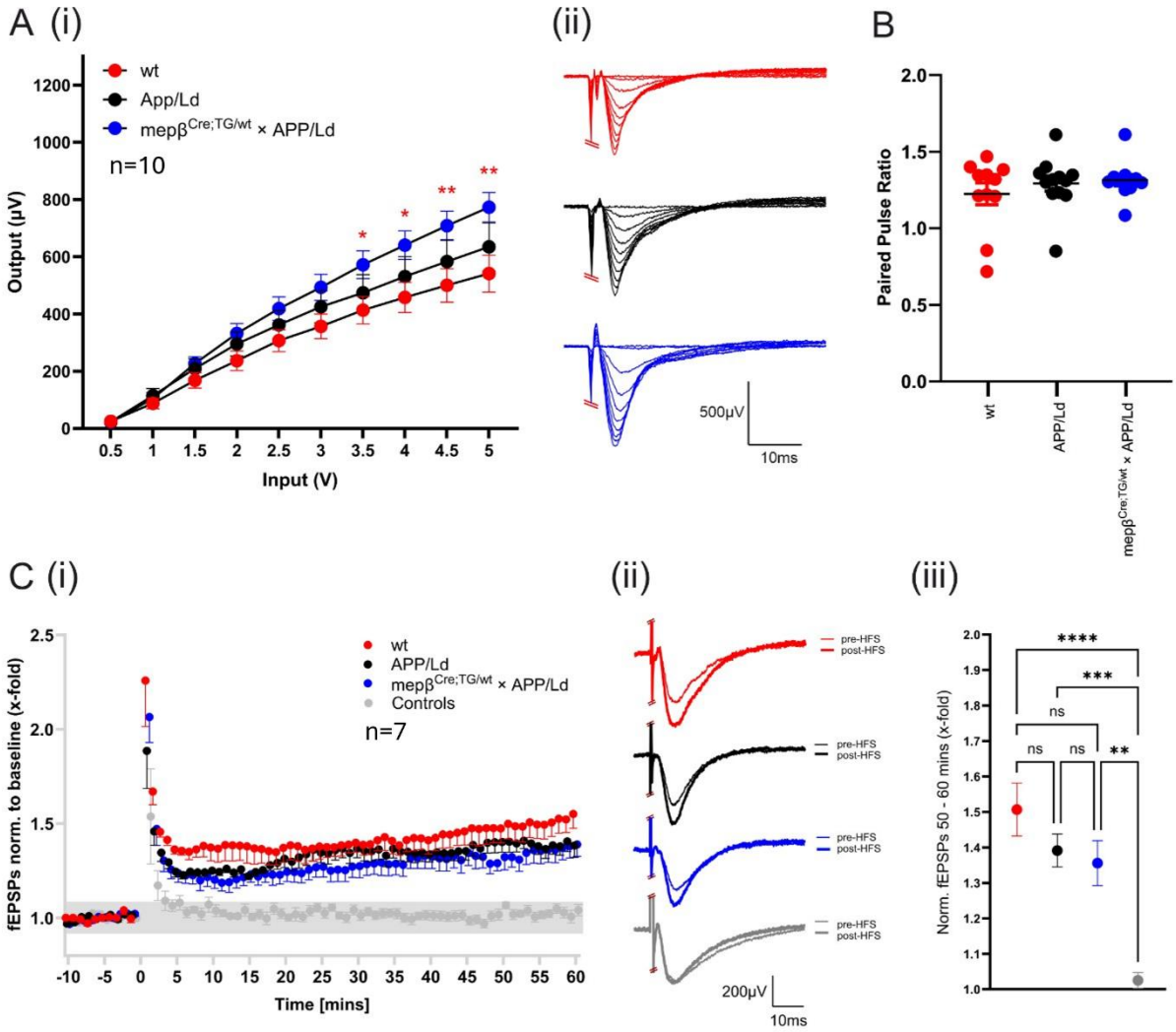

Figure 26 - Mepβ$^{Cre;TG/wt}$ × APP/Ld animals show increased excitability of hippocampal neurons but no change in LTP induction. (A) (i) Input/output (I/O) curves demonstrating the evoked field excitatory synaptic potential (fEPSP) amplitudes in CA1 from wild-type (red), APP/Ld (black) and mepβ$^{Cre;TG/wt}$ × APP/Ld (blue) mice. **(ii)** Representative traces of the evoked I/O fEPSPs from 0.5 – 5 V stimulations in 0.5 V-step increments. **(B)** Paired-pulse ratio (PPR) between the amplitude of the second and the first evoked fEPSP, with a 50 ms inter-stimulus interval (ISI), from a stimulation intensity that evoked an amplitude that is ~30% of the maximum evoked amplitude for each slice. **(C) (i)** Long-term potentiation (LTP) induction along the Schaffer collateral pathway using a 100 Hz high-frequency stimulation (HFS) protocol and recorded in area CA1 in wt (red), APP/Ld (black) and mepβ$^{Cre;TG/wt}$ × APP/Ld (blue) mice. Grey dots represent the recordings taken from the independent control pathway. **(ii)** Representative LTP fEPSP traces from wt (red), APP/Ld (black) and mepβ$^{Cre;TG/wt}$ × APP/Ld (blue) genotypes, along with the traces from the independent control pathway (grey). The thinner trace of each color shows fEPSP before the 100Hz stimulation, while the thicker trace of each color shows fEPSP 60 minutes after the tetanic stimulation. **(iii)** The mean relative strength of potentiation of the fEPSPs recorded at 50 to 60 minutes after the 100 Hz stimulation for each genotype, as well as the independent control pathway. Statistical analysis using one-way ANOVA with post-hoc Tukey's multiple comparisons test. Graphs show mean +/- S.E.M. $p < 0.05$.

In order to clarify the possible contribution of meprin β or APP/Ld to neuronal functional alterations, we carried out electrophysiological experiments using the multielectrode array (MEA). These experiments consisted of varying protocols along the Schaffer Collaterals from

the hippocampal regions CA3 to CA1. Basal neuronal excitability was first measured by generating an I/O curve for each genotype. Input simulations ranging from 0.5 V to 5 V and which increased in 0.5 V steps with a 40-second interstimulus interval, were applied to the CA3 region. Output-evoked fEPSPs were recorded in the CA1 region, where it was found that mep$\beta^{Cre;TG/wt}$ × APP/Ld fEPSPs had significantly larger amplitudes at inputs 3.5 – 5V when compared to wild-type animals but showed no differences when compared to APP/Ld fEPSPs (Figure 26A(i)). Overlaid representative traces for each genotype can be seen in Figure 26A(ii). Since these evoked fEPSPs mostly reflect activity from postsynaptic AMPA receptors, we also investigated potential presynaptic alterations by performing an electrical paired-pulse protocol. The stimulation intensity was decided upon on a slice-by-slice basis and equated to the stimulation intensity that produced an fEPSP amplitude that was approximately 30% of the maximum evoked fEPSP amplitude from the I/O curve protocol. The paired-pulse had a 50 ms interstimulus interval (ISI) and the amplitude of the second response was divided by the amplitude of the first to generate the paired-pulse ratios (PPR) for each genotype. PPRs were comparable across all three genotypes (Figure 26B), suggesting no major functional presynaptic alterations relative to wild-type animals. Finally, we wanted to elucidate any possible changes in synaptic long-term plasticity. An LTP protocol, a cellular model for learning and memory, was executed. Here, initial baseline fEPSPs were evoked for 10 minutes in the CA1 region. Next, a high-frequency stimulation (HFS) of 100 Hz with a duration of 1 second was applied to the Schaffer collaterals. Subsequently, baseline stimulation was performed for the following 60 minutes to disclose any potentiation of the evoked fEPSPs. The potentiation of the fEPSP amplitude for each slice was measured relative to its baseline fEPSPs and the mean was plotted for each genotype in Figure 26C(i). The grey dots represent an independent control pathway measured in the non-potentiating direction from CA1 to CA3. Representative fEPSPs for each genotype before (thin trace) and after (thick trace) the HFS are shown in Figure 26C(ii). All genotypes showed successful induction of LTP; however, the level of the LTP was comparable between all genotypes (Figure 26C(iii)), indicating that the APP/Ld mutation and meprin β in animals with an APP/LD background do not significantly influence hippocampal LTP induction.

4.2.5 Mepβ$^{Cre;TG/wt}$ × APP/Ld mice Show No Impairment in Learning and Memory Compared to APP/Ld Animals

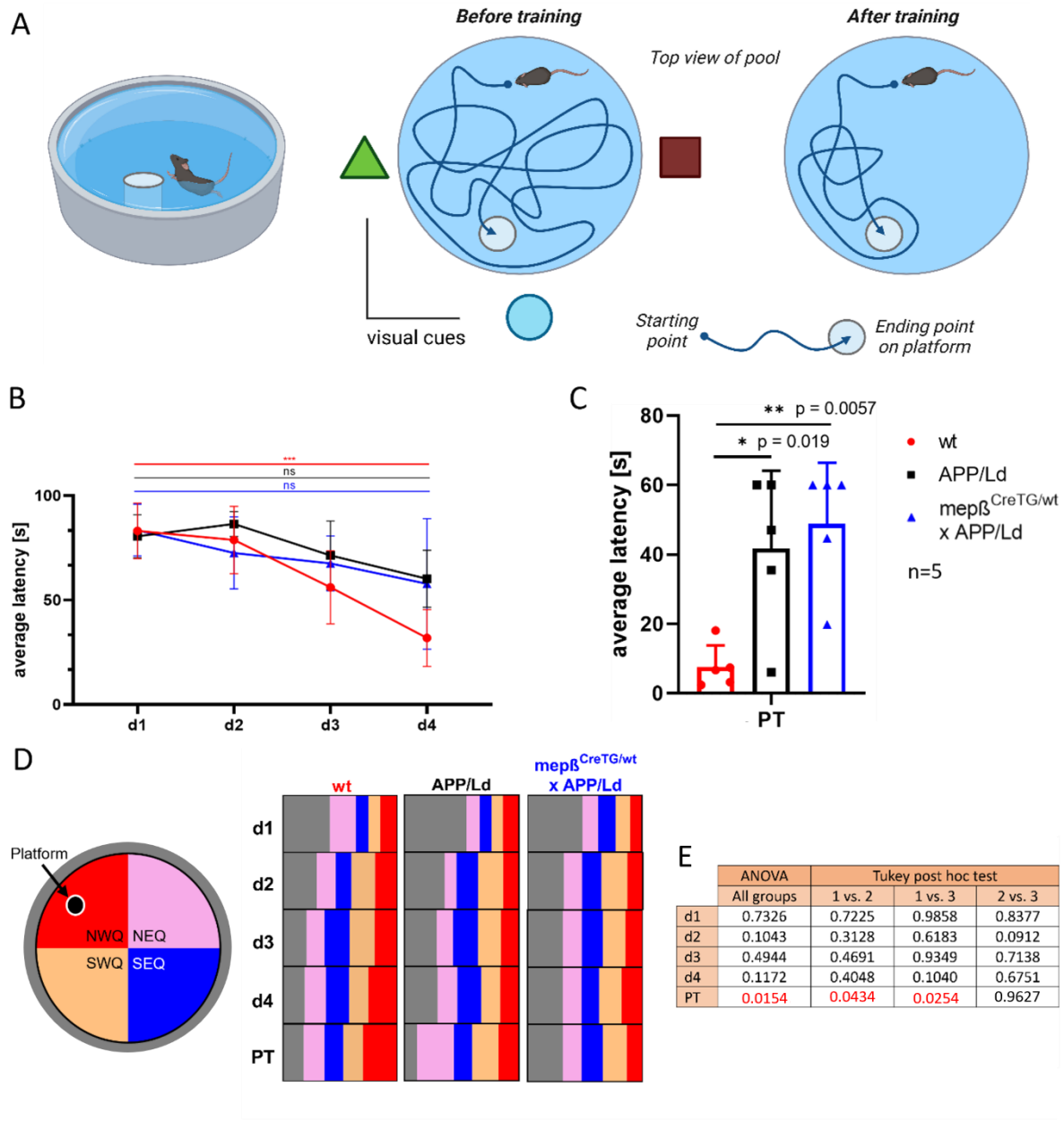

	ANOVA	Tukey post hoc test		
	All groups	1 vs. 2	1 vs. 3	2 vs. 3
d1	0.7326	0.7225	0.9858	0.8377
d2	0.1043	0.3128	0.6183	0.0912
d3	0.4944	0.4691	0.9349	0.7138
d4	0.1172	0.4048	0.1040	0.6751
PT	0.0154	0.0434	0.0254	0.9627

Figure 27 - APP/Ld animals exhibited cognitive impairment compared to wild-type controls in the Morris' Water Maze, but no additional deficits were observed in the mepβ$^{Cre;TG/wt}$ × APP/Ld group. Spatial learning and memory tests utilizing the Morris' water maze (MWM) paradigm were carried out on 8-month-old meprin β-overexpressing mice and their wild-type counterparts (n=5). **(A)** Schematic overview of the MWM paradigm: the hidden platform is submerged below the water surface, while visual cues on the tank walls help animals orient. Training is conducted over four days, with four trials each day. **(B)** Average escape latency was recorded for each trial across the four training days, but no significant differences were observed between the groups. The data shown is the mean ±SEM of four different trials performed on each day. Statistical analysis was performed using one-way ANOVA. Additionally, we compared the first and the last training day for each group to assess potential improvement using a paired t-test. Here, we could detect that only the latency for the wild-type group significantly decreases, whereas no difference could be observed for APP/Ld and mepβ$^{Cre;TG/wt}$ × APP/Ld, between the first and last training day. **(C)** On probe trial (PT) day, the platform was removed and the latency to reach the former platform location was measured. Significant cognitive deficits can be observed for APP/Ld and mepβ$^{Cre;TG/wt}$ × APP/Ld mice compared to wt animals. Statistical analysis was conducted applying one-way ANOVA

followed by Tukey's post-hoc test. **(D)** The water tank was divided into four equal quarters, with the platform located in the north-west quarter (NWQ). No differences were observed in time spent circling the tank (grey area) or across quadrants during training. On the probe trial day, significant differences emerged between wt (1) & APP/Ld (2) and wt (1) & mepβ$^{Cre;TG/wt}$ × APP/Ld (3) groups, in line with average latency results. Statistical analysis was performed using one-way ANOVA followed by Tukey's HSD post-hoc test. **(E)** The numbers shown in the table represent the calculated p-values of (D).

We aimed to compare learning and memory performance in a behavioral experiment involving three groups: mepβ$^{Cre;wt/wt}$ (wt), APP/Ld, and mepβ$^{Cre;TG/wt}$ × APP/Ld mice, using the Morris Water Maze paradigm, where a hidden platform is submerged below the water surface, while visual cues on the tank walls help animals orient (Figure 27A). The animals have a certain period to find the platform, which is measured, as described in the methods section.

The animals underwent training over four consecutive days (Figure 27B), during which no significant differences emerged among the groups. However, on the fourth training day, a measurable yet non-significant trend indicated potential differences between the wt animals and the APP/Ld + mepβ$^{Cre;TG/wt}$ × APP/Ld groups. This observed trend was consistent with the results from the probe trial (PT): APP/Ld animals displayed cognitive impairment compared to wt controls, while no additional impairment was detected in the mepβ$^{Cre;TG/wt}$ × APP/Ld group (Figure 27C). Thus, the presence of the meprin β overexpression did not further exacerbate cognitive deficits.

Wild-type animals showed significant improvement compared to APP/Ld mice, locating the platform faster from the first to the fourth training day (Figure 27B). Conversely, APP/Ld and mepβ$^{Cre;TG/wt}$ × APP/Ld mice showed no improvement, with the time needed to locate the platform remaining unchanged across the training days (Figure 27B), indicating substantial learning impairment. To confirm that the differences are not due to locomotion impairment, the mean swimming velocity of the animals was measured throughout the experiment, showing no differences between all groups (Figure 28).

During analysis, the water tank was divided into four quadrants (Figure 27D). Throughout the training sessions, no significant differences were found in either circling behavior (grey area) or time spent across the four quadrants (Figure 27D). In the PT, however, wild-type mice exhibited a clear preference for the correct quadrant compared to the other groups (Figure 27E). This preference highlights effective spatial learning and memory, aligning with the observed differences in escape latency (Figure 27C&D).

In summary, transgenic mice demonstrated significant learning deficits in the MWM test, consistent with typical Alzheimer's disease-related symptoms. Nonetheless, introducing meprin β-overexpression did not worsen cognitive impairment beyond that observed in APP/Ld mice.

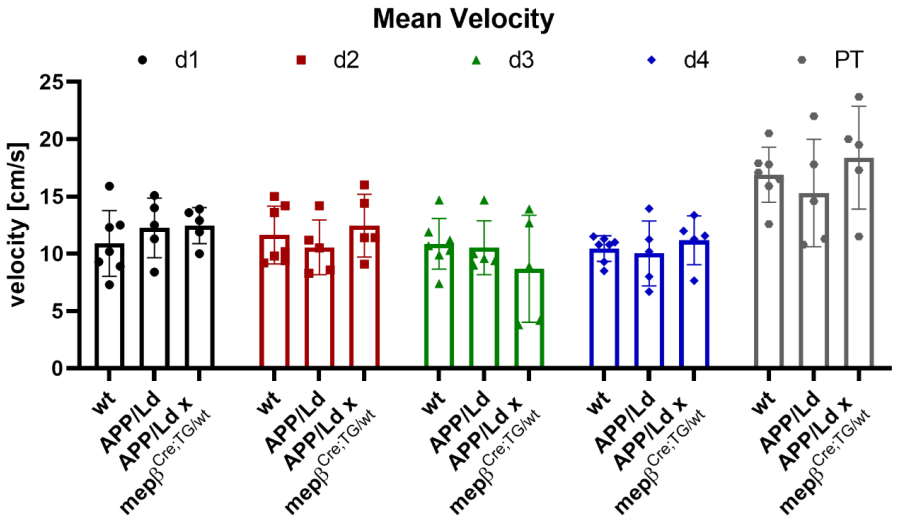

Figure 28 – Mean swimming velocity of mice used for Morris Water Maze experiment. No differences could be detected for the swimming speed of the animals, showing that neither the APP/Ld mutation nor the meprin β overexpression had any influence on locomotion.

4.2.6 Identification of Meprin β Substrates in the mepβ$^{Cre;TG/wt}$ × APP/Ld Mouse Model

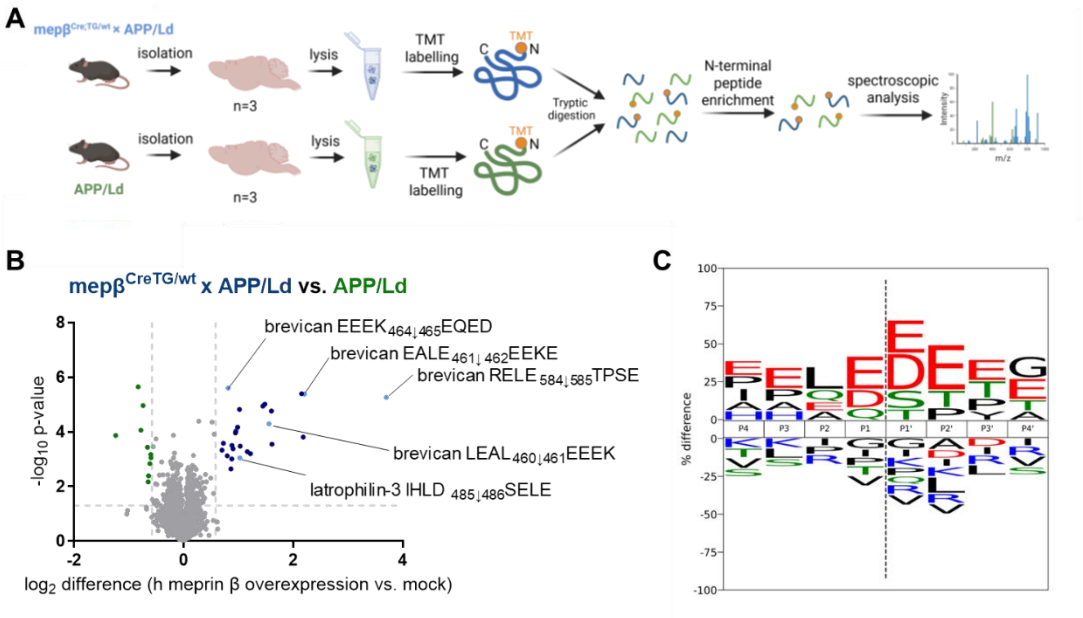

Figure 29 - Utilization of N-terminomics for the identification of substrates within the brain of mepβ$^{Cre;TG/wt}$ × APP/Ld animals. (A) Schematic overview of the TMT HUNTER-based N-terminomics approach: pooled proteins from brain lysates from mepβ$^{Cre;TG/wt}$ × APP/Ld mice and APP/Ld mice (n=3) were extracted and labeled with tandem mass tags (TMT) at their N-terminus. Afterward, proteins were digested into peptides with trypsin. In a negative selection via hydrophobic tagging, internal tryptic peptides are removed to enrich the neo N-termini that are measured via mass spectrometry and quantified. **(B)** Volcano plots showing all identified proteolytic events detected by TMT HUNTER-based N-terminomics approach of brain lysates from mepβ$^{Cre;TG/wt}$ × APP/Ld

mice compared to APP/Ld mice. Grey lines represent threshold values (±0.58 for $\log_2$ difference, p = 0.05). Selected cleavage events within known substrates are highlighted (light blue). **(C)** Native protein substrate cleavage specificities of meprin β calculated from significantly elevated neo N-termini in lysates from mepβ$^{Cre;TG/wt}$ × APP/Ld mice presented in specificity logos (including P4 to P4' positions).

To further investigate the causes of the electrophysiological effects, we performed an N-terminomics screen to identify cerebral substrates of meprin β in mepβ$^{Cre;TG/wt}$ × APP/Ld mice. We used TMT-based HUNTER analysis to compare brain lysates from mepβ$^{Cre;TG/wt}$ × APP/Ld mice and APP/Ld control mice (Figure 29A). Through this method, we identified 5174 novel N-terminal peptides and 25 significantly altered neo N-termini when comparing brains from meprin β-overexpressing mice to APP/Ld controls (cutoff set at ±0.58 for $\log_2$ difference, p = 0.05) (Figure 29B). Remarkably, one recently validated cerebral substrate of meprin β, latrophilin-3 (Armbrust et al., 2025), emerged among the most prominent candidates identified in mepβ$^{Cre;TG/wt}$ × APP/Ld mice. For Latrophilin-3, cleavage sites identical or differing by only one amino acid from those found in previous N-terminomic studies were identified, reinforcing the notion of enhanced meprin β proteolytic activity specifically in mepβ$^{Cre;TG/wt}$ × APP/Ld mice. Additionally, we identified further potential substrates associated with the extracellular matrix (ECM), such as previously described brevican (Q61361), neurocan (P55066) and hyaluronan and proteoglycan link protein 1 (Q9QUR5), again suggesting a possible role for meprin β in remodeling the extracellular matrix (ECM). Further confirmation arises from native substrate specificity profiling, where a cleavage specificity logo derived from significantly enriched neo N-termini demonstrates the typical specificity profile for meprin β (Becker-Pauly et al., 2011), prominently featuring acidic amino acids near the cleavage site, particularly at the P1 and P1' position (Figure 29C).

4.2.7 Knock-Out of Meprin β Leads to Weight Gain in Mice

We additionally investigated knockout (KO) animals that have previously been characterized with respect to amyloid-β deposition (Marengo et al., 2022). Interestingly, these mice developed a pronounced metabolic phenotype, as they exhibited progressive weight gain compared to wild-type controls. To quantify this effect, we monitored body weight over a period of several months, beginning at six months of age, and confirmed that KO animals became significantly heavier after the fifth month of measuring (Figure 30A). Assessment of liver tissue further revealed abundant lipid accumulation, indicative of hepatic steatosis, in contrast to the livers of wild-type animals (Figure 30B). These findings raise the possibility that the observed phenotype may be linked to alterations in soluble Aβ, which is downregulated in

the KO animals on an AD mouse model background. Additionally, a contribution of elevated endogenous Aβ levels cannot be excluded.

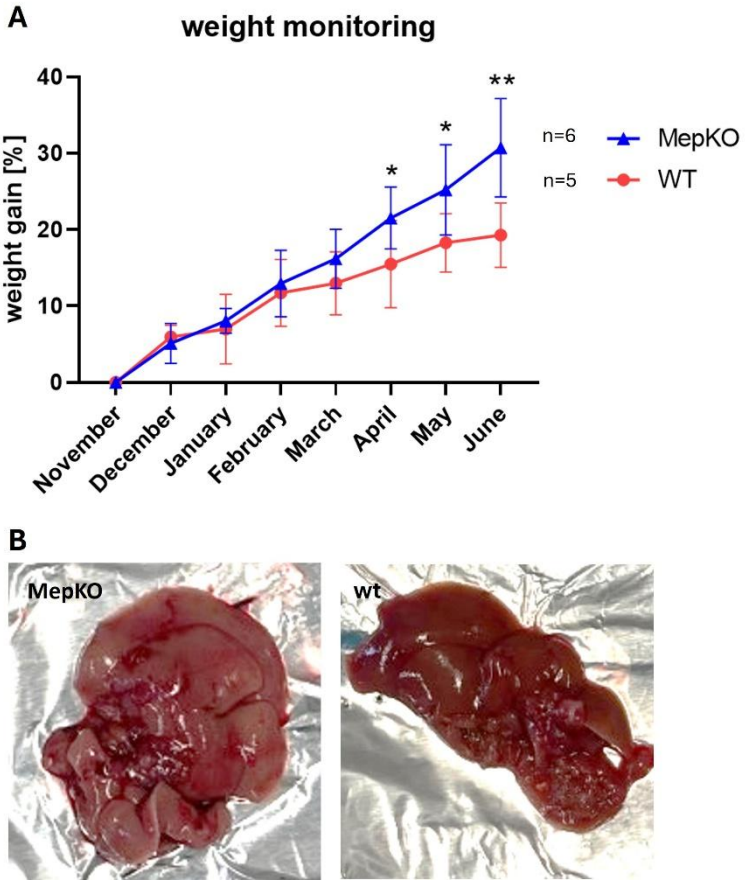

Figure 30 – KO animals previously described in the context of amyloid-β deposition developed a metabolic phenotype with progressive weight gain compared to wild-type controls. (A) Monitoring of the weight of 6-month-old animals revealed a significant weight gain after 11 months of age. **(B)** Liver examination revealed pronounced hepatic steatosis with abundant lipid accumulation in KO livers, in contrast to wild-type animals.

After observing significant weight gain in MepKO animals, we aimed to identify potential biochemical mechanisms underlying this phenotype by assessing protein expression levels relevant to lipid metabolism using Western blotting. In initial analyses, no differences were detected in LRP β-chain, LDLR, PCSK9, or FOXO1 expression between groups. Interestingly, however, MepKO animals exhibited reduced expression of GSK3β, MDR1 (ABCB1), and ApoE.

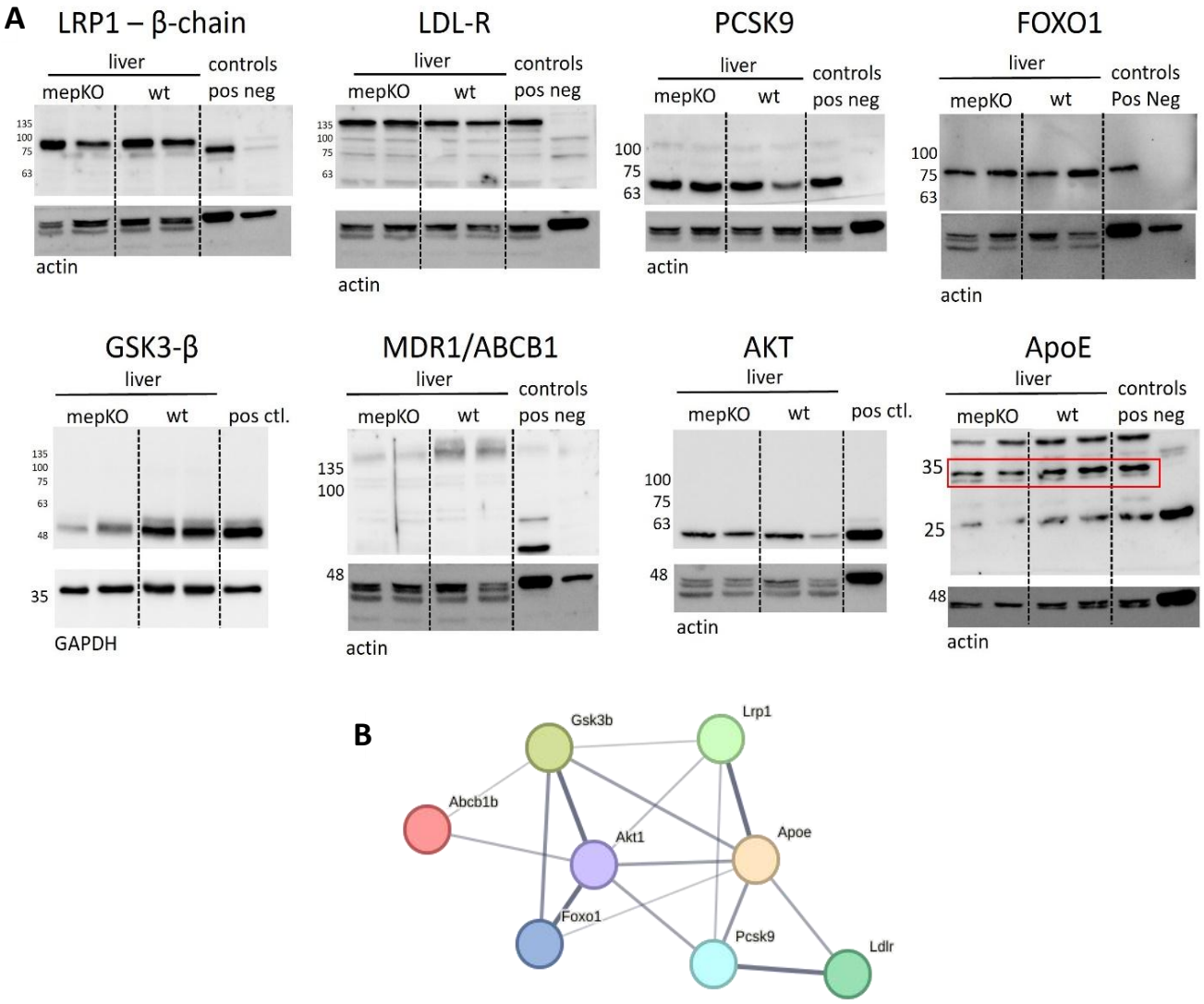

Figure 31 – Analysis of proteins involved in lipid metabolism in the liver. (A) Western blot analysis of proteins involved in lipid metabolism revealed no differences in LRP β-chain, LDLR, PCSK9, or FOXO1 expression between groups. In contrast, MepKO animals showed reduced expression of GSK3β, MDR1 (ABCB1), and ApoE. **(B)** STRING analysis highlighted functional links between these proteins, with GSK3β and AKT emerging as central hubs connected to both ApoE and ABCB1.

Notably, GSK3β is a key regulator of multiple pathways, including glucose uptake and lipid metabolism, and plays a central role in the Wnt/β-catenin signaling cascade, which controls gene transcription relevant to cell proliferation and metabolism. ApoE, in addition to being a well-established genetic risk factor for AD, is also critically involved in lipid transport and metabolism. Importantly, these factors are functionally interconnected, with GSK3β emerging as a central hub: analysis using the STRING database (Szklarczyk et al., 2024) revealed links between GSK3β, ABCB1, and ApoE. While the predicted connection between ABCB1 and GSK3β is relatively weak, their interaction cannot be excluded and may contribute to the observed phenotype.

5. Discussion

5.1 Part I:

5.1.1 Brevican Cleavage Influences LTP Formation and Learning Behavior of Meprin β-Overexpressing Animals

Brevican is expressed in both neurons and glial cells, where it is predominantly localized at perisynaptic sites. Together with other lecticans, hyaluronic acid, and tenascin-R, brevican plays a crucial role in the formation of perineuronal nets (PNNs). These nets are structures that surround the proximal dendrites and neuronal cell bodies, stabilizing synapses by acting as a barrier against the growth of nearby axons or dendrites (Van't Spijker et al., 2017; Karetko, 2009; Sorg et al., 2016). Moreover, PNNs are essential for long-term memory consolidation (Saroja et al., 2014), extending the importance of brevican in the neuronal ECM and its role in synaptic transmission to behavioral and cognitive aspects. Brevican is a key contributor to spatial memory and memory retrieval function, as found previously through hippocampal proteoglycan isolation and characterization in rats that underwent the Morris Water Maze (MWM) spatial paradigm test (Saroja et al., 2014). Brevican-deficient mice have also displayed impaired hippocampal CA1 LTP in previous studies, with LTP considered the most widely established underlying cellular mechanism for learning and memory consolidation (Brakebusch et al., 2002). Even within clinical cohorts, patients suffering from vascular dementia were found to have significantly decreased serum brevican levels compared to those of healthy controls (Pantazopoulos et al., 2020; Minta et al., 2019; Jonesco et al., 2020; Minta et al., 2021; Höhn et al., 2023; Chia et al., 2024), which prompted the suggestion of the use of fluid brevican as a biomarker for dementia- and cognitive impairment-related brain pathologies. In a recent study by Liu et al. (2024), brevican was further implicated in axonal-cerebral degeneration (ACD), Alzheimer's disease (AD), stroke, and depression, underscoring its potential utility as a biomarker for a more diverse array of diseases. Notably, Liu et al. demonstrated that brevican exhibited no influence on movement, a finding that aligns with our observations, since we cannot detect any locomotion changes between the tested groups.

To better understand how meprin β overexpression influences synaptic function, we examined its subcellular localization using confocal microscopy on sagittal brain slices, specifically targeting the CA3 region of the hippocampus. This region was selected due to

previously observed deficits in spatial learning in the MWM in meprin β-overexpressing mice. Wild-type animals showed meprin β predominantly localized around the nucleus, likely reflecting the endoplasmic reticulum. In contrast, overexpressing mice exhibited strong meprin β expression in the soma, axons and notably, at synaptic sites. Co-staining with the postsynaptic marker PSD-95 revealed a higher degree of overlap compared to the presynaptic marker VGLUT, supporting postsynaptic enrichment of meprin β. This subcellular distribution provides a potential anatomical correlation to the observed electrophysiological and behavioral changes.

While LTP induction is primarily an NMDA receptor (NMDAR)-dependent mechanism, brevican has also been highlighted for its associations with AMPA receptors (AMPAR); namely, their mobility and diffusion (Frischknecht et al., 2009; Pantazopoulos et al., 2020) and the capacity at which they can facilitate short-term synaptic plasticity (Yuan et al., 2002; Sonntag et al., 2018). Knockout of AMPAR subunit GluR1 in mice exhibits impaired learning and memory, which also highlights AMPA's role in synaptic plasticity and associative learning (Feyder et al., 2007; Chater et al., 2014). On discovering that overexpression of meprin β resulted in the cleavage of such a main component of the neuronal ECM as brevican, the electrophysiology and behavioral results also became more coherent. The increase in basal excitability, seen by the significantly larger evoked input/output curve amplitudes in meprin β-overexpressing mice compared to mepβ$^{Cre;wt/wt}$ mice, is likely due to the increased AMPAR mobility and lateral diffusion in the postsynaptic CA1 pyramidal cells (Frischknecht et al., 2009). Interestingly, it was shown that the surface compartments formed by the ECM - of which brevican is a main component - hinder lateral diffusion of AMPA receptors and may therefore decrease the capacity for short-term synaptic plasticity (Frischknecht et al., 2009). With the digestion of brevican and therefore an at least partial breakdown of the impeding ECM, AMPARs, which are desensitized from use, can quickly be replaced by naïve AMPARs moving from the extrasynaptic space to the postsynaptic density (PSD), ready for activation. This means that the number of postsynaptic receptors that are available for activation can be consistently replenished, enhancing the AMPAR-dependent evoked activity responses seen from the input/output curve. A study by Favuzzi et al. (2017) supports previous findings by demonstrating that the PNN surrounding parvalbumin (PV+) interneurons plays a critical role in regulating plasticity. The authors propose that brevican, a key component of the PNN,

modulates cellular and synaptic plasticity by influencing the localization of potassium channels and AMPA receptors (Favuzzi et al., 2017).

5.1.2 Meprin β Overexpression Does Not Affect Glutamatergic Receptor Levels at the Synapse

The fact that meprin β cleaves a protein of the ECM within which the receptors are immobilized - allowing a more fluid diffusion of synaptic receptors in the membrane, rather than cleaving or affecting those receptors directly - brings with it some further inquiries. This assumes that total AMPAR and/or NMDAR subunit protein expression levels in the meprin β-overexpressing mouse line should not be different from those of the mepβ$^{Cre;wt/wt}$ controls, despite electrophysiological changes which are normally receptor concentration-dependent. Indeed, quantitative Western blot analysis confirmed that total expression levels for AMPAR and NMDAR subunits were equivalent for both animal groups (Figures 11 & 13), owing to the point that it is not about whether the receptors (or their subunits) are increased or decreased in expression, but rather where they are in the membrane/ECM at any given moment. If meprin β was in fact actively degrading both NMDA and AMPA receptors, it would likely result in early mortality, given their developmental roles (Nakazawa et al., 2004). Even if mortality did not occur, it would likely cause a distinct phenotype in the transgenic animals, since the meprin β overexpression occurs from birth. Meprin β-overexpressing mice, however, exhibit no developmental abnormalities and appear phenotypically normal (own observations). The absence of a clear phenotype of meprin β-overexpressing mice might relate to the fact that the natural increase of brevican expression only normally occurs *after* birth (Yamada et al., 1997). Supposedly, brevican is disposable in early development and not essential for fetal growth or embryonic development.

Additionally, the significant intergroup electrophysiological changes could be specifically due to receptor expression on the membrane surface, rather than to total expression. This was also thoroughly considered. Since there was a significant increase in evoked fEPSPs concomitantly with a significant decrease/loss of LTP in the meprin β-overexpressing mice, a metaplasticity effect was hypothesized. In order to investigate this, a surface biotinylation assay on primary hippocampal neurons from mepβ$^{Cre;wt/wt}$ and meprin β KO mouse brains was undertaken (Figure 13). This assay showed no changes in membrane surface AMPAR subunit or NMDAR subunit expression, verifying that membrane surface receptor composition was

not quantitatively altered between these groups, as well as implying that meprin β does not influence membrane surface receptor expression. Furthermore, we would like to emphasize that Brakebusch et al. (2002) reported an impairment in LTP maintenance in brevican KO mice, which was attributed to structural and functional changes in the ECM affecting synaptic signaling and maintenance. This finding supports our theory, since a similar effect is observed in meprin β-overexpressing mice.

5.1.3 Electrophysiological Effects Are Most Likely Due to Postsynaptic Morphological Changes

While the evoked network excitability and the LTP experiments proved significant differences between groups, the additional electrophysiological paired-pulse ratio (PPR) experiments did not (Figure 20). Although an increase in synaptic facilitation is generally seen with an accompanying increase in PPR, the significant increase of both the first and the second evoked response from the PPR protocol in these meprin β-overexpressing mice meant that the overall ratio of the second response relative to the first was equivalent across groups. This is, however, in line with our hypothesis that the postsynaptic replenishment of naive AMPARs causes the significant enhancement of the evoked response amplitudes—something which does not concern the presynaptic release probability (which is reflected by the PPR) but rather the postsynaptic AMPAR functional efficiency.

Of course, meprin β overexpression could also be due to morphological changes in neurons or their connectivity. The composition of ECM proteins critically impacts neuronal spine density and synaptic plasticity, which are vital for learning and memory (Sharma et al., 2023). Enzymes like MMP-9 cleave ECM components, enhancing dendritic spine formation and stability (Stawarski et al., 2014). Such modifications may, of course, contribute to impairments in synaptic function and cognitive processes in the brain, showing the large impact proteolytic enzymes have on the ECM. For example, ADAMTS4 - a brevican-cleaving proteolytic enzyme- strongly influences neuronal spine density and is essential for synaptic plasticity (Jefferson et al., 2013; Gottschall & Howell, 2015) as well as being linked to LTP (Brakebusch et al., 2022). Our data strongly reflect these changes: meprin β overexpression leads to lower brevican protein levels and ECM proteolysis, which then influences LTP formation and ultimately impacts learning and memory.

In conclusion, brevican emerges as a pivotal ECM component integral to synaptic plasticity, memory formation, and cognitive function. The interplay between brevican and meprin β highlights the dynamic regulation of synaptic receptors and neuronal connectivity, emphasizing how ECM proteolysis impacts neuronal signaling and plasticity. These findings not only underscore meprin β's role in memory and synaptic transmission but also put forward its potential as a biomarker for cognitive disorders.

5.2 Part II:

5.2.1 Triple-Transgenic Mepβ$^{Cre;TG/wt}$ × APP/Ld Animals Circumvent BACE1-Generated Bias

This part of the thesis aimed to investigate the role of the metalloprotease meprin β in Aβ generation using a mouse model overexpressing APP with the London (Ld) mutation, either alone or in combination with meprin β overexpression. Rather than modeling AD symptoms per sé, our primary objective was to circumvent the common bias introduced by BACE1-dependent APP processing. Most conventional AD mouse models rely on the use of APP/swe-based mutations that are characterized by BACE1-dependent Aβ generation (Armbrust et al., 2022), which primarily generate Aβ species starting at positions 1 and 11 (Aβ1–40/42 and Aβ11–40/42) (De Strooper et al., 2021). However, these models do not adequately reflect the diversity of N-terminally truncated Aβ variants observed in patients with sporadic AD. Since meprin β can generate such N-terminally cleaved Aβ peptides in addition to the Aβ1-x peptides, we aimed to establish a more suitable model for studying these variants. To circumvent BACE1-biased processing, we used human APP carrying the Ld mutation and overexpressed murine meprin β. Interestingly, the murine form of meprin β is also capable of cleaving human substrates, such as APP, as demonstrated by Armbrust et al. (2024), and therefore generating Aβ1/2-x species. Although there are differences between human and murine meprin β, the catalytic domain remains highly conserved.

5.2.2 Vulnerability to Neurodegeneration is Increased in the Hippocampus Compared to Other Brain Tissue in Meprin β-Overexpressing Animals

We clearly demonstrate that meprin β facilitates the proteolytic cleavage of APP, resulting in significantly elevated levels of soluble Aβ peptides in the hippocampus of mepβ$^{Cre;TG/wt}$ × APP/Ld animals when compared to APP/Ld animals. This increase was specific to the

hippocampus and absent in the cortex, suggesting region-specific enzymatic activity of meprin β. Previously, we showed that the expression of endogenous meprin β is elevated in the murine hippocampus compared to cortical areas (Marengo et al., 2022). This likely reflects regional differences in substrate availability, expression of co-factors, or metabolic demand in the hippocampus (Aldana et al., 2021; Pamplona et al., 2021; Liu et al., 2018). The observed pattern aligns with the concept of hippocampal vulnerability, which posits that the hippocampus is particularly prone to early AD pathology due to elevated APP expression, increased excitability and lower antioxidant capacity relative to other brain regions (Busi et al., 2024; Krishnamurthy et al., 2022; Jiang et al., 2020; Duara et al., 2021). This vulnerability is further supported by differential gene expression profiles, such as increased levels of SERPINA5 in hippocampal neurons (Duara et al., 2021). It has been demonstrated that increased expression of SERPINA5 in the hippocampus correlates with greater susceptibility to AD pathology, particularly through its interaction with tau protein, potentially representing a critical “tipping point” in their development and the progression of hippocampal damage (Crist et al., 2020). Increased excitability of neurons was also observed in electrophysiological experiments in our study (Figure 26A), which further supports the theory of hippocampal vulnerability in our mouse model.

Moreover, the hippocampus stands out as a focal point for early pathology. Numerous studies have identified higher levels of APP expression, increased metabolic stress, and more pronounced synaptic decline in this region relative to others (Reddy et al., 2018; Berger et al., 2023; Aldana et al., 2021; Ostrowski et al., 2024). In disease models, synaptic protein loss is more severe in the hippocampus than in the cortex, particularly in aged or epileptic mice (Sasaki et al., 2022; Tapia-Rojas et al., 2020; Van Der Kolk et al., 2005). Our study highlights the hippocampus as a uniquely susceptible site, making it an ideal target for studying early molecular changes in AD.

5.2.3 Intracellular Accumulation of Aβ in Mepβ$^{Cre;TG/wt}$ × APP/Ld Animals

The accumulation of Aβ within cells is attributable to differences in Aβ processing, aggregation, and clearance pathways. Intracellular deposition of Aβ often precedes and promotes the development of extracellular plaques, with impaired degradation and export mechanisms playing central roles. In this thesis, we demonstrate that genetic modifications

prevented intracellular Aβ from being transported outside the cell, leading to its intracellular retention. This accumulation was clearly detectable by histochemical and immunofluorescence approaches in different age groups (4-, 12 and 18-month-old).

Generally, Aβ is derived from APP and can accumulate within late endosomes and lysosomes. Among its isoforms, Aβ1–42 is particularly prone to aggregation and exhibits resistance to degradation in these compartments, contributing to persistent intracellular buildup. Aggregated Aβ species are less susceptible to proteolytic clearance, especially when forming high molecular weight assemblies. Their localization in dense organelles such as late endosomes and lysosomes further limits enzymatic accessibility (Knauer et al., 1992; Takahashi et al., 2017; Gowrishankar et al., 2015). In 18-month-old animals, we can detect accumulations of Aβ that appear to be retained within vesicles, possibly endosomes (Figure 25C), which supports the findings from these studies. Additionally, neurons and other brain cell types are capable of internalizing soluble extracellular Aβ, which subsequently accumulates in acidic vesicles where it undergoes aggregation. These aggregates may then act as nucleation sites for further amyloid formation inside the cell (Hu et al., 2009; Han et al., 2017). Another noteworthy aspect is the influence of meprin β on the blood-brain barrier (BBB). We showed before that meprin β activity leads to increased permeability of the BBB by cleavage of Claudin-5, a tight junction protein (Gindorf et al., 2021). In addition to the LRP1-mediated transport of Aβ into the blood, the leaky BBB may represent an alternative way for Aβ clearance from the brain and could explain the absence of plaque formation.

One possible explanation for the observed intracellular accumulation of Aβ is the presence of mutations in the AD mouse model employed in this study. Specifically, the γ-secretase cleavage site of APP is mutated, which may delay the second proteolytic cleavage step (following α/β cleavage), thereby contributing to intracellular Aβ retention. An additional factor could involve meprin β, which may cleave APP in an alternative manner. Supporting this, APP/Ld meprin β KO animals display fewer extracellular plaques, indicating that meprin β contributes to APP cleavage (Marengo et al., 2022). In this thesis, we provide evidence that meprin β indeed cleaves APP, as reflected by elevated levels of soluble intracellular Aβ. However, the precise mechanism remains unresolved. Importantly, the reduction in plaque deposition observed in KO animals cannot be conclusively attributed to impairment of the canonical amyloidogenic pathway. Instead, meprin β may participate in a distinct plaque-

forming mechanism, which may explain why this protease has received limited attention in AD research to date.

Mutations proximal to the γ-secretase cleavage site of APP are well-established drivers of familial AD and are closely associated with intracellular Aβ accumulation. Variants such as T714I, V715M, I716V, and V717I/L alter γ-secretase cleavage specificity and efficiency, resulting in an elevated Aβ42/Aβ40 ratio and, in some instances, stabilization of APP C-terminal fragments within neurons (e.g., C99), which also could be detected by the pAb77 and IC16 antibodies we used for stainings (Jonghe et al., 2001; Dimitrov et al., 2013; Suzuki et al., 2023). These fragments, being less efficiently processed, accumulate intracellularly without showing a phenotype. Other mutations, such as E693Δ (deletion of E693), enhance Aβ oligomerization and promote accumulation in diverse organelles, including the endoplasmic reticulum, Golgi apparatus, endosomes, and lysosomes (Jonghe et al., 2001; Schilling et al., 2023). Evidence suggests that intracellular and secreted Aβ may arise from distinct γ-secretase cleavage dynamics, with late Golgi and trans-Golgi network compartments serving as key intracellular sites of Aβ generation. Furthermore, some mutations alter the trafficking and subcellular localization of APP and its fragments, thereby intensifying intracellular retention (Grimm et al., 2003; Schilling et al., 2023). Collectively, these findings underscore the mechanistic diversity of APP mutations, ranging from altered cleavage preferences to impaired trafficking and degradation, and highlight their pivotal role in shaping disease progression (Jonghe et al., 2001; Suzuki et al., 2023; Grimm et al., 2003).

Intriguingly, mepβ$^{Cre;TG/wt}$ × APP/Ld mice show no obvious phenotype besides intracellular Aβ accumulation and memory deficits, even at advanced ages of up to two years (own observation). In contrast, APP/Ld animals develop severe symptoms by that age (Herl et al., 2009). A possible explanation is that intracellular meprin β-derived, N-truncated Aβ may not be pathogenic as long as neurons remain viable. Only once advanced neurodegeneration occurs are these intracellular pools released into the extracellular space, where truncated Aβ species can aggregate and contribute to plaque formation. This could explain why plaques in human AD are rich in N-truncated Aβ, while transgenic meprin β-overexpressing mice show only intracellular accumulation and elevated levels in Western blotting experiments, as their neurons largely remain intact. In the absence of plaque formation or toxic extracellular Aβ levels, microglial activation would be absent, which may explain why these animals do not

exhibit neurodegeneration or a distinct phenotype. To better replicate AD pathology, this novel mouse model could be crossed with another model that develops age-dependent neurodegeneration independent of APP processing. Our findings suggest that while Aβ plays a critical role in the early stages of the disease, elevated levels alone are insufficient to trigger a pathological response. Instead, the transport of Aβ to the extracellular space may be equally important.

5.2.4 Higher Excitability of Hippocampal Neurons of Mepβ$^{Cre;TG/wt}$ × APP/Ld Animals Does Not Translate into Changes in Learning and Memory

In support of a broader role for meprin β, electrophysiological analyses revealed significant changes in synaptic excitability in young mepβ$^{Cre;TG/wt}$ × APP/Ld mice compared to wt animals. These early effects suggest that meprin β impacts neuronal function during development, perhaps independently of Aβ. Proteomics analyses identified potential non-APP substrates, including brevican, neurocan, HAPLN1, and latrophilin-3. Recent studies have further confirmed that brevican and latrophilin-3 are substrates of meprin β in the brain - the former playing a crucial role in the structural organization of PNNs. Its cleavage by meprin β leads to lower brevican level (Keller et al., 2025). Brevican enwraps synapses and neurons, playing a crucial role in regulating neuronal plasticity (Sharma et al., 2023; Yamada et al., 1997; Sorg et al., 2016; Brakebusch et al., 2002) and likely influencing AMPA-mediated excitability in hippocampal neurons. Additionally, Latrophilin-3 emerged as a potential substrate in our proteomic data. It was recently confirmed as a murine meprin β substrate in astrocytes and neurons, with potential implications for cognition and links to hyperactivity (Armbrust et al., 2025). These findings extend our understanding of meprin β's activity from APP cleavage to more generalized roles in ECM remodeling and neuronal physiology.

Nevertheless, studies have shown that low levels of Aβ during early brain development can have beneficial effects on synaptic growth, suggesting that the observed electrophysiological changes in the mepβ$^{Cre;TG/wt}$ × APP/Ld animals might also be attributed to the elevated Aβ concentrations in this group (Cai et al., 2023). Additionally, Zott and colleagues (2019) reported that soluble Aβ oligomers impair glutamate reuptake, leading to sustained synaptic glutamate levels and hyperexcitability in neurons that are already active. This hyperactivation establishes a self-reinforcing "vicious cycle", as excessive neuronal firing further intensifies Aβ-dependent dysfunction. Importantly, these effects emerge before amyloid plaques form,

implicating early glutamatergic dysregulation as a trigger of hippocampal circuit hyperexcitability. Interestingly, we previously showed that the KO of meprin β did not affect GFAP protein levels in the brains of animals of an advanced age (15 months), owing to the point that genetic modifications of meprin β expression do not alter the inflammatory pathology of AD (Dissertation Liana Marengo). It would be interesting to further investigate whether meprin β-generated soluble Aβ is influencing this "vicious cycle" and glutamate reuptake. Interestingly, we detected EAAT-2, a major glutamate transporter, as a possible substrate in our N-terminomics data (Figure 16) and initial Western blot experiments showed promising results (Figure 15).

Another intriguing aspect of our findings is the observation of electrophysiological changes in very young animals. These precede behavioral changes and may reflect synaptogenic roles of Aβ during development. Our results raise the possibility that overexpression models may unintentionally obscure beneficial functions of Aβ by exceeding physiological levels (Cai et al., 2023). Investigating the effects of moderate Aβ elevations on developing circuits could provide new insights into both disease mechanisms and normal neurobiology.

Interestingly, despite molecular differences between APP/Ld and mepβ$^{Cre;TG/wt}$ × APP/Ld animals, no significant behavioral differences were detected in the MWM test. While both groups showed deficits relative to wild-type animals, the mepβ$^{Cre;TG/wt}$ × APP/Ld group did not display additional impairments, implying that the cognitive decline induced by APP/Ld overexpression may already saturate the measurable phenotype (Figure 26). This ceiling effect may hide subtle behavioral impacts of meprin β activity and the associated increase in Aβ levels. Additionally, mice with sole meprin β overexpression exhibit no signs of learning behavior or memory formation, further supporting the observation that a ceiling effect becomes apparent in this behavioral test (Figure 5).

5.2.5 Aβ Generation of the Novel Mepβ$^{Cre;TG/wt}$ × APP/Ld Model

APP/Ld mice express a mutant form of APP that promotes γ-secretase cleavage at the Aβ42 position of Aβ (Kujoth et al., 2014; Hyman et al., 2021). Generation of Aβ1–40 and Aβ1–42 peptides requires several previous cleavage steps that are separated from each other. To produce Aβ1–40 peptides, the γ-secretase sequentially cleaves at positions Aβ49, Aβ46, Aβ43 and finally at Aβ40. Similar to this sequence, Aβ1–42 is obtained by sequential cleavage at

Aβ48, Aβ45 and Aβ42. This latter process is increased in the APP/Ld model, resulting in an elevated amount of Aβ42 (Steiner et al., 2008; Dewachter et al., 2000). Comparison between healthy individuals and AD patients shows that the Aβ1–42 to Aβ1–40 ratio is usually skewed toward Aβ1–42, with Aβ1–42 serving as the aggregation-prone core of plaques due to its increased hydrophobicity (Jenkins et al., 1996; Xu et al., 2022; Wall et al., 2016; Nguyen et al., 2016). Although our model shows a shift toward a higher Aβ1-42 proportion relative to what is commonly seen in AD patients, the Aβ1–42/Aβ1–40 ratio in our triple-transgenic mice did not differ substantially, especially when compared to highly aggressive models such as 5xFAD (Dewachter et al., 2000). Our results suggest that while meprin β increases the absolute levels of Aβ, it does not dramatically alter the peptide profile established by APP/Ld. This supports the idea that the mepβ$^{Cre;TG/wt}$ × APP/Ld model represents a more physiologically relevant spectrum of Aβ species.

It is essential to place these findings in the context of species-specific differences in Aβ metabolism. Mouse Aβ differs from its human counterpart by three amino acids—R5G, Y10F, and H13R—which reduce its tendency to form β-sheet structures and aggregate into plaques (T´Syen et al., 2020; Jiang et al., 2021). This structural difference explains why wild-type mice do not spontaneously form amyloid plaques, even at advanced ages. To address this limitation, many models incorporate humanized APP sequences, introduce additional presenilin mutations, or utilize gene knock-ins targeting various components of AD pathology to enhance amyloid formation and better replicate disease features. However, such models may introduce confounding variables such as protein overexpression, metabolic overload, and ectopic protease activity, complicating data interpretation. Overexpression models, in particular, may produce non-physiological levels of APP or Aβ, leading to artifacts unrelated to AD, such as increased cellular stress or off-target effects (Saido et al., 2017; Jankowsky et al., 2017; Cai et al., 2024; Tatsumi et al., 2022). We successfully developed a mouse model showing a moderate increase in Aβ peptides in the hippocampus without severe phenotypic effects harming the animal.

5.2.6 GSK3β may be Modulated by Meprin β Expression and Could Serve as a Central Node in Lipid Metabolism in Meprin β KO Animals

The systemic deletion of meprin β produced an unexpected effect, as demonstrated by our results. Preliminary liver protein analyses revealed reduced levels of GSK3β and ApoE, accompanied by a phenotype of increased adiposity and fatty liver in affected animals. This raises the question of whether reduced GSK3β expression may underlie these metabolic alterations, and, if so, through which mechanisms this connection could be established.

Loss of GSK3β activity has the potential to promote hepatic lipid accumulation via multiple, interrelated mechanisms. Under normal conditions, GSK3β phosphorylates and thereby inhibits lipogenic transcription factors such as SREBP1c (Kim et al., 2004). Reduced GSK3β activity diminishes this inhibitory effect, leading to enhanced lipogenesis and upregulation of enzymes, including fatty acid synthase (FASN) and acetyl-CoA carboxylase (ACC) (Brownsey et al., 2006). In addition, GSK3β functions downstream of AKT within the insulin signaling pathway. Its reduced activity can disrupt feedback regulation, thereby promoting systemic insulin resistance and facilitating hepatic triglyceride deposition (Xu et al., 2016; Bo et al., 2024; Zhang et al., 2022). GSK3β also exerts control over glycogen metabolism by phosphorylating and inhibiting glycogen synthase (GS). When this regulatory function is impaired, GS remains constitutively active, altering hepatic glucose handling and redirecting carbon flux toward lipid storage (Wang et al., 2021; Summers et al., 1999; Oreña et al., 2000). Furthermore, GSK3β plays a central role in regulating β-catenin stability; its loss leads to β-catenin accumulation, which influences hepatocyte metabolic reprogramming and proliferation, thereby favoring lipid accumulation (Huang et al., 2017).

Despite these numerous possibilities, no direct link has been established between reduced hepatic GSK3β expression and the development of obesity. In fact, the current evidence suggests the opposite: decreased GSK3β activity has been associated with protective metabolic effects. Studies in murine models have demonstrated that hepatocyte- or adipocyte-specific GSK3β deficiency often results in improved insulin sensitivity, reduced inflammatory signaling, and healthier adipose tissue remodeling, thereby diminishing obesity-related metabolic dysfunction (Wang et al., 2024; Dewidar et al., 2023; Fromenty et al., 2022; Ye et al., 2023). These beneficial effects are supported by data showing enhanced AMPK activation and increased adiponectin production, both of which promote metabolic resilience

(Wang et al., 2024). Consequently, the current literature does not support the hypothesis that reduced hepatic GSK3β expression causally drives obesity or fatty liver. Instead, compensatory and protective pathways appear to dominate, complicating the interpretation of the observed phenotype in systemic meprin β KO animals (Wang et al., 2024; Dewidar et al., 2023; Fromenty et al., 2022; Ye et al., 2023).

Interestingly, in connection with previous electrophysiological results of this thesis, Aβ increases neuronal firing by inhibiting K+ currents via caspase and GSK3β activation, contributing to network dysfunction (Sciaccaluga et al., 2021; Scala et al., 2015). It would be interesting to examine GSK3β protein levels in animals that overexpress meprin β, and to assess how KO animals perform in electrophysiological experiments. This could further reveal that meprin β has a broader impact in the brain, not only in influencing the AMPA receptor, but also in modulating Aβ levels and, consequently, promoting neuronal hyperexcitability.

6. References

Abramson, J., Adler, J., Dunger, J. *et al.* Accurate structure prediction of biomolecular interactions with AlphaFold 3. *Nature* **630**, 493–500 (2024). https://doi.org/10.1038/s41586-024-07487-w

Al-Kuraishy, H., Jabir, M., Al-Gareeb, A., Albuhadily, A., Albukhaty, S., Sulaiman, G., & Batiha, G. (2023). Evaluation and targeting of amyloid precursor protein (APP)/amyloid beta (Aβ) axis in amyloidogenic and non-amyloidogenic pathways: A time outside the tunnel. Ageing Research Reviews, 92. https://doi.org/10.1016/j.arr.2023.102119.

Almonte, A., & Sweatt, J. (2011). Serine proteases, serine protease inhibitors, and protease-activated receptors: Roles in synaptic function and behavior. Brain Research, 1407, 107-122. https://doi.org/10.1016/j.brainres.2011.06.042.

Andrade-Guerrero, J., Santiago-Balmaseda, A., Jeronimo-Aguilar, P., Vargas-Rodríguez, I., Cadena-Suárez, A., Sánchez-Garibay, C., Pozo-Molina, G., Méndez-Catalá, C., Cárdenas-Aguayo, M., Díaz-Cintra, S., Pacheco-Herrero, M., Luna-Muñoz, J., & Soto-Rojas, L. (2023). Alzheimer's Disease: An Updated Overview of Its Genetics. International Journal of Molecular Sciences, 24. https://doi.org/10.3390/ijms24043754 .

Anyomi, B., Fosu, K., Lamptey, E., Agegnehu, S., Quarshie, J., Kampo, S., & Wei, J. (2025). Decreased Expression of Alzheimer's Disease-Related Genes in Cancer May Contribute to the Inverse-Relationship-a Computational Study. ACS Omega, 10, 17651 - 17660. https://doi.org/10.1021/acsomega.4c11571.

Arbo, B., Cechinel, L., Palazzo, R., & Siqueira, I. (2019). Endosomal dysfunction impacts extracellular vesicle release: Central role in Aβ pathology. Ageing Research Reviews, 58. https://doi.org/10.1016/j.arr.2019.101006.

Armbrust F, Bickenbach K, Koudelka T, Joos C, Keller M, Tholey A, Pietrzik CU, Becker-Pauly C. HYTANE-Identified Latrophilin-3 Cleavage by Meprin β Leads to Loss of the Interaction Domains. J Proteome Res. 2025 Apr 4;24(4):1832-1844. doi: 10.1021/acs.jproteome.4c00912. Epub 2025 Mar 26. PMID: 40135725; PMCID: PMC11976865.

Armbrust F, Bickenbach K, Altmeppen H, Foggetti A, Winkelmann A, Wulff P, Glatzel M, Pietrzik CU, Becker-Pauly C. A novel mouse model for N-terminal truncated Aβ2-x generation through meprin β overexpression in astrocytes. Cell Mol Life Sci. 2024 Mar 13;81(1):139. doi: 10.1007/s00018-024-05139-w. PMID: 38480559; PMCID: PMC10937767.

Armbrust F, Bickenbach K, Marengo L, Pietrzik C, Becker-Pauly C. The Swedish dilemma - the almost exclusive use of APPswe-based mouse models impedes adequate evaluation of alternative β-secretases. Biochim Biophys Acta Mol Cell Res. 2022 Mar;1869(3):11914. doi: 10.1016/j.bbamcr.2021.119164. Epub 2021 Oct 23. PMID: 34699873.

Arnold, P., Boll, I., Rothaug, M., Schumacher, N., Schmidt, F., Wichert, R., Schneppenheim, J., Lokau, J., Pickhinke, U., Koudelka, T., Tholey, A., Rabe, B., Scheller, J., Lucius, R., Garbers, C., Rose-John, S., & Becker-Pauly, C. (2017). Meprin Metalloproteases Generate Biologically Active Soluble Interleukin-6 Receptor to Induce Trans-Signaling. Scientific Reports, 7. https://doi.org/10.1038/srep44053.

Arolas, J., Broder, C., Jefferson, T., Guevara, T., Sterchi, E., Bode, W., Stöcker, W., Becker-Pauly, C., & Gomis-Rüth, F. (2012). Structural basis for the sheddase function of human meprin β metalloproteinase at the plasma membrane. Proceedings of the National Academy of Sciences, 109, 16131 - 16136. https://doi.org/10.1073/pnas.1211076109.

Bae, J., Kim, Y., Park, M., & Rezaie, A. (2009). Concentration dependent dual effect of thrombin in endothelial cells via Par-1 and Pi3 Kinase. Journal of Cellular Physiology, 219. https://doi.org/10.1002/jcp.21718.

Bai, G., & Pfaff, S. (2011). Protease Regulation: The Yin and Yang of Neural Development and Disease. Neuron, 72, 9-21. https://doi.org/10.1016/j.neuron.2011.09.012.

Baranowski, B., Marko, D., Fenech, R., Yang, A., & MacPherson, R. (2020). Healthy Brain, Healthy Life: a review of diet and exercise interventions to promote brain health and reduce Alzheimer's disease risk.. Applied physiology, nutrition, and metabolism = Physiologie appliquee, nutrition et metabolisme. https://doi.org/10.1139/apnm-2019-0910 .

Baudry, M., & Bi, X. (2024). Revisiting the calpain hypothesis of learning and memory 40 years later. Frontiers in Molecular Neuroscience, 17. https://doi.org/10.3389/fnmol.2024.1337850.

Baudry, M., & Bi, X. (2016). Calpain-1 and Calpain-2: The Yin and Yang of Synaptic Plasticity and Neurodegeneration. Trends in Neurosciences, 39, 235-245. https://doi.org/10.1016/j.tins.2016.01.007.

Bayer TA, Wirths O. Focusing the amyloid cascade hypothesis on N-truncated Abeta peptides as drug targets against Alzheimer's disease. Acta Neuropathol. 2014;127(6):787-801. doi: 10.1007/s00401-014-1287-x. Epub 2014 May 7. PMID: 24803226; PMCID: PMC4024135.

Bayer TA. N-Truncated Aβ Starting at Position Four-Biochemical Features, Preclinical Models, and Potential as Drug Target in Alzheimer's Disease. Front Aging Neurosci. 2021 Aug 20;13:710579. doi: 10.3389/fnagi.2021.710579. PMID: 34489680; PMCID: PMC8417877.

Becker-Pauly C, Barré O, Schilling O, Auf dem Keller U, Ohler A, Broder C, Schütte A, Kappelhoff R, Stöcker W, Overall CM. Proteomic analyses reveal an acidic prime side specificity for the astacin metalloprotease family reflected by physiological substrates. Mol Cell Proteomics. 2011 Sep;10(9):M111.009233. doi: 10.1074/mcp.M111.009233. Epub 2011 Jun 21. PMID: 21693781; PMCID: PMC3186203.

Becker-Pauly, C., Höwel, M., Walker, T., Vlad, A., Aufenvenne, K., Oji, V., Lottaz, D., Sterchi, E., Debela, M., Magdolen, V., Traupe, H., & Stöcker, W. (2007). The alpha and beta subunits of the metalloprotease meprin are expressed in separate layers of human epidermis, revealing different functions in keratinocyte proliferation and differentiation.. The Journal of investigative dermatology, 127 5, 1115-25 .

Bellenguez, C., Küçükali, F., Jansen, I., Ruiz, A., Ramírez, A., & Lambert, J. (2022). New insights into the genetic etiology of Alzheimer’s disease and related dementias. Nature Genetics, 54, 412 - 436. https://doi.org/10.1038/s41588-022-01024-z .

Berger, E., Naia, L., Leal, N., Ankarcrona, M., Giraud, R., Li, X., Nilsson, P., Dentoni, G., Bereczki, E., Liu, J., Pinho, C., Shimozawa, M., Falk, V., & Jiang, R. Mitochondrial hypermetabolism precedes impaired autophagy and synaptic disorganization in App knock-in Alzheimer mouse models. Molecular Psychiatry. 2023; 28. doi: 10.1038/s41380-023-02289-4. Epub 2023 Nov 1. PMID: 37907591; PMCID: PMC10730401.

Bernard, M. (2020). UPDATE ON NIH INCLUSION ACROSS THE LIFESPAN. Innovation in Aging, 4, 825 - 825. https://doi.org/10.1093/geroni/igaa057.3012.

Berner DK, Wessolowski L, Armbrust F, et al. Meprin β cleaves TREM2 and controls its phagocytic activity on macrophages. The FASEB Journal. 2020; 34: 6675–6687. https://doi.org/10.1096/fj.201902183R

Bertenshaw GP, Norcum MT, Bond JS. Structure of homo- and hetero-oligomeric meprin metalloproteases. Dimers, tetramers, and high molecular mass multimers. J Biol Chem. 2003 Jan 24;278(4):2522-32. doi: 10.1074/jbc.M208808200. Epub 2002 Oct 23. PMID: 12399461.

Beshir, S., Aadithsoorya, A., Parveen, A., Goh, S., Hussain, N., & Menon, V. (2022). Aducanumab Therapy to Treat Alzheimer's Disease: A Narrative Review. International Journal of Alzheimer's Disease, 2022. https://doi.org/10.1155/2022/9343514 .

Bhardwaj, A., Liyanage, S., & Weaver, D. (2023). Cancer and Alzheimer’s Inverse Correlation: an Immunogenetic Analysis. Molecular Neurobiology, 60, 3086 - 3099. https://doi.org/10.1007/s12035-023-03260-8.

Bhattacharjee, A., & Roy, P. (2022). Conjoint hepatobiliary-enterohepatic cycles for amyloid excretion and enhancing its drug-induced clearance: a systems biology approach to Alzheimer's disease. Journal of Biomolecular Structure and Dynamics, 41, 10507 - 10524. https://doi.org/10.1080/07391102.2022.2154842.

Bickenbach, K., David, N., Koudelka, T., Joos, C., Scharfenberg, F., Rüffer, M., Armbrust, F., Georgiadis, D., Beau, F., Stahmer, L., Rahn, S., Tholey, A., Pietrzik, C., & Becker-Pauly, C. (2025). Targeted approach to determine the impact of cancer-associated protease variants. Science Advances, 11. https://doi.org/10.1126/sciadv.adp5958.

Bingol, B., & Schuman, E. (2006). Activity-dependent dynamics and sequestration of proteasomes in dendritic spines. Nature, 441, 1144-1148. https://doi.org/10.1038/nature04769.

Bingol, B., & Sheng, M. (2011). Deconstruction for Reconstruction: The Role of Proteolysis in Neural Plasticity and Disease. Neuron, 69, 22-32. https://doi.org/10.1016/j.neuron.2010.11.006.

Bird, T. (1994). Familial Alzheimer's disease. Annals of Neurology, 36. https://doi.org/10.1002/ana.410360303.

Bo, T., Gao, L., Yao, Z., Shao, S., Wang, X., Proud, C., & Zhao, J. (2024). Hepatic selective insulin resistance at the intersection of insulin signaling and metabolic dysfunction-associated steatotic liver disease.. *Cell metabolism*, 36 5, 947-968 . https://doi.org/10.1016/j.cmet.2024.04.006.

Bond, J., Matters, G., Banerjee, S., & Dusheck, R. (2005). Meprin metalloprotease expression and regulation in kidney, intestine, urinary tract infections and cancer. FEBS Letters, 579. https://doi.org/10.1016/j.febslet.2005.03.045.

Bondi, M., Edmonds, E., & Salmon, D. (2017). Alzheimer's Disease: Past, Present, and Future. Journal of the International Neuropsychological Society, 23, 818 - 831. https://doi.org/10.1017/S135561771700100X.

Brakebusch, C., Seidenbecher, C. I., Asztely, F., Rauch, U., Matthies, H., Meyer, H., … Fässler, R. (2002). Brevican-Deficient Mice Display Impaired Hippocampal CA1 Long-Term Potentiation but Show No Obvious Deficits in Learning and Memory. Molecular and Cellular Biology, 22(21), 7417–7427. https://doi.org/10.1128/MCB.22.21.7417-7427.2002

Breijyeh, Z., & Karaman, R. (2020). Comprehensive Review on Alzheimer's Disease: Causes and Treatment. Molecules, 25. https://doi.org/10.3390/molecules25245789.

Breitner, J., & Folstein, M. (1984). Familial Alzheimer Dementia: a prevalent disorder with specific clinical features. Psychological Medicine, 14, 63 - 80. https://doi.org/10.1017/S0033291700003081.

Broder, C., & Becker-Pauly, C. (2013). The metalloproteases3 meprin α and meprin β: unique enzymes in inflammation, neurodegeneration, cancer and fibrosis. Biochemical Journal, 450, 253 - 264. https://doi.org/10.1042/BJ20121751.

Brody, D., Jiang, H., Wildburger, N., & Esparza, T. (2017). Non-canonical soluble amyloid-beta aggregates and plaque buffering: controversies and future directions for target discovery in Alzheimer's disease. Alzheimer's Research & Therapy, 9. https://doi.org/10.1186/s13195-017-0293-3.

Brown JC, Higgins ES, George MS. Synaptic Plasticity 101: The Story of the AMPA Receptor for the Brain Stimulation Practitioner. Neuromodulation. 2022 Dec;25(8):1289-1298. doi: 10.1016/j.neurom.2021.09.003. Epub 2021 Dec 18. PMID: 35088731; PMCID: PMC10479373.

Brownsey, R., Boone, A., Elliott, J., Kulpa, J., & Lee, W. (2006). Regulation of acetyl-CoA carboxylase.. *Biochemical Society transactions*, 34 Pt 2, 223-7 . https://doi.org/10.1042/BST20060223.

Bu, X., Xiang, Y., Ws, J., Wang, J., Shen, L., Zl, H., Zhang, K., Liu, Y., Zeng, F., Liu, J., Liu, J., Sun, H., Zq, Z., Chen, S., Yao, X., Giunta, B., Yc, S., Tan, J., Chen, X., Zf, D., Zhou, H., Zhou, X., Song, W., & Wang, Y. (2018). Blood-derived amyloid-β protein induces Alzheimer's disease pathologies. Molecular Psychiatry, 23, 1948-1956. https://doi.org/10.1038/mp.2017.204.

Buccellato, F., D'Anca, M., Tartaglia, G., Del Fabbro, M., Scarpini, E., & Galimberti, D. (2023). Treatment of Alzheimer's Disease: Beyond Symptomatic Therapies. International Journal of Molecular Sciences, 24. https://doi.org/10.3390/ijms241813900 .

Buchanan, P., Boylan, K., Walcheck, B., Heinze, R., Geller, M., Argenta, P., & Skubitz, A. (2017). Ectodomain shedding of the cell adhesion molecule Nectin-4 in ovarian cancer is mediated by ADAM10 and ADAM17. The Journal of Biological Chemistry, 292, 6339 - 6351. https://doi.org/10.1074/jbc.M116.746859.

Busi, G., Berron, D., Baumeister, H., Mohanty, R., Misirocchi, F., Mutti, C., Zilioli, A., Westman, E., Spallazzi, M., Florindo, I., Morelli, N., & Pancaldi, B. Unveiling the hippocampal subfield changes across the Alzheimer's disease continuum: a systematic review of neuroimaging studies. Brain imaging and behavior (2024). doi: 10.1007/s11682-024-00952-0. Epub 2024 Oct 23. PMID: 39443362.

Cai W, Li L, Sang S, Pan X, Zhong C. Physiological Roles of β-amyloid in Regulating Synaptic Function: Implications for AD Pathophysiology. Neurosci Bull. 2023 Aug;39(8):1289-1308. doi: 10.1007/s12264-022-00985-9. Epub 2022 Nov 28. PMID: 36443453; PMCID: PMC10387033.

Cai, D., Wang, M., Peng, T., Zhong, M., & Duarte, M. Updates on mouse models of Alzheimer's disease. Molecular Neurodegeneration. 2024; 19. https://doi.org/10.1186/s13024-024-00712-0

Carulli, D., Broersen, R., De Winter, F., Muir, E., Mešković, M., De Waal, M., De Vries, S., Boele, H., Canto, C., De Zeeuw, C., & Verhaagen, J. (2019). Cerebellar plasticity and associative memories are controlled by perineuronal nets. Proceedings of the National Academy of Sciences of the United States of America, 117, 6855 - 6865. https://doi.org/10.1073/pnas.1916163117.

Chater T. E. and Goda Y., "The Role of AMPA Receptors in Postsynaptic Mechanisms of Synaptic Plasticity," Frontiers in Cellular Neuroscience 8 (2014): 401, 10.3389/fncel.2014.00401

Chia R. S. L., Minta K., Wu L. Y., et al., "Serum Brevican as a Biomarker of Cerebrovascular Disease in an Elderly Cognitively Impaired Cohort," Biomolecules 14, no. 1 (2024): 75, 10.3390/biom14010075

Cho, Y., Bae, H., Okun, E., Arumugam, T., & Jo, D. (2022). Physiology and pharmacology of amyloid precursor protein.. Pharmacology & therapeutics, 108122 . https://doi.org/10.1016/j.pharmthera.2022.108122.

Chocron, E., Munkácsy, E., Kim, H., Karpowicz, P., Jiang, N., Van Skike, C., DeRosa, N., Banh, A., Palavicini, J., Wityk, P., Kalinowski, L., Galvan, V., Osmulski, P., Jankowska, E., Gaczynska, M., & Pickering, A. (2022). Genetic and pharmacologic proteasome augmentation ameliorates Alzheimer's-like pathology in mouse and fly APP overexpression models. Science Advances, 8. https://doi.org/10.1126/sciadv.abk2252.

Church, T., & Margolis, S. (2025). Mechanisms of ubiquitin-independent proteasomal degradation and their roles in age-related neurodegenerative disease. Frontiers in Cell and Developmental Biology, 12. https://doi.org/10.3389/fcell.2024.1531797.

Cole SL, Vassar R. The role of amyloid precursor protein processing by BACE1, the beta-secretase, in Alzheimer disease pathophysiology. J Biol Chem. 2008 Oct 31;283(44):29621-5. doi: 10.1074/jbc.R800015200. Epub 2008 Jul 23. PMID: 18650431; PMCID: PMC2662048.

Corder, E., Saunders, A., Risch, N., Strittmatter, W., Schmechel, D., Gaskell, P., Rimmler, J., Locke, P., Conneally, P., Schmader, K., Small, G., Roses, A., Haines, J., & Pericak-Vance, M. (1994). Protective effect of apolipoprotein E type 2 allele for late onset Alzheimer disease. Nature Genetics, 7, 180-184. https://doi.org/10.1038/NG0694-180.

Coronel, R., Bernabeu-Zornoza, A., Palmer, C., Muñiz-Moreno, M., Zambrano, A., Cano, E., & Liste, I. (2018). Role of Amyloid Precursor Protein (APP) and Its Derivatives in the Biology and Cell Fate Specification of Neural Stem Cells. Molecular Neurobiology, 55, 7107 - 7117. https://doi.org/10.1007/s12035-018-0914-2.

Crapser, J., Spangenberg, E., Barahona, R., Arreola, M., Hohsfield, L., & Green, K. (2020). Microglia facilitate loss of perineuronal nets in the Alzheimer's disease brain. EBioMedicine, 58. https://doi.org/10.1016/j.ebiom.2020.102919.

Crist AM, Kelly M. Hinkle, Xue Wang, Christina M. Moloney, Billie J. Matchett, Sydney A. Labuzan, Isabelle Frankenhauser. Leveraging selective hippocampal vulnerability among Alzheimer's disease subtypes reveals a novel tau binding partner SERPINA5. bioRxiv 2020.12.18.423469; doi: https://doi.org/10.1101/2020.12.18.423469

Cruchaga, C., Del-Aguila, J., Saef, B., Black, K., Fernández, M., Budde, J., Ibañez, L., Deming, Y., Kapoor, M., Tosto, G., Mayeux, R., Holtzman, D., Fagan, A., Morris, J., Bateman, R., Goate, A., & Harari, O. (2018). Polygenic risk score of sporadic late-onset Alzheimer's disease reveals a shared architecture with the familial and early-onset forms. Alzheimer's & Dementia, 14, 205-214. https://doi.org/10.1016/j.jalz.2017.08.013 .

Cummings, B., Satou, T., Head, E., Milgram, N., Cole, G., Savage, M., Podlisny, M., Selkoe, D., Siman, R., Greenberg, B., & Cotman, C. (1996). Diffuse plaques contain C-terminal Aβ 42 and not Aβ 40: Evidence from cats and dogs. Neurobiology of Aging, 17, 653-659. https://doi.org/10.1016/0197-4580(96)00062-0.

Davidson, K., & Pickering, A. (2023). The proteasome: A key modulator of nervous system function, brain aging, and neurodegenerative disease. Frontiers in Cell and Developmental Biology, 11. https://doi.org/10.3389/fcell.2023.1124907.

De La Rosa, A., Olaso-González, G., Arc-Chagnaud, C., Millan, F., Salvador-Pascual, A., García-Lucerga, C., Blasco-Lafarga, C., García-Domínguez, E., Carretero, A., Correas, A., Viña, J., & Gómez-Cabrera, M. (2020). Physical exercise in the prevention and treatment of Alzheimer's disease. Journal of Sport and Health Science, 9, 394 - 404. https://doi.org/10.1016/j.jshs.2020.01.004 .

De Strooper, B., Yarenis, L., Timmers, M., Monfared, A., Albala, B., Imbimbo, B., Watanabe, N., Hampel, H., Vanmechelen, E., Willem, M., Kimura, T., Streffer, J., Voytyuk, I., Irizarry, M., Zhou, J., Hardy, J., Vassar, R., Koyama, A., Yan, R., Vergallo, A., De Vos, A., Corbo, M., Lista, S., Nisticò, R., Kramer, L., & Singh, N. The β-Secretase BACE1 in Alzheimer's Disease. Biological Psychiatry (2021). doi: 10.1016/j.biopsych.2020.02.001. Epub 2020 Feb 13. PMID: 32223911; PMCID: PMC7533042.

Deng, Z., Wang, J., Xiao, Y., Li, F., Niu, L., Liu, X., Meng, L., & Zheng, H. (2021). Ultrasound-mediated augmented exosome release from astrocytes alleviates amyloid-β-induced neurotoxicity. Theranostics, 11, 4351 - 4362. https://doi.org/10.7150/thno.52436.

Dewachter I, Van Dorpe J, Smeijers L, Gilis M, Kuipéri C, Laenen I, Caluwaerts N, Moechars D, Checler F, Vanderstichele H, Van Leuven F. Aging increased amyloid peptide and caused amyloid plaques in brain of old APP/V717I transgenic mice by a different mechanism than mutant presenilin1. J Neurosci. 2000 Sep 1;20(17):6452-8. doi: 10.1523/JNEUROSCI.20-17-06452.2000. PMID: 10964951; PMCID: PMC6772965.

Drummond, E., Kavanagh, T., Pires, G., Martá-Ariza, M., Kanshin, E., Nayak, S., Faustin, A., Berdah, V., Ueberheide, B., & Wisniewski, T. (2022). The amyloid plaque proteome in early onset Alzheimer's disease and Down syndrome. Acta Neuropathologica Communications, 10. https://doi.org/10.1186/s40478-022-01356-1.

Duara, R., Dickson, D., Murray, M., Carter, R., DeTure, M., Asmann, Y., Lesser, E., Ertekin-Taner, N., Hinkle, K., Graff-Radford, N., Allen, M., Moloney, C., Wang, X., Carnwath, T., Serie, D., Matchett, B., Li, H., Liesinger, A., Carrasquillo, M., Tang, X., Petersen, R., Frankenhauser, I., Azu, N., Patel, T., Quicksall, Z., Crist, A., Ross, O., & Labuzan, S. Transcriptomic analysis to identify genes associated with selective hippocampal vulnerability in Alzheimer's disease. Nature Communications (2021). https://doi.org/10.1038/s41467-021-22399-3

Dunys J., Audrey Valverde, Frédéric Checler. Are N- and C-terminally truncated Aβ species key pathological triggers in Alzheimer's disease?, Journal of Biological Chemistry, Volume 293, Issue 40, 2018, Pages 15419-15428, ISSN 0021-9258. doi: 10.1074/jbc.R118.003999. Epub 2018 Aug 24. PMID: 30143530; PMCID: PMC6177599.

Duyckaerts, C., Clavaguera, F., & Potier, M. (2019). The prion-like propagation hypothesis in Alzheimer's and Parkinson's disease. Current Opinion in Neurology, 32, 266–271. https://doi.org/10.1097/WCO.0000000000000672.

Eckhard, U., Huesgen, P., Schilling, O., Bellac, C., Butler, G., Cox, J., Dufour, A., Goebeler, V., Kappelhoff, R., Keller, U., Klein, T., Lange, P., Marino, G., Morrison, C., Prudova, A., Rodríguez, D., Starr, A., Wang, Y., & Overall, C. (2016). Active site specificity profiling of the matrix metalloproteinase family: Proteomic identification of 4300 cleavage sites by nine MMPs explored with structural and synthetic peptide cleavage analyses.. Matrix biology : journal of the International Society for Matrix Biology, 49, 37-60. https://doi.org/10.1016/j.matbio.2015.09.003.

Fani G., Benedetta Mannini, Giulia Vecchi, Roberta Cascella, Cristina Cecchi, Christopher M. Dobson, Michele Vendruscolo, and Fabrizio Chiti. Aβ Oligomers Dysregulate Calcium Homeostasis by Mechanosensitive Activation of AMPA and NMDA Receptors. ACS Chemical Neuroscience 2021 12 (4), 766-781. DOI: 10.1021/acschemneuro.0c00811

Fatemi, S. (2005). Reelin glycoprotein: structure, biology and roles in health and disease. Molecular Psychiatry, 10, 251-257. https://doi.org/10.1038/sj.mp.4001613.

Favuzzi E., Marques-Smith A., Deogracias R., et al., “Activity-Dependent Gating of Parvalbumin Interneuron Function by the Perineuronal Net Protein Brevican,” Neuron 95, no. 3 (2017): 639–655, 10.1016/j.neuron.2017.06.028.

Fawcett, J., Oohashi, T., & Pizzorusso, T. (2019). The roles of perineuronal nets and the perinodal extracellular matrix in neuronal function. Nature Reviews Neuroscience, 20, 451 - 465. https://doi.org/10.1038/s41583-019-0196-3.

Ferrer-Ferrer, M., & Dityatev, A. (2018). Shaping Synapses by the Neural Extracellular Matrix. Frontiers in Neuroanatomy, 12. https://doi.org/10.3389/fnana.2018.00040.

Feyder M., Wiedholz L., Sprengel R., and Holmes A., “Impaired Associative Fear Learning in Mice With Complete Loss or Haploinsufficiency of AMPA GluR1 Receptors,” Frontiers in Behavioral Neuroscience 1 (2007): 149, 10.3389/neuro.08.004.2007

Fornari, S., Schäfer, A., Jucker, M., Goriely, A., & Kuhl, E. (2019). Prion-like spreading of Alzheimer’s disease within the brain’s connectome. Journal of the Royal Society Interface, 16. https://doi.org/10.1098/rsif.2019.0356.

Frischknecht R., Heine M., Perrais D., Seidenbecher C. I., Choquet D., and Gundelfinger E. D., “Brain Extracellular Matrix Affects AMPA Receptor Lateral Mobility and Short-Term Synaptic Plasticity,” Nature Neuroscience 12, no. 7 (2009): 897–904, 10.1038/nn.2338

Frischknecht, R., Fejtová, A., Viesti, M., Stephan, A., & Sonderegger, P. (2008). Activity-Induced Synaptic Capture and Exocytosis of the Neuronal Serine Protease Neurotrypsin. The Journal of Neuroscience, 28, 1568 - 1579. https://doi.org/10.1523/JNEUROSCI.3398-07.2008.

Frisoni, G., Altomare, D., Thal, D., Ribaldi, F., Van Der Kant, R., Ossenkoppele, R., Blennow, K., Cummings, J., Van Duijn, C., Nilsson, P., Dietrich, P., Scheltens, P., & Dubois, B. (2021). The probabilistic model of Alzheimer disease: the amyloid hypothesis revised. Nature Reviews Neuroscience, 23, 53 - 66. https://doi.org/10.1038/s41583-021-00533-w .

Galanis, C., Fellenz, M., Becker, D., Bold, C., Lichtenthaler, S., Müller, U., Deller, T., & Vlachos, A. (2020). Amyloid-Beta Mediates Homeostatic Synaptic Plasticity. The Journal of Neuroscience, 41, 5157 - 5172. https://doi.org/10.1523/JNEUROSCI.1820-20.2021.

Gao, J., Wang, L., Huntley, M., Perry, G., & Wang, X. (2018). Pathomechanisms of TDP-43 in neurodegeneration. Journal of Neurochemistry, 146. https://doi.org/10.1111/jnc.14327 .

Gellrich, A., Scharfenberg, F., Peters, F., Sammel, M., Helm, O., Armbrust, F., Schmidt, F., Lokau, J., Garbers, C., Sebens, S., Arnold, P., & Becker-Pauly, C. (2021). Characterization of the Cancer-Associated Meprin Beta Variants G45R and G89R. Frontiers in Molecular Biosciences, 8. https://doi.org/10.3389/fmolb.2021.702341.

Ghiso, J., Shayo, M., Calero, M., Ng, D., Tomidokoro, Y., Gandy, S., Rostagno, A., & Frangione, B. (2004). Systemic catabolism of Alzheimer's Abeta40 and Abeta42.. The Journal of biological chemistry, 279 44, 45897-908 .

Gindorf, M., Storck, S., Ohler, A., Scharfenberg, F., Becker-Pauly, C., & Pietrzik, C. (2020). Meprin β: A novel regulator of blood–brain barrier integrity. Journal of Cerebral Blood Flow & Metabolism, 41, 31 - 44. https://doi.org/10.1177/0271678X20905206.

Gnosa, S., Puig-Blasco, L., Piotrowski, K., Freiberg, M., Savickas, S., Madsen, D., Keller, A., Kronqvist, P., & Kveiborg, M. (2022). ADAM17-mediated EGFR ligand shedding directs macrophage-promoted cancer cell invasion. JCI Insight, 7. https://doi.org/10.1172/jci.insight.155296.

Goebbels S, Bormuth I, Bode U, Hermanson O, Schwab MH, Nave KA. Genetic targeting of principal neurons in neocortex and hippocampus of NEX-Cre mice. Genesis. 2006 Dec;44(12):611-21. doi: 10.1002/dvg.20256. PMID: 17146780.

Goedert, M. (2015). Alzheimer's and Parkinson's diseases: The prion concept in relation to assembled Aβ, tau, and α-synuclein. Science, 349. https://doi.org/10.1126/science.1255555.

Gorbea, C., Marchand, P., Jiang, W., Copeland, N. G., Gilbert, D. J., Jenkins, N. A., & Bond, J. S. (1993). Cloning, expression, and chromosomal localization of the mouse meprin beta subunit. Journal of Biological Chemistry, 268(28), 21035–21043. https://doi.org/10.1016/S0021-9258(19)36890-5

Gottschall P. E. and Howell M. D., "ADAMTS Expression and Function in Central Nervous System Injury and Disorders," Matrix Biology: Journal of the International Society for Matrix Biology 44 (2015): 70–76, 10.1016/j.matbio.2015.01.014.

Goutagny, R., & Krantic, S. (2013). Hippocampal oscillatory activity in Alzheimer's disease: toward the identification of early biomarkers?. Aging and disease, 4 3, 134-40

Gu, L., Tran, J., Jiang, L., & Guo, Z. (2016). A new structural model of Alzheimer's Aβ42 fibrils based on electron paramagnetic resonance data and Rosetta modeling.. Journal of structural biology, 194 1, 61-7 . https://doi.org/10.1016/j.jsb.2016.01.013.

Güntert, A., Döbeli, H., & Bohrmann, B. (2006). High sensitivity analysis of amyloid-beta peptide composition in amyloid deposits from human and PS2APP mouse brain. Neuroscience, 143, 461-475. https://doi.org/10.1016/j.neuroscience.2006.08.027.

Guo, Q., Li, H., Gaddam, S., Justice, N., Robertson, C., & Zheng, H. (2011). Amyloid Precursor Protein Revisited. The Journal of Biological Chemistry, 287, 2437 - 2445. https://doi.org/10.1074/jbc.M111.315051.

Hamm, V., Héraud, C., Bott, J., Herbeaux, K., Strittmatter, C., Mathis, C., & Goutagny, R. (2017). Differential contribution of APP metabolites to early cognitive deficits in a TgCRND8 mouse model of Alzheimer's disease. Science Advances, 3. https://doi.org/10.1126/sciadv.1601068.

Harris, S., & Harris, E. (2018). Molecular Mechanisms for Herpes Simplex Virus Type 1 Pathogenesis in Alzheimer's Disease. Frontiers in Aging Neuroscience, 10. https://doi.org/10.3389/fnagi.2018.00048.

Hebert, L., Beckett, L., Scherr, P., & Evans, D. (2001). Annual Incidence of Alzheimer Disease in the United States Projected to the Years 2000 Through 2050. Alzheimer Disease and Associated Disorders, 15, 169-173. https://doi.org/10.1097/00002093-200110000-00002.

Hegde, A. (2017). Proteolysis, synaptic plasticity and memory. Neurobiology of Learning and Memory, 138, 98-110. https://doi.org/10.1016/j.nlm.2016.09.003.

Hegde, A., & Upadhya, S. (2007). The ubiquitin–proteasome pathway in health and disease of the nervous system. Trends in Neurosciences, 30, 587-595. https://doi.org/10.1016/j.tins.2007.08.005.

Herl L, Thomas AV, Lill CM, Banks M, Deng A, Jones PB, Spoelgen R, Hyman BT, Berezovska O. Mutations in amyloid precursor protein affect its interactions with presenilin/gamma-secretase. Mol Cell Neurosci. 2009 Jun;41(2):166-74. doi: 10.1016/j.mcn.2009.02.008. Epub 2009 Mar 9. PMID: 19281847; PMCID: PMC2732195.

Höhn L., Hußler W., Richter A., et al., "Extracellular Matrix Changes in Subcellular Brain Fractions and Cerebrospinal Fluid of Alzheimer's Disease Patients," International Journal of Molecular Sciences 24, no. 6 (2023): 5532, 10.3390/ijms24065532.

Hone, E., Martins, I., Fonte, J., & Martins, R. (2003). Apolipoprotein E influences amyloid-beta clearance from the murine periphery. Journal of Alzheimer's Disease, 5, 1 - 8. https://doi.org/10.3233/JAD-2003-5101.

Hou, Y., Dan, X., Babbar, M., Wei, Y., Hasselbalch, S., Croteau, D., & Bohr, V. (2019). Ageing as a risk factor for neurodegenerative disease. Nature Reviews Neurology, 1-17. https://doi.org/10.1038/s41582-019-0244-7 .

Huang, Z., Lin, H., Zhang, Q., & Zong, X. (2022). Targeting Alzheimer's Disease: The Critical Crosstalk between the Liver and Brain. Nutrients, 14. https://doi.org/10.3390/nu14204298.

Huang, J., Guo, X., Li, W., & Zhang, H. (2017). Activation of Wnt/β-catenin signalling via GSK3 inhibitors direct differentiation of human adipose stem cells into functional hepatocytes. *Scientific Reports*, 7. https://doi.org/10.1038/srep40716.

Huguenin, M., Müller, E., Trachsel-Rösmann, S., Oneda, B., Ambort, D., Sterchi, E., & Lottaz, D. (2008). The Metalloprotease Meprinβ Processes E-Cadherin and Weakens Intercellular Adhesion. PLoS ONE, 3. https://doi.org/10.1371/journal.pone.0002153.

Hussain, I., Powell, D., Howlett, D., Chapman, G., Gilmour, L., Murdock, P., Tew, D., Meek, T., Chapman, C., Schneider, K., Ratcliffe, S., Tattersall, D., Testa, T., Southan, C., Ryan, D., Simmons, D., Walsh, F., Dingwall, C., & Christie, G. (2000). ASP1 (BACE2) cleaves the amyloid precursor protein at the beta-secretase site.. Molecular and cellular neurosciences, 16 5, 609-19 .

Hyman, B., Frosch, M., Pei, X., Stern, M., Saqran, L., William, C., & Ramani, M. Impairment of visual cortical plasticity by amyloid-beta species. Neurobiology of Disease. 2021; 154. doi: 10.1016/j.nbd.2021.105344. Epub 2021 Mar 22. PMID: 33766652; PMCID: PMC8113107.

Jack, C., Knopman, D., Jagust, W., Shaw, L., Aisen, P., Weiner, M., Petersen, R., & Trojanowski, J. (2010). Hypothetical model of dynamic biomarkers of the Alzheimer's pathological cascade. The Lancet Neurology, 9, 119-128. https://doi.org/10.1016/S1474-4422(09)70299-6.

Jacobsen, K., & Galanis Iverfeldt, K. (2011). O-GlcNAcylation increases non-amyloidogenic processing of the amyloid-β precursor protein (APP). Molecular Neurodegeneration, 8, P21 - P21. https://doi.org/10.1186/1750-1326-8-S1-P21.

Jäger M., Alexandra Schoberth, Peter Ruf, Jürgen Hess, Horst Lindhofer; The Trifunctional Antibody Ertumaxomab Destroys Tumor Cells That Express Low Levels of Human Epidermal Growth Factor Receptor 2. Cancer Res 15 May 2009; 69 (10): 4270–4276. https://doi.org/10.1158/0008-5472.CAN-08-2861

Jankowsky, J., & Zheng, H. Practical considerations for choosing a mouse model of Alzheimer's disease. Molecular Neurodegeneration. 2017; https://doi.org/10.1186/s13024-017-0231-7

Javaid, S., Giebel, C., Khan, M., & Hashim, M. (2021). Epidemiology of Alzheimer's disease and other dementias: rising global burden and forecasted trends. F1000Research, 10, 425. https://doi.org/10.12688/F1000RESEARCH.50786.1 .

Jefferson, T., Keller, A., Bellac, C., Metz, V., Broder, C., Hedrich, J., Ohler, A., Maier, W., Magdolen, V., Sterchi, E., Bond, J., Jayakumar, A., Traupe, H., Chalaris, A., Rose-John, S., Pietrzik, C., Postina, R., Overall, C., & Becker-Pauly, C. (2012). The substrate degradome of meprin metalloproteases reveals an unexpected proteolytic link between meprin β and ADAM10. Cellular and Molecular Life Sciences: CMLS, 70, 309 - 333. https://doi.org/10.1007/s00018-012-1106-2.

Jenkins, N., Wang, R., Sisodia, S., Gandy, S., Copeland, N., Price, D., Yager, D., Prada, C., Lee, M., Seekins, S., Ratovitsky, T., Thinakaran, G., Levey, A., Younkin, S., Borchelt, D., Davenport, F., Seeger, M., Eckman, C., Kim, G., & Slunt, H. Familial Alzheimer's Disease–Linked Presenilin 1 Variants Elevate Aβ1–42/1–40 Ratio In Vitro and In Vivo. Neuron. 1996; 17. https://doi.org/10.1016/S0896-6273(00)80230-5

Ji, Q., Chen, J., Li, Y., Tao, E., & Zhan, Y. (2024). Incidence and prevalence of Alzheimer's disease in China: a systematic review and meta-analysis.. European journal of epidemiology. https://doi.org/10.1007/s10654-024-01144-2 .

Jiang, J., Sachdev, P., Koch, F., Thalamuthu, A., Wen, W., Mather, K., & Foo, H. Associations between Alzheimer's disease polygenic risk scores and hippocampal subfield volumes in 17,161 UK Biobank participants. Neurobiology of Aging. 2020; 98. DOI: 10.1016/j.neurobiolaging.2020.11.002

Jiang, S., Green, K., Garcia, F., Tenner, A., Rodriguez-Ortiz, C., Wood, M., Matheos, D., Da Cunha, C., Phan, J., Trujillo-Estrada, L., Swarup, V., Mortazavi, A., Kramár, E., Moreno-Gonzalez, I., Balderrama-Gutierrez, G., , X., Soto, C., Shahnawaz, M., Tran, K., Walls, K., Javonillo, D., LaFerla, F., Gutiérrez, A., García-León, J., Ager, R., Huynh, K., Nguyen, M., Childs, J., Forner, S., Martini, A., Baglietto-Vargas, D., Cai, L., Kitazawa, M., MacGregor, G., & Nuñez-Diaz, C. Generation of a humanized Aβ expressing mouse demonstrating aspects of Alzheimer's disease-like pathology. Nature Communications. 2021; 12. https://doi.org/10.1038/s41467-021-22624-z

Jiang, W., Kumar, J., Matters, G., & Bond, J. (2000). Structure of the mouse metalloprotease meprin beta gene (Mep1b): alternative splicing in cancer cells.. Gene, 248 1-2, 77-87 . https://doi.org/10.1016/S0378-1119(00)00143-8.

Jin, K., Simpkins, J., Ji, X., Leis, M., & Stambler, I. (2015). The Critical Need to Promote Research of Aging and Aging-related Diseases to Improve Health and Longevity of the Elderly Population.. Aging and disease, 6 1, 1-5 . https://doi.org/10.14336/AD.2014.1210.

Jin, W., Shen, L., Bu, X., Zhang, W., Chen, S., Huang, Z., Xiong, J., Gao, C., Dong, Z., He, Y., Hu, Z., Zhou, H., Song, W., Zhou, X., Wang, Y., & Wang, Y. (2017). Peritoneal dialysis reduces amyloid-beta plasma levels in humans and attenuates Alzheimer-associated phenotypes in an APP/PS1 mouse model. Acta Neuropathologica, 134, 207-220. https://doi.org/10.1007/s00401-017-1721-y.

Jonesco D. S., Karsdal M. A., and Henriksen K., "The CNS-Specific Proteoglycan, Brevican, and Its ADAMTS4-Cleaved Fragment Show Differential Serological Levels in Alzheimer's Disease, Other Types of Dementia and Non-Demented Controls: A Cross-Sectional Study," PLoS One 15, no. 6 (2020): e0234632, 10.1371/journal.pone.0234632.

Jónsson, T., Atwal, J., Steinberg, S., Snaedal, J., Jonsson, P., Bjornsson, S., Stefánsson, H., Sulem, P., Gudbjartsson, D., Maloney, J., Hoyte, K., Gustafson, A., Liu, Y., Lu, Y., Bhangale, T., Graham, R., Huttenlocher, J., Bjornsdottir, G., Andreassen, O., Jönsson, E., Palotie, A., Behrens, T., Magnusson, O., Kong, A., Thorsteinsdóttir, U., Watts, R., & Stefánsson, K. (2012). A mutation in APP protects against Alzheimer's disease and age-related cognitive decline. Nature, 488, 96-99. https://doi.org/10.1038/nature11283 .

Kalaria, R., Maestre, G., Mahinrad, S., Acosta, D., Akinyemi, R., Alladi, S., Allegri, R., Arshad, F., Babalola, D., Baiyewu, O., Bak, T., Bellaj, T., Brodie-Mends, D., Zewde, Y., & Ismail, O. (2024). The 2022 symposium on dementia and brain aging in low- and middle-income countries: Highlights on research, diagnosis, care, and impact. Alzheimer's & Dementia, 20, 4290 - 4314. https://doi.org/10.1002/alz.13836.

Kametani, F., & Hasegawa, M. (2018). Reconsideration of Amyloid Hypothesis and Tau Hypothesis in Alzheimer's Disease. Frontiers in Neuroscience, 12. https://doi.org/10.3389/fnins.2018.00025 .

Karch, C., & Goate, A. (2015). Alzheimer's Disease Risk Genes and Mechanisms of Disease Pathogenesis. Biological Psychiatry, 77, 43-51. https://doi.org/10.1016/j.biopsych.2014.05.006 .

Karetko M. and Skangiel-Kramska J., "Diverse Functions of Perineuronal Nets," Acta Neurobiologiae Experimentalis 69, no. 4 (2009): 564–577.

Karran, E., & De Strooper, B. (2022). The amyloid hypothesis in Alzheimer disease: new insights from new therapeutics. Nature Reviews Drug Discovery, 21, 306 - 318. https://doi.org/10.1038/s41573-022-00391-w .

Katakowski, M., Jiang, F., Zheng, X., Gutierrez, J., Szalad, A., & Chopp, M. (2009). Tumorigenicity of cortical astrocyte cell line induced by the protease ADAM17. Cancer Science, 100. https://doi.org/10.1111/j.1349-7006.2009.01221.x.

Katiyar, P., Nagy, C., Sauma, S., & Bernard, M. (2020). Attracting New Investigators to Alzheimer's Disease Research: Outcomes of Increased Funding and Outreach.. The Gerontologist. https://doi.org/10.1093/geront/gnaa056 .

Keller M, Gallagher C, Kreiselmaier S, Bickenbach K, Schmitt U, Marengo L, Taghikhah D, Abukhalaf M, Tholey A, Becker-Pauly C, Mittmann T, Pietrzik CU. Meprin β Modulates Brevican Proteolysis Impairing Neural Plasticity and Memory Formation. FASEB J. 2025 May 31;39(10):e70616. doi: 10.1096/fj.202500017R. PMID: 40396346; PMCID: PMC12093287.

Kępka, A., Ochocińska, A., Borzym-Kluczyk, M., Chojnowska, S., Skorupa, E., Przychodzeń, M., & Waszkiewicz, N. (2022). Healthy Food Pyramid as Well as Physical and Mental Activity in the Prevention of Alzheimer's Disease. Nutrients, 14. https://doi.org/10.3390/nu14081534.

Kesika, P., Suganthy, N., Sivamaruthi, B., & Chaiyasut, C. (2020). Role of gut-brain axis, gut microbial composition, and probiotic intervention in Alzheimer's disease.. Life sciences, 118627 . https://doi.org/10.1016/j.lfs.2020.118627.

Khemka, S., Reddy, A., Garcia, R., Jacobs, M., Reddy, R., Roghani, A., Pattoor, V., Basu, T., Sehar, U., & Reddy, P. (2023). Role of diet and exercise in aging, Alzheimer's disease, and other chronic diseases. Ageing Research Reviews, 91. https://doi.org/10.1016/j.arr.2023.102091 .

Kienlen-Campard, P., Tasiaux, B., Van Hees, J., Li, M., Huysseune, S., Sato, T., Fei, J., Aimoto, S., Courtoy, P., Smith, S., Constantinescu, S., & Octave, J. (2008). Amyloidogenic Processing but Not Amyloid Precursor Protein (APP) Intracellular C-terminal Domain Production Requires a Precisely Oriented APP Dimer Assembled by Transmembrane GXXXG Motifs*. Journal of Biological Chemistry, 283, 7733 - 7744. https://doi.org/10.1074/jbc.M707142200.

Kim, K., Song, M., Yoo, E., Choe, S., Park, S., & Kim, J. (2004). Regulatory Role of Glycogen Synthase Kinase 3 for Transcriptional Activity of ADD1/SREBP1c*. *Journal of Biological Chemistry*, 279, 51999 - 52006. https://doi.org/10.1074/JBC.M405522200.

Kim, J., Jeong, M., Stiles, W., & Choi, H. (2022). Neuroimaging Modalities in Alzheimer's Disease: Diagnosis and Clinical Features. International Journal of Molecular Sciences, 23. https://doi.org/10.3390/ijms23116079.

Kim, K., Lee, S., Kegelman, T., Su, Z., Das, S., Dash, R., Dasgupta, S., Barral, P., Hedvat, M., Diaz, P., Reed, J., Stebbins, J., Pellecchia, M., Sarkar, D., & Fisher, P. (2011). Role of Excitatory Amino Acid Transporter-2 (EAAT2) and glutamate in neurodegeneration: Opportunities for developing novel therapeutics. Journal of Cellular Physiology, 226. https://doi.org/10.1002/jcp.22609.

Kim, M., & Bezprozvanny, I. (2021). Conformational Models of APP Processing by Gamma Secretase Based on Analysis of Pathogenic Mutations. International Journal of Molecular Sciences, 22. https://doi.org/10.3390/ijms222413600.

Klimczak P, Rizzo A, Castillo-Gómez E, Perez-Rando M, Gramuntell Y, Beltran M, Nacher J. Parvalbumin Interneurons and Perineuronal Nets in the Hippocampus and Retrosplenial Cortex of Adult Male Mice After Early Social Isolation Stress and Perinatal NMDA Receptor Antagonist Treatment. Front Synaptic Neurosci. 2021 Sep 22;13:733989. doi: 10.3389/fnsyn.2021.733989. PMID: 34630066; PMCID: PMC8493248.

Korte, N., Nortley, R., & Attwell, D. (2020). Cerebral blood flow decrease as an early pathological mechanism in Alzheimer's disease. Acta Neuropathologica, 140, 793 - 810. https://doi.org/10.1007/s00401-020-02215-w.

Krishnamurthy, A., Agrawal, A., Murlimanju, B., Joy, T., Ganaraja, B., & Rao, Y. Hippocampus and its involvement in Alzheimer's disease: a review. 3 Biotech. 2022; 12. doi: 10.1007/s13205-022-03123-4. Epub 2022 Feb 1. PMID: 35116217; PMCID: PMC8807768.

Kronenberg, D., Bruns, B., Moali, C., Goff, V., Sterchi, E., Traupe, H., Böhm, M., Hulmes, D., Stöcker, W., & Becker-Pauly, C. (2010). Processing of procollagen III by meprins: new players in extracellular matrix assembly?. The Journal of investigative dermatology, 130 12, 2727-35 . https://doi.org/10.1038/jid.2010.202.

Kruse, M., Becker, C., Lottaz, D., Köhler, D., Yiallouros, I., Krell, H., Sterchi, E., & Stöcker, W. (2004). Human meprin alpha and beta homo-oligomers: cleavage of basement membrane proteins and sensitivity to metalloprotease inhibitors.. The Biochemical journal, 378 Pt 2, 383-9 . https://doi.org/10.1042/BJ20031163.

Kujoth, G., Kukreja, L., Prolla, T., Van Leuven, F., & Vassar, R. Increased mtDNA mutations with aging promotes amyloid accumulation and brain atrophy in the APP/Ld transgenic mouse model of Alzheimer's disease. Molecular Neurodegeneration. 2014; 9. https://doi.org/10.1186/1750-1326-9-16

Kukreja, L., Kujoth, G., Prolla, T., Van Leuven, F., & Vassar, R. (2014). Increased mtDNA mutations with aging promotes amyloid accumulation and brain atrophy in the APP/Ld transgenic mouse model of Alzheimer's disease. Molecular Neurodegeneration, 9, 16 - 16. https://doi.org/10.1186/1750-1326-9-16.

Kumar, Y. (2019). Nature's Derivative(s) as Alternative Anti-Alzheimer's Disease Treatments. Journal of Alzheimer's Disease Reports, 3, 279 - 297. https://doi.org/10.3233/ADR-190137 .

Langa, K. (2015). Is the risk of Alzheimer's disease and dementia declining?. Alzheimer's Research & Therapy, 7. https://doi.org/10.1186/s13195-015-0118-1.

Lanni, C., Masi, M., Racchi, M., & Govoni, S. (2020). Cancer and Alzheimer's disease inverse relationship: an age-associated diverging derailment of shared pathways. Molecular Psychiatry, 26, 280-295. https://doi.org/10.1038/s41380-020-0760-2.

Lech, A., Wiera, G., & Mozrzymas, J. (2019). Matrix metalloproteinase-3 in brain physiology and neurodegeneration.. Advances in clinical and experimental medicine : official organ Wroclaw Medical University. https://doi.org/10.17219/acem/110319.

Lesnikova, A., Casarotto, P., Biojone, C., & Castrén, E. (2021). Perineuronal Net Receptor PTPσ Regulates Retention of Memories. Frontiers in Synaptic Neuroscience, 13. https://doi.org/10.3389/fnsyn.2021.672475.

Li, D. (2019). Analysis of Funded Projects by National Institutes of Health in the Field of Aging from 2008 to 2017 (P01-006-19).. Current developments in nutrition, 3 Suppl 1. https://doi.org/10.1093/cdn/nzz028.P01-006-19.

Li, W., Wang, D., Sun, X., Zhang, Y., Wang, L., & Suo, J. (2018). ADAM17 promotes lymph node metastasis in gastric cancer via activation of the Notch and Wnt signaling pathways. International Journal of Molecular Medicine, 43, 914 - 926. https://doi.org/10.3892/ijmm.2018.4028.

Li, X., Feng, X., Sun, X., Hou, N., Han, F., & Liu, Y. (2022). Global, regional, and national burden of Alzheimer's disease and other dementias, 1990–2019. Frontiers in Aging Neuroscience, 14. https://doi.org/10.3389/fnagi.2022.937486

Li, X., Li, N., Zhao, P., Ren, D., Luo, B., & Zhou, T. (2023). Perineuronal Nets: From Structure to Neurological Disorders.. Current medicinal chemistry. https://doi.org/10.2174/0109298673258290231009111633.

Li, X., Wang, P., & Xie, Y. (2020). Protease nexin-1 protects against Alzheimer's disease by regulating the sonic hedgehog signaling pathway. International Journal of Neuroscience, 131, 1087 - 1096. https://doi.org/10.1080/00207454.2020.1773821.

Li, X., Wu, X., Lu, T., Kuang, C., Si, Y., Zheng, W., Li, Z., & Xue, Y. (2024). Perineuronal Nets in the CNS: Architects of Memory and Potential Therapeutic Target in Neuropsychiatric Disorders. International Journal of Molecular Sciences, 25. https://doi.org/10.3390/ijms25063412.

Limegrover, C., Levine, H., Izzo, N., Yurko, R., Mozzoni, K., Rehak, C., Sadlek, K., Safferstein, H., & Catalano, S. (2020). Alzheimer's protection effect of A673T mutation may be driven by lower Aβ oligomer binding affinity. Journal of Neurochemistry, 157, 1316 - 1330. https://doi.org/10.1111/jnc.15212.

Liu W. S., You J., Chen S. D., et al., "Plasma Proteomics Identify Biomarkers and Undulating Changes of Brain Aging," Nature Aging 5 (2024): 99–112, 10.1038/s43587-024-00753-6.

Liu, Z., Choi, W., Maletić-Savatić, M., Semerci, F., Tosun, M., Jeong, H., & Karakas, C. Metabolomics of mammalian brain reveals regional differences. BMC Systems Biology. 2018; 12. doi: 10.1186/s12918-018-0644-0. PMID: 30577853; PMCID: PMC6302375

Luo, X., Prior, M., He, W., Hu, X., Tang, X., Shen, W., Yadav, S., Kiryu-Seo, S., Miller, R., Trapp, B., & Yan, R. (2011). Cleavage of Neuregulin-1 by BACE1 or ADAM10 Protein Produces Differential Effects on Myelination*. The Journal of Biological Chemistry, 286, 23967 - 23974. https://doi.org/10.1074/jbc.M111.251538.

Mackic, J., Bading, J., Ghiso, J., Walker, L., Wisniewski, T., Frangione, B., & Zlokovic, B. (2002). Circulating amyloid-beta peptide crosses the blood-brain barrier in aged monkeys and contributes to Alzheimer's disease lesions.. Vascular pharmacology, 38 6, 303-13 . https://doi.org/10.1016/S1537-1891(02)00198-2.

Madani, R., Hulo, S., Toni, N., Madani, H., Steimer, T., Muller, D., & Vassalli, J. (1999). Enhanced hippocampal long-term potentiation and learning by increased neuronal expression of tissue-type plasminogen activator in transgenic mice. The EMBO Journal, 18. https://doi.org/10.1093/emboj/18.11.3007.

Maloney, J., Bainbridge, T., Gustafson, A., Zhang, S., Kyauk, R., , P., , S., Brug, M., Liu, Y., Ernst, J., Watts, R., Jasvinder, K., & , A. (2014). Molecular Mechanisms of Alzheimer's Disease Protection by the A673T Allele of Amyloid Precursor Protein. .

Mañucat-Tan, N., Saadipour, K., Wang, Y., Bobrovskaya, L., & Zhou, X. (2018). Cellular Trafficking of Amyloid Precursor Protein in Amyloidogenesis Physiological and Pathological Significance. Molecular Neurobiology, 56, 812 - 830. https://doi.org/10.1007/s12035-018-1106-9.

Masters, C., Bateman, R., Blennow, K., Rowe, C., Sperling, R., & Cummings, J. (2015). Alzheimer's disease. Nature Reviews Disease Primers. https://doi.org/10.1038/nrdp.2015.56.

Mathews, P., & Levy, E. (2016). Cystatin C in aging and in Alzheimer's disease. Ageing Research Reviews, 32, 38-50. https://doi.org/10.1016/j.arr.2016.06.003.

Mckhann, G., Drachman, D., Folstein, M., Katzman, R., Price, D., & Stadlan, E. (1984). Clinical diagnosis of Alzheimer's disease. Neurology, 34, 939 - 939. https://doi.org/10.1212/WNL.34.7.939.

Medoro, A., Bartollino, S., Mignogna, D., Marziliano, N., Porcile, C., Nizzari, M., Florio, T., Pagano, A., Raimo, G., Intrieri, M., & Russo, C. (2019). Proteases Upregulation in Sporadic Alzheimer's Disease Brain. Journal of Alzheimer's Disease, 68, 931 - 938. https://doi.org/10.3233/JAD-181284.

Meighan, S., Meighan, P., Choudhury, P., Davis, C., Olson, M., Zornes, P., Wright, J., & Harding, J. (2006). Effects of extracellular matrix-degrading proteases matrix metalloproteinases 3 and 9 on spatial learning and synaptic plasticity. Journal of Neurochemistry, 96. https://doi.org/10.1111/j.1471-4159.2005.03565.x.

Minta K., Brinkmalm G., Portelius E., et al., "Brevican and Neurocan Peptides as Potential Cerebrospinal Fluid Biomarkers for Differentiation Between Vascular Dementia and Alzheimer's Disease," Journal of Alzheimer's Disease 79, no. 2 (2021): 729–741, 10.3233/JAD-201039

Minta K., Portelius E., Janelidze S., et al., "Cerebrospinal Fluid Concentrations of Extracellular Matrix Proteins in Alzheimer's Disease," Journal of Alzheimer's Disease 69, no. 4 (2019): 1213–1220, 10.3233/JAD-190187.

Mirzadeh, Z., Alonge, K., Cabrales, E., Herranz-Pérez, V., Scarlett, J., Brown, J., Hassouna, R., Matsen, M., Nguyen, H., García-Verdugo, J., Zeltser, L., & Schwartz, M. (2018). Perineuronal Net Formation during the Critical Period for Neuronal Maturation in the Hypothalamic Arcuate Nucleus. Nature metabolism, 1, 212 - 221. https://doi.org/10.1038/s42255-018-0029-0.

Monfared, A., Byrnes, M., White, L., & Zhang, Q. (2022). Alzheimer's Disease: Epidemiology and Clinical Progression. Neurology and Therapy, 11, 553 - 569. https://doi.org/10.1007/s40120-022-00338-8.

Morawski, M., Brückner, G., Jäger, C., Seeger, G., Matthews, R., & Arendt, T. (2012). Involvement of Perineuronal and Perisynaptic Extracellular Matrix in Alzheimer's Disease Neuropathology. Brain Pathology, 22. https://doi.org/10.1111/j.1750-3639.2011.00557.x .

Morawski, M., Brückner, M., Riederer, P., Brückner, G., & Arendt, T. (2004). Perineuronal nets potentially protect against oxidative stress. Experimental Neurology, 188, 309-315. https://doi.org/10.1016/j.expneurol.2004.04.017.

Morawski, M., Reinert, T., Meyer-Klaucke, W., Wagner, F., Tröger, W., Reinert, A., Jäger, C., Brückner, G., & Arendt, T. (2015). Ion exchanger in the brain: Quantitative analysis of perineuronally fixed anionic binding sites suggests diffusion barriers with ion sorting properties. Scientific Reports, 5. https://doi.org/10.1038/srep16471.

Müller, U., & Zheng, H. (2012). Physiological functions of APP family proteins.. Cold Spring Harbor perspectives in medicine, 2 2, a006288 . https://doi.org/10.1101/cshperspect.a006288.

Mueller-Buehl, C., Pakusch, J., Bader, V., Winklhofer, K., Mark, M., & Faissner, A. (2025). Combined loss of brevican, neurocan, tenascin-C and tenascin-R leads to impaired fear retrieval due to perineuronal net loss. *Scientific Reports*, 15. https://doi.org/10.1038/s41598-025-89580-2.

Multhaup, G. (1994). Identification and regulation of the high affinity binding site of the Alzheimer's disease amyloid protein precursor (APP) to glycosaminoglycans.. Biochimie, 76 3-4, 304-11 . https://doi.org/10.1016/0300-9084(94)90163-5.

Musicco, M., Adorni, F., Di Santo, S., Prinelli, F., Pettenati, C., Caltagirone, C., Palmer, K., & Russo, A. (2013). Inverse occurrence of cancer and Alzheimer disease. Neurology, 81, 322 - 328. https://doi.org/10.1212/WNL.0b013e31829c5ec1.

Naguib S, Lopez-Lee C, Torres ER, Lee SI, Zhu J, Zhu D, Ye P, Norman K, Zhao M, Wong MY, Ambaw YA, Muñoz-Castañeda R, Wang W, Patel T, Bhagwat M, Norinsky R, Mok SA, Walther TC, Farese RV Jr, Luo W, Sinha SC, Wu Z, Fan L, Gong S, Gan L. The R136S mutation in the APOE3 gene confers resilience against tau pathology via inhibition

of the cGAS-STING-IFN pathway. Immunity. 2025 Aug 12;58(8):1931-1947.e9. doi: 10.1016/j.immuni.2025.05.023. Epub 2025 Jun 23. PMID: 40555238; PMCID: PMC12406129.Selkoe

Nagy, V., Bozdagi, O., & Huntley, G. (2007). The extracellular protease matrix metalloproteinase-9 is activated by inhibitory avoidance learning and required for long-term memory.. Learning & memory, 14 10, 655-64 . https://doi.org/10.1101/LM.678307.

Nakamura, H., Fujii, Y., Inoki, I., Sugimoto, K., Tanzawa, K., Matsuki, H., Miura, R., Yamaguchi, Y., & Okada, Y. (2000). Brevican Is Degraded by Matrix Metalloproteinases and Aggrecanase-1 (ADAMTS4) at Different Sites*. The Journal of Biological Chemistry, 275, 38885 - 38890. https://doi.org/10.1074/JBC.M003875200.

Nakazawa K., McHugh T. J., Wilson M. A., and Tonegawa S., "NMDA Receptors, Place Cells and Hippocampal Spatial Memory," Nature Reviews Neuroscience 5, no. 5 (2004): 361–372

Nguyen, P., Chen, Y., Lan, P., Truong, P., Li, M., Nguyen, H., Man, V., Thu, T., & Tu, L. Aβ41 Aggregates More Like Aβ40 than Like Aβ42: In Silico and in Vitro Study.. The journal of physical chemistry. B. 2016; 120 30. doi: 10.1021/acs.jpcb.6b06368. Epub 2016 Jul 21. PMID: 27388669.

Nilsson, P., Loganathan, K., Sekiguchi, M., Matsuba, Y., Hui, K., Tsubuki, S., Tanaka, M., Iwata, N., Saito, T., & Saido, T. (2013). Aβ secretion and plaque formation depend on autophagy.. Cell reports, 5 1, 61-9 . https://doi.org/10.1016/j.celrep.2013.08.042.

Noori, A., Mezlini, A., Hyman, B., Serrano-Pozo, A., & Das, S. (2020). Systematic review and meta-analysis of human transcriptomics reveals neuroinflammation, deficient energy metabolism, and proteostasis failure across neurodegeneration. Neurobiology of disease, 149, 105225 - 105225. https://doi.org/10.1016/j.nbd.2020.105225.

Oreña, S., Torchia, A., & Garofalo, R. (2000). Inhibition of Glycogen-synthase Kinase 3 Stimulates Glycogen Synthase and Glucose Transport by Distinct Mechanisms in 3T3-L1 Adipocytes*. *The Journal of Biological Chemistry*, 275, 15765 - 15772. https://doi.org/10.1074/jbc.M910002199.

Ospina-Romero, M., Ospina-Romero, M., Glymour, M., Hayes-Larson, E., Mayeda, E., Graff, R., Brenowitz, W., Ackley, S., Witte, J., & Kobayashi, L. (2020). Association Between Alzheimer Disease and Cancer With Evaluation of Study Biases. JAMA Network Open, 3. https://doi.org/10.1001/jamanetworkopen.2020.25515.

Ostrowski, D., Ramsey, J., Ostrowski, T., Han, B., Chimienti, K., & Schodl, T. Synaptic Profile and Oxidative Stress Associated with Amyloid-β in the Hippocampus. Physiology (2024). DOI:10.1152/physiol.2024.39.S1.2465

Paillard, T., Blain, H., & Bernard, P. (2024). The impact of exercise on Alzheimer's disease progression. Expert Review of Neurotherapeutics, 24, 333 - 342. https://doi.org/10.1080/14737175.2024.2319766.

Pamplona, R., Domínguez-González, M., Piñol-Ripoll, G., Portero-Otín, M., Ferrer, I., Berdún, R., Gil-Villar, M., Cabré, R., Mota-Martorell, N., Jové, M., Naudí, A., Ayala, V., & Òbis, È. Specific Metabolomics Adaptations Define a Differential Regional Vulnerability in the Adult Human Cerebral Cortex. Frontiers in Molecular Neuroscience (2016); 9. doi: 10.3389/fnmol.2016.00138. PMID: 28008307; PMCID: PMC5143679.

Pantazopoulos H., Gisabella B., Rexrode L., et al., "Circadian Rhythms of Perineuronal Net Composition," Eneuro 7, no. 4 (2020) ENEURO.0034-19.2020, 10.1523/ENEURO.0034-19.2020.

Patel T., K. J. Brookes, J. Turton, S. Chaudhury, T. Guetta-Baranes, R. Guerreiro, J. Bras, D. Hernandez, A. Singleton, P. T. Francis, J. Hardy and K. Morgan. (2018) Neuropathology and Applied Neurobiology 44, 506–521 Whole-exome sequencing of the BDR cohort: evidence to support the role of the PILRA gene in Alzheimer's disease. https://doi.org/10.1111/nan.12452

Patrick, M., Omar, N., Werner, C., Mitra, S., & Jarome, T. (2023). The ubiquitin-proteasome system and learning-dependent synaptic plasticity – A 10 year update. Neuroscience & Biobehavioral Reviews, 152. https://doi.org/10.1016/j.neubiorev.2023.105280.

Peng, Y., Chen, Q., Xue, Y., Jin, H., Liu, S., Du, M., & Yao, S. (2024). Ginkgo biloba and Its Chemical Components in the Management of Alzheimer's Disease.. The American journal of Chinese medicine, 1-42 . https://doi.org/10.1142/S0192415X24500277 .

Peters F., Rahn S., Mengel M., et al., "Syndecan-1 Shedding by Meprin β Impairs Keratinocyte Adhesion and Differentiation in Hyperkeratosis," Matrix Biology 102 (2021): 37–69, 10.1016/j.matbio.2021.08.002.

Peters, F., & Becker-Pauly, C. (2019). Role of meprin metalloproteases in metastasis and tumor microenvironment. Cancer and Metastasis Reviews, 38, 347 - 356. https://doi.org/10.1007/s10555-019-09805-5.

Petrushanko, I., Mitkevich, V., & Makarov, A. (2023). Effect of β-amyloid on blood-brain barrier properties and function. Biophysical Reviews, 15, 183-197. https://doi.org/10.1007/s12551-023-01052-x.

Piaceri, I., Nacmias, B., & Sorbi, S. (2013). Genetics of familial and sporadic Alzheimer's disease.. Frontiers in bioscience, 5, 167-77 . https://doi.org/10.2741/E605 .

Pietrzik, Claus U., Busse, Tracy, Merriam, David E., Weggen, Sascha, Koo, Edward H. The cytoplasmic domain of the LDL receptor-related protein regulates multiple steps in APP processing (2002); The EMBO Journal; 5691-5700;0261-4189; https://doi.org/10.1093/emboj/cdf568; https://www.embopress.org/doi/abs/10.1093/emboj/cdf568

Pimplikar, S. (2009). Reassessing the amyloid cascade hypothesis of Alzheimer's disease.. The international journal of biochemistry & cell biology, 41 6, 1261-8 . https://doi.org/10.1016/j.biocel.2008.12.015 .

Rahman, A., Hossen, M., Chowdhury, M., Bari, S., Tamanna, N., Sultana, S., Haque, S., Masud, A., & Saif-Ur-Rahman, K. (2023). Aducanumab for the treatment of Alzheimer's disease: a systematic review. Psychogeriatrics, 23, 512 - 522. https://doi.org/10.1111/psyg.12944.

Rajabli, F., Benchek, P., Tosto, G., Reitz, C., & Naj, A. (2023). Multi-ancestry genome-wide meta-analysis of 56,241 individuals identifies LRRC4C, LHX5-AS1 and nominates ancestry-specific loci PTPRK, GRB14, and KIAA0825 as novel risk loci for Alzheimer disease: the Alzheimer Disease Genetics Consortium. medRxiv : the preprint server for health sciences. https://doi.org/10.1101/2023.07.06.23292311.

Rajendran, L., Honsho, M., Zahn, T., Keller, P., Geiger, K., Verkade, P., & Simons, K. (2006). Alzheimer's disease beta-amyloid peptides are released in association with exosomes.. Proceedings of the National Academy of Sciences of the United States of America, 103 30, 11172-7 . https://doi.org/10.1073/PNAS.0603838103.

Rauch, U et al., Cloning and primary structure of neurocan, a developmentally regulated, aggregating chondroitin sulfate proteoglycan of brain. Journal of Biological Chemistry, Volume 267, Issue 27, 19536 – 19547.

Rawlings N., Alan J Barrett, Paul D Thomas, Xiaosong Huang, Alex Bateman, Robert D Finn, The MEROPS database of proteolytic enzymes, their substrates and inhibitors in 2017 and a comparison with peptidases in the PANTHER database, Nucleic Acids Research, Volume 46, Issue D1, 4 January 2018, Pages D624–D632, https://doi.org/10.1093/nar/gkx1134

Reddy, P., Kandimalla, R., Yin, X., & Mańczak, M. Hippocampal mutant APP and amyloid beta-induced cognitive decline, dendritic spine loss, defective autophagy, mitophagy and mitochondrial abnormalities in a mouse model of Alzheimer's disease. Human Molecular Genetics. 2018; 27. doi: 10.1093/hmg/ddad147. PMID: 29408999; PMCID: PMC6455948.

Reichelt, A. (2020). Is loss of perineuronal nets a critical pathological event in Alzheimer's disease?. EBioMedicine, 59. https://doi.org/10.1016/j.ebiom.2020.102946.

Reichelt, A., Hare, D., Bussey, T., & Saksida, L. (2019). Perineuronal Nets: Plasticity, Protection, and Therapeutic Potential. Trends in Neurosciences, 42, 458-470. https://doi.org/10.1016/j.tins.2019.04.003.

Ricciarelli, R., & Fedele, E. (2017). The Amyloid Cascade Hypothesis in Alzheimer's Disease: It's Time to Change Our Mind. Current Neuropharmacology, 15, 926 - 935. https://doi.org/10.2174/1570159X15666170116143743 .

Ridler, C. BACE1 inhibitors block new Aβ plaque formation. Nat Rev Neurol 14, 126 (2018). https://doi.org/10.1038/nrneurol.2018.12

Rodkin, S., Dzreyan, V., Khaitin, A., Pitinova, M., Eid, M., & Demyanenko, S. (2021). Expression and Localization of C-APP and N-APP in Peripheral Neurons of Rats and Crayfish After Axotomy. . https://doi.org/10.21203/RS.3.RS-721350/V1.

Saido, T., Winblad, B., Saito, T., De Strooper, B., Hardy, J., Nagata, K., Sasaguri, H., Hashimoto, S., Vassar, R., & Nilsson, P. APP mouse models for Alzheimer's disease preclinical studies. The EMBO Journal. 2017; 36. doi: 10.15252/embj.201797397. Epub 2017 Aug 1. PMID: 28768718; PMCID: PMC5579350.

Salazar, I., Caldeira, M., Curcio, M., & Duarte, C. (2015). The Role of Proteases in Hippocampal Synaptic Plasticity: Putting Together Small Pieces of a Complex Puzzle. Neurochemical Research, 41, 156 - 182. https://doi.org/10.1007/s11064-015-1752-5.

Samaey, C., Schreurs, A., Stroobants, S., & Balschun, D. (2019). Early Cognitive and Behavioral Deficits in Mouse Models for Tauopathy and Alzheimer's Disease. Frontiers in Aging Neuroscience, 11. https://doi.org/10.3389/fnagi.2019.00335 .

Sanchez, B., Kraszewski, P., Lee, S., & Cope, E. (2023). From molecules to behavior: Implications for perineuronal net remodeling in learning and memory. Journal of Neurochemistry, 168, 1854 - 1876. https://doi.org/10.1111/jnc.16036.

Sanghai, N., & Tranmer, G. (2023). Biochemical and Molecular Pathways in Neurodegenerative Diseases: An Integrated View. Cells, 12. https://doi.org/10.3390/cells12182318 .

Saroja S. R., Sase A., Kircher S. G., et al., "Hippocampal Proteoglycans Brevican and Versican Are Linked to Spatial Memory of Sprague-Dawley Rats in the Morris Water Maze," Journal of Neurochemistry 130, no. 6 (2014): 797–804, 10.1111/jnc.12783.

Sasaki, T., Zhu, R., Zhang, Y., Shi, Y., Zhang, L., Li, J., Lu, Y., Liu, X., Chen, X., Jiang, G., Huo, D., Wei, Z., Hu, B., Ye, W., Li, Z., Han, F., & Song, H. Decreased synapse-associated proteins are associated with the onset of epileptic memory impairment in endothelial CDK5-deficient mice. MedComm. 2022; 3. doi: 10.1002/mco2.128. PMID: 35770064; PMCID: PMC9209881.

Savastano, S., Tarantino, G., D'Esposito, V. et al. Bisphenol-A plasma levels are related to inflammatory markers, visceral obesity and insulin-resistance: a cross-sectional study on adult male population. J Transl Med 13, 169 (2015). https://doi.org/10.1186/s12967-015-0532-y

Scala, F., Fusco, S., Ripoli, C., Piacentini, R., Puma, D., Spinelli, M., Laezza, F., Grassi, C., & D'Ascenzo, M. (2015). Intraneuronal Aβ accumulation induces hippocampal neuron hyperexcitability through A-type K+ current inhibition mediated by activation of caspases and GSK-3. Neurobiology of Aging, 36, 886-900. https://doi.org/10.1016/j.neurobiolaging.2014.10.034.)

Schäffler H., Li W., Helm O., et al., "The Cancer-Associated Meprin β Variant G32R Provides an Additional Activation Site and Promotes Cancer Cell Invasion," Journal of Cell Science 132, no. 11 (2019): jcs220665, 10.1242/jcs.220665.

Schönherr, C., Bien, J., Isbert, S., Wichert, R., Prox, J., Altmeppen, H., Kumar, S., Walter, J., Lichtenthaler, S., Weggen, S., Glatzel, M., Becker-Pauly, C., & Pietrzik, C. (2016). Generation of aggregation prone N-terminally

truncated amyloid β peptides by meprin β depends on the sequence specificity at the cleavage site. Molecular Neurodegeneration, 11. https://doi.org/10.1186/s13024-016-0084-5.

Sciaccaluga, M., Megaro, A., Bellomo, G., Ruffolo, G., Romoli, M., Palma, E., & Costa, C. (2021). An Unbalanced Synaptic Transmission: Cause or Consequence of the Amyloid Oligomers Neurotoxicity?. International Journal of Molecular Sciences, 22. https://doi.org/10.3390/ijms22115991.

Selkoe, D., & Hardy, J. (2016). The amyloid hypothesis of Alzheimer's disease at 25 years. EMBO Molecular Medicine, 8, 595 - 608. https://doi.org/10.15252/emmm.201606210 .

Selkoe, D., Yamazaki, T., Citron, M., Podlisny, M., Koo, E., Teplow, D., & Haass, C. (1996). The role of APP processing and trafficking pathways in the formation of amyloid beta-protein.. Annals of the New York Academy of Sciences, 777, 57-64 .

Semyachkina-Glushkovskaya, O., Penzel, T., Poluektov, M., Fedosov, I., Tzoy, M., Terskov, A., Blokhina, I., Sidorov, V., & Kurths, J. (2023). Phototherapy of Alzheimer's Disease: Photostimulation of Brain Lymphatics during Sleep: A Systematic Review. International Journal of Molecular Sciences, 24. https://doi.org/10.3390/ijms241310946.

Sergeant N, Bombois S, Ghestem A, Drobecq H, Kostanjevecki V, Missiaen C, Wattez A, David JP, Vanmechelen E, Sergheraert C, Delacourte A. Truncated beta-amyloid peptide species in pre-clinical Alzheimer's disease as new targets for the vaccination approach. J Neurochem. 2003 Jun;85(6):1581-91. doi: 10.1046/j.1471-4159.2003.01818.x. PMID: 12787077.

Shafi, O. (2016). Inverse relationship between Alzheimer's disease and cancer, and other factors contributing to Alzheimer's disease: a systematic review. BMC Neurology, 16. https://doi.org/10.1186/s12883-016-0765-2.

Sharma A., Hill K. E., and Schwarzbauer J. E., "Extracellular Matrix Composition Affects Outgrowth of Dendrites and Dendritic Spines on Cortical Neurons," Frontiers in Cellular Neuroscience 17 (2023): 1177663, 10.3389/fncel.2023.1177663.

Sigal Y. H., H. Bae, L.J. Bogart, T.K. Hensch, & X. Zhuang, Structural maturation of cortical perineuronal nets and their perforating synapses revealed by superresolution imaging, Proc. Natl. Acad. Sci. U.S.A. 116 (14) 7071-7076, https://doi.org/10.1073/pnas.1817222116 (2019).

Shigemori, K., Nomura, S., Umeda, T., Takeda, S., & Tomiyama, T. (2022). Peripheral Aβ acts as a negative modulator of insulin secretion. Proceedings of the National Academy of Sciences of the United States of America, 119. https://doi.org/10.1073/pnas.2117723119.

Shimohama, S., Fujioka, R., Mihira, N., Sekiguchi, M., Sartori, L., Joho, D., Saito, T., Saido, T., Nakahara, J., Hino, T., Hoshino, A., & Sasaguri, H. (2024). The Icelandic Mutation (APP-A673T) Is Protective against Amyloid Pathology In Vivo. The Journal of Neuroscience, 44. https://doi.org/10.1523/JNEUROSCI.0223-24.2024.

Sims JR, Zimmer JA, Evans CD, Lu M, Ardayfio P, Sparks J, Wessels AM, Shcherbinin S, Wang H, Monkul Nery ES, Collins EC, Solomon P, Salloway S, Apostolova LG, Hansson O, Ritchie C, Brooks DA, Mintun M, Skovronsky DM; TRAILBLAZER-ALZ 2 Investigators. Donanemab in Early Symptomatic Alzheimer Disease: The TRAILBLAZER-ALZ 2 Randomized Clinical Trial. JAMA. 2023 Aug 8;330(6):512-527. doi: 10.1001/jama.2023.13239. PMID: 37459141; PMCID: PMC10352931.

Singh, J., Habean, M., & Panicker, N. (2023). Inflammasome assembly in neurodegenerative diseases. Trends in neurosciences. https://doi.org/10.1016/j.tins.2023.07.009.

Sinha, S., & Lieberburg, I. (1999). Cellular mechanisms of beta-amyloid production and secretion.. Proceedings of the National Academy of Sciences of the United States of America, 96 20, 11049-53 . https://doi.org/10.1073/PNAS.96.20.11049.

Szklarczyk D., Katerina Nastou, Mikaela Koutrouli, Rebecca Kirsch, Farrokh Mehryary, Radja Hachilif, Dewei Hu, Matteo E Peluso, Qingyao Huang, Tao Fang, Nadezhda T Doncheva, Sampo Pyysalo, Peer Bork, Lars J Jensen, Christian von Mering, The STRING database in 2025: protein networks with directionality of regulation, *Nucleic Acids Research*, Volume 53, Issue D1, 6 January 2025, Pages D730–D737, https://doi.org/10.1093/nar/gkae1113

Sonntag M., Blosa M., Schmidt S., et al., "Synaptic Coupling of Inner Ear Sensory Cells Is Controlled by Brevican-Based Extracellular Matrix Baskets Resembling Perineuronal Nets," BMC Biology 16, no. 1 (2018): 99, 10.1186/s12915-018-0566-8.

Sorg B. A., Berretta S., Blacktop J. M., et al., "Casting a Wide Net: Role of Perineuronal Nets in Neural Plasticity," Journal of Neuroscience 36, no. 45 (2016): 11459–11468.

Sosa, L., Cáceres, A., Dupraz, S., Oksdath, M., Quiroga, S., & Lorenzo, A. (2017). The physiological role of the amyloid precursor protein as an adhesion molecule in the developing nervous system. Journal of Neurochemistry, 143. https://doi.org/10.1111/jnc.14122.

Şovrea, A., Boşca, A., Dronca, E., Constantin, A., Crintea, A., Sufleţel, R., Ştefan, R., Ştefan, P., Onofrei, M., Tschall, C., & Crivii, C. (2025). Non-Drug and Non-Invasive Therapeutic Options in Alzheimer's Disease. Biomedicines, 13. https://doi.org/10.3390/biomedicines13010084 .

Spires-Jones, T., Attems, J., & Thal, D. (2017). Interactions of pathological proteins in neurodegenerative diseases. Acta Neuropathologica, 134, 187 - 205. https://doi.org/10.1007/s00401-017-1709-7 .

Stanton H., James Melrose, Christopher B. Little, Amanda J. Fosang. Proteoglycan degradation by the ADAMTS family of proteinases. Biochimica et Biophysica Acta (BBA), 2011 - Molecular Basis of Disease. https://doi.org/10.1016/j.bbadis.2011.08.009.

Stawarski M., Stefaniuk M., and Wlodarczyk J., "Matrix Metalloproteinase-9 Involvement in the Structural Plasticity of Dendritic Spines," Frontiers in Neuroanatomy 8 (2014): 68, 10.3389/fnana.2014.00068.

Stefaniak, O., Dobrzyńska, M., Drzymała-Czyż, S., & Przysławski, J. (2022). Diet in the Prevention of Alzheimer's Disease: Current Knowledge and Future Research Requirements. Nutrients, 14. https://doi.org/10.3390/nu14214564.

Steiner H., Regina Fluhrer, Christian Haass, (2008). Intramembrane Proteolysis by γ-Secretase*, Journal of Biological Chemistry, Volume 283, Issue 44, 2008, Pages 29627-29631, ISSN 0021-9258, https://doi.org/10.1074/jbc.R800010200.

Stephan, B., Birdi, R., Tang, E., Cosco, T., Cosco, T., Donini, L., Licher, S., Ikram, M., Siervo, M., & Robinson, L. (2018). Secular Trends in Dementia Prevalence and Incidence Worldwide: A Systematic Review. Journal of Alzheimer's Disease, 66, 653 - 680. https://doi.org/10.3233/JAD-180375.

Stevenson-Hoare, J., Schalkamp, A., Sandor, C., Hardy, J., & Escott-Price, V. (2023). New cases of dementia are rising in elderly populations in Wales, UK. Journal of the Neurological Sciences, 451. https://doi.org/10.1016/j.jns.2023.120715.

Steullet, P., Cabungcal, J., Bukhari, S., Ardelt, M., Pantazopoulos, H., Hamati, F., Salt, T., Cuénod, M., , K., & Berretta, S. (2017). The Thalamic Reticular Nucleus in Schizophrenia and Bipolar Disorder: Role of Parvalbumin-Expressing Neuron Networks and Oxidative Stress. *Molecular psychiatry*, 23, 2057 - 2065. https://doi.org/10.1038/mp.2017.230.

Storck, S., Hartz, A., Bernard, J., Wolf, A., Kachlmeier, A., Mahringer, A., Weggen, S., Pahnke, J., & Pietrzik, C. (2018). The concerted amyloid-beta clearance of LRP1 and ABCB1/P-gp across the blood-brain barrier is linked by PICALM. Brain, Behavior, and Immunity, 73, 21-33. https://doi.org/10.1016/j.bbi.2018.07.017.

Summers, S., Kao, A., Kohn, A., Backus, G., Roth, R., Pessin, J., & Birnbaum, M. (1999). The Role of Glycogen Synthase Kinase 3β in Insulin-stimulated Glucose Metabolism*. *The Journal of Biological Chemistry*, 274, 17934 - 17940. https://doi.org/10.1074/jbc.274.25.17934.

T'Syen, D., Serneels, L., Pérez-Benito, L., De Strooper, B., Holt, M., & Theys, T. Modeling the β-secretase cleavage site and humanizing amyloid-beta precursor protein in rat and mouse to study Alzheimer's disease. Molecular Neurodegeneration. 2020; 15. https://doi.org/10.1186/s13024-020-00399-z

Taheri-Targhi, S., Gjedde, A., Araj-Khodaei, M., Rikhtegar, R., Parsian, Z., Zarrintan, S., Torbati, M., & Vafaee, M. (2019). Avicenna (980–1037 CE) and his Early Description and Classification of Dementia. Journal of Alzheimer's Disease, 71, 1093 - 1098. https://doi.org/10.3233/JAD-190345 .

Takahashi, R., Nam, E., Edgar, M., & Gouras, G. (2002). Alzheimer beta-amyloid peptides: normal and abnormal localization.. Histology and histopathology, 17 1, 239-46 . https://doi.org/10.14670/HH-17.239.

Tan, S., Karri, V., Tay, N., Chang, K., Ah, H., Ng, P., Ho, H., Keh, H., & Candasamy, M. (2019). Emerging pathways to neurodegeneration: Dissecting the critical molecular mechanisms in Alzheimer's disease, Parkinson's disease.. Biomedicine & pharmacotherapy = Biomedecine & pharmacotherapie, 111, 765-777 . https://doi.org/10.1016/j.biopha.2018.12.101.

Tang, B. (2005). Alzheimer's disease: channeling APP to non-amyloidogenic processing.. Biochemical and biophysical research communications, 331 2, 375-8 . https://doi.org/10.1016/J.BBRC.2005.03.074.

Tang, M., Ryman, D., McDade, E., Jasielec, M., & Bateman, R. (2016). Neurological manifestations of autosomal dominant familial Alzheimer's disease: a comparison of the published literature with the Dominantly Inherited Alzheimer Network observational study (DIAN-OBS). The Lancet Neurology, 15, 1317-1325. https://doi.org/10.1016/S1474-4422(16)30229-0 .

Tanghe A, Termont A, Merchiers P, Schilling S, Demuth HU, Scrocchi L, Van Leuven F, Griffioen G, Van Dooren T. Pathological Hallmarks, Clinical Parallels, and Value for Drug Testing in Alzheimer's Disease of the APP[V717I] London Transgenic Mouse Model. Int J Alzheimers Dis. 2010 Sep 2;2010:417314. doi: 10.4061/2010/417314. PMID: 20862386; PMCID: PMC2939388.

Tapia-Rojas, C., Olesen, M., Jara, C., Murphy, M., & Torres, A. Premature synaptic mitochondrial dysfunction in the hippocampus during aging contributes to memory loss. Redox Biology. 2020; 34. doi: 10.1016/j.redox.2020.101558. Epub 2020 May 5. PMID: 32447261; PMCID: PMC7248293.

Tatsumi, L., Kobayashi, H., Yokoyama, M., & Tomita, T. Mouse Models of Alzheimer's Disease. Frontiers in Molecular Neuroscience. 2022; 15. https://doi.org/10.3389/fnmol.2022.912995

Testa, D., Prochiantz, A., & Di Nardo, A. (2019). Perineuronal nets in brain physiology and disease.. Seminars in cell & developmental biology, 89, 125-135 . https://doi.org/10.1016/j.semcdb.2018.09.011.

Thal DR, Rüb U, Orantes M, Braak H. Phases of A beta-deposition in the human brain and its relevance for the development of AD. Neurology. 2002 Jun 25;58(12):1791-800. doi: 10.1212/wnl.58.12.1791. PMID: 12084879.

Theron, D., Hopkins, L., Sutherland, H., Griffiths, L., & Fernandez, F. (2023). Can Genetic Markers Predict the Sporadic Form of Alzheimer's Disease? An Updated Review on Genetic Peripheral Markers. International Journal of Molecular Sciences, 24. https://doi.org/10.3390/ijms241713480.

Thompson, E., Lensjø, K., Wigestrand, M., Malthe-Sørenssen, A., Hafting, T., & Fyhn, M. (2017). Removal of perineuronal nets disrupts recall of a remote fear memory. Proceedings of the National Academy of Sciences of the United States of America, 115, 607 - 612. https://doi.org/10.1073/pnas.1713530115.

Tremblay, J., Guyon, A., Rousseau, J., Tremblay, G., Bégin, F., & Lamothe, G. (2021). Insertion of the protective APP A673T mutation by CRISPR/Cas9 base editing or PRIME editing. Innovation in Aging. https://doi.org/10.1093/geroni/igab046.2505.

Tsilibary, E., Tzinia, A., Radenović, L., Stamenković, V., Lebitko, T., Mucha, M., Pawlak, R., Frischknecht, R., & Kaczmarek, L. (2014). Neural ECM proteases in learning and synaptic plasticity.. Progress in brain research, 214, 135-57 . https://doi.org/10.1016/B978-0-444-63486-3.00006-2.

Tsoy, A., Umbayev, B., Kassenova, A., Kaupbayeva, B., & Askarova, S. (2024). Pathology of Amyloid-β (Aβ) Peptide Peripheral Clearance in Alzheimer's Disease. International Journal of Molecular Sciences, 25. https://doi.org/10.3390/ijms252010964.

Türker, F., Cook, E., & Margolis, S. (2021). The proteasome and its role in the nervous system.. Cell chemical biology. https://doi.org/10.1016/j.chembiol.2021.04.003.

Vafadari, B., Salamian, A., & Kaczmarek, L. (2016). MMP-9 in translation: from molecule to brain physiology, pathology, and therapy. Journal of Neurochemistry, 139. https://doi.org/10.1111/jnc.13415.

Van Der Kolk, N., Schmitz, C., Bayer, T., Steinbusch, H., Schafer, S., Rutten, B., & Van Zandvoort, M. Age-related loss of synaptophysin immunoreactive presynaptic boutons within the hippocampus of APP751SL, PS1M146L, and APP751SL/PS1M146L transgenic mice. The American journal of pathology. 2005; 167 1. doi: 10.1016/S0002-9440(10)62963-X. PMID: 15972962; PMCID: PMC1603440.

Van Dyck et al. Lecanemab in Early Alzheimer's Disease. New England Journal of Medicine (2023). doi:10.1056/NEJMoa2212948

Van't Spijker H. M. and Kwok J. C., "A Sweet Talk: The Molecular Systems of Perineuronal Nets in Controlling Neuronal Communication," Frontiers in Integrative Neuroscience 11 (2017): 33.

Vassar, R., Bennett, B., Babu-Khan, S., Kahn, S., Mendiaz, E., Denis, P., Teplow, D., Ross, S., Amarante, P., Loeloff, R., Luo, Y., Fisher, S., Fuller, J., Edenson, S., Lile, J., Jarosinski, M., Biere, A., Curran, E., Burgess, T., Louis, J., Collins, F., Treanor, J., Rogers, G., & Citron, M. (1999). Beta-secretase cleavage of Alzheimer's amyloid precursor protein by the transmembrane aspartic protease BACE.. Science, 286 5440, 735-41 . https://doi.org/10.1126/SCIENCE.286.5440.735.

Vatanabe, I., Manzine, P., & Cominetti, M. (2020). Historic concepts of dementia and Alzheimer's disease: From ancient times to the present. Revue neurologique. https://doi.org/10.1016/j.neurol.2019.03.004.

Vetrivel, K., & Thinakaran, G. (2006). Amyloidogenic processing of β-amyloid precursor protein in intracellular compartments. Neurology, 66, S69 - S73. https://doi.org/10.1212/01.wnl.0000192107.17175.39.

Walker, L., Schelle, J., & Jucker, M. (2016). The Prion-Like Properties of Amyloid-β Assemblies: Implications for Alzheimer's Disease.. Cold Spring Harbor perspectives in medicine, 6 7. https://doi.org/10.1101/cshperspect.a024398.

Wall, J., Donovan, K., Rosay, M., Michael, B., Silvers, R., Can, T., Colvin, M., Ni, Q., Griffin, R., Sergeyev, I., & Linse, S. Atomic Resolution Structure of Monomorphic Aβ42 Amyloid Fibrils. Journal of the American Chemical Society. 2016; 138 30. doi: 10.1021/jacs.6b05129. Epub 2016 Jul 14. PMID: 27355699; PMCID: PMC5389415.

Walter, S., Jumpertz, T., Hüttenrauch, M. *et al.* The metalloprotease ADAMTS4 generates N-truncated Aβ4–x species and marks oligodendrocytes as a source of amyloidogenic peptides in Alzheimer's disease. *Acta Neuropathol* **137**, 239–257 (2019). https://doi.org/10.1007/s00401-018-1929-5

Wang, L., Li, J., & Di, L. (2021). Glycogen synthesis and beyond, a comprehensive review of GSK3 as a key regulator of metabolic pathways and a therapeutic target for treating metabolic diseases. *Medicinal Research Reviews*, 42, 946 - 982. https://doi.org/10.1002/med.21867.

Wang, M., Dinarvand, D., Chan, C., Bragin, A., & Li, L. (2024). Photobiomodulation as a Potential Treatment for Alzheimer's Disease: A Review Paper. Brain Sciences, 14. https://doi.org/10.3390/brainsci14111064 .

Wang, Y., Liu, Y., Bi, X., & Baudry, M. (2020). Calpain-1 and Calpain-2 in the Brain: New Evidence for a Critical Role of Calpain-2 in Neuronal Death. Cells, 9. https://doi.org/10.3390/cells9122698.

Watts, J., & Prusiner, S. (2018). β-Amyloid Prions and the Pathobiology of Alzheimer's Disease.. Cold Spring Harbor perspectives in medicine, 8 5. https://doi.org/10.1101/cshperspect.a023507.

Welikovitch, L., Carmo, S., Maglóczky, Z., Malcolm, J., Oke, J., Klein, W., Freund, T., & Cuello, C. (2020). Early intraneuronal amyloid triggers neuron-derived inflammatory signaling in APP transgenic rats and human brain. Proceedings of the National Academy of Sciences of the United States of America, 117, 6844 - 6854. https://doi.org/10.1073/pnas.1914593117.

Weller, J., & Budson, A. (2018). Current understanding of Alzheimer's disease diagnosis and treatment. F1000Research, 7. https://doi.org/10.12688/f1000research.14506.1 .

Weng S. S. H., Demir F., Ergin E. K., et al., "Sensitive Determination of Proteolytic Proteoforms in Limited Microscale Proteome Samples," Molecular & Cellular Proteomics 18, no. 11 (2019): 2335–2347, 10.1074/mcp.TIR119.001560

Wildburger, N.C., Esparza, T.J., LeDuc, R.D. et al. Diversity of Amyloid-beta Proteoforms in the Alzheimer's Disease Brain. Sci Rep 7, 9520 (2017). https://doi.org/10.1038/s41598-017-10422-x.

Wiltfang J, Esselmann H, Cupers P, Neumann M, Kretzschmar H, Beyermann M, Schleuder D, Jahn H, Rüther E, Kornhuber J, Annaert W, De Strooper B, Saftig P. Elevation of beta-amyloid peptide 2-42 in sporadic and familial Alzheimer's disease and its generation in PS1 knockout cells. J Biol Chem. 2001 Nov 16;276(46):42645-57. doi: 10.1074/jbc.M102790200. Epub 2001 Aug 28. PMID: 11526104.

Wingert JC, Sorg BA. Impact of Perineuronal Nets on Electrophysiology of Parvalbumin Interneurons, Principal Neurons, and Brain Oscillations: A Review. Front Synaptic Neurosci. 2021 May 10;13:673210. doi: 10.3389/fnsyn.2021.673210. PMID: 34040511; PMCID: PMC8141737.

Wirths, Oliver & Zampar, Silvia. (2019). Emerging roles of N- and C-terminally truncated Aβ species in Alzheimer's disease. Expert Opinion on Therapeutic Targets. 23. DOI: 10.1080/14728222.2019.1702972.

Wittrahm, R., Takalo, M., Kuulasmaa, T., & Hiltunen, M. (2023). Protective Alzheimer's disease-associated APP A673T variant predominantly decreases sAPPβ levels in cerebrospinal fluid and 2D/3D cell culture models. Neurobiology of Disease, 182. https://doi.org/10.1016/j.nbd.2023.106140 .

Woodruff, G., Reyna, S., & Goldstein, L. (2014). A PRESENILIN 1 MUTATION ALTERS APP LOCALIZATION IN HUMAN NEURONS. Alzheimer's & Dementia, 10. https://doi.org/10.1016/j.jalz.2014.05.305.

Woźniak, M., Mee, A., & Itzhaki, R. (2009). Herpes simplex virus type 1 DNA is located within Alzheimer's disease amyloid plaques. The Journal of Pathology, 217. https://doi.org/10.1002/path.2449.

Xu, C., Dong, C., & Zhao, L. A Review of Application of Aβ42/40 Ratio in Diagnosis and Prognosis of Alzheimer's Disease. Journal of Alzheimer's Disease. 2022; 90. doi: 10.3233/JAD-220673. PMID: 36155521.

Xu, H., Zhou, Y., Liu, Y., Ping, J., Shou, Q., Chen, F., & Ruo, R. (2016). Metformin improves hepatic IRS2/PI3K/Akt signaling in insulin-resistant rats of NASH and cirrhosis.. *The Journal of endocrinology*, 229 2, 133-44 . https://doi.org/10.1530/JOE-15-0409.

Yamada H., Fredette B., Shitara K., et al., "The Brain Chondroitin Sulfate Proteoglycan Brevican Associates With Astrocytes Ensheathing Cerebellar Glomeruli and Inhibits Neurite Outgrowth From Granule Neurons," Journal of Neuroscience 17, no. 20 (1997): 7784–7795

Yang, S., Gigout, S., Molinaro, A., Naito-Matsui, Y., Hilton, S., Foscarin, S., Nieuwenhuis, B., Tan, C., Verhaagen, J., Pizzorusso, T., Saksida, L., Bussey, T., Kitagawa, H., Kwok, J., & Fawcett, J. (2021). Chondroitin 6-sulphate is required for neuroplasticity and memory in ageing. Molecular Psychiatry, 26, 5658 - 5668. https://doi.org/10.1038/s41380-021-01208-9.

Yang, S., Hilton, S., Alves, J., Saksida, L., Bussey, T., Matthews, R., Kitagawa, H., Spillantini, M., Kwok, J., & Fawcett, J. (2017). Antibody recognizing 4-sulfated chondroitin sulfate proteoglycans restores memory in tauopathy-induced neurodegeneration. Neurobiology of Aging, 59, 197-209. https://doi.org/10.1016/j.neurobiolaging.2017.08.002.

Yi, Y., Lee, J., & Lim, M. (2024). Amyloid-β-interacting proteins in peripheral fluids of Alzheimer's disease. Trends in Chemistry. https://doi.org/10.1016/j.trechm.2024.01.003.

Yoshida, S., & Shiosaka, S. (1999). Plasticity-related serine proteases in the brain (review). International journal of molecular medicine, 3 4, 405-9 . https://doi.org/10.3892/IJMM.3.4.405.

Yuan W., Matthews R. T., Sandy J. D., and Gottschall P. E., "Association Between Protease-Specific Proteolytic Cleavage of Brevican and Synaptic Loss in the Dentate Gyrus of Kainate-Treated Rats," Neuroscience 114, no. 4 (2002): 1091–1101, 10.1016/s0306-4522(02)00347-0.

Zabel, P., Przekoracka-Krawczyk, A., Jaworski, D. et al. Assessment of individual retinal layer thickness and vascular changes in Alzheimer's disease. Sci Rep 15, 17287 (2025). https://doi.org/10.1038/s41598-025-02377-1

Zhang, M., Zhao, D., Zhou, G., & Li, C. (2020). Dietary pattern, Gut microbiota and Alzheimer's disease.. Journal of agricultural and food chemistry. https://doi.org/10.1021/acs.jafc.9b08309 .

Zhang, Q., Guo, S., Zhang, X., Tang, S., Shao, W., Han, X., Wang, L., & Du, Y. (2015). Inverse relationship between cancer and Alzheimer's disease: a systemic review meta-analysis. Neurological Sciences, 36, 1987-1994. https://doi.org/10.1007/s10072-015-2282-2.

Zhang, R., Jiang, H., Liu, Y., & He, G. (2022). Structure, function, and pathology of Neurexin-3. Genes & Diseases, 10, 1908 - 1919. https://doi.org/10.1016/j.gendis.2022.04.008.

Zhang, Y., Chen, H., Li, R., Sterling, K., & Song, W. (2023). Amyloid β-based therapy for Alzheimer's disease: challenges, successes and future. Signal Transduction and Targeted Therapy, 8. https://doi.org/10.1038/s41392-023-01484-7 .

Zhang, Y., Thompson, R., Zhang, H., & Xu, H. (2011). APP processing in Alzheimer's disease. Molecular Brain, 4, 3 - 3. https://doi.org/10.1186/1756-6606-4-3.

Zhang, X., Liu, A., Zhang, Y., Zhou, M., Li, X., Fu, M., Pan, Y., Xu, J., & Zhang, J. (2022). A diarylheptanoid compound from Alpinia officinarum Hance ameliorates high glucose-induced insulin resistance by regulating PI3K/AKT-Nrf2-GSK3β signaling pathways in HepG2 cells.. *Journal of ethnopharmacology*, 115397 . https://doi.org/10.2139/ssrn.4055988.

Zhao, J., Liu, X., Xia, W., Zhang, Y., & Wang, C. (2020). Targeting Amyloidogenic Processing of APP in Alzheimer's Disease. Frontiers in Molecular Neuroscience, 13. https://doi.org/10.3389/fnmol.2020.00137.

Zhao, L., Yue, Z., Wang, Y., Wang, J., Ullah, I., Muhammad, F., Zhou, Y., Zhu, H., Wang, X., & Li, H. (2022). Autophagy activation by Terminalia chebula Retz. reduce Aβ generation by shifting APP processing toward non-amyloidogenic pathway in APPswe transgenic SH-SY5Y cells.. Phytomedicine : international journal of phytotherapy and phytopharmacology, 103, 154245 . https://doi.org/10.1016/j.phymed.2022.154245.

Zhou, J., Tang, M., Fang, R., Tang, C., & Wang, Q. (2023). Diet and physical activity influence the composition of gut microbiota, benefit on Alzheimer's Disease. Food Science and Human Wellness. https://doi.org/10.26599/fshw.2022.9250049.

Zlokovic, B., Ghiso, J., Mackic, J., McComb, J., Weiss, M., & Frangione, B. (1993). Blood-brain barrier transport of circulating Alzheimer's amyloid beta.. Biochemical and biophysical research communications, 197 3, 1034-40 . https://doi.org/10.1006/BBRC.1993.2582.

Zott B, Simon MM, Hong W, Unger F, Chen-Engerer HJ, Frosch MP, Sakmann B, Walsh DM, Konnerth A. A vicious cycle of β amyloid-dependent neuronal hyperactivation. Science. 2019 Aug 9;365(6453):559-565. doi: 10.1126/science.aay0198. PMID: 31395777; PMCID: PMC6690382.

Curriculum Vitae

Full name: Maximilian Keller

Adress: Rheinallee 15, 55118 Mainz

Work experience

Position	Graduate student
Period	March 2022 – October 2025
Institution	University Medical Center Mainz, Pathobiochemistry, Pietrzik Lab
Obtained skills	- animal work in transgenic mouse models - standard biochemical methods - immunofluorescence - transcytosis in a cellular BBB model

Position	Teaching
Period	March 2022 – November 2025
Institution	University Medical Center Mainz
Obtained skills	- tutoring medicine students in biochemical practical (photometry)

Position	Private Tutor (online)
Period	January 2024 – May 2025
Institution	GoStudent Online Tutoring GmbH
Obtained skills	improved on: - communication and explanation skills - digital teaching and time management skills

Position	Research Assistant
Period	October 2020 – December 2021
Institution	University Medical Center Mainz, Institute for Molecular Medicine, Waisman Lab
Obtained skills	- animal work (weaning cages, breeding) - genotyping

Position	Intern (Chemical laboratory)
Period	June 2012 – August 2012
Institution	Carrier Kältetechnik GmbH
Obtained skills	- assessment of rubber seals in refrigerators - quality control of different industrial oil formulations

Educational background

Degree	Master of Science in Biomedicine
Period	October 2019 – February 2022
Institution	Johannes Gutenberg University Mainz
Title Thesis	Exploring NKp30-redirected, TCR-negative CAR T cells for cellular therapy of B7H6-positive malignancies (Udo Hartwig Lab)

Degree	Bachelor of Science in Biology
Period	March 2017 – March 2019
Institution	Goethe University Frankfurt
Title Thesis	Radioresistance of agonist-selected T cells (Andreas Krueger Lab)

Degree	Biophysics
Period	October 2012 – March 2016
Institution	Goethe University Frankfurt
Title Thesis	-

List of Publications

First author:

- Meprin β Modulates Brevican Proteolysis Impairing Neural Plasticity and Memory Formation @FASEB journal (IF 4.8): https://doi.org/10.1096/fj.202500017R (2025)

- Meprin β Elevates Hippocampal Soluble Aβ in an APP/V717I Mouse Model (under review @ Experimental Neurology)

Co-Author:

- CRISPR/Cas9 TCR-Edited NKp30 CAR T Cells Exhibit Superior Anti-Tumor Immunity to B7H6-Expressing Leukemia and Melanoma @International Journal of Molecular Sciences (IF 4.9): https://doi.org/10.3390/ijms26178235 (2025)

- HYTANE-Identified Latrophilin-3 Cleavage by Meprin β Leads to Loss of the Interaction Domains @Journal of Proteome Research (IF 3.6): https://doi.org/10.1021/acs.jproteome.4c00912 (2025)

- The solute carrier SLC7A1 may act as a protein transporter at the blood-brain barrier @European Journal of Cell Biology (IF 4.3): https://doi.org/10.1016/j.ejcb.2024.151406 (2024)

- Shedding of transferrin receptor I by meprin β regulates cellular iron uptake and iron homeostasis *in vivo* (under review)

Acknowledgements

First and foremost, I would like to express my deepest gratitude to Prof. for his constant support, optimism, and encouragement throughout my PhD. His guidance and positive attitude made every challenge seem manageable. I truly can't and don't want to say anything negative about you. I also wish to thank Prof. for kindly accepting the official supervision of my thesis. Even though our interactions were rare, I truly appreciated your patience and genuine interest when I had the chance to present my data to you (during the FTN seminar).

My heartfelt thanks go to all my colleagues -
- for creating such a friendly, supportive, and inspiring working environment. It was a pleasure sharing this journey with you and I hope our paths cross a lot of times after we all finish our theses!

I am also grateful for the fruitful collaborations with the lab: , for the important input; , for her help with primary cell cultures; , for assisting with the staining of brain slices; and especially , who was an integral part of my PhD from start to finish. You did an incredible amount of work - even if you sometimes forget just how much! From the lab, I would like to thank , with whom I had close and enjoyable collaboration, and for their contributions and great insight into all meprin-related problems. , you were not just colleagues but became true friends along the way, and I'm very thankful for that.

My sincere thanks also go to (for helping with behavioral experiments), (for assisting with brain slices), (for her thoughtful advice and kind words about my work), (for his valuable input and expertise), and , who was always fair and helpful—especially when I occasionally forgot things in the animal facility!

To my parents, thank you for always being there for me, for your endless support, and for giving me the strength and freedom to pursue this path. To my friends, thank you for the good times, for helping me stay grounded, and for being my balance when things got stressful. You made everything better just by being there.

And finally, - you are truly the personification of "the best comes last." Thank you so much for helping me push through to the very end. I don't know if I could have done it without you. You came into my life at exactly the right moment, and for that, I am endlessly grateful!

Declarations

I hereby declare that the submitted scientific work has not been submitted to any other German or foreign university or comparable institution for the conferral of an academic degree.

Maximilian Keller

Date

I hereby declare that I have not unsuccessfully ended another doctoral or equivalent program in the subject area of the current doctoral program.

Maximilian Keller

Date

I hereby declare that I wrote the dissertation submitted without any unauthorized external assistance and used only sources acknowledged in the work. All textual passages that are appropriated verbatim or paraphrased from published and unpublished texts, as well as all information obtained from oral sources, are duly indicated and listed in accordance with bibliographical rules. In carrying out this research, I complied with the rules of standard scientific practice as formulated in the statutes of Johannes Gutenberg University Mainz to ensure standard scientific practice.

Maximilian Keller

Date